Environmental Science

Rong Sun
Li Fei *Editors*

Sustainable Development of Water and Environment

Proceedings of the ICSDWE 2019

Springer

Environmental Science and Engineering

Environmental Science

The protection of our environment is one of the most important challenges facing today's society. At the focus of efforts to solve environmental problems are strategies to determine the actual damage, to manage problems in a viable manner, and to provide technical protection. Similar to the companion subseries Environmental Engineering, Environmental Science reports the newest results of research. The subjects covered include: air pollution; water and soil pollution; renaturation of rivers; lakes and wet areas; biological ecological; and geochemical evaluation of larger regions undergoing rehabilitation; avoidance of environmental damage. The newest research results are presented in concise presentations written in easy to understand language, ready to be put into practice.

More information about this series at http://www.springer.com/series/3234

Rong Sun · Li Fei
Editors

Sustainable Development of Water and Environment

Proceedings of the ICSDWE 2019

Springer

Editors
Rong Sun
Department of Environmental Science and Engineering, School of Chemical Engineering
Huaqiao University
Xiamen, China

Li Fei
Research Center for Environment and Health
Zhongnan University of Economics and Law
Wuhan, China

ISSN 1863-5520 ISSN 1863-5539 (electronic)
Environmental Science and Engineering
ISSN 1431-6250 ISSN 2661-8222 (electronic)
Environmental Science
ISBN 978-3-030-16728-8 ISBN 978-3-030-16729-5 (eBook)
https://doi.org/10.1007/978-3-030-16729-5

This Springer imprint is published by the registered company Springer Nature Switzerland AG
The registered company address is: Gewerbestrasse 11, 6330 Cham, Switzerland

Preface

Dear Distinguished Authors and Guests,

It was a great pleasure to welcome all the participants to the 2019 2nd International Conference on Sustainable Development of Water and Environment (ICSDWE2019) held in Hong Kong, China. ICSDWE2019 is dedicated to new research development and advances in the field of Sustainable Development, Water Resource, Environmental Monitoring, and Environmental Chemistry.

The aim of ICSDWE2019 is to present the latest research and results of scientists (professors, students, Ph.D. students, engineers, and postdoc scientist) related to sustainable development of water and environment. The key goal of the conference provides opportunities for academic scientists, engineers, and industry researchers to exchange and share their expertise, experience, new ideas, or research result and discuss the challenges and future in their expertise. This conference also provides a platform for the students, researchers, and engineers to interact with experts and specialists on the technical matters and future direction of their research area.

The papers were selected after the peer review process by conference committee members and international reviewers. The submitted papers were selected on the basis of originality, significance, and clarity for the purpose of the conference. The papers should provide the reader with an overview of many recent advances in the field related to Sustainable Development, Water Resource, Environmental Monitoring, and Environmental Chemistry. The conference program is extremely rich, featuring high-impact presentation. We hope that the conference results constituted a significant contribution to the knowledge in this up-to-date scientific field.

On behalf of the organizing committee, I would like to especially thank all technology committee members, reviewers, speakers, chairpersons, sponsors, and conference participants for their support and contributions to this volume. We look forward to your participation in the 3rd ICSDWE 2020.

With our warmest regards

Xiamen, China — Rong Sun
Wuhan, China — Li Fei

Contents

Part I
Environmental Monitoring

Microbiological Monitoring of Cryohydrological Geosystems of the Cryolithozone

Andrey Subbotin, Sergey Petrov, Lyubov Gnatchenko and Maksim Narushko

Abstract The degradation of permafrost as a result of the development of destructive cryogenic processes leads to the fact that microorganisms, which for a long time were preserved in the permafrost strata, are carried out into modern aquatic biocenoses, belonging to earlier geological epochs with different climatic and ecological conditions than modern ones. The aim of the work was to study the influence of the metabolites of bacteria of the genera *Bacillus*, *Pseudomonas*, *Acinetobacter*, *Listeria*, isolated from the permafrost of the Subarctic zone of Russia, on the morphophysiological parameters of the unicellular hydrobionts *Paramecium caudatum Ehrenberg*. It has been shown that the secondary metabolites of bacteria of ancient natural cryolithozone ecosystems may have a negative effect on the physiological parameters of single-cell hydrobionts. The bacterial metabolites obtained at different temperatures vary in the severity of the effects on the biological parameters of *Paramecium caudatum Ehrenberg*. Secondary metabolites of bacteria, obtained at a temperature of +4 °C, in most cases have a less pronounced toxic effect. Considering global climate change in the direction of warming and anthropogenic conditions leading to the degradation of permafrost and subsequent removal of microorganisms into aquatic biocenoses, it is necessary to systematically monitor the aquatic environment to determine the biological activity of both microorganisms and their metabolites with the purpose of predicting possible environmental impacts.

Keywords Cryohydrological systems · Microbiota · Secondary metabolites · Cryolithozone · *Paramecium caudatum ehrenbe*

A. Subbotin · S. Petrov (✉) · L. Gnatchenko · M. Narushko
Tyumen Scientific Center of the Siberian Branch of the Russian Academy of Sciences, Tyumen, Russia
e-mail: tumiki@yandex.ru

R. Sun and L. Fei (eds.), *Sustainable Development of Water and Environment*, Environmental Science and Engineering,
https://doi.org/10.1007/978-3-030-16729-5_1

1 Introduction

The development of the Subarctic and Arctic territories poses a number of new tasks for researchers. In particular, the functioning and interaction of various elements of paleo-ecosystems occurring against the background of global climate change and the increasing anthropogenic load associated with the development of mineral and natural resources of the Arctic and subarctic territories remain little studied. The degradation of permafrost as a result of the development of destructive cryogenic processes leads to the fact that microorganisms, which for a long time were preserved in the permafrost strata, are carried out into modern aquatic biocenoses, belonging to earlier geological epochs with different climatic and ecological conditions than modern ones.

In the last decade, a large number of works have appeared, showing that the cryocolithozone paleo-ecosystems contain a significant variety of viable forms of microorganisms (Kudryashova et al. 2013; Gubin et al. 2003; Skladnev et al. 2016; Gilichinsky et al. 2008; Bakermans and Skidmore 2011; Melnikov et al. 2011; Pecheritsyna et al. 2007). Keeping their vitality, being in a state of hypometabolism under peculiar environmental conditions of permafrost, they could form new biochemical adaptation mechanisms, therefore, they can be a source of biologically active molecules with unique physiological properties that influence the physiological processes of modern organisms (Subbotin et al. 2016; Kalenova et al. 2013, 2015; Kalyonova et al. 2015).

When destructive processes occur in permafrost, microorganisms in them, first of all get into the aquatic environment. This is due to the destruction of permafrost onshore sediments of rivers, pumping of drilling and quarry waters, the transfer of large volumes of permafrost, and their subsequent thawing when opening mineral deposits. As a result, microorganisms that have been in cryopreservation for a long time, the hypometabolic state begins to actively proliferate in modern aquatic ecosystems. The effects of the interaction of microorganisms and their metabolites of ancient natural ecosystems with modern representatives of aquatic ecosystems are poorly understood and are of considerable interest.

The aim of the work was to study the influence of the metabolites of bacteria, isolated from the permafrost on the morphophysiological parameters of the unicellular hydrobionts *Paramecium caudatum Ehrenberg*.

2 Materials and Methods

We used bacterial strains isolated from cores obtained by drilling wells to a depth of 35 m in the Tarko-Sale area of the Yamalo-Nenets Autonomous District of Russia (the age of rocks for sampling is from 2 to 40 thousand years). A also from the permafrost of the Mamontova Mountain (above-flood terrace of the left bank of the Aldan River (Yakutia), the age of rocks for sampling can reach up to 3 million years) and outcrops of permafrost of the floodplain terrace of the right bank of the r. Chara

9 km upstream from the village New Chara (age of rocks from 2 to 14 thousand years). Strains identified by the method of the 16S rRNA sequence.

We used secondary protein metabolites derived from bacterial strains. Suspensions of bacterial cultures with a density of 1×10^9 microbial cells/ml for obtaining secondary metabolites were incubated in a thermostat at two temperatures: +36 and +4 °C for 5 days (Kalyonova et al. 2015). The total mass of peptide complexes in the metabolites was determined by the method of liquid preparative chromatography, on a Gilson chromatograph, and was 200 μg/ml.

For biological testing of bacterial metabolites from permafrost, a culture of infusoria *Paramecium caudatum Ehrenberg*, widely used to study the effects of the toxic effects of various substances in the aquatic environment, was used. Ciliates were cultured in dairy medium. In each variant of the experiment, 5 tubes with 50 ml of medium for containing ciliates were used. On the first day of the experiment, 10 *Paramecium caudatum* infusoria were placed in each tube. The bacterial metabolites were added to the ciliates nutrient medium at a dose of 30 μl (6 μg for the protein complex). In the control, washings from the surface of sterile nutrient bacteriological agar were added. After 96 h, the density of ciliates, motor activity, and chemotaxis was determined. The results obtained, after statistical data processing, were expressed as a percentage relative to the control (the results obtained in the control were taken as 100%).

3 Results of the Study

It was established that identical doses of metabolites (6 μg/ml) obtained at different cultivation temperatures of bacterial cultures (+36 and +4 °C) mainly have toxic activity, reducing the studied physiological indices of infusoria (Table 1).

The decrease in the density of cultures of ciliates (suppression of reproduction) is more pronounced in metabolites obtained at +36 °C of the genus *Bacillus* (strains: 3/12, 875, 9/48p, 1/04). The same metabolites have a more pronounced negative effect on the motional activity of ciliates than the metabolites obtained at +4 °C. Metabolites of the strain *Bacillus cereus* 3M have a more pronounced negative effect on the motor activity of ciliates, as compared with others. When evaluating chemotaxis, its values are higher for metabolites of bacteria of the genus *Bacillus strains* 3/12, 875, 1/04, obtained at a temperature of +36 °C, than for metabolites obtained at a temperature of +4 °C. It is likely that the metabolites of bacteria of the genus *Bacillus*, obtained at the cultivation temperature of the strains +36 °C, have a higher toxicity than the metabolites obtained at the cultivation temperature of the strains +4 °C.

Metabolites of the strain *Acinetobacter sp.* 4/25, obtained at a temperature of +36 °C, have a less pronounced toxic effect on the culture of ciliates, than metabolites obtained at a temperature of +4 °C, but stimulate chemotaxis in ciliates.

Metabolites of strains *Pseudomonas putida* 3/09 and *Acinetobacter sp*. 3/14, obtained at different temperatures of cultivation of strains, have the same effect

Table 1 Physiological parameters of ciliates when exposed to metabolites of bacterial cultures obtained at different cultivation temperatures (in % relative to the control)

Metabolites of microorganisms	Metabolites obtained at +36 °C			Metabolites obtained at +4 °C		
	Density	Physical activity	Chemotaxis	Density	Physical activity	Chemotaxis
Bacillus megaterium 3/12	46.7	100.0	94.5	57.5	158.0	46.6
Bacillus megaterium 875	49.1	51.5	94.7	62.7	74.4	88.4
Bacillus sp. 9/48п	53.4	48.9	68.4	60.2	73.3	95.4
Bacillus subtilus 1/04	59.8	63.5	99.0	63.9	82.3	65.7
Bacillus cereus 3M	77.9	22.6	84.6	61.0	48.7	90.8
Pseudomonas putida 3/09	66.8	64.9	96.0	65.0	67.5	98,6
Acinetobacter sp. 3/14	56.7	100.0	83.7	55.5	95.5	71.9
Acinetobacter sp. 4/25	61.8	88.3	136.1	48.1	56.3	70.8
Listeria sp. 4/19	57.5	76.9	67.9	65.8	64.1	104.2

on the studied parameters, regardless of the temperature of cultivation of bacterial strains. The differences between them are not significant ($p > 0.05$).

Metabolites of *Bacillus megaterium* 3/12 and *Acinetobacter sp*. 3/14 do not have a negative effect on the motor activity of the ciliates, unlike the other metabolites studied, but exhibit a toxic effect, significantly inhibiting the ciliate multiplication ($p < 0.05$).

Adding metabolites to *Listeria sp.* 4/19, obtained at temperatures of +36 and +4 °C, there was a statistically significant decrease in the density of the ciliates culture compared with the control ($p < 0.05$). Under the action of the filtrate obtained at a temperature of +36 °C on the 3rd day of the experiment, a decrease ($p < 0.05$) in the density of the culture and the ciliate chemotaxis was observed. Under the action of the filtrate obtained at a temperature of +4 °C, a less pronounced decrease in culture density ($p < 0.05$) and a high chemotaxis at the control level ($p > 0.05$) are observed.

The decrease in the chemotaxis index in cultures of ciliates to which the studied metabolites were added can be explained by the fact that the cultures are accustomed

to these toxicants; in most of the experimental options, it remains quite high. It should be noted that this indicator is higher in the study of metabolites obtained at +36 °C.

4 Conclusions and Suggestions

The results of the study indicate that the metabolites of bacteria isolated from permafrost contained in the medium of cultivation of ciliate *Paramecium caudatum*, may have a negative impact on the physiological parameters of eukaryotic single-cell hydrobionts. The bacterial metabolites obtained at different temperatures differ in the severity of the impact on the biological parameters of ciliates. Metabolites of bacteria, obtained at a temperature of +4 °C, in most cases have a less pronounced toxic effect.

Considering the change in climatic and anthropogenic conditions leading to the degradation of permafrost and subsequent removal of relict microorganisms into aquatic biocenoses, it is necessary to systematically monitor the aquatic environment to determine the biological activity of both the microorganisms and their metabolites. Such studies will make it possible to predict the effects of reproduction of relict microorganisms in modern hydrobiocenoses and to evaluate the potential effects on the biological components of these biocenoses.

Acknowledgements The work was carried out according to the state project, according to the Research Plan of the Tyumen Scientific Center of the SB RAS for 2018–2020, Protocol No. 2 of December 8, 2017 (Priority IX.133 Program IX.133.1 Project: IX.133.1.4 Cryobiological processes on land and in the coastal part of the Kara Sea in conditions of increasing average annual temperatures).

References

Bakermans C, Skidmore ML (2011) Microbial metabolism in ice and brine at 5 °C. Microbiology 13(8):2269–2278

Gilichinsky DA, Vishnivetskaya TA, Petrova MA et al (2008) Bacteria in permafrost. In: Margesin R et al (eds) Psychrophiles: from biodiversity to biotechnology. Springer, Berlin, Rosa, pp 83–102

Gubin SV, Maksimovich SV, Davydov SP, Gilichinsky DA, Shatilovich AV, Spirina EV, Yashina SG (2003) About the possibility of the participation of Late Pleistocene biota in the formation of the biodiversity of the modern cryolithozone. J General Biol 64(2):160–165

Kalenova LF, Subbotin AM, Bazhin AS (2013) The influence of permafrost bacteria of different geological age on the immune system. Bull New Med Technol (Electron J) 1:2–105

Kalenova LF, Novikova MA, Subbotin AM (2015) Effects of permafrost microorganisms on skin wound reparation. Bull Exp Biol Med 158(4):478–482

Kalyonova LF, Novikova MA, Subbotin AM, Bazhin AS (2015) Effects of temperature on biological activity of permafrost microorganisms. Bull Exp Biol Med 158(6):772–775

Kudryashova EB, Chernousova EY, Suzina NE, Ariskina EV, Gilichinsky DA (2013) Microbial diversity of samples of Late Pleistocene permafrost of the Siberia. Microbiology 82(3):351–361
Melnikov VP, Rogov VV, Kurchatova AN et al (2011) Distribution of microorganisms in frozen soils. Earth's Cryosphere 15(4):86–90
Pecheritsyna SA, Scherbakova VA, Kholodov AL (2007) Microbiological analysis of cryopegs of the Varandey peninsula on the coast of the Barents Sea. Microbiology 76(5):694–701
Skladnev DA, Mulyukin AL, Filippova SN et al (2016) Modeling of the process of microbial cell spread and phage particles from the melting sites of the permafrost layers. Microbiology 580–587
Subbotin AM, Narushko MV, Bome NA et al (2016) The influence of permafrost microorganisms on the morphophysiological indicators of spring wheat. Vavilovsky J Genet Breed 20(5):666–672

Survey of Physical, Chemical and Microbial Water Quality of Irrigation Sources in Tarlac, Philippines

Edmar N. Franquera, Cielito A. Beltran, Ma. Asuncion G. Beltran and Ruth Thesa B. Franquera

Abstract The main sources of irrigation water for irrigating crops comes from major rivers. Usually these water sources which can be used for irrigating various crops could be very vulnerable to contamination. The aim of the study was to determine the physical, chemical and microbial water quality of the different irrigation sources in Tarlac and to compare it with the existing water quality guidelines stipulated in the DENR AO 08 Series of 2016. The water samples collected from the surface water of different rivers were subjected to laboratory analysis. Higher TSS was found to be during wet season as compared during the dry season. Higher COD was found both in dry and wet seasons in Benig river. All of the major rivers have a less than 0.05 mg/l lead and 0.0002 mg/l mercury based from the result of the laboratory analysis. The highest dissolved oxygen was found to be within the Tarlac River both during the dry and wet season. Comparing with the National standards from the DENR the major rivers of Tarlac surpasses the minimum standards of classification of water bodies with dissolved oxygen ranging from 2 to 6 mg/l. The lowest dissolved oxygen was found in Concepcion River during the dry season (5.0 mg/l) and in Rio Chico River (4.8 mg/l) during the wet season. Higher total dissolved solids were observed in the different rivers during the dry season which ranges from 300 to 560 mg/l as compared during the wet season which ranges from 169 to 540 mg/l respectively. The nitrate concentrations of the different rivers in Tarlac shows to be within the range of the National Standards of the DENR. Higher concentrations of *E. coli* and fecal coliform count were also noted within the different rivers of Tarlac.

Keywords Water quality · River · Irrigation · Tarlac

E. N. Franquera (✉) · C. A. Beltran (✉) · Ma. A. G. Beltran (✉) · R. T. B. Franquera (✉)
Tarlac Agricultural University, Malacampa, Camiling, Tarlac, Philippines
e-mail: edmarfranquera123@gmail.com

C. A. Beltran
e-mail: tolitsbeltran@yahoo.com

Ma. A. G. Beltran
e-mail: marizonbeltran@yahoo.com

R. T. B. Franquera
e-mail: edmarfranquera@yahoo.com

R. Sun and L. Fei (eds.), *Sustainable Development of Water and Environment*, Environmental Science and Engineering,
https://doi.org/10.1007/978-3-030-16729-5_2

1 Introduction

Water is life. All living organisms on earth need fresh water. The major user of freshwater in most countries is agriculture. The largest single user of freshwater in the world today which consumes an average of 70% globally is accounted in agriculture.[1] However, the availability of freshwater is already decreasing due to water pollution. Agriculture is considered to be a casualty of water pollution but it also causes and contributes to water pollution due to excess nutrients by too much application of fertilizers, excessive use of pesticides and other pollutants. Globally, agriculture is also considered to be the major cause of degradation of surface including groundwater resources as a result of erosion, excessive farming contaminating freshwater like wastewater coming from large poultries and piggeries, chemical run off and other indiscriminate human activities and improper agricultural management practices. Waste coming from swine is significant source of fecal pollution leading to water pollution by contaminating of ground and surface water from lagoon overflow and the use of lagoon surface water for irrigation. Thus, it is important to test a system or test a technology such as potential aquatic plants to decontaminate the wastewaters so that this will resolve the problem.

In the Philippines, agriculture wastewater is one of the major sources of water pollution which accounted 37%.[2] In addition, only 10% of wastewater is treated while 58% of groundwater is contaminated. Regions which had unsatisfactory ratings for their water quality criteria include National Capital Region (NCR), Southern Tagalog Region, Central Luzon (Region 3) and Central Visayas. Hence, there is a need to address the global implications of water quality and there is a need for wastewater treatments. In central Luzon, the agricultural land area is 653,607 km^2 and 9.1% contributed to the agricultural BOD generation, 9.0% industrial BOD generation and 9.9% domestic BOD generation leading to water quality degradation and contamination.[3]

Generally, the availability of clean freshwater is becoming a primary limitation to human activities expansion and also the scope or capacity of our agricultural lands to feed the tremendous population growth not only in the Philippines but globally. There are an estimated 2.2 million metric tons of organic water pollution that occur in the Philippines each year and the annual economic losses caused by water pollution are estimated at Php67 Billion which is equivalent to more or less US$1.3 billion.[4] Hence, this study aims to quantify the physical, chemical and microbiological water qualities of the different river waters in Tarlac, Philippines.

[1] www.fao.org. Last accessed 30 Nov 2017.

[2] www.greenpeace.org. Last accessed 30 Nov 2017.

[3] www.wipo.int/wipo_ip_mnl_15_t4. Last accessed 27 Nov 2017.

[4] www.wepa-db.net.philippines.overview. Last accessed 30 Nov 2017.

2 Methodology

2.1 Gathering/Collection of Data of Existing Irrigation Water Sources in Tarlac

The existing data on the type of irrigation systems and the irrigation sources were gathered. This was done in collaboration with National Irrigation Administration (NIA). The water qualities that were gathered were compared to the existing standards of the Department of Environment and Natural Resources (DENR).

2.2 Water Sample Collection

Representative water samples were collected in seven major rivers of Tarlac based from the data of the National Irrigation Administration (NIA) and the Department of Environment and Natural Resources and the collection was done from 9:00 AM in the morning until 4:00 PM in the afternoon. A total of six liters of water samples were collected in each sampling sites based from the recommendation of the Department of Science and Technology. The water sampling collection was done on the onset of 2018 dry and wet season productions of rice.

2.3 Water Quality Analysis

Collected water samples were analyzed for its physical, chemical and microbiological qualities (Total suspended solids, chemical oxygen demand, total coliform bacteria, *E. coli*, lead and mercury content). These parameters were analyzed using the standard methods in analysis of water samples. Portable instruments were used for the analysis of the following parameters such as dissolved oxygen (portable oxygen meter), pH (HM pH-200) total dissolved solids and electrical conductivity (HM COM-100). For the nitrate quantification a Horiba portable nitrate meter was used.

2.4 Analysis of Data

Laboratory results from the collected water samples were analyzed and compared with the Water Quality Guidelines and General Effluent Standards of 2016 based on the Department of Environment and Natural resources (DENR) Administrative Order No. 08 Series of 2016.

3 Results and Discussions

See Table 1.

3.1 Total Soluble Solids and Chemical Oxygen Demand

Table 2 presents the data of the different major rivers of Tarlac in terms of the total soluble solids and chemical oxygen demand. Results showed that the different river water has a varied total suspended solids and chemical oxygen demand. Higher TSS was found to be during wet season as compared during the dry season. This was also evident in terms of the chemical oxygen demand except for the two rivers, the Rio Chico and the Camiling river which exhibited a lower COD during the wet season with less than. For the TSS, based from the standard water qualifications, Tarlac and Concepcion rivers exceeded the numerical value which a body of water could be classified ranging only from 25 to 110 but for the two rivers it has both 169 mg/l total suspended solids during the wet season. Higher COD was found both in dry and wet seasons in Benig river with 27 and 22 mg/l respectively. Result of the COD laboratory test from the Benig river was also in consonance with the result of research conducted by Fernandez and David (2008) [5] which also shows high COD in Benig River. This implies that the higher COD in the sampling area, the higher level of water pollution. The wastewater discharge coming from the different industries within the area such as the presence of piggery farms could contribute to the higher COD of the water samples which maybe contributed to the deterioration of water quality within the sampling area (Al-Badaii et al. 2013).

3.2 Heavy Metals (Lead and Mercury)

The heavy metal concentrations (lead and mercury) in the different major rivers of Tarlac are presented in Table 3. All of the major rivers have a less than 0.05 mg/l lead and 0.0002 mg/l mercury based from the result of the laboratory analysis. Compared to the standards for the water quality the result both of the lead and mercury content of all the major rivers showed lesser than that of the standards. This implies that the rivers were not contaminated with heavy metals. This could be due to the non-presence of mining sites within the areas where the different rivers were located. Heavy metals were considered to be toxic and dangerous. The presence of higher concentrations of heavy metals in rivers as source of irrigation for the crops could lead also to the decline in production and these heavy metals could bio accumulate affecting also the humans whom will consume the crops irrigated with higher concentrations of heavy

[5] www.bgr.bund.de.Veranstaltungen. Last accessed 15 Dec 2017.

Table 1 Water quality guidelines (DENR AO 08 Series 2016)

Parameter	Water body qualifications								
	AA	A	B	C	D	SA	SB	SC	SD
Dissolved oxygen (mg/l)	5	5	5	5	2	6	6	5	2
Fecal coliform (MPN/100 ml)	<1.1	<1.1	100	200	400	<1.1	100	200	400
Nitrate (mg/l)	7	7	7	7	15	10	10	10	15
pH	6.5–8.5	6.5–8.5	6.5–8.5	6.5–9.0	6.5–9.0	7.0–8.5	7.0–8.5	6.5–8.5	6.5–9.0
TSS	25	50	65	80	110	25	50	80	110
Lead (mg/l)	0.01	0.01	0.01	0.05	0.1	0.01	0.01	0.05	0.01
Mercury (mg/l)	0.001	0.001	0.001	0.002	0.004	0.001	0.001	0.002	0.004

Table 2 Total soluble solids and chemical oxygen demand data of different major rivers of Tarlac province, Philippines during wet and dry season of 2018

River	Total suspended solids (mg/l)		Chemical oxygen demand (mg/l)	
	Dry season	Wet season	Dry season	Wet season
Benig	32	40	27	22
Tarlac	40	169	10	14
Bamban	58	32	11	15
Concepcion	52	169	21	19
Lapaz	223	91	11	28
Rio Chico	103	66	10	<10
Camiling	17	45	6.9	<10

Table 3 Heavy metals concentration of different major rivers of Tarlac province, Philippines during wet and dry season of 2018

River	Lead (mg/l)		Mercury (mg/l)	
	Dry season	Wet season	Dry season	Wet season
Benig	<0.05	<0.05	<0.0002	<0.0002
Tarlac	<0.05	<0.05	<0.0002	<0.0002
Bamban	<0.05	<0.05	<0.0002	<0.0002
Concepcion	<0.05	<0.05	<0.0002	<0.0002
Lapaz	<0.05	<0.05	<0.0002	<0.0002
Rio Chico	<0.05	<0.05	<0.0002	<0.0002
Camiling	<0.05	<0.05	<0.0002	<0.0002

metals. When crops were irrigated with water contaminated with heavy metals, the soils will also be polluted (Verma and Dwivedi 2013).

3.3 Dissolved Oxygen and pH

Table 4 presents the data on the dissolved oxygen and pH of the different major rivers of Tarlac province Philippines. Based from the result the highest dissolved oxygen was found to be within the Tarlac River both during the dry and wet season with 16.0 and 14.8 mg/l respectively.

The lowest dissolved oxygen was found in Concepcion River during the dry season (5.0 mg/l) and in Rio Chico River (4.8 mg/l) during the wet season. Comparing with the National standards from the DENR the major rivers of Tarlac surpasses the minimum standards of classification of water bodies with dissolved oxygen ranging from 2 to 6 mg/l. Low DO is also caused by fertilizer and manure runoff from streets, lawns and farms. The growth of too much algae which could be due to the overuse of fertilizers and the presence of fecal matters causes the speeding up of using the

Table 4 Dissolve oxygen and pH of different major rivers of Tarlac province, Philippines during wet and dry season of 2018

River	Dissolved oxygen (mg/l)		pH	
	Dry season	Wet season	Dry season	Wet season
Benig	5.3	5.4	8.0	8.26
Tarlac	16.0	14.8	8.1	8.29
Bamban	9.2	6.0	8.0	7.96
Concepcion	5.0	5.0	7.0	6.78
Lapaz	8.0	5.0	7.2	7.98
Rio Chico	7.9	4.8	7.3	7.96
Camiling	15.0	14.0	8.0	8.26

oxygen quickly resulting to a lower DO.[6] The dissolved oxygen which drops below 5.0 mg/l causes stress to many aquatic lives. However based from the results, all of the rivers surpass or equal to 5.0 mg/l except for the Rio Chico River during the wet season with 4.8 mg/l.[7] In terms of pH, the major rivers of Tarlac are within the minimum and maximum standard of pH range within the DENR standards. The pH ranges from 6.78 to 8.29 during the wet season and 7.0–8.1 during the dry season.

3.4 Total Dissolved Solids and Electrical Conductivity

Higher total dissolved solids were observed in the different rivers during the dry season which ranges from 300 to 560 mg/l as compared during the wet season which ranges from 169 to 540 mg/l respectively. Too high or too low concentrations of TDS may limit the growth and may lead to the death of many aquatic organisms.[8] The reduction of water clarity, which contributes to a decrease in photosynthesis and lead to an increase in water temperature, could be due to the high concentrations of TDS. The EC during the dry season ranges from 389 to 423 while during the wet season it ranges from 280 to 420 respectively (Table 5).

3.5 Nitrate

The nitrate concentrations of the different rivers in Tarlac shows to be within the range indicated in Table 1. During the dry season, the nitrate concentrations from

[6] http://www.ririvers.org/wsp/CLASS_3/DissolvedOxygen.htm. Last accessed 30 Nov 2017.

[7] http://www.mymobilebay.com/stationdata/whatisDO.htm. Last accessed 30 Nov 2017.

[8] http://www.ei.lehigh.edu/envirosci/watershed/wq/wqbackground/tdsbg.html. Last accessed 15 Dec 2017.

Table 5 Total dissolved solids and electrical conductivity of different major rivers of Tarlac province, Philippines during wet and dry season of 2018

River	Total dissolved solids (mg/l)		Electrical conductivity (μS)	
	Dry season	Wet season	Dry season	Wet season
Benig	323	218	400	323
Tarlac	308	169	420	416
Bamban	300	254	418	375
Concepcion	560	540	423	420
Lapaz	300	220	400	291
Rio Chico	305	250	412	281
Camiling	320	200	389	280

Table 6 Nitrate content of different major rivers of Tarlac province, Philippines during wet and dry season of 2018

River	Nitrate (mg/l)	
	Dry season	Wet season
Benig	14	59
Tarlac	10	48
Bamban	10	17
Concepcion	10	48
Lapaz	14	38
Rio Chico	10	45
Camiling	10	38

the different major rivers had a range of 10–14 mg/l. While during the dry season, it ranges from 17 to 59 mg/l with Benig River as the highest. The higher nutrient concentrations within the area could be due to the wastewater from the swine farm lagoons which may be discharged from the nearby farms within the area. Less than 5 mg/l N has little effect, even on nitrogen sensitive crops, but may stimulate nuisance growth of algae and aquatic plants in streams, lakes, canals and drainage ditches (Table 6).[9]

3.6 Fecal Coliform and E. coli

In terms of the microbiological parameters such as fecal coliforms and *E. coli*, the different river waters of Tarlac was higher than the standards particularly in Benig River with 11,000 MPN/100 ml and within the Concepcion river which exceeds the National standards for safe water with fecal coliform count of 140,000. Higher concentrations of *E. coli* were also noted in Benig and Concepcion River both with

[9] http://www.fao.org/docrep/003/T0234E/T0234E06.htm. Last accessed 15 Dec 2017.

Table 7 Fecal coliform and *E. coli* concentration of different major rivers of Tarlac province, Philippines during wet and dry season of 2018

River	Fecal coliform (MPN/100 ml)	*E. coli* (MPN/100 ml)
	Wet season	Wet season
Benig	11,000	1700
Tarlac	390	21
Bamban	270	17
Concepcion	140,000	1700
Lapaz	2600	170
Rio Chico	2800	330
Camiling	330	<1.8

1700 MPN/100 ml. The high concentrations within the said rivers could be due to the wastewater discharged from the nearby areas contributing to the higher Fecal coliform and *E. coli* in the said areas of concern. The higher concentrations as observed in the two rivers could have a potential to reduce the water quality thus reducing also the recreational value (Table 7).[10]

4 Conclusions

The water samples collected from major rivers of Tarlac revealed that there were variations in the results in terms of the different parameters used to quantify the concentrations of the physical, chemical and microbiological quality of the river waters for irrigation purposes. Based from the result, the different river waters were also in accordance with the National Standards set by the Department of Environment and Natural Resources (DENR).

Acknowledgements The authors would like to acknowledge the Department of Agriculture Regional Field Office (DA-RFO 3) for funding this research and sincere acknowledgement was also to the management of the Tarlac Agricultural University.

References

Al-Badaii F, Shuhaimi-Othman M, Gasim MB (2013) Water quality assessment of the Semenyih River, Selangor, Malaysia. J Chem Article ID 871056, 10 p. https://doi.org/10.1155/2013/871056

Fernandez XD, David ME (2008) Water quality assessment of the benig river: implication to environmental management accessed through https://www.bgr.bund.de/EN/Themen/Wasser/Veranstaltungen/symp_sanitat-gwprotect/poster_fernandez_pdf.pdf?__blob=publicationFile&v=2 December 2017

[10] https://pubs.usgs.gov/wri/wri004139/pdf/wrir00-4139.pdf. Last accessed 15 Dec 2017.

Verma R, Dwivedi P (2013) Heavy metal water pollution—a case study. Recent Res Sci Technol 5(5):98–99. ISSN: 2076-5061. Available Online http://recent-science.com/

Study on the Inactivation of *E. coli* in Water by UV-LED

Zhilin Ran, Zhe Wang, Meng Yao and Shaofeng Li

Abstract In this study, the effects of UV-LED on the inactivation of *Escherichia coli* in water were studied. The effects of turbidity, humic acid and inorganic cation on this process were examined and a preliminary analysis of the mechanism by which UV-LED inactivates *E. coli* was performed. Our results showed that turbidity and HA had no significant effects on *E. coli* inactivation under a UV radiation dose of 24.48 mJ/cm^2. Cu^{2+} promoted UV-LED-mediated *Escherichia coli* inactivation while Ca^{2+} inhibited the process. Zn^{2+}, Cl^-, $CO_3{}^{2-}$ and $SO_4{}^{2-}$ had no significant effects on the inactivation of *E. coli* by UV-LED. Nucleic acids released in the system indicated that the bactericidal effect of UV-LED was primarily mediated through damage to the nucleic acids.

Keywords UV-LED · *Escherichia coli* · Influencing factors · Inactivation mechanism

1 Introduction

Water is the source of life. It is one of the indispensable resources on which human survival and development depend. Freshwater that can be directly used by humans only accounts for 0.25% of the global water resource (Ke 2003). The rapid growth in population, industry and agriculture has led to an accelerated increase in the global use

Z. Ran (✉) · M. Yao
Institute of Innovational Education Research, School of Transportation and Environment, Shenzhen Institute of Information Technology, Shenzhen 518172, China
e-mail: zhilinran1980@gmail.com

Z. Wang
College of Environmental and Municipal Engineering, Shenyang Jianzhu University, Shenyang 110168, China

S. Li
Department of Building and Environmental Engineering, Shenzhen Polytechnic Institute, Shenzhen 518055, China

R. Sun and L. Fei (eds.), *Sustainable Development of Water and Environment*, Environmental Science and Engineering,
https://doi.org/10.1007/978-3-030-16729-5_3

of freshwater, and the disparity between supply and demand of freshwater resources is an increasing concern in the world (Hao 2000). Meanwhile, the standards for drinking water quality, sewage treatment and recycled water are also becoming more stringent (Liu 2004). Currently used methods for water disinfection include chlorination, ozone disinfection and heavy metal ion disinfection (Lanzhi et al. 2012). However, these disinfection methods are more or less prone to problems in terms of safety and cost. UV-LED is a new type of UV light source that has bactericidal properties. It does not require additional chemical agents, does not produce disinfection by-products and is environmentally friendly and energy efficient. Therefore, UV-LED has broad application prospects in the field of water treatment (Taniyasu et al. 2006; Wurtele et al. 2011; Vilhunen et al. 2009; Mori et al. 2007; Oguma et al. 2013).

In this study, we examined the effects of UV-LED on the inactivation of *Escherichia coli* in water using a customized UV-LED reactor, assessed the impact of turbidity, humic acid (HA) concentration and anion and cation levels on this inactivation process, and preliminarily elucidated the mechanism of inactivation. We found that turbidity and HA had no significant effects on *E. coli* inactivation under a UV radiation dose of 24.48 mJ/cm^2. Cu^{2+} promoted UV-LED-mediated *E. coli* inactivation while Ca^{2+} inhibited the process. Zn^{2+}, Cl^-, $CO_3{}^{2-}$ and $SO_4{}^{2-}$ had no significant effects on the inactivation of *E. coli* by UV-LED. Nucleic acids released in the system indicated that the bactericidal effect of UV-LED is primarily mediated through damages to the nucleic acids of *E. coli*. Our study holds great value and significance towards the search for highly efficient, environmentally friendly and low-risk disinfection techniques, and provides insights into the rapid development of UV-LED disinfection.

2 Materials and Methods

2.1 Experimental Apparatus and Methods

The experimental apparatus (Fig. 1) is comprised of two UVC-LED arrays placed within a quartz tube. Each array is composed of 40 UVC-LED beads that are evenly mounted (7 mm apart) on a circuit board. The peak emission wavelength is 275 nm, and each UVC-LED array is operated under 40 mA constant forward current, 6.9 V forward voltage and 2.8 mW output power. The inner chamber volume of the reactor is 500 mL, and the exterior of the inner tube is covered with aluminum foil to prevent interference from other light sources. The outer chamber of the reactor is connected to the constant cryostat to ensure that the entire reactor system is maintained at a certain constant temperature. For the disinfection experiment, bacterial suspension was added into the inner chamber and irradiated using the immersed UVC-LED. The bacterial suspension was also aerated during the UVC-LED irradiation to ensure that every part of the system was exposed to a consistent UV radiation intensity. After turning on the power, the bacterial suspension was irradiated by UVC-LED for

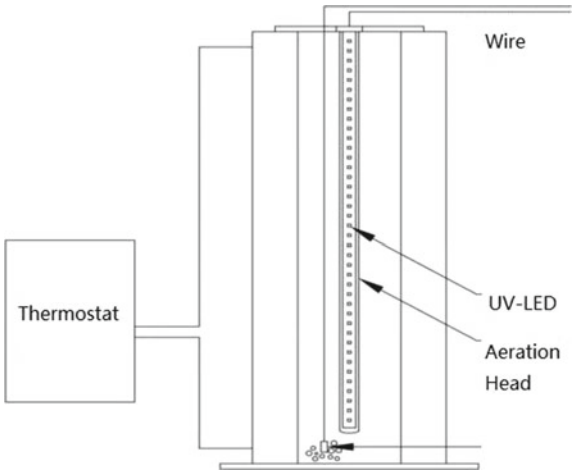

Fig. 1 Experiment apparatus of UVC-LED

10 min. Samples were collected at 0.5, 1, 2, 3, 4, 5 and 10 min post-irradiation, and the number of *E. coli* in the water samples was enumerated.

2.2 Materials

Escherichia coli ATCC8099 was used as the experimental strain in this study. Yeast extract powder, tryptone, sodium chloride, bacteriological agar powder, concentrated hydrochloric acid, sodium hydroxide, kaolinite, humic acid, sodium dihydrogen phosphate, anhydrous ethanol, disodium hydrogen phosphate, and deionized water, 0.1 mol/L sodium thiosulfate standard solution, 25% glutaraldehyde, anhydrous calcium chloride anhydrous sodium carbonate, isoamyl acetate, sodium sulfate.

2.3 Analytical Methods

2.3.1 Evaluation of *E. coli* Inactivation

The bactericidal effects of UV-LED on *E. coli* were assessed by the log inactivation value. The formula for log inactivation value is as follows (1):

$$\text{Log inactivation value} = -\log(N/N_0) \tag{1}$$

where: N is the *E. coli* count (CFU/L; determined by plate count method) in the water sample irradiated by UV-LED;

N_0 is the *E. coli* count (CFU/L; determined by plate count method) in the original bacterial suspension.

Plate counting method: Bacterial suspension (100 μL) was mixed with 900 μL of sterile 4% saline and serially diluted 10-fold. Autoclaved LB agar (unsolidified) was poured into sterile petri dishes and cooled. Bacterial suspension (100 μL) from each dilution was spread plated onto agar using a triangular cell spreader, and the plates were inverted and incubated at 37 °C. After 24 h of incubation, the number of colonies were counted (plates with 30–300 CFUs were selected). All procedures were performed under sterile conditions, and each dilution was plated in triplicates (Liu et al. 2017). In order to reduce experimental error, each experiment was repeated 3 times and the mean and standard deviation were calculated.

2.3.2 Detection of Nucleic Acid in the System

Although the nucleic acid concentration in the system cannot accurately reflect the nucleic acid level in *E. coli*, it can indicate the release of nucleic acid from *E. coli*. The nucleic acid backbone is primarily composed of purines and pyrimidines. These nucleobases contain conjugated double bonds that have a maximum absorbance at 260 nm, which renders a positive correlation between optical density (OD) at 260 nm and nucleic acid concentration (Zhang et al. 2011). Changes in OD260nm of the solution in the system were determined using Nanodrop 2000.

3 Results and Discussion

3.1 Effect of Turbidity on Escherichia coli *Inactivation by UV-LED*

The effect of different turbidities on *E. coli* inactivation at 25 ± 0.1 °C and pH 7 ± 0.1 was determined. Bacterial suspensions with different turbidities were prepared by the addition of kaolinite (Fig. 2). It was previously shown that turbidity has a substantial impact on traditional UV disinfection. Particles in the water can scatter UV energy and reduce the level of UV radiation on microorganisms. Therefore, the disinfection effect of traditional UV method is decreased as turbidity increases. Our results showed that turbidity had no significant effect on *E. coli* inactivation by UVC-LED. The log *E. coli* inactivation value remained relatively high (4.35, 4.34, 4.47, 4.63, 4.71 and 4.75) after 5 min of UV irradiation of bacterial suspension with various turbidities (1, 5, 10, 20, 30 and 60NTU, respectively).

Compared with traditional UV mercury lamp, disinfection by UV-LED is not significantly affected by turbidity, and this may be attributed to the fact that UV-LED emits UV through light-emitting diodes in which the energy is highly concentrated

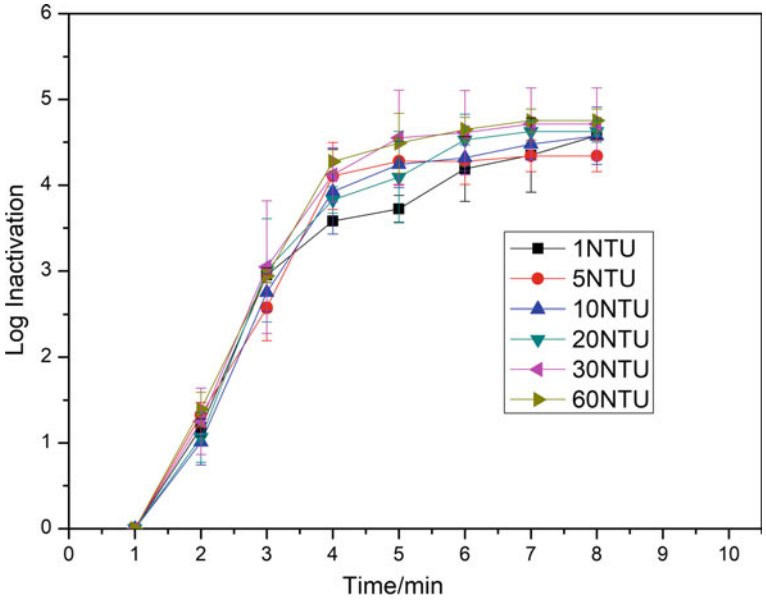

Fig. 2 Effect of turbidity on *E. coli* inactivation by UV-LED

in a narrow waveband near the desired wavelength. In contrast, traditional mercury lamp involves full spectrum radiation and the energy that has bactericidal effects comprises only a portion of the total energy. The ultraviolet wavelengths emitted by UVC-LED are highly concentrated near 275 nm and hence are higher in energy. Therefore, high turbidity (60NTU) has no effect on the highly concentrated energy emitted by UVC-LED when it is at a radiation intensity of 0.102 mW/cm^2. This feature increased the range and value of UV-LED application in water treatment.

3.2 Effect of Humic Acid (HA) on E. coli *Inactivation Rate*

HA is an organic macromolecule that is widely found in nature. It is generated primarily from the decomposition and transformation of animal and plant remains by microorganisms, as well as a series of chemical reactions. The level of organic substances in water may affect the effect of disinfection. Here, we selected HA as a representative organic acid in water and examined the effect of different HA concentrations on *E. coli* inactivation by UV-LED at 25 ± 0.1 °C, pH 7 ± 0.1 and 1NTU (Fig. 3).

The log of inactivated *E. coli* was the highest when HA was present at 0.5 mg/L. In addition, the log of inactivated *E. coli* was not significantly changed as HA concentration increased (1, 2, 5, 10 and 20 mg/L). The rate of *E. coli* inactivation was the

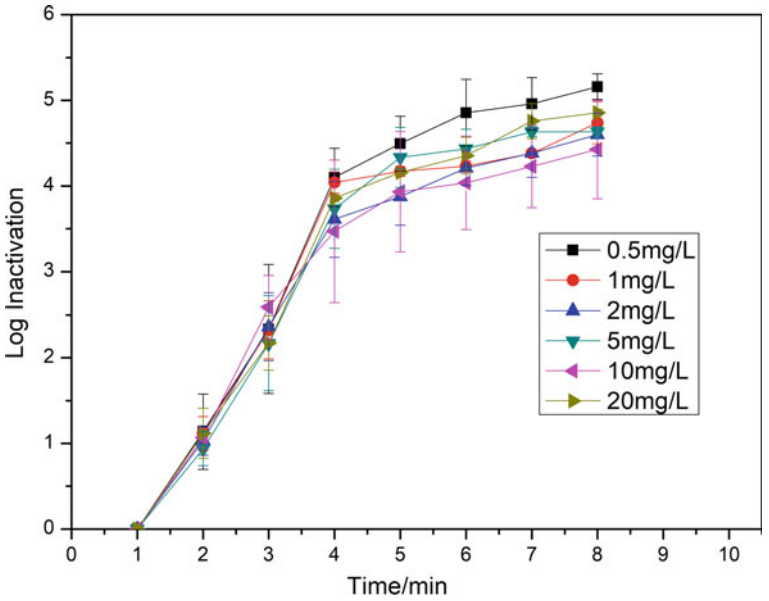

Fig. 3 Effect of humic acid on inactivation of *E. coli*

fastest within 0–2 min of irradiation. At 2 min of irradiation, the log of inactivated *E. coli* was 4.1, 4.04, 3.61, 3.73, 3.47 and 3.86 in the presence of 0.5, 1, 2, 5, 10 and 20 mg/L HA, respectively. At 5 min of irradiation, the log of inactivated *E. coli* increased to 4.96, 4.38, 4.38, 4.63, 4.23 and 4.76 at 0.5, 1, 2, 5, 10 and 20 mg/L of HA, respectively. Therefore, UV-LED has an optimal disinfection effect when the concentration of HA in water is 0.5 mg/L.

3.3 Effect of Common Inorganic Cations on the Inactivation Rate of E. coli *in Water*

Zn^{2+}, Ca^{2+} and Cu^{2+} are inorganic cations that are commonly found in natural water sources. We examined the effect of these three cations (0.5 mg/L) on *E. coli* inactivation rate (Fig. 4).

As shown in Fig. 4, after 5 min of irradiation, the log of inactivated *E. coli* was the highest (5.09) in the presence of Cu^{2+}, lowest (4.67) in the presence of Ca^{2+} and unaffected in the presence of Zn^{2+}. After 10 min of irradiation, the log of inactivated *E. coli* barely increased in the presence of the inorganic cations. In summary, *E. coli* inactivation by UV-LED is promoted by Cu^{2+} (0.5 mg/L), inhibited by Ca^{2+} (0.5 mg/L) and not affected by Zn^{2+} (0.5 mg/L).

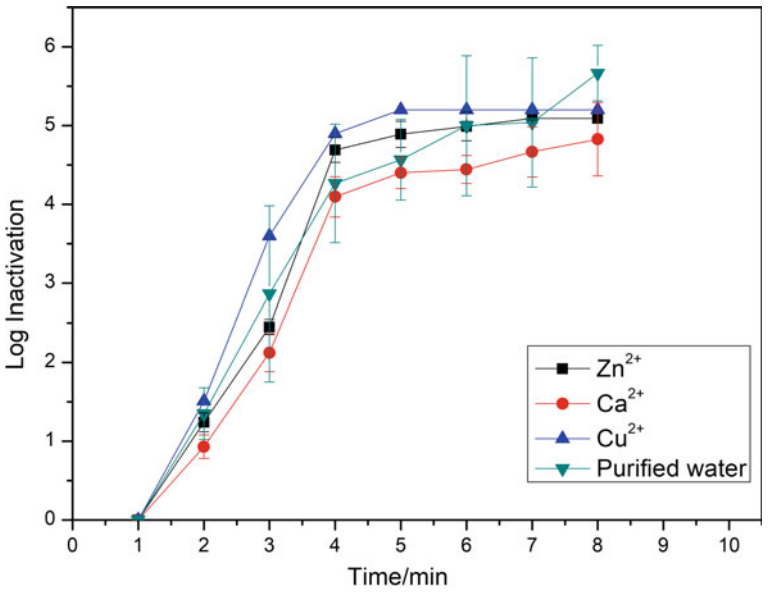

Fig. 4 Effect of common inorganic cations on inactivation of *E. coli*

3.4 Effect of Common Inorganic Anions on the Inactivation Rate of E. coli *in Water*

Cl^-, CO_3^{2-} and SO_4^{2-} are inorganic anions that are commonly found in natural water sources. We examined the effect of these three anions (50 mg/L) on *E. coli* inactivation by UV-LED at 25 ± 0.1 °C, pH 7 ± 0.1 and 1NTU (Fig. 5). After 10 min of irradiation, the log of inactivated *E. coli* was 5.43, 5.48, 5.03 and 5.67 in the presence of purified water, for Cl^-, CO_3^{2-} and SO_4^{2-}, respectively. In summary, Cl^-, CO_3^{2-} and SO_4^{2-} (50 mg/L) had no significant effects on *E. coli* inactivation by UV-LED.

3.5 Detection of Nucleic Acid Release in the Solution

The nucleic acid backbone is primarily composed of purines and pyrimidines. These nucleobases contain conjugated double bonds that have a maximum absorbance at 260 nm. We measured the change in absorbance at 260 nm of the solution using Nanodrop 2000. *E. coli* suspension was irradiated by UVC-LED (275 nm) at 25 ± 0.1 °C, pH 7 ± 0.1 and 1NTU for 0–10 min, and 1 mL of sample was collected at various time points. The samples were centrifuged and the absorbance of the supernatants was measured at 260 nm (Fig. 6).

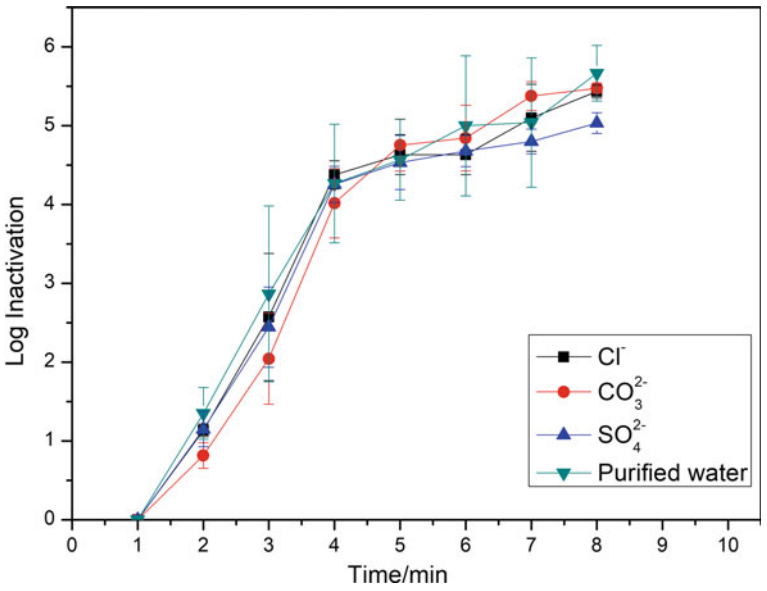

Fig. 5 Effect of common inorganic anions on inactivation of *E. coli*

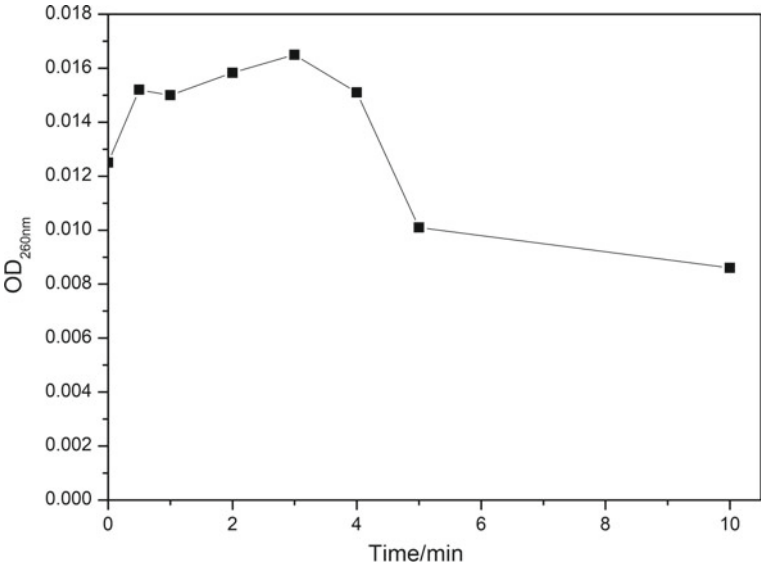

Fig. 6 Absorbance changes of the solution at 260 nm under UVC-LED

The changes in absorbance (260 nm) can indirectly reflect the release of nucleic acids from *E. coli*. As shown in Fig. 6, OD260nm increased from 0.0125 to 0.0152 after 0.5 min of UVC-LED irradiation, and gradually increased from 0.015 to 0.0165 after 0.5–3 min of irradiation. However, OD260nm rapidly decreased to 0.0101 after 5 min of irradiation. This suggests that UVC-LED irradiation caused certain damage to the cell wall and cell membrane of *E. coli* that resulted in changes in cell membrane permeability and hence the release of nucleic acids. Within the first 3 min of irradiation, UV-LED-mediated damage of the double-stranded DNA resulted in the exposure of nucleotides and hence the slight increase in OD260nm. As the duration of UV irradiation increased, adjacent pyrimidines crosslinked into pyrimidine dimers and caused DNA damage leading to completely altered genetic sequences. As the number of pyrimidine dimers increased, the OD260nm of the solution decreased. This is the major form of damage that UV inflicts upon microorganisms.

4 Conclusion

In this study, the inactivation of *E. coli* in water by UVC-LED was examined and how this process is affected by turbidity, humic acid and common ions, and the release of nucleic acid into the solution was studied. We concluded that:

(1) Turbidity and HA concentration have no significant effects on *E. coli* inactivation by UVC-LED at 0.102 mw/cm^2 and pH7 for 5 min;
(2) After 0–5 min of UVC-LED irradiation, *E. coli* inactivation was enhanced in the presence of Cu^{2+}, inhibited in the presence of Ca^{2+}, and unaffected in the presence of Zn^{2+}, Cl^-, $CO_3{}^{2-}$ and $SO_4{}^{2-}$;
(3) UVC-LED can cause certain damage to the *E. coli* cell wall and cell membrane soon after irradiation begins, leading to changes in cell membrane permeability and release of nucleic acids.

Acknowledgements This research was jointly funded by Shenzhen Science and Technology Innovation Committee, China (JCYJ20160226092135176), the project of Shenzhen Institute Information Technology (PT201703), and Innovation and Enhancing College Project of Guangdong Province, China (2017GKTSCX065).

References

Hao Y (2000) World water symposium was held in The Hague, The Netherlands. World Agriculture 255(7):48 (in chinese)
Ke S (2003) World water resources. Global Technol Econ Outlook 213(9):60 (in chinese)
Liu W (2004) Forecast on advanced water disinfection. Water Wastewater Eng 30(1):2–5 (in chinese)
Liu Y, Jing E, Hu X et al (2017) Comparison of enzyme substrate method and plate counting method for determination of total number of colonies in water. China Water Wastewater 33(2):111–114 (in chinese)

Mori M, Hamamoto A, Takahashi A et al (2007) Development of a new water sterilization device with a 365 nm UV-LED. Med Biol Eng Comput 45(12):1237–1241

Oguma K, Kita R, Sakai H et al (2013) Application of UV light emitting diodes to batch and flow-through water disinfection systems. Desalination 328:24–30

Taniyasu Y, Kasu M, Makimoto T (2006) Aluminum nitride deep-ultraviolet light-emitting diodes. NTT Technol Rev 4(12):54–58

Vilhunen S, Sarkka H, Sillanpaa M (2009) Ultraviolet light-emitting diodes in water disinfection. Environ Sci Pollut Res 16(4):439–442

Wurtele MA, Kolbe T, Lipsz M et al (2011) Application of GaN-based ultraviolet-C light emitting diodes-UV LEDs-for water disinfection. Water Res 45(3):1481–1489

Xiao L, Gao J, Wang D (2012) Comparison of several common water treatment and disinfection processes. Wastewater Eng 38:96–98 (in chinese)

Zhang A, Wang R, Xie H et al (2011) Summarization on the methodology study of protein detection. Lett Biotechnol 22(1):130–134 (in chinese)

Radionuclides' Activity Analysis in the Environmental Samples

Eva Singovszka, Adriana Estokova and Magdalena Balintova

Abstract Sediment quality monitoring are amongst the highest priorities of environmental protection policy. Their main objective is to control and minimise the incidence of pollutant—oriented problems, and to provide for water of appropriate quality to serve various purposes such as drinking water supply, irrigation water etc. The present work aimed to investigate the pollutants levels of some heavy metals (Fe, Mn, Al, Cu, Zn, As, Cd, Pb) in the sediments relate to acid mine drainage (AMD) producing from abandoned sulphide mine in Smolnik in eastern of Slovakia. Studies on environmental radioactivity in this area is scarce. Therefore, a baseline study of natural (238U, 226Ra, 40K) radionuclides was carried out on Smolnik Creek surface sediments and on their radiological significance. Grab surface sediment samples were collected from 5 stations and their radioactivity concentrations measured by gamma spectrometry. The estimated radionuclide activity index, total absorbed dose rate in air (D), radium equivalent activity (Raeq), external hazard index (Hex), annual effective dose equivalent (AEDE) and indicated no significant radiological risks from the sediment radioactivity concentrations.

Keywords Acid mine drainage · Heavy metals · Natural radioactivity · Radiological parameters

1 Introduction

Radionuclides such as ^{226}Ra, ^{228}Th and ^{40}K are widely distributed in the environment as a result of their natural occurrence in the Earth's crust or the atmosphere. The human population worldwide receives an average annual radiation dose of 2.4 mSv/y, about 80% of which comes from naturally-occurring radionuclides, the remaining part is largely due to artificial sources of which fallout radionuclides account for only

E. Singovszka (✉) · A. Estokova · M. Balintova
Technical University of Kosice, Faculty of Civil Engineering, Institute of Environmental Engineering, Vysokoskolska 4, 042 00 Kosice, Slovakia
e-mail: eva.singovszka@tuke.sk

R. Sun and L. Fei (eds.), *Sustainable Development of Water and Environment*, Environmental Science and Engineering,
https://doi.org/10.1007/978-3-030-16729-5_4

0.4% (UNSCEAR 2000). Sediment contamination by radionuclides of the ^{238}U and ^{232}Th decay-series and ^{40}K is of particular interest from radiological point of view, as they can form the basis of radiological assessments for the human population. The Environmental Risk from Ionising Contaminants Assessment and Management tool (ERICA) developed by the European Commission provides an integrated approach to the assessment and management of environmental risks from ionising radiation (Beresford et al. 2007) and can be applied to assess the potential ecological impact of radionuclide-contaminated environments.

The activity concentrations of various radionuclides in natural resources play an essential role as regards the public and environmental health. The naturally occurring radioisotopes ^{40}K-as well as ^{238}U-series and ^{232}Th-series are the main sources of gamma radiation in rocks, soils and water. Human body could be subjected to such radiation sources, either externally or internally (through inhalation and/or ingestion ways). During the last decades, there has been an increasing interest in the study of radioactivity in environmental samples such as bottom sediment (Ahmed et al. 2006; Harb et al. 2008; El Mamoney and Khater 2004; Abdel-Razek et al. 2008; EL Saharty and Dar 2008; El-Taher and Madkour 2011; Orgun et al. 2007). In the Slovak Republic, overflowed mine Smolnik produces acid mine drainage with high metal concentrations and low value of the pH (about 3–4) as a result of chemical oxidation of sulphides and other chemical processes. This was the reason for starting a systematic monitoring of geochemical development (Singovszka et al. 2016). The most critical values of heavy metals were observed also in the abandoned deposit Smolnik (Balintova and Petrilakova 2011; Singovszka et al. 2017). Another significant issue could be connected with the possible radiological risk of sediment. The aim of this study was to assess the mass activities of natural radionuclides in bottom sediments from Smolnik creek in the East of Slovakia and their radiological significance to provide a prognosis in terms of environmental risk.

2 Materials and Methods

The samples of the sediment were collected from the Smolnik creek from five sampling stations (S1–S5) creek in November 2018. The sampling sites were located at 48° south latitude and 20° east longitude (Fig. 1). The two sampling sites were situated in the upper part of the Smolnik creek not contaminated by acid mine water from the Pech shaft and another two sampling localities were located under the shaft. The outflow of AMD from Pech shaft (Smolnik mine) is numbered as Site 3 (Balintova and Petrilakova 2011). The sediment samples are marked as S1, S2, S3, S4 and S5 according to the location of sampling.

The samples of sediment were air-dried and ground by using a planetary mill to a fraction of 0.063 mm. TFirst af all the samples were characterized by its chemical composition using of X-ray fluorescence (XRF) method (SPECTRO iQ II, Ametek, Germany). The measured concentration of heavy metals in sediment were compared

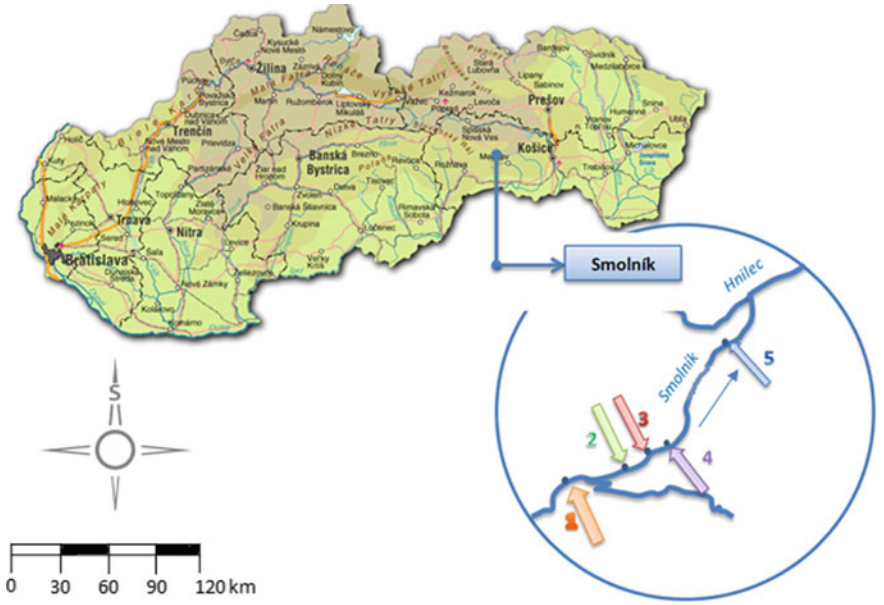

Fig. 1 Location of five sediment samples from Smolnik Creek

with limit value by Slovak legislation (Act. No. 188/2003 Coll of Laws on the application of treated sludge and bottom sediments to fields) (188/2003).

Afterwards, the powdered samples were under radiological investigation. The samples were weighted and stored in the Marinelli containers until radioactive equilibrium was stated.

The mass activities of radionuclides (^{226}Ra, ^{232}Th and ^{40}K) in sediment were measured by gamma ray spectrometry. Measurements were carried out using an EMS-1A SH (Empos, Prague, Czech Republic) detection system equipped with a NaI/Tl scintillation detection probe and a MC4K multichannel analyzer with optimized resolution of 818 V, 4.096 channel and with 9 cm of lead shielding and internal lining of 2 mm tinned copper.

The specific activity concentrations of ^{226}Ra, ^{232}Th and ^{40}K were determined in Bq.kg^{-1} using the count spectra. The ^{40}K radionuclide was measured directly through its gamma ray energy peak at 1461 keV, while activities of ^{226}Ra and ^{232}Th were calculated based on the mean value of their respective decay products. Activity of ^{226}Ra was measured using the 351.9 keV gamma rays from ^{214}Pb and the activity of ^{232}Th was measured using the 238.6 keV gamma rays of ^{212}Pb. The same counting time of 86,400 s (24 h) was used for all measured samples.

2.1 Radiological Risk Assessment

Characterisation of associated potential radiological risk is essential to protection for human and appropriate handling of radioactive—contaminated sediments, Radionuclide activity index, radium equivalent activity (Raeq), total absorbed dose rate in air (D), external hazard index (Hex), annual effective dose rate (AEDR) and gamma radiation representative level index (RLI) are six most often used radiological hazard indices for radiological assessment.

UNSCEAR 2000 defined index of radionuclide activity. The gamma index of materials recommend limit values depending on the dose criterion ($I\gamma \leq 1$) (UNSCEAR 2000). Radionuclides' activity index, Iγ is exúressed according to the following Eq. (1):

$$I\gamma = (A_{Ra}/300) + (A_{Th}/200) + (A_K/3000) \tag{1}$$

According to Sugandhi et al. (2014), Botwe et al. (2017) the Ra_{eq} is weight sum of activity concentration of measured radionuclides in a study sediment, which allows comparison with their individual ^{226}Ra, ^{232}Th and ^{40}K activity concentration. Radium equivalent activity is expressed by the following Eq. (2).

$$Ra_{eq} = A_{Ra} + 1.43A_{Th} + 0.077A_K \text{ (Bq/kg)} \tag{2}$$

The total absorbed dose rate in air (D) expresses the rate of exposure to gamma radiation in air at 1 m above the ground due to measured activities in sediment samples (Sugandhi et al. 2014). The D rates were calculated using the Eq. (3).

$$D = 0.462A_{Ra} + 0.604A_{Th} + 0.0417A_K \text{ (nGy/h)} \tag{3}$$

Beretka and Mathew (1995) defined index that represent External hazard index, which is obtained from Rae_q expression, that its allowed maximum value corresponds to the upper limit of Ra_{eq} (370 Bq/kg). The limit value for H_{ex} must not exceed 1.0 for human health (UNSCEAR 2000; Beretka and Mathew 1995). The H_{ex} can be defined as:

$$H_{ex} = (A_{Ra}/370) + (A_{Th}/259) + (A_K/4810) \tag{4}$$

Annual effective dose rate as a result from total absorbed dose values was calculated using the next equal (4) (Ravisankar et al. 2012; Kurnaz et al. 2007):

$$AEDR = D \times 1.23 \times 10^{-3} \text{ (mSv/y)} \tag{5}$$

Association with different concentration of some specific radionuclide can be estimated by level of gamma radioactivity known as the representative level index (RLI)

Gamma radiation representative level index is given as:

$$RLI = (A_{Ra}/150) + (A_{Th}/100) + (A_K/1500) \quad (6)$$

where A_{Ra} is average activity concentration of ^{236}Ra in Bq/kg, A_{Th} is average activity concentration of ^{232}Th in Bq/kg and A_K is average activity concentration of ^{40}K in Bq/kg.

3 Result and Discussion

3.1 Chemical Analysis

The results of the chemical analysis of sediment samples, originated from the Smolnik creek are presented in Table 1.

Based on the analyses of sediments quality in the Smolnik creek oriented towards the influence of heavy metals concentration; and on the comparison of limit values, it can be stated that the sediment does not show a significant risk with respect to the heavy metal content except copper and arsenic. The concentration of popper was higher than the limit value in all sediment samples while arsenic in one sample (S3) of the Site 3 (1406 mg/kg). This points to the extra high content of arsenic in AMD since Site S3 was located at the outflow of the contaminated water from the mine.

Table 1 Chemical analysis of sediments regarding the metals content from the Smolnik creek

Metals	Sediment samples					Limits
(mg/kg)	S1	S2	S3	S4	S5	(mg/kg)
Fe	29510	27910	302100	85540	64840	–
Mn	568.5	426.4	383	558	755	–
Al	62,450	54,520	8267	5,7460	7,4320	–
Cu	**113.0**	**147.4**	**360**	**249.5**	**338.1**	100
Zn	121.0	135.2	1.0	94.6	215.8	2500
As	2.1	6.1	**1406**	18.7	39.2	20
Cd	5.1	3.2	5.1	5.1	1.7	10
Pb	5.9	22.8	222	4.5	20.3	750

Table 2 Natural activity of radionuclides and gamma indexes of the samples $I\gamma$

	Sample	^{226}Ra	^{232}Th	^{40}K	$I\gamma$
		Bq/kg			
Sediment sample sites	S1	11.11	76.96	1148.75	0.80
	S2	9.18	81.84	1082.38	0.79
	S3	4.30	53.97	350.39	0.40
	S4	10.01	64.16	846.57	0.66
	S5	7.52	69.29	946.77	0.68

Table 3 Radiological parameters in bottom sediment samples from Smolnik creek

	Ra_{eq}	D	H_{ex}	AEDR	RLI
	Bq/kg	nGy/h	–	mSv/y	–
S1	201.58	99.86	0.57	0.12	1.61
S2	201.98	99.13	0.57	0.12	1.60
S3	106.02	49.31	0.29	0.06	0.80
S4	168.17	81.95	0.47	0.10	1.32
S5	172.88	85.09	0.48	0.10	1.37

3.2 Radiological Risk Assessment

3.2.1 Concentrations of Radionuclides

The activity concentration of ^{226}Ra, ^{232}Th and ^{40}K in the bottom sediment are shown in Table 2.

The natural activity concentration of radionuclide ^{40}K is relatively higher than of radionuclides ^{226}Ra and ^{232}Th, ranging from 350.39 to 1148.75 Bq/kg. The activities range for ^{226}Ra and ^{232}Th are 4.30–11.11 and 53.96–81.84 Bq/kg, respectively. The comparison of the measured radionuclides in our study with the worldwide average values (35 Bq/kg for ^{226}Ra, 30 Bq/kg for ^{232}Th and 400 Bq/kg for ^{40}K) show that radionuclides ^{232}Th and ^{40}K exceed multiply worldwide average values (UNSCEAR 2000) measured in sediments.

3.2.2 Assessment of the Radiological Hazard

The results of six radiological hazard indexes are given in Table 3. The radium equivalent activity Ra_{eq} was calculating according Eq (2). The maximum admissible value of Ra_{eq} is 370 Bq/kg (Beretka and Mathew 1995). As it can be seen in Table 3, the Ra_{eq} values for the bottom sediments rangeg from 106.02 to 201.98 Bq/kg. Any values of Ra_{eq} did not exceed the allowed value.

The absorbed gamma dose rates D ranged from 49,31 to 99,86 nGy/h. In this study, estimated mean value of absorbed gamma dose rate.

The range of annual effective dose rate AEDR is between 0.06 and 0.12 mSv/y and mean value is 0.1 mSv/y. According (UNSCEAR 1993) the average annual indoor effective dose from natural radionuclides in normal background areas is 0.46 mSv/y. The calculated mean value (0.1 mSv/y) from five evaluated sediment samples is lower than average value. The values for external hazard index are between 0.29 and 0.57 (Table 3). The recommended values of the Hex should be <1. It is observed in Table 3 that the values of H_{ex} is below the criterion value (<1). The RLI values for the evaluated sediment samples varies from 0.80 to 1.61. The limit values of RLI is ≤ 1 (Mahur et al. 2008). Except one location (S3) all sediment sample exceed recommend value.

4 Conclusion

The radioactivity levels of ^{226}Ra, ^{232}Th and ^{40}K in bottom sediment from Smolnik creek in Slovakia have not been studied before. The measured activity concentrations of the radionuclides were the basis for the calculation of the main radiological hazard indicators to determine a possible risk effect from natural radionuclides in sediments. The result indicated that values of all radiological hazard parameters were under the world average value reported in (UNSCEAR 2000), expect for RLI for sediment sample site S1, S2, S4, S5.

Assessment of radioactivity in the environment is useful for the protection of human health and environment from dangerous ionizing radiation. Consequently the assessed radiological parameter in this study can be used as a basis for next research.

Acknowledgements This work has been supported by the Slovak Grant Agency for Science (Grant No. 1/0648/17).

References

Abdel-Razek YA, Bakhit AF, Nada AA (2008) Measurements of the natural radioactivity along wadi nugrus, Egypt. In: IX radiation physics and protection conference, Nasr city—Cairo, Egypt, pp 225–231

Ahmed NK, Abbady A, El Arabi AM, Mitchel R (2006) Comparative study of natural radioactivity of some selected rocks from Egypt and Germany. Indian J Pure Appl Phys 44:209–215

Balintova M, Petrilakova A (2011) Study of pH influence on selective precipitation of heavy metals from acid mine drainage. Chem Eng Trans 25:345–350. https://doi.org/10.3303/CET1125058

Beresford N, Brown J, Copplestone D, Garnier-Laplace J, Howard B, Larsson C-M (2007) D-ERICA: an integrated approach to the assessment and management of environmental risk from ionising radiation, description of purpose, methodology and application, p 82

Beretka J, Mathew PJ (1995) Natural radioactivity of Australian building materials, industrial wastes and byproducts. Health Phys 48:87–95

Botwe B, Schirone A, Delbono I, Barsanti M, Delfanti R, Kelderma P, Nyarko E, Lens PNL (2017) Radioactivity concentrations and their radiological significance in sediments of the Tema Harbour (Greater Accra, Ghana). J Radiat Res Appl Sci 10(1):63–71

El Mamoney MH, Khater AEM (2004) Environmental characterization and radio-ecological impacts of non-nuclear industries on the Red Sea coast. J Environ Radioact 73:151–168

EL Saharty AA, Dar MA (2008) The concentration levels of some isotopic radionuclides in the coastal sediments of the Red Sea. Egypt Isot Radiat Resid 42(1):11–27

El-Taher A, Madkour A (2011) Distribution and environmental impacts of metals and natural radionuclides in marine sediments in-front of different wadies mouth along the Egyptian red sea coast. Appl Radiat Isot 69:550–558

Harb S, El-Kamel AH, Abd El-Mageed AI, Abbady A, Rashed W (2008) Concentration of U-238, U-235, Ra-226, Th-232 AND K-40 for some granite samples in Eastern Desert of Egypt. In: Proceedings of the 3rd environmental physics conference, Aswan, Egypt, pp 19–23 (2008)

Kurnaz A, Küçükömeroğlu B, Keser R, Okumusoglu N, Korkmaz F, Karahan G (2007) Determination of radioactivity levels and hazards of soil and sediment samples in Fırtına Valley (Rize, Turkey). Appl Radiat Isot 65(11):1281–1289

Mahur AK, Rajesh Kumar RG, Sonkawade D, Sengupta RP (2008) Measurement of natural radioactivity and radon exhalation rate from rock samples of Jaduguda uranium mines and its radiological implications. Nucl Instrum Methods Phys Res Sect B: Beam Interact Mater At 266:1591–1597

Orgun Y, Altinsoy N, Sahin SY, Gungor Y, Gultekin AH, Karaham G (2007) Natural and anthropogenic radionuclide in rocks and beach sands from Ezine region, Western Anatolia Turkey. Appl Radiat Isot 65:739–747

Ravisankar R, Vanasundari K, Chandrasekaran A, Rajalakshmi A, Suganya M, Vijayagopal P, Meenakshisundram V (2012) Measurement of natural radioactivity in building materials of Namakkal, Tamilnadu, India using gamma-ray spectrometry. Appl Radioact Isot 70:699–704

Singovszka E, Balintova M, Holub M (2016) Heavy metal contamination and its indexing approach for sediment in Smolnik creek (Slovakia). Clean Technol Environ Police 18(1):305–313

Singovszka E, Balintova M, Demcak S, Pavlikova P (2017) Metal pollution indices of bottom sediment and surface water affected by acid mine drainage. Metals 7(8):1–11

Slovak Act. No. 188/2003 Coll of laws on the application of treated sludge and bottom sediments to fields

Sugandhi S, Joshi VM, Ravi P (2014) Studies on natural and anthropogenic radionuclides in sediment and biota of Mumbai Harbour Bay. J Radioanal Nucl Chem 300(1):67–70

United Nations Scientific Committee on the Effects of Atomic (UNSCEAR) (2000) Sources and effects of ionizing radiation: sources, vol 1. United Nation Publications, New York

United Nations Scientific Committee on the Effects of Atomic Radiation (UNSCEAR) (1993) Sources and effects of ionizing radiation united nations, New York

Analysis of Shanghai Urban Expansion Based on Multi-temporal Remote Sensing Images

Yi Lin, Yuan Hu and Jie Yu

Abstract Being different from the traditional analysis of urban expansion in Shanghai from the perspective of humanities or urban geography, this study applies the Remote Sensing (RS) and Geographical Information System (GIS) spatial information technologies to analyze the spatio-temporal characteristics and evolution of urban land expansion in Shanghai's urbanization process. It provides a basis for further research on the mechanism of urbanization process. In this study, we processed and analyzed the multi-temporal remote sensing images (Landsat series) in Shanghai from 1995 to 2016. A multidimensional feature space was constructed. Then the image classification was carried out by the support vector machine (SVM). On the basis of classification results, the central city zone was extracted by method of regional connectivity. After analyzing the change of area, center of gravity, location and spatial distribution of the central city zone, the spatial layout and trend of urban expansion are obtained. Finally, the driving force of urban expansion in Shanghai is analyzed. The analysis results accurately reflect the process of Shanghai's urban expansion.

Keywords Urban expansion · Remote sensing · Spatial analysis · Driving force

1 Introduction

The development of spatial information technologies such as RS and GIS provides favorable technical support for the study of urban expansion. Kantakumar et al. (2016) applied Landsat images to study land cover changes in Indian cities and analyzed the patterns and processes of urban development. Zhan Xin et al. 2017) applied GIS and RS to analyze the spatio-temporal characteristics, the morphological evolution of Xiamen's urban expansion, and the coordination measure of economic development. Based on the previous researches, it can be seen that the dynamic monitoring of urban

Y. Lin · Y. Hu · J. Yu (✉)
Tongji University, Shanghai 200092, China
e-mail: 2011_jieyu@tongji.edu.cn

R. Sun and L. Fei (eds.), *Sustainable Development of Water and Environment*, Environmental Science and Engineering,
https://doi.org/10.1007/978-3-030-16729-5_5

expansion and the analysis of the driving force are benefit to grasp the law of urban expansion. On the other hand, it can also reflect the comprehensive development of the city at the present stage, which is conducive to the protection of limited arable land resources and ecological environment. This provides macroscopical and reliable management information and scientific decision-making basis for the government.

In the past 20 years, Shanghai has become the most dramatic urbanization area in China. The researches on the urbanization of Shanghai were mainly focused on analyzing the spatial structure and function of Shanghai from the perspective of humanity or urban geography. But there were too few studies on the spatio-temporal characteristics of urban land expansion in the process of urbanization and its evolution. Thus, this study applies Landsat satellite images from 1995 to 2016 to extract the central urban boundary with a machine-learning algorithm (SVM) (Huang et al. 2002). Additionally, overlapping analysis was generated as well. This study provides a basis for further research on the mechanism of urbanization.

2 The Study Area

The research area of this paper is Shanghai with 6,340 km^2 (excluding Chongming Island, Changxing Island and Hengsha Island). Its location is unique, ranging from 120°51′E to 122°12′E and 30°40′N to 31°53′N. As a municipality directly under the central government of China, Shanghai has seized the historic opportunity of reform and development and become one of the first batch of open coastal cities (Shanghai Statistics Bureau 2016). It is one of the most populous cities in the world with the largest urban area as well. In the rapid development of the economy in recent years, activities such as social economy and humanities construction have made its land use structure and industrial structure have undergone earth-shaking changes. With the contradiction between human and land becoming increasingly acute, how to coordinate the fierce contradiction between human and land and promote the construction of a benign ecological environment in Shanghai is a problem that needs to be solved urgently.

3 Data Source and Pre-processing

3.1 Classification of Remote Sensing Images

Considering the suitability, spatial resolution, spectral resolution, and seasonality of cloudless spatial coverage, the research data consists of the Landsat4-5TM, Landsat7 ETM, and Landsat8 OLI data from 1995 to 2016. Most of the data were in the period from June to August. Due to the cloud of remote sensing data in Shanghai during

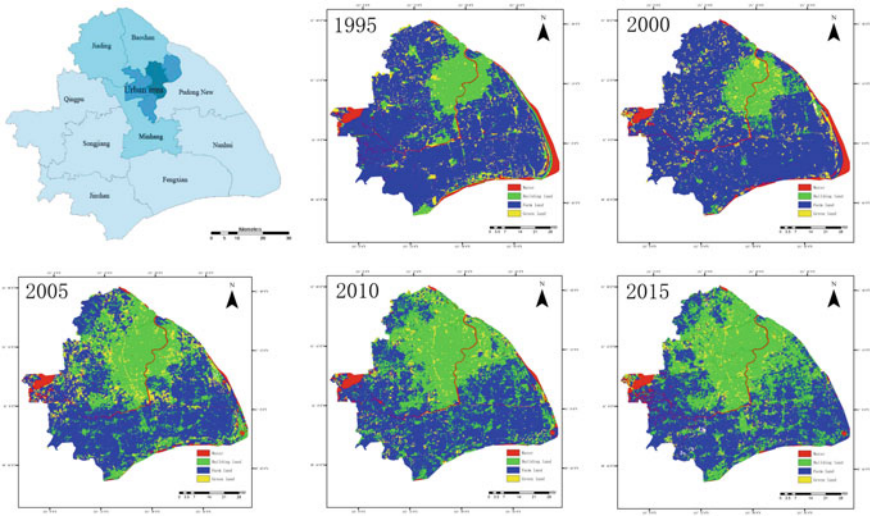

Fig. 1 SVM classification map

2011 was too large to not be suitable for classification research, the data of 2011 was not selected. Then the data of 20 remote sensing images were preprocessed.

Based on the pre-processed remote sensing data, the improved normalized water body index (MNDWI) (Han-qiu 2005), soil conditioning index (SAVI) (Huete 1988), and normalized building index (NDBI) (Chen and Chen 2006) were calculated to represent water body, vegetation and building land in the remote sensing image, respectively. A six dimensional feature space including SWIR, NIR, RED, NDBI, MNDWI and SAVI was constructed in this study. Then the machine learning method (SVM) as used to classify the images into four categories: water body, built-up area, vegetation and farmland. By evaluating the classification accuracy, the accuracy of all classification images is all greater than 90% and the Kappa coefficient (Thompson and Walter 1988) is all greater than 0.85, as shown in Fig. 1, meeting the requirements of expansion analysis. The classified remote sensing image is used as the basic data of boundary extraction for subsequent experiments.

3.2 Boundary Extraction of Central City Zone

At present, the main methods of extracting boundary could be divided into two classes: artificial extraction and edge detection, but these two extraction methods have lower efficiency. Generally speaking, the surface of the central city zone is cement surface, and its spectral characteristics are the same. Considering that the central city zone maintains continuity in space, it is a combination type and large-scale target. Buildings, streets and squares, industrial areas, etc., as well as smaller areas of

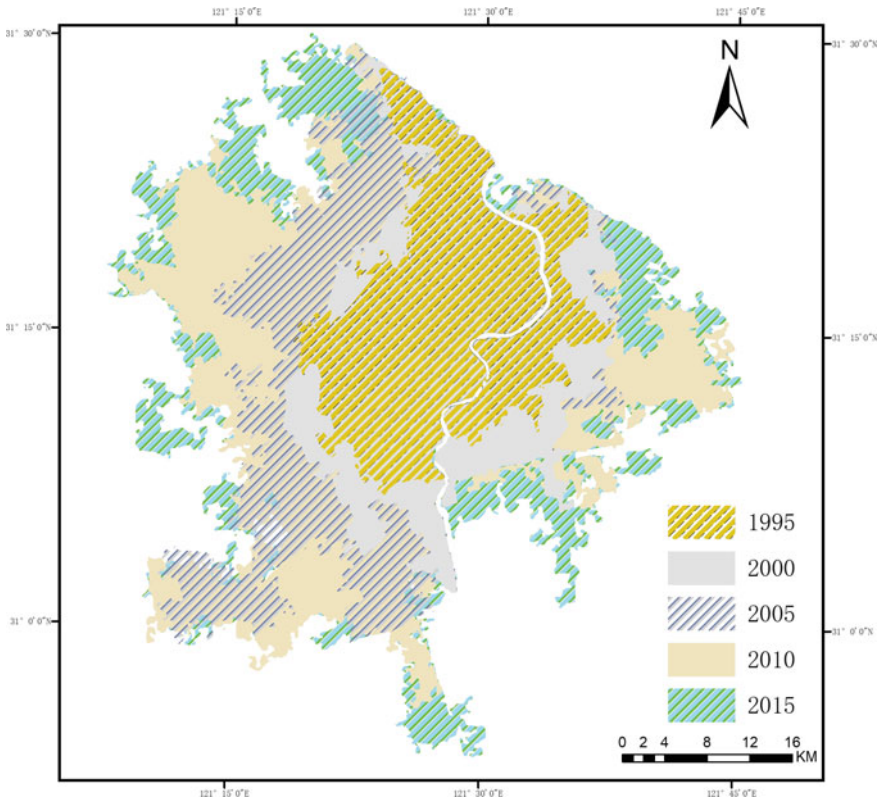

Fig. 2 Superimposed map of Shanghai central city zone

non-urban land (such as water bodies, etc.) in the space are regarded as a whole central city zone for extraction. Therefore, this study uses a regional connectivity method to directly extract central city zone. The boundary of the central city zone is finally obtained, as shown in Fig. 2.

4 Spatial Analysis of Central City Zone

The spatial expansion is analyzed with the boundary of the central city zone of Shanghai extracted from the classified images. In the time interval of the study, the area, gravity position and spatial distribution of the central urban area were all changed. The layout and trend of urban expansion were obtained through data analysis.

4.1 Spatial Area Change Analysis

According to the boundary of the central city zone extracted, the corresponding area of the central city zone of each year center can be obtained statistically, and the two indicators of urban space expansion rate and expansion intensity are calculated for each year.

As shown Fig. 3, the central city zone of Shanghai developed rapidly from 1995 to 2016, with the area increasing year by year. The central city zone of Shanghai increased 1174.3736 km^2 during the past 21 years. In 2016, the area expanded by 2.78 times compared with 1995, with an average annual expansion of 56 km^2. In 2004, 2005, 2013 and 2014, the expansion broke through 100 km^2, showing the characteristics of high-speed expansion.

In the study for the past 21 years, the expansion intensity of the central city zone of Shanghai changed dramatically, and the rapid growth of the central city zone was mainly distributed in Baoshan District, Minhang District, Jiading District and Pudong new District. According to the method of equidistant classification, the expansion intensity index of the central city zone is divided into four levels: low (>1–4%), medium (>4–7%), rapid (>7–10%) and high speed extension (>10–13%).The analysis of every five years for a phase shows that the expansion area of the central city zone increased year by year, and the expansion intensity increased firstly and then decreased. From 1995 to 2000, the central city zone showed a slow expansion trend, with 3.91% expansion intensity. From 2000 to 2005, the expansion intensity was 7%, which was twice as the previous stage, implying it entered the rapid expansion stage. From 2010 to 2015, due to the constraint of Shanghai's own development load and the government's Macro-control on land use, the expansion intensity sank to 4.3% and entered to the stage of medium speed expansion. The expansion intensity shows that Shanghai's central city zone has expanded into S-type development since 1995, with slow development in the early stage, rapid development in the middle stage, and the development speed has slowed down in the later period. It can be seen that the government's Macro-control of land use has been effective.

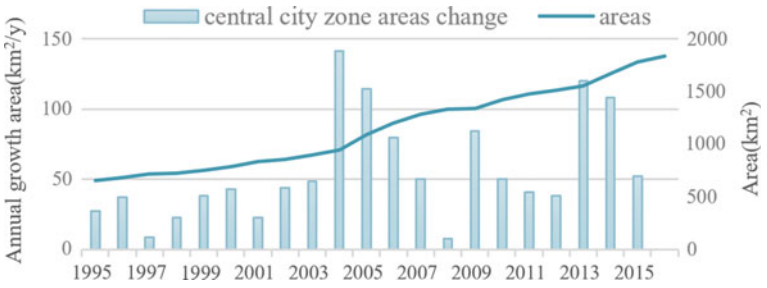

Fig. 3 Area and spatial expansion rate of Shanghai central city zone

Table 1 Compactness and fractal dimension table

Year	1995	2000	2005	2010	2015
Compactness	0.3203	0.2952	0.2529	0.2396	0.1927
Fractal dimension	1.3135	1.3296	1.3586	1.3585	1.4074

4.2 Analysis of Spatial Morphological Changes

In terms of the analysis of urban spatial morphological changes, two indices of spatial compactness C (Zhang et al. 2013) and fractal dimension D (Tan et al. 2009) of spatial shape were selected to analyze the spatial morphological changes in central Shanghai. The two indices of 1995, 2000, 2005, 2010 and 2015 were calculated respectively to analyze urban spatial distribution and structural changes.

The spatial compactness index is one of the important indicators that measure the change of urban spatial shape, whose value range is 0–1. The higher the compactness is, the more compact the urban space will be. On the contrary, the lower the compactness of the space, the greater dispersion of the city (Zhang et al. 2013).

The central boundary of Shanghai has an irregular shape and is complex and nonlinear, with fractal features. The fractal dimension of urban spatial shape is a characteristic index describing the fractal structure, which can describe the complexity of the boundary shape of the central city zone of Shanghai, and quantitatively reflect the change of shape and the degree of human interference. The larger the value is, the more complex the shape is. The urban space compactness and fractal dimension of spatial shape from 1995 to 2015 can be obtained. As shown in Table 1.

From Table 1, it can be seen that the compactness index of the central city zone decreased from 0.3203 to 0.1927 during the period from 1995 to 2016, showing a downward trend overall. The fractal dimensions of the two stages increased gradually from 1995 to 2005 and 2010 to 2015, increasing by 0.0451 and 0.0488 respectively, indicating that the central city zone in these two periods mainly expanded outward and to a large extent. The fractal dimension decreased slightly from 2005 to 2010, which was consistent with the change law of compactness. During this period, influenced by the Shanghai World Expo in 2010, Shanghai carried out a two-pronged urban construction of the old city reconstruction and the new city construction. A large number of Expo pavilions were built, which promoted the improvement of urban infrastructure, transportation facilities, public facilities, and promoted the renewal of the city (Such as Hongqiao Airport, Shanghai-Nanjing Intercity High-speed Railway, Shanghai-Changzhou Expressway, etc.) (Xu 2010). The central city zone at this stage is mainly based on internal structure adjustment.

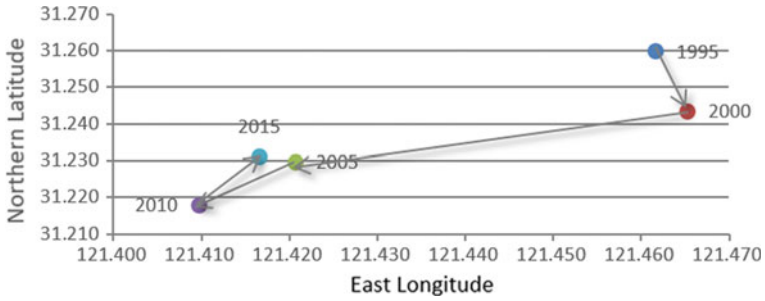

Fig. 4 Center of gravity moving process of Shanghai central city zone from 1995 to 2016

4.3 Center of Gravity Index Analysis

The urban center of gravity index is the balance point of urban uniform distribution, which is an important index to describe urban spatial distribution. By tracking the center movement of gravity coordinates in urban space during different periods, we can understand the trajectory of urban expansion and predict the spatial development trend of the city, and Fig. 4 is obtained.

After the establishment of first subway rail in 1993, totally 14 routs have been built till 2016 in Shanghai. The subway traffic network forms a mixture of grid, ring and radial. The improvement of road capacity has driven the change of land use types around and accelerated the urbanization development around the subway. As can be seen in Fig. 4, in 1990, the development strategy of Pudong drove the expansion of the Puxi central city. It not only changed the pattern of Shanghai's development, but also strengthened the east-west urban expansion. On the whole, after 2000, the central city zone entered the stage of rapid expansion, the construction land area rose sharply, and the center of gravity shifted significantly. The expansion of the central city zone of Shanghai mainly focused on the west and southwest directions (Minhang and Songjiang). The east and northeast region (Pudong New District) is limited by the coastal boundaries and has a small expansion intensity. The development of the central city zone in the southeast direction (Pudong New District) is mainly to expand along the Huangpu River.

5 Driving Force Analysis

Based on the statistical data of the central urban areas and the relevant socio-economic statistical data (Shanghai Statistics Bureau 2016) of Shanghai from 1995 to 2015, the statistical software SPSS was used for correlation analysis and principal component analysis. Then the driving factors of the change of central urban area were further analyzed and discussed. Through the analysis, the expansion of the central

city zone of Shanghai is the result of the mutual drive of population, economy, policy, environmental protection and energy, as described below.

(1) Population driven. Since the uncertainty of floating population is strong. The permanent population becomes one of the most dynamic driving forces. The growth of population accelerated the encroachment of urban construction land on farmland. Increased investment in fixed assets projects, real estate development and urban infrastructure has accelerated the reconstruction, construction and expansion of built-up areas. It has led to an increase not only in the scale of urban and rural residential construction land, but also in urbanization levels. In addition, the public infrastructure is improved as well.
(2) Economic production driven. Shanghai takes the tertiary industry as the leading industry, and vigorously develops the secondary industry. The proportion of the primary industry decreases year by year. By 2015, the primary industry in Shanghai accounted for 0.4% of the GDP, while the secondary and tertiary industry occupied 31.8 and 67.8%, respectively. Although the farmland decreases, with the development of science and technology, the single yield of grain increased, alleviating the contradiction between population and food demand. The substantial increase in GDP and household consumption have prompted an increase in various types of non-agricultural land.
(3) Policy driven. By taking the lead in integrating with the international market, the first largest Waigaoqiao free trade zone in China and the only Jinqiao export processing zone named after export processing were established. The government adopted policies to attract foreign direct investment, and also attracted talents and labor force to gather in Shanghai, which drives the economic development of Shanghai and promotes the increase of construction land.
(4) Environmentally friendly energy driven. With the acceleration of industrialization, Shanghai has become the largest comprehensive industrial city in China, which has increased employment opportunities and attracted more talents to Shanghai. In 1995, the investment in environmental protection was 4.649 billion yuan. However it reached 70.83 billion yuan in 2015, an increase of 14.15 times. Sustainable and large-scale investment in environmental protection can gradually improve the quality of life, improve the happiness and satisfaction of urban residents and attract more talents to Shanghai.

6 Conclusion

Due to the differences in politics, economy and population, the mechanism of urbanization expansion is complicated. The analysis of the evolution law of urban space expansion from a long time series is of great significance for optimizing urban spatial structure and promoting urban development. Through the remote sensing imagery from 1995 to 2016, this study quickly and effectively monitors the expansion process

of Shanghai's central city zone in the past 21 years, and systematically analyzes the spatio-temporal changes of its expansion.

There remained some deficiencies in the research process of this study: (1) in the process of extracting the boundary of downtown, the setting of the morphological processing threshold is determined subjectively. Thus, how to improve the algorithm to achieve full objective automatic extraction still needs further research. (2) The study of Shanghai's regional urbanization expansion is only a macroscopic view of the Shanghai area and surrounding areas, which are regarded as a single expansion model. But in fact, Shanghai has gradually developed into a multi-core city with multiple regions and simultaneous development. Therefore, it is further possible to study the expansion of various districts in Shanghai by taking each district as a unit, combined with the economic and population factors of each district to refine the expansion region.

Acknowledgements This study has been supported by the National Science Foundation of China (41771449).

References

Chen Z, Chen J (2006) Urban land image recognition analysis and mapping based on NDBI index method. Geo-inf Sci 8(2):137–140

Han-qiu X (2005) Research on water information extraction by using improved normalized difference water body index (MNDWI). J Remote Sens 9(5):590–595

Huang C, Davis LS, Townshend J (2002) An assessment of support vector machines for land cover classification. Int J Remote Sens 23(4):725–749

Huete AR (1988) A soil-adjusted vegetation index(SAVI). Remote Sens Environ 25(3):295

Kantakumar LN, Kumar S, Schneider K (2016) Spatiotemporal urban expansion in Pune metropolis India using remote sensing. Habitat Int 51:11–22

Li A, Liu S, Lü A (2011) Research on expansion of built-up area in Zhengzhou during 1999 2007 based on multi-original remote sensing images. J Zhengzhou University 32(2):125–128

Tan W, Liu B, zhang Z et al (2009) Remote sensing monitoring and analysis of the built-up area of Kunming city in the past three decades. Geo-Inf Sci 11(01):117–124

Thompson WD, Walter SD (1988) A reappraisal of the kappa coefficient. J Clin Epidemiol 41(10):949

Xu L (2010) Analysis of the impact of Shanghai world expo 2010 on Shanghai urban economy. Market Weekly Heoretical Res (5):28–30

Shanghai statistics bureau. Shanghai statistical book [Z]. Statistical Press, Beijing, China

Zhang Z, Jia D et al (2013) Quantitative analysis of urban spatial morphology and characteristics—a case study of the main urban area of chongqing. Geo-Inf Sci 15(2):297–306

Zhan Xin, Pan Wen-bin, et al (2017) Research of urban expansion measures based on multi-source remote sensing data-a case study of Xiamen City. J Fuzhou Univ (Natural Science Edition) 45:355–361

The Innovation Model Research of Roof Garden of Green Building

Xiuyun Fan

Abstract The green and low carbon is a development trend of the city in the future. One of the ways to realize the green low carbon is the construction of roof garden. The roof garden plays an important role in improving the local microclimate to realize the sustainable development, such as improving the effect of urban heat island, beautifying the environment, reducing pollution, etc. The paper concluded the rule of the roof garden of green building in making low carbon city and beautifying the environment, and put forward a kind of innovative design pattern of roof garden scenery that can meet the needs of people.

Keywords Roof garden · Low-carbon city · Green building · Landscape pattern heat island effect

The world today has entered a low-carbon era, and low-carbon development has become a core issue in the development of the world's cities. With the rapid development of the economy and the accelerating urbanization process, urban environmental problems have become more and more serious, and various environmental problems such as noise pollution, PM2.5, "heat island effect" and garbage siege are directly threatens the survival and development of mankind.

In order to improve the living environment, improve the quality of life, and create a green ecological space, people are constantly exploring the problem of insufficient greening area per capita through greening methods. Roof gardens can play an active role in improving such problems. This paper is a discussion of the new model of landscape design for roof gardens in low-carbon cities.

X. Fan (✉)
Huali College Guangdong University of Technology, Zengcheng District, Guangzhou City 511325, Guangdong Province, China
e-mail: 249106637@qq.com

R. Sun and L. Fei (eds.), *Sustainable Development of Water and Environment*, Environmental Science and Engineering,
https://doi.org/10.1007/978-3-030-16729-5_6

1 Related Notion

1.1 Roof Garden

It is a form of gardening that is not directly connected to the ground. It refers to the landscaping activities in the open areas of all buildings, rooftops, terraces, etc. (Lv 2013).

1.2 Urban Heat Island Effect

It refers to the phenomenon that the temperature in the city is higher than the temperature in the surrounding suburbs. The high temperature zone formed over the urban area is like an island relative to the suburbs, so it is called the urban heat island effect (Han 2014).

2 The Function and Significance of the Roof Garden

Beautify the environment and improve urban green coverage. An important means of reducing the "heat island" effect of the city. Solve the problem of garbage siege from the source. Give a miracle effect to governing PM2.5 (Zhang 2014). Save electrical energy. Have the effect of cultivating sentiment, relieving mental stress, and rehabilitation, medical care and pension. Improve urban waterlogging. Protect the building and extend its service life (Ren 2010).

3 The Design Factor Difference Between Roof Garden and Ground Garden

The roof garden belongs to the "fifth facade" of the building and therefore has a unique difference from the general garden. The area is not large, limited by the spatial topography, so the vertical change space is not large. The planting soil is artificially synthesized, the soil layer is relatively thin, not connected to the earth, and the water source is limited. The construction of landscape elements such as landscape architecture, small and brief buildings, plants, and road pavements is limited by factors such as roof bearing capacity. Located at the top of the high-rise building, there are fewer people, the view is wider, and the environment is quieter. It is not affected by the surrounding environment, and it does not need to consider factors such as the influence of underground pipelines.

4 Plant Selection Requirements for Roof Gardens

(1) Choose low-quality shrubs, potted flowers or ground cover plants that are not afraid of cold and high temperature.
(2) Select a shallow-rooted plant that is heliophilous and resistant to infertile.
(3) In order to achieve the purpose of improving green coverage, sterilizing and anti-pollution, and purifying the air, try to use the evergreen plants or the colored aromatic flowers with obvious seasonal colors.
(4) The principle of adapting to the appropriate land. Choose slow-growing plants which easy to transplant, survival rate is high, resistance to trim, easy to be managed and anti-pollution. This can save costs and stabilize the effect of the scene.

5 Roof Greening Survey

Questionnaire survey: The targets of this investigation are the residents and units of roof garden in Guangzhou and the region of Foshan, applied with the method of integrating bearer on site and telephone interview, 4 kinds of questionnaires are designed for the residents and units of roofless garden and residents and units of roof garden respectively, each kind of questionnaire is released for 50 pcs with 200 pcs in total. 200 pcs are recycled, the recycling rate is 100%.

Interview survey: Through the methods of face to face deep interview and telephone interview, the interview is conducted for the land in Guangzhou and Foshan City where Country Garden is located and the surrounding areas, 23 units including the holiday village of Country Garden, school of Country Garden at Beijiao Town, headquarter of Country Garden, public health bureau of Yuexiu District and South China Agricultural University etc. and 27 units and neighborhood residents of Zengcheng Region in Guangzhou are interviewed, The investigation is conducted for the advantages and disadvantages, types, preference and the essentials for Technology development of roof garden. 48 pieces of feedback information are received in total. The feedback rate is 96%.

Data statistics and analysis: EXCEL2003 software was used for statistical analysis.

5.1 Investigation Display I (See Fig. 1)

There are four types in general for the green method of roof garden in these regions: Ground cover, potted flower combination, canopy frame and garden style. Each type has its advantages and shortages. The residents hold different opinions on the roof garden of each type, their preferences are different. But generally the ratio of residents who like roof garden of garden type is low which is 10%. The investigation shows

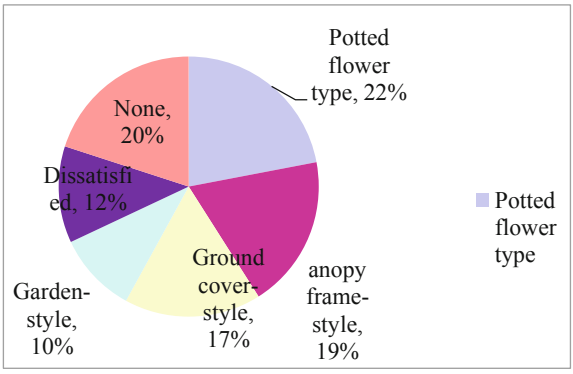

Fig. 1 Statistics of type and preference degree of Table 1 statistics of type and preference degree of roof garden

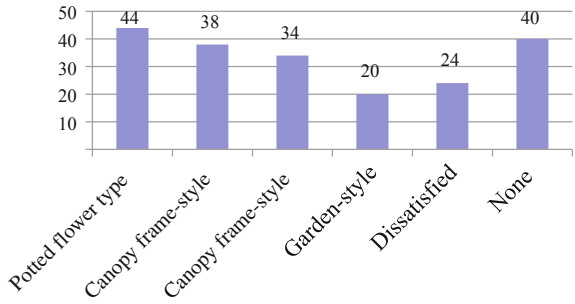

Fig. 2 Survey of type and preference degree of roof garden

that the advantages and disadvantages of the roof gardens of the major types are as follows (Sun 2017) (Fig. 2):

Garden type: The plant varieties are abundant, well-proportioned and easy to assort or arrange in pairs or groups, the stratification of landscape is beautiful. However, the weight of landscape materials is larger and cost is high.

Potted flower: The body of the plants applied is small, the weight is light, Most of them are short plants, the landscape level is unclear, potted flowers need fertilization, watering and more frequent hoeing.

Ground cover: Light and simple, light load, quick setting speed, easy management, low cost, small number of plant varieties, small plants and high safety performance. Fewer plant varieties and poor ornamental performance affect people's leisure and entertainment activities.

Scaffolding: Liana has special aesthetic feeling and landscape effect. However, scaffolding stability needs input, can not be built too high.

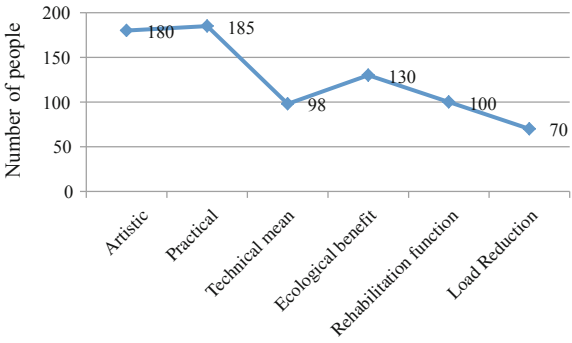

Fig. 3 Improvement element of existing roof garden

5.2 Investigation Display I (See Fig. 3)

65% of people think it is necessary to further improve the roof garden design pattern, and are not satisfied with the existing roof greening. The main factors that need to be improved include: beauty, utility, technical means, ecological benefits, rehabilitation function, reducing load and so on. People pay more and more attention to the problem of keeping in good health. People hope that the plants used can recover and recuperate the body, reduce the load and hope that a new ecological design mode with low input and high output will emerge at the same time. They demand that four seasons be green and three seasons have flowers (Li and Li 2012).

5.3 The Third Aspect of the Survey

80% questioned the safety of rooftop gardens, mainly water leakage, mosquitoes, lodging, funding, conservation and some other questions. For example, where plants exist, there must be some mosquitoes, and even in the south there will be poisonous snakes that like to inhabit aromatherapy plants. This may bring inconvenience to the safety and life of the occupants. When the storm comes, some plants are prone to lodging, some will uproot, damage the roof planting layer and cause roof leakage. 44% expressed concern about the source of funding needed for regular pruning. 23% of the people think that the roof garden is a common ownership, only the top floor residents will be very good to benefit, easy to enjoy, not related to their own, reported have no attitude.

6 An Approach to a Recreational Ecological Comprehensive Roof Garden Model

6.1 Measurement of Temperature and Humidity in Different Types of Roof Garden Buildings (Wang 2011)

Testing site: The testing site is located in the rooftop garden of a few buildings not far from the city area. Four types of roof gardens were selected, including garden type, scaffolding type, ground quilt type, potted flower type, and bare roof as control (see Table 1).

Testing tools: Use DWS508C type thermometer, hygrometer (the precision of humidity measurement is 0.1% RH and the precision of temperature measurement is 0.10 °C) and illumination meter ZDS-10.

Inspection method: A total of 7 times, only once a day, temperature and relative humidity were measured at the same height (distance from ground) at the center of different types of roof garden.

Data statistics and analysis: EXCEL2003 software was used for statistical analysis. Figure 4 is the result.

Results and analysis: The temperature of bare roof is the highest, reaching 37 °C, the lowest temperature of garden is only 29 °C, the cooling effect is obvious, the relative humidity of bare roof is also the lowest, only 26%, and the relative humidity of ground cover is the highest. The temperature of these kinds of roof garden is as

Table 1 Basic situation of roof garden Laboratory Building in Zengcheng District, Guangzhou

Address	Name	Nature of building	Type of roof garden	Growth situation	Management situation
No. 23, Qianjin Road, Zengcheng	Phoenix Mountains Park	Unit	Canopy frame-style	Good	Specialist management
No. 6, Guangming West Road, Zengcheng	Family dormitory building	Private household	Potted flower-style	General	Private management
Zengcheng tap water company	Family dormitory building	Private household	Garden-style	Good	Private management
No. 23, Xicheng Road, Zengcheng	Building 3, Taifu Plaza	Unit	Ground cover-style	Good	Specialist management
No. 21, Qianjin Road, Zengcheng	Changshou Temple	Unit	Exposed roof		

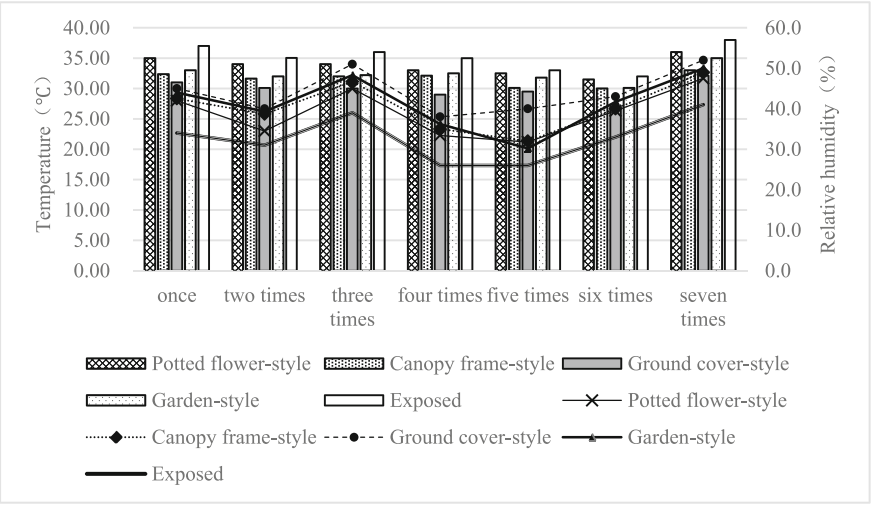

Fig. 4 Comparison of temperature and humidity of different types of roof gardens

follows: bare roof > potted flower > garden > scaffold > ground cover, and the order of relative humidity is ground cover > garden > scaffold > pot flower > bare roof.

It can be seen that different types of roof gardens have different effects in regulating temperature and humidity, which determines that different types of roof gardens play a different role in saving electricity, reducing PM2.5, and improving heat island effect. Each has its advantages and disadvantages.

On this basis, a comprehensive ecological roof garden innovation model is proposed to maximize the effectiveness of different types of roof garden and complement each other.

6.2 General Objective

On the people-oriented principle, in the scientific artistic method, by adhering to the ecological, economic and innovative principle, reasonably arrange the multilevel new design pattern of landscape elements such as plant, artificial hill, gallery frame, small and brief building, etc. in order to provide people a multi-functional circular hanging garden integrating ecology, environmental protection, rehabilitation and recuperation, leisure and entertainment.

6.3 Structural Design

Such kind of mode could be divided into three layers: Upper layer, middle layer and lower layer.

Upper layer: It sets up the gallery frame equipped with the vine and covered with the grape, Chinese wistaria, campsis grandiflora and other flowers or fruit-effect plants, which could reduce the load compared with the tall tress.

Lower layer: It is close to the first floor of roof, is equipped with the water tank, and could adopt the prefabricated water tank where the fish, shrimp and tortoise are fed, matched with the water plants, seaweed and other aquatic plants. And some cobbles could be put in water for decoration. Some potted plant group scenes are configured.

Middle layer: The facilities where the birds could inhabit, such as coop, birdcage, etc. could be put in different layers at the dangling parts between the gallery frame and the water tank on lower layer. The pigeon, parrot and ornamental chicken could be raised, which could not only attract the birds to stop, could also kill the plant and mosquito.

In this way, the canopy frame on which the vine crawls could overshadow the birds on the middle layer. The bird manure could fall in the water tank below to feed fish, forming a low-carbon green organic sustainable ecological cycle mode including the upper layer, middle layer and lower layer. Besides, the spare space is paved with the road, is laid with turf, and sets up the artificial hill, pavilion, seats and other recreational facilities. The design and building style combines with the surrounding environment by reasonably matching plants.

6.4 Plant Design

For the purpose of reflecting its rehabilitation efficacy, the relation with the twelve meridians is considered in the plant design. The human body could play a role in rehabilitation, salubrity and longevity after inhaling the beneficial chemical gas from plants. For example: “type good for the spleen and stomach channel: dungarunga—pomegranate and Aesculus chinensis Bunge. Type good for liver channel: Dungarunga—Armeniaca vulgaris Lam. Type good for kidney channel: dungarunga—Ulmus parvifolia Jacq, (Cerasus serrulata (Lindl.) *G. Don ex London*).

6.5 Design of Ecological Chain

Canopy plant—bird—fish pond—grassland—garden, simple ecological cycle mode. Such kind of mode Could completely alleviate people’s psychological pressure from the vision, audition, smell, touch and taste, cultivate one’s taste, enrich the spiritual

life, and embody the ecological and low-carbon cycle design concept that the human and nature have the harmonious coexistence and promote each other.

7 Conclusion[1]

Most of people supports the construction of roof garden. People have different preferences on different types of roof gardens, in which 12% of people are dissatisfied with the existing type and mode, and people expect a kind of ecological rehabilitation-type roof garden with more perfect function.

The existing roof garden has obvious effect in thermal insulation and moisturizing, but some factors shall be improved: such as the ecological income, load reduction, technical mean, etc., and the economic investment and technical support shall be increased.

The economic investment and maintenance management of roof garden shall be solved. The maintenance personnel and the management system shall be fully implemented and the following several aspects shall be strengthened: propaganda, guidance, investment and management, indicating their importance.

References

Han C (2014) Research on influence mechanism of regional urbanization to heat island effect based on RS. China University of Geosciences, Beijing

Li W and Li W (2012) Research on expression of landscape ecology and culture of modern residential area in Shaanxi Wubao County of China. J Landscape Res

Lv J (2013) Analysis of roof garden design of commercial building in China. Hangzhou Normal University, Hangzhou

Ren B (2010) Urbanization solving of "garbage siege". Ningbo Econ: Financ View 8

Sun C (2017) Planning and design of Mudanshan Mountain based on the integration of characteristic culture in Jiangning District of Nanjing City. Tianjin University, Tianjin

Wang W (2011) Study on plant application, landscape and ecological benefit roof garden in Hangzhou City. Zhejiang Agricultural and Forestry University

Zhang Y (2014) Research on slow traffic system planning in mountain cities. Chongqing Jiaotong University

[1]**Note**: This thesis is a featured innovative projects of key platform and scientific research innovation projects for 2017 undergraduate colleges and universities in the Department of Education of Guangdong Province. One of the innovative research (subject No.: 2017GXJK224) results of practical teaching of garden planning and design based on multi-functional training.

Part II
Environmental Chemistry

The Preparation of Sulfonated PS Microspheres Supported nZVFe/Ag Bimetals and Its Using in the Catalytic Reduction of 3-CP

Lixia Li, Lin Li, Wenqiang Qu, Kejun Dong, Gulisitan and Duoduo Chen

Abstract Based on soapless emulsion polymerization and dispersion polymerization, two kinds of sulfonated polystyrene microspheres were synthesized. Taking them as carrier, four kinds of SPS@Ag microspheres were prepared, i.e. SPS_1@Ag($NaBH_4$), SPS_1@Ag(PVP), SPS_2@Ag($NaBH_4$), and SPS_2@Ag(PVP), by $NaBH_4$/PVP reduction methods. SPS_1@Ag(PVP) was the best one, the nZVAg was about 20 nm and uniformly supported on SPS; the loading capacity was maximum. SPS supported nZVFe/Ag (SPS@nZVFe/Ag) was successfully prepared by chemical reduction. Part of nZVI was homogeneously covered on the surface of SPS_1@nZVAg and others existed as particles with size of 30–100 nm. The loading content of nZVI was 0.254 g/g. Taking 3-chlorophenol (3-CP) as model pollutant, the reactivity of SPS@nZVFe/Ag was carefully studied. The influence of the mole ratio of Ag/Fe and initial solution pH on the reactivity of SPS@nZVFe/Ag were investigated. At optimal reaction condition, 97% 3-CP in 50 mL 20 mg/L 3-CP solution (pH = 5) was reduced into phenol by about 0.344 g SPS@nZVFe/Ag (Ag/Fe = 0.041) at 20 °C, under stirring (110 r/min) within 10 min. The reaction was agreed with the pseudo first-order kinetics model. The reaction rate was very fast and the K_{obs} was 0.684 min^{-1}, which should attribute to both the electrochemical effect between Fe^0 and Ag^0, and the good hydrophily of SPS@nZVFe/Ag due to the $–HSO_3$ group on the carrier. In generally, SPS@nZVFe/Ag showed excellent reductive activity which suggested SPS@nZVFe/Ag had high potential practical application value in the reductive degradation of chlorophenol pollutant.

Keywords Sulfonated PS microspheres · Supported nZVFe/Ag · Catalytic reduction · 3-chlorophenol

L. Li (✉) · L. Li · W. Qu · K. Dong · Gulisitan · D. Chen
School of Environment and Safety Engineering, Jiangsu University, 212013 Zhenjiang, China
e-mail: qingpipa@ujs.edu.cn

R. Sun and L. Fei (eds.), *Sustainable Development of Water and Environment*, Environmental Science and Engineering,
https://doi.org/10.1007/978-3-030-16729-5_7

1 Introduction

In 1994, Gillham reported firstly that nZVI could be effectively used in situ remediation of groundwater (Gillham and O'Hannesin 1994). Since then nZVI, as a reducing agent, was quickly demonstrated successful in the elimination of various contaminants (Lofrano et al. 2017). At the same time, bimetallic Fe nanoparticles, such as Fe/Pd, Fe/Ag, Fe/Pt, Fe/Ni, Fe/Cu were reported to show more reducing capacity than nZVI, the bimetallic Fe nanoparticles could reduce many refractory substances such as aromatic hydrocarbons, polychlorinated aliphatic hydrocarbons, heavy metals, and nitro and azoaromatic hydrocarbons (Liu et al. 2014; Liu et al. 2017; Yuan et al. 2017). However, because of their small size, nZVI and other nanoscale metal particles showed strong tendency to aggregate and difficult separation of nano iron from the purified matrix (Liu et al. 2014; Noubactep et al. 2012). Supporting nanoscale metal-particles on solid carriers was proved to be an efficient method to overcome these insufficiencies. Till now, a lots of solid carriers were studied, such as clay (Ezzatahmadi et al. 2017), silica, activated carbon (Choi et al. 2008), zeolites, kaolinite (Zhou et al. 2018), diatomite (Ezzatahmadi et al. 2018) graphere, carbon nanotubes, PS, PGE/PVDF, polyaniline, PAA/PVA and so on (Zhao et al. 2011; Stefaniuk et al. 2016). These studies showed that carrier-supported nZVI and bimetallic Fe nanoparticles generally showed higher efficiency, improved stabilization and easy separation compared to their unsupported counterpart. Meanwhile a fact was found that not only the load amount, particle size and agglomerating behavior of the supported nanoscale metal particles but also the reduction reaction between supported nanoscale metal particles and substrate pollutants were affected by the kind of carrier and even the surface group of carrier (Liu et al. 2014; Parshetti and Doong 2009; Zhang et al. 2013). It was inferred that carrier played an important role in the preparation and the use of carrier-supported nanoscale metal particles.

Polystyrene (PS) is widely used as a carrier material because of its easy preparation protocol from inexpensive material, high environmental stability, and functionalizable properties. Some studies showed that the surface functional groups on PS could affect the formation and properties of the supported nZVI because of steric effect, electrostatic double layer repulsion interaction and van der Waals attraction forces (Jiang et al. 2011; Park et al. 2009). These results prompted us to fabricate functionalized PS microspheres supported nZVI or bimetallic Fe nanoparticles and investigate the efficiency of them in the elimination of environmental pollutants. In beginning of the year, our research group has reported our research about nitrobenzene reduction using nanoscale zero-valent iron supported by polystyrene microspheres with different surface functional groups, where it was found according to the synergistic effect of PS-CH_2-N + $(C_2H_5)_3Cl^-$ carrier for the supported nZVI, an excellent reduction efficiency and a very fast reduction rate was obtained. But unfortunately, PS-CH_2-N + $(C_2H_5)_3Cl^-$ supported nZVI showed low reducing capacity for CP (Li et al. 2018). Here, two kinds of sulfonated PS microspheres were prepared to support nZVFe/Ag; taking 3-CP as model pollutant, the catalytic reductive activity of SPS@ nZVFe/Ag were studied carefully. The introduction of –HSO_3 group into the PS microspheres

was supposed to help the adsorption capacity of Fe^{3+} and Ag^{+} and the hydrophily of carrier microspheres in water.

2 Experimental

2.1 Materials and Methods

Styrene (St, AR), anhydrous ethanol (AR), concentrated sulfuric acid (AR), polyvinyl pyrrolidone (PVP, GR), silver nitrate (AR), ferric chloride hexahydrate ($FeCl_3 \cdot 6H_2O$, AR), sodium hydroxide (AR), sodium borohydride ($NaBH_4$, AR), methanol (HPLC), hydrochloric acid (36–38%, AR), Diethylene benzene (DVB, 55%), chlorophenol (3-CP, AR), phenol (AR), and, azodiisobutyronitrile (AIBN, 98%) were all commercially available. AIBN was used after purifying by recrystallization in methanol and drying under a vacuum. St was used after purifying by vacuum distillation.

FTIR spectra were recorded using a Nicolee Nexus 670 FTIR spectrometer. X-ray diffractometer (XRD, D8 ADVANCE, BRUKER-AXS, Germany) defined crystallinity and detected composition of investigated particles using Cu K a radiation operating at 40 kV and 40 mA at scanning speed of $2° \text{ min}^{-1}$ between scanning angle 5° and 80°. Microscopic morphology and fixed point quantitative analysis of hybrid reducers were tested using a JEOL JSM-7001F thermal Field Emission SEM combined with GENESIS XM EDS instrument. The working voltage of SEM is 15 kV. The accelerated voltage of EDS was 20 kV. It needs special attention to prevent the supported NZVI from oxidation during pretreatment. 3-CP and phenol concentration were detected using LC-2010Aup HT Shimadzu HPLC instrument with WAT054275 C18 column and UV detector, determination wavelength was 375 nm. The mobile phase was methanol-water (70:30), the flow rate was 1.0 mL/min. The detected temperature was 30 °C.

2.2 Synthesis of Sulfonated Polystyrene Microspheres

First, two kinds of polystyrene microsphere, i.e. PS_1 and PS_2 were synthesized based on two synthetic methods.

PS_1 microspheres were prepared based on the published articles (Fontanals et al. 2008). 9.8 mL St and 0.2 mL DVB were added into 250 mL deoxygenated water in a 500 mL 3-neck flask at 75 °C. 0.2 g AIBN was dissolved in 10 mL deionized water and the solution was added into, dropwise, the mixture of reactant. The reaction was carried out at 75 °C with 300 rpm mechanical agitation under nitrogen protection for 11 h. Then, PS_2 microspheres were separated from the mixture by centrifugation, and washed with alcohol and distilled water in sequence, and then dried under vacuum at 30 °C for 12 h.

PS_2 microspheres were prepared according to the reports (Hong et al. 2007). 3 g PVP was added into 250 mL ethanol aqueous solution (V_{C2H6O} V_{H2O} = 95:5) in a 500 mL 3-neck flask at 70 °C. Next, the mixture of 15 mL St and 0.2 g AIBN was added into the above prepared mixture. The reaction was carried out at 70 °C with 300 rpm under nitrogen protection for 24 h. Then, PS_2 microspheres were separated from the mixture by centrifugation, and washed with distilled water several times, and then dried under vacuum at 30 °C for 12 h.

Second, 3 g PS_1 microspheres or PS_2 microspheres were added into 100 mL concentrated sulfuric acid (Jang and Han 2013). The mixture was dispersed by ultrasonic vibration. Then the reaction was carried out at 45 °C with 300 rpm mechanical agitation for 6 h. The mixture was chilled by ice water, and then the mixture was layered naturally. SPS microspheres were separated from the above layer by centrifugation, and washed with distilled water several times, and then dried under vacuum at 30 °C for 12 h.

2.3 Preparation of SPS@Ag

SPS supported nanoscale zero-valent Ag, recorded as SPS@Ag, were prepared by two kinds of supported methods.

The one was solution chemical reduction method using $NaBH_4$ as reducing agent (Zhang et al. 2018). 0.25 g SPS was added into 20 mL deionized water and dispersed by ultrasonic vibration. 5 mL 0.1 mM silver nitrate solution was added into SPS suspension. The mixture was placed at room temperature with stirring (100 rpm) for 3 h. Then, the above mixture was added dropwise into 25 mL $NaBH_4$ solution (0.5 M). The reaction was carried out at 4 °C for 1 h. Then, the SPS@Ag was separated out by 10000 rpm centrifugation and washed by deionized water twice and added into 10 mL anhydrous ethanol to preserve.

The second was chemical reduction method using PVP as reducing agent (Liao et al. 2016). 0.25 g SPS and 1 g PVP were added into 68 mL distilled water in a 250 mL 3-neck flask with a reflux condenser. The mixture was dispersed by ultrasonic vibration and deoxygenated by N_2 for 30 min. Then, 5 mL 0.1 mM silver nitrate solution was added into SPS emulsion. The reaction was carried out at 70 °C with stirring (100 rpm) for 7 h. Then, the SPS@Ag was separated out by 10000 rpm centrifugation and washed by anhydrous ethanol and deionized water alternately for six times and added into 10 mL anhydrous ethanol to preserve.

2.4 Preparation of SPS@nZVFe/Ag

The above prepared emulsion of SPS@Ag and anhydrous ethanol was added into 40 mL ethanol solution of $FeCl_3$ (100 g/L) for 12 h to absorb $FeCl_3$ on the surface of SPS@Ag. The mixture was filtered, and the obtained powder was washed with

ethanol two times and was added into a 100 mL wild-mouth bottle with 20 mL ethanol. Then, 40 mL $NaBH_4$ solution (0.5 M) was added drop wise to the powder suspension while swirling by hand. After the completion of the addition, the mixture was left to settle till no bubbles were produced. Then SPS@nZVFe/Ag was separated out by 10000 rpm centrifugation and washed by deionized water for several times and dried under vacuum at 30 °C for 12 h.

2.5 Catalytic Reduction of 3-CP by SPS@nZVFe/Ag

Reduction experiments of 3-CP were performed in 250 mL, 3-neck, round bottom flask, at 20 °C under stirring (110 r/min). The flask was initially filled with 50 mL 20 mg/L 3-CP solution which was deoxygenated by N_2 for 10 min. The initial pH value of the solution was adjusted by HCl (0.5 M) or NaOH (0.5 M). Certain amount of freshly prepared SPS@nZVFe/Ag was added into the flask. Reaction was carried out at 20 °C with stirring (110 r/min) under N_2 protection. During the reaction 1.5 mL solution was withdrawn at pre-determined time interval and filtered, dilute and analyzed for 3-CP and phonel concentration using LC-2010Aup HT Shimadzu instrument or Waters1525 HPLC instrument.

3 Results and Discussion

3.1 The Preparation and Characterization of SPS, SPS@Ag and SPS@nZVFe/Ag

Taking St as reaction monomer, deionized water as solvent, DVB as crosslinking agent, and AIBN as Initiator, PS_1 microspheres were prepared by soapless emulsion polymerization. Taking St as reaction monomer, ethanol aqueous solution $\left(V_{C_2H_6O} : V_{H_2O} = 95 : 5\right)$ as solvent, PVP as dispersion agent, and AIBN as Initiator, PS_2 microspheres were prepared by dispersion polymerization. After optimizing the reaction conditions, the two kinds of PS microsphere were prepared. Then both of them were sulfonated by concentrated sulfuric acid. The IR spectra of PS and SPS were showed in Fig. 1. Comparing the two FTIR spectra of PS and SPS, a peak at 1177 cm^{-1} which was the characteristic peak of $–HSO_3$ (Merche et al. 2010) arose in the spectrum of SPS which indicated that SPS was successfully synthesized.

The micro morphology of PS_1, PS_2, SPS_1 and SPS_2 were shown in Fig. 2. It can be seen that both PS_1 and PS_2 were globular. The diameter of PS_1 was about 340–380 nm. After sulfonation, SPS_1 became uniform globular with diameter of 390 nm. Comparing the shape of PS_1, PS_2 was uniform globular with lager diameter, about 580 nm. When PS_2 was sulfonated, the size of SPS_2 grew slightly and adhesion were happened which should be disadvantage to their application as carrier.

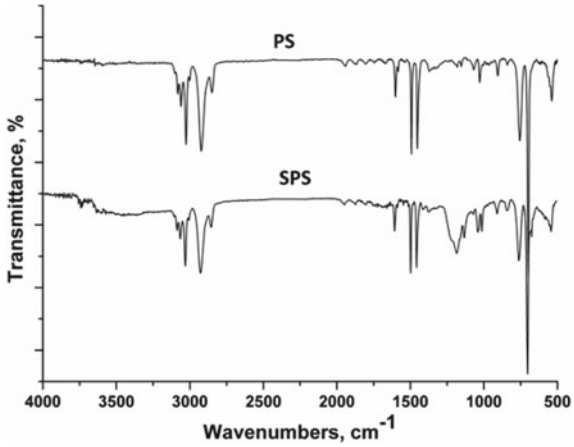

Fig. 1 The FT-IR spectra of PS and SPS

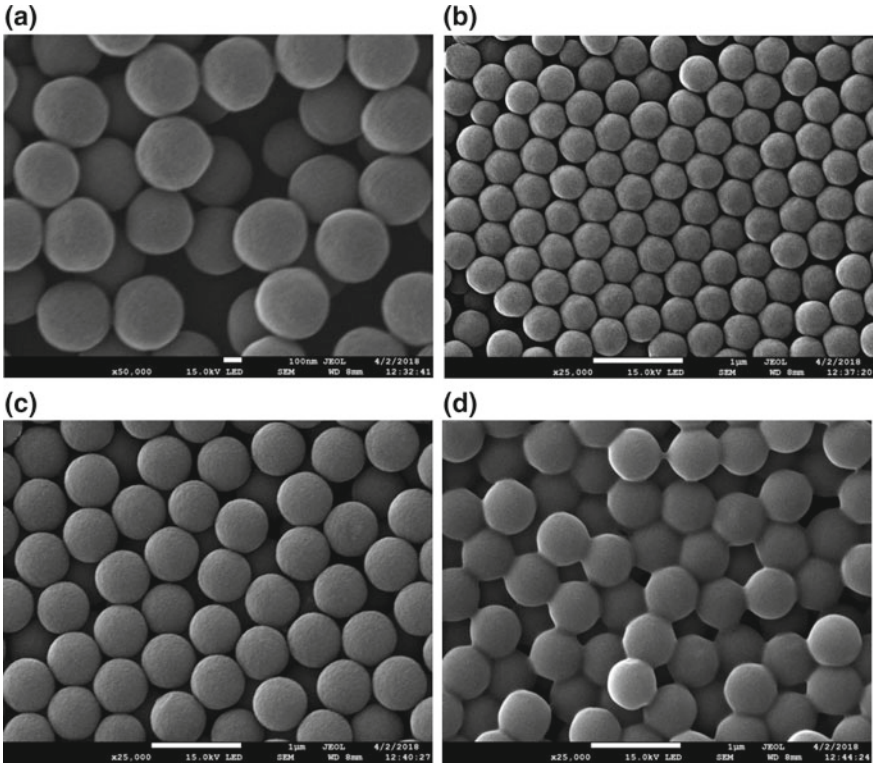

Fig. 2 SEM images of PS_1 (**a**), SPS_1 (**b**), PS_2 (**c**) and SPS_2 (**d**) microspheres

$NaBH_4$ reduction method and PVP reduction method were used to prepare SPS@Ag. The SPS@Ag using $NaBH_4$ as reducing agent was recorded as SPS@Ag($NaBH_4$), and using PVP as reducing agent was recorded as SPS@Ag(PVP). Four kinds of SPS@Ag particles were obtained, i.e. SPS_1@Ag($NaBH_4$), SPS_1@Ag(PVP), SPS_2@Ag($NaBH_4$), and SPS_2@Ag(PVP). Because of the strong reducibility of $NaBH_4$, it easy to react with water to produce H_2, the reduction between Ag^+ and $NaBH_4$ should be carried out at lower temperature. PVP was weak reducibility, so the reduction of Ag^+ with PVP should be carried out at higher temperature and no oxygen environment. The micro morphology of SPS_1@Ag($NaBH_4$), SPS_1@Ag(PVP), SPS_2@Ag($NaBH_4$), and SPS_2@Ag(PVP) were shown in Fig. 3. For SPS_1@Ag($NaBH_4$), nZVAg particles were unevenly anchored on the surface of SPS microspheres, and the size of them was difference from 20 to 70 nm which should be attributed to the rapid reaction rate of Ag^+ and $NaBH_4$. The nZVAg particles in SPS_1@Ag(PVP), by contrast, were well distributed and the size of them was uniform 20 nm. Comparing the SEM images of the SPS_1@Ag($NaBH_4$) and SPS_2@Ag($NaBH_4$), SPS_1@Ag(PVP) and SPS_2@Ag(PVP), it can be seen that similar regular was got for SPS_2@Ag($NaBH_4$) and SPS_2@Ag(PVP). But, the loading content of nZVAg on SPS_2@Ag was much less than that on SPS_1@Ag. The loading content of nZVAg on SPS_1@Ag(PVP) was maximum. So the SPS_1@Ag(PVP) was the best one and was selected to the following research. Stated thus, the loading of nZVAg was influenced by many factors which was worth further studied.

The Loading of nZVI on SPS@Ag microspheres was carried out by chemical reduction. First, the Fe^{3+} dissociated from $FeCl_3$ in ethanol was absorbed onto the surface of SPS_1@nZVAg microspheres by physical adsorption. When the SPS_1@nZVAg's color changed from white to dark yellow. Then the absorbed ferric ions were reduced to nZVI using $NaBH_4$ solution when the color of the hybrid particles turned into black which indicated that the loading of nZVI was successful. This can also be confirmed by the EDS detection of hybrid reducer. The SEM images of SPS@nZVFe/Ag microspheres was showed in Fig. 4. It can be seen that part of nZVI was homogeneously covered on the surface of SPS@nZVAg and the others existed as particles (the size were different from 30 to 100 nm) which also appeared in document (Li et al. 2018). Both the homogeneous disperse winkle structure and the particles structure of nZVI showed good limitation of nanoparticle agglomeration and aggregation. The loading quantity of nZVAg and nZVI mainly determined by the adsorption quantity of Ag^+ and Fe^{3+}, which could be controlled by regulating the concentration of $AgNO_3$ and $FeCl_3$ solution. According to the EDS spectra of SPS@nZVAg and SPS@nZVFe/Ag (Fig. 5), both the nZVAg and nZVI were supported successfully, and the loading content of nZVI/Ag of SPS@nZVFe/Ag was 0.254 g/g which was higher than documents (Zhang et al. 2013; Li et al. 2018; Bai et al. 2009) which should be attributed to the attraction Fe^{3+} and $–SO_3^-$ on the surface of carrier. Three mole ratio of Ag/Fe, 0.023, 0.041 and 0.058, were prepared and obtained.

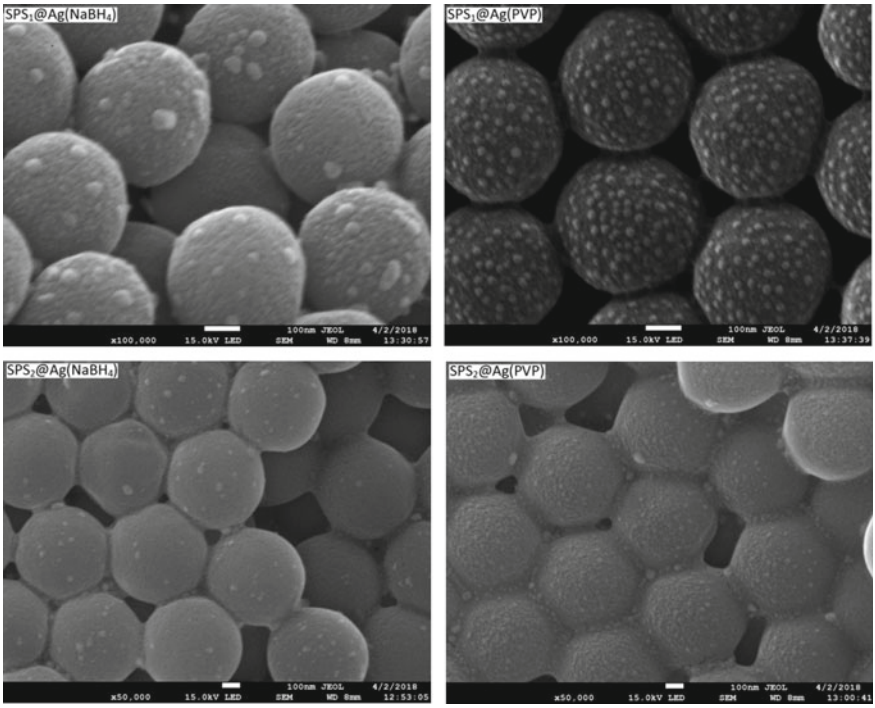

Fig. 3 SEM images of SPS1@Ag(NaBH4), SPS1@Ag(PVP), SPS2@Ag(NaBH4), and SPS2@Ag(PVP) microspheres

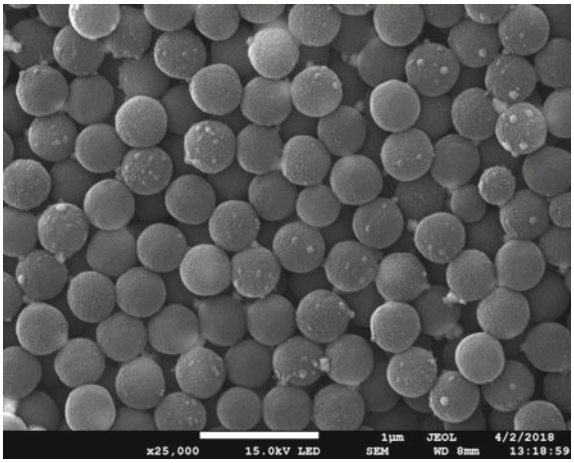

Fig. 4 The SEM images of SPS@nZVFe/Ag microspheres

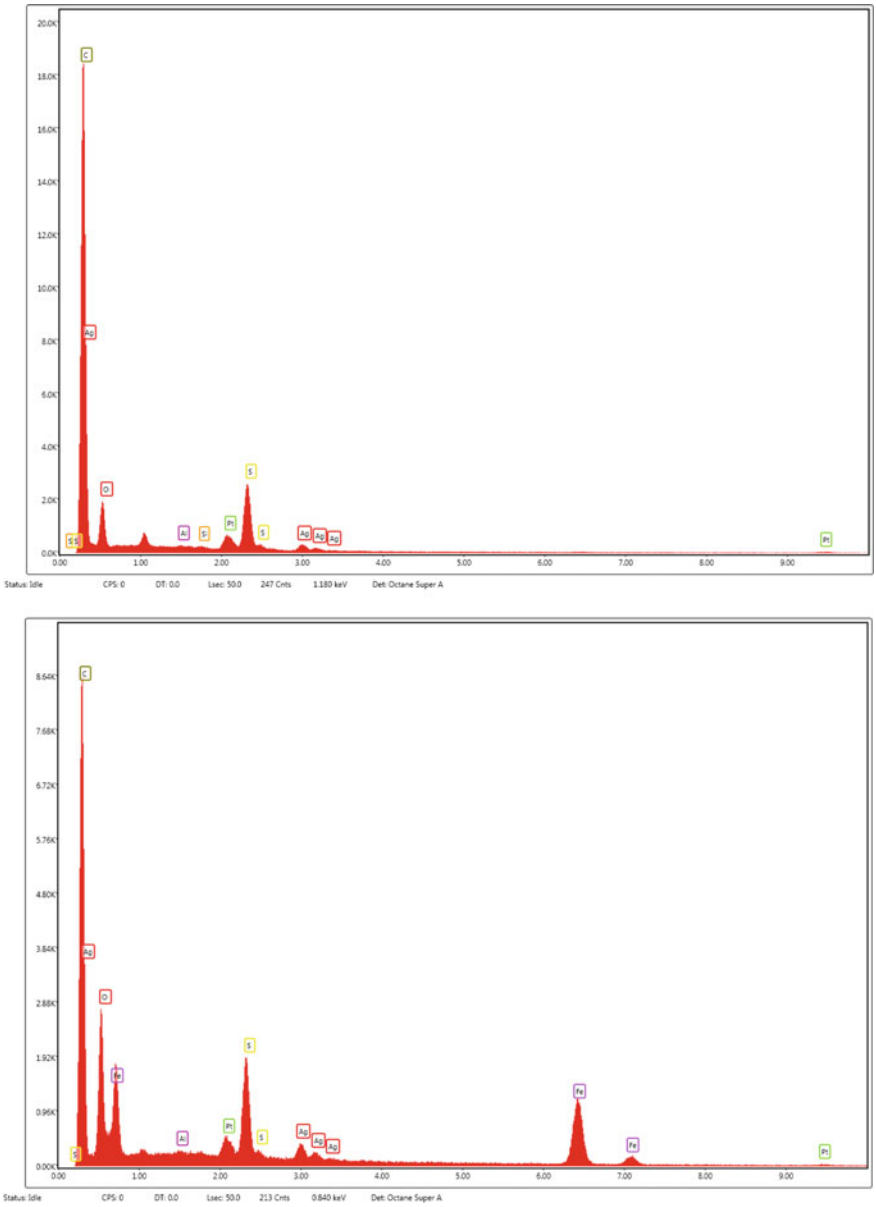

Fig. 5 The EDS spectra of SPS@nZVAg and SPS@nZVFe/Ag

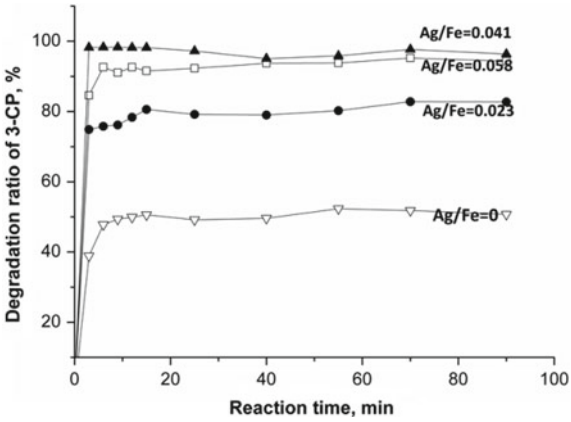

Fig. 6 The influence of mole ratio of Ag/Fe on the degradation ratio of 3-CP

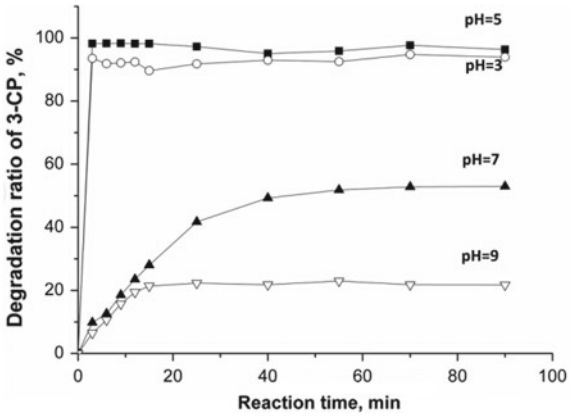

Fig. 7 The influence of pH on the degradation ratio of 3-CP

3.2 The Preparation and Characterization of SPS, SPS@Ag and SPS@nZVFe/Ag

Taking the 3-CP as model contaminant, the activity of the SPS@nZVFe/Ag at room temperature (20 °C) was studied. The 3-CP in 50 mL 20 mg/L 3-CP solution was catalytic reducted by about 0.344 g SPS@nZVFe/Ag, which was prepared based on 0.25 g SPS_1. The influence of mole ratio of Ag/Fe and initial solution pH on the activity of SPS@nZVFe/Ag were investigated. Each reaction was monitored by LC-2010Aup HT Shimadzu HPLC instrument during the course of reaction. The results were showed in Figs. 6 and 7. The data showed that most of the reaction reach the equilibrium within 10 min, showing that the activity of SPS@nZVFe/Ag was very high.

It can be seen from Fig. 6 that the degradation ratio of 3-CP at the case of Ag/Fe mole ratio = 0, 0.023, 0.041, 0.058 were 51, 82.8, 97 and 95.2% respectively after the reactions reached equilibrium. At the same condition, the degradation ratio of 3-CP

increased with the increasing of Ag/Fe mole ratio which showed that the existence of nZVg could heighten the activity of nZVI. The reason was nZVI adjacent to nZVAg could produce electrochemical effect, nZVI was negative pole and nZVAg was positive pole, which accelerated the oxidation of nZVI and produce more H_2, thereby promoting the reduction of 3-CP. But when the Ag/Fe mole ratio was excessive the nZVAg, wrapped in the surface of the SPS carrier, could hinder the loading of nZVI. So the best Ag/Fe mole ratio was about 0.041.

From the Fig. 7, it can be seen the degradation ratio of 3-CP at the case of pH = 3, 5, 7, and 9 were 94, 96, 52, and 21% respectively after the reactions reached equilibrium. The degradation ratio of 3-CP increased first and then decreased sonly with the increase of pH value. The possible reason was that when pH = 3, any of the nZVI were wasted by the reaction of Fe^0 and H^+ so that there was not enough Fe^0 to reduce the 3-CP. Under alkaline conditions, some solid $Fe(OH)_3$ could be produced by the reaction of Fe^{3+} with OH^- and which should settle on the surface of nZVI and hinder the reaction. While under weak acid conditions, the dissociated proton hydrogen from the acid was not enough to react with Fe^0 to produce H_2 but enough to promote the reaction (Liang et al. 2015; Li et al. 2016). So best degradation ratio of 96% was obtained when the pH value was 5.

According the above studies, the best reaction condition for the reduction of 3-CP and SPS@nZVFe/Ag was pH = 5, 20 °C, 110 r/min magnetic stirring. In such a condition, 97% 3-CP in 50 mL 20 mg/L 3-CP solution could be degraded by about 0.344 g fresh supported SPS@nZVFe/Ag in 10 min. At optimal reaction condition, the HPLC spectrum of reaction was showed in Fig. 8. It showed that there was no intermediate product during the reduction reaction. The kinetic was tested and showed in Fig. 9. The kinetic rate equation is expressed in Eq. (1).

$$\ln C_t/C_0 = -K_{obs}t \tag{1}$$

where C_t and C_0 (mg/L) are the residual concentration of 3-CP at time t and the initial concentration, respectively; K_{obs} (min^{-1}) is the apparent rate constant.

It can be seen from Fig. 9 that the linear relationship between C_t/C_0 and t had relatively high correlation coefficients. The results showed the reduction reaction were well fitted by the pseudo-first-order model. The apparent rate constant for the reaction at optimal reaction condition was 0.684 min^{-1} which should be attributed to not only the electrochemical effect between Fe^0 and Ag^0 but the good hydrophilic of SPS@nZVFe/Ag resulted from the introduction of $–HSO_3$ group on the surface of SPS.

4 Conclusions

Two kinds of sulfonated polystyrene microspheres carrier, i.e. SPS_1 and SPS_2, were synthesized successfully by soapless emulsion polymerization, dispersion polymer-

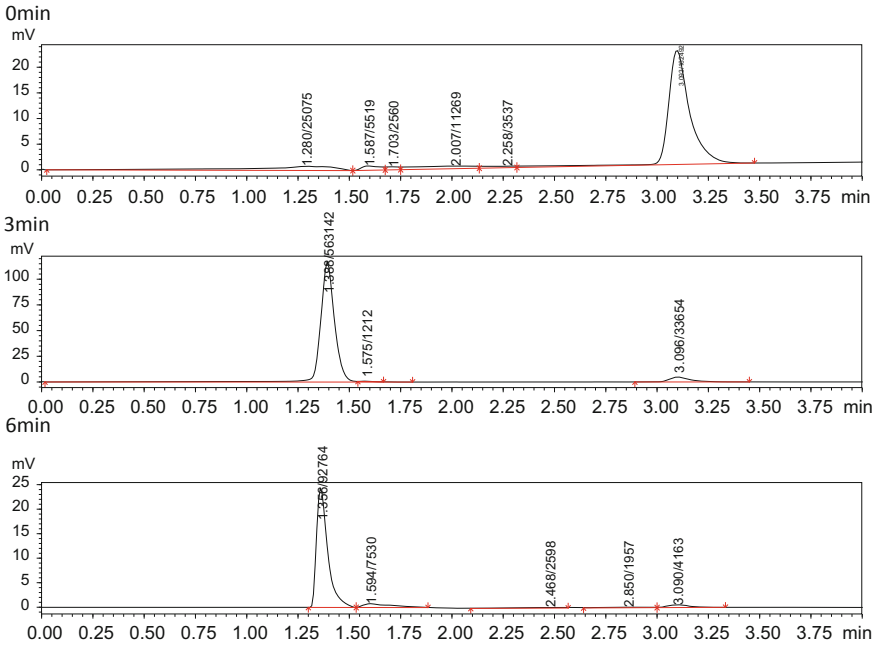

Fig. 8 The HPLC spectrum of reaction at optimal reaction condition

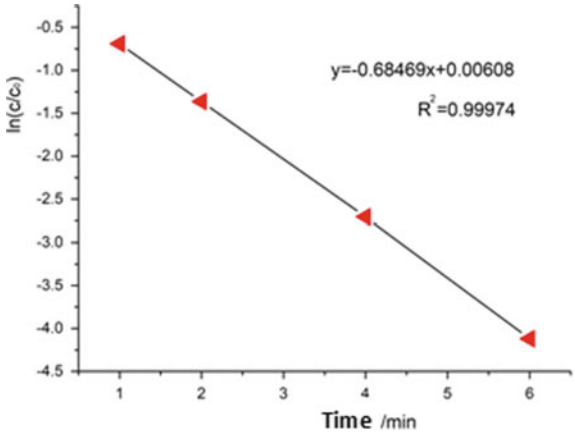

Fig. 9 The kinetic data of 3-CP at optimal reaction condition

ization and sulfonation reaction. Then, using $NaBH_4$ reduction method and PVP reduction method, SPS supported nanoscale zero-valent Ag were prepared and four kinds of SPS@Ag particles were obtained, i.e. SPS_1@Ag($NaBH_4$), SPS_1@Ag(PVP), SPS_2@Ag($NaBH_4$), and SPS_2@Ag(PVP). Comparing the micro morphology and the loading capacity of the supported nZVAg, the loading content of nZVAg on SPS_1@Ag(PVP) was maximum, and the supported nZVAg on SPS_1@Ag(PVP) was uniform size of 20 nm, so SPS_1@nZVAg(PVP) was selected to supported nZVI. Then, based on SPS_1@Ag(PVP), SPS@nZVFe/Ag was successfully synthesized by chemical reduction. The SEM images showed that part of nZVI was homogeneously covered on the surface of SPS@Ag and the others existed as particles with size from 30 to 100 nm. According to the attraction between Fe^{3+} and $–SO_3^-$ on the SPS, high loading content of nZVI, 0.254 g/g, was obtained. Four SPS@nZVFe/Ag with mole ratio of Ag/Fe = 0, 0.023, 0.041 and 0.058 were prepared. Taking 3-CP as model pollutant, the reactivity of SPS@nZVFe/Ag was carefully studied. The influence of mole ratio of Ag/Fe and initial pH on the reduction of 3-CP by SPS@nZVFe/Ag were studied successively. SPS@nZVFe/Ag showed excellent reductive activity. At optimal reaction condition, 97% 3-CP in 50 mL 20 mg/L 3-CP solution (pH = 5) could be reduced into phenol by about 0.344 g SPS@nZVFe/Ag (Ag/ Fe = 0.041) at 20 °C, under stirring (110 r/min) within 10 min which was very fast. The reduction of 3-CP by SPS@nZVFe/Ag was agreed with the pseudo first-order kinetics model. Because of the electrochemical effect between Fe^0 and Ag^0, and the good hydrophily of SPS@nZVFe/Ag due to the introduction of $–HSO_3$ group on the surface of the carrier, the reaction rate was very fast and the K_{obs} was 0.684 min^{-1}. In generally, the above results suggested that SPS@nZVFe/Ag had high potential practical application value in the reductive degradation of chlorophenol pollutant.

Acknowledgements The authors acknowledge the support by the by the National Natural Science Foundation of China [Grant No. 51508233], and Jiangsu Collaborative Innovation Center of Technology and Material of Water Treatment.

References

Bai X, Ye Z-F, Qu Y-Z, Li Y-F, Wang Z-Y (2009) Immobilization of nanoscale Fe^0 in and on PVA microspheres for nitrobenzene reduction. J Hazard Mater 172:1357–1364

Choi H, Al-Abed SR, Agarwal S, Dionysios DD, Choi H (2008) Synthesis of reactive nano-Fe/Pd bimetallic system-impregnated activated carbon for the simultaneous adsorption and dechlorination of PCBs. Chem Mater 20(11):3649–3655

Ezzatahmadi N, Ayoko GA, Millar GJ, Speight R, Yan C, Li JH, Li SZ (2017) Clay-supported nanoscale zero-valent iron composite materials for the remediation of contaminated aqueous solutions: a review. Chem Eng J 312:336–350

Ezzatahmadi N, Bao T, Liu HM, Xi YF (2018) Catalytic degradation of Orange II in aqueous solution using diatomite-supported bimetallic Fe/Ni nanoparticles. RSC Adv 8(14):7687–7696

Fontanals N, Manesiotis P, Sherrington DC, Cormack PAG (2008) Synthesis of spherical ultra-high-surface-area monodisperse amphipathic polymer sponges in the low-micrometer size range. Adv Mater 20:1298–1302

Gillham RW, O'Hannesin SF (1994) Enhanced degradation of halogenated aliphatics by zero-valent iron. Ground Water 32:958–967

Hong J, Hong CK, Shim SE (2007) Synthesis of polystyrene microspheres by dispersion polymerization using poly(vinyl alcohol) as a steric stabilizer in aqueous alcohol media. Colloids Surf A Physicochem Eng Aspects 302:225–233

Jang SY, Han SH (2013) Characterization of sulfonated polystyrene-block-poly (ethyl-ranpropylene)-block-polystyrene copolymer for proton exchange membranes (PEMs). J Membr Sci 444:1–8

Jiang ZM, Lv L, Zhang WM, Du Q, Pan BC, Yang L, Zhang QX (2011) Nitrate reduction using nanosized zero-valent iron supported by polystyrene resins: role of surface functional groups. Water Res 45:2191–2198

Li L, Hu J, Fan M, Luo J, Wei X (2016) Nanoscale zero-valent metals: a review of synthesis, characterization, and applications to environmental remediation. Environ Sci Pollut Res 23:17880–17900

Li LX, Zhang SS, Lu B, Zhu F, Cheng J, Sun ZH (2018) Nitrobenzene reduction using nanoscale zero-valent iron supported by polystyrene microspheres with different surface functional groups. Environ Sci Pollut Res 25(8):7916–7923

Liang C-J, Lin Y-T, Shiu JW (2015) Reduction of nitrobenzene with alkaline ascorbic acid: kinetics and pathways. J Hazard Mater 302:137–143

Liao GF, Chen J, Zeng WG, Yu CH, Yi CF, Xu ZS (2016) Facile preparation of uniform nanocomposite spheres with loading silver nanoparticles on polystyrene-methyl acrylic acid spheres for catalytic reduction of 4-nitrophenol. J Phys Chem 120:25935–25944

Liu WJ, Qian TT, Jiang H (2014) Bimetallic Fe nanoparticles: recent advances in synthesis and application in catalytic elimination of environmental pollutants. Chem Eng J 236:448–463

Liu J, Zhu H, Xu FY, Zhao JZ (2017) Enhanced hydrodechlorination of 4-chlorophenol by Cu/Fe bimetallic system via ball-milling. Desalin Water Treat 64:157–164

Lofrano G, Libralato G, Brown J (2017) Nanotechnologies for environmental remediation: applications and implications. In: Nanomaterials for adsorption and heterogeneous reaction in water decontamination. Springer International Publishing AG, pp 200–201

Merche D, Hubert J, Poleunis C, Yunus S, Bertrand P, Keyzer PD, Reniers F (2010) One step polymerization of sulfonated polystyrene films in a dielectric barrier discharge. Plasma Process Polym 7(9–10):836–845

Noubactep C, Caré S, Crane R (2012) Nanoscale metallic iron for environmental remediation: prospects and limitations. Water Air Soil Pollut 223:1363–1382

Park H, Park YM, Lee SH (2009) Reduction of nitrate by resin-supported nanoscale zero-valent iron. Water Sci Technol 59:2153–2157

Parshetti GK, Doong RA (2009) Dechlorination of trichloroethylene by Ni/Fe nanoparticles immobilized in PEG/PVDF and PEG/nylon 66 membranes. Water Res 43:3086–3094

Stefaniuk M, Oleszczuk P, Ok YS (2016) Review on nano zerovalent iron (nZVI): from synthesis to environmental applications. Chem Eng J 287:618–632

Yuan Y, Yuan DH, Zhang YH, Lai B (2017) Exploring the mechanism and kinetics of Fe-Cu-Ag trimetallic particles for p-nitrophenol reduction. Chemosphere 186:132–139

Zhang QR, Du Q, Hua M, Jiao TF, Gao FM, Pan BC (2013) Sorption enhancement of lead ions from water by surface charged polystyrene-supported nano-zirconium oxide composites. Environ Sci Technol 47:6536–6544

Zhang Z, Shen WF, Xue J, Liu YM, Liu YW, Yan PP, Liu JX, Tang JG (2018) Recent advances in synthetic methods and applications of silver nanostructures. Nanoscale Res Lett 13:1931–7573

Zhao X, Lv L, Pan BC, Zhang WM, Zhang SJ, Zhang QX (2011) Polymer-supported nanocomposites for environmental application: a review. Chem Eng J 170:381–394

Zhou SW, Xu R, He JZ, Huang YC, Cai ZJ, Xu MG, Song ZG (2018) Preparation of Fe-Cu-kaolinite for catalytic wet peroxide oxidation of 4-chlorophenol. Environ Sci Pollut Res 25(5):4924–4933

Development of a Fluidized Bed Gas Heater Using Solar Heat for Waste Steam Reuse in the Plant

Sung Won Kim and Sae Han Park

Abstract Due to serious environmental impact from huge amount of energy and water resource consumption in industrial processes, the industries have been looking for new systems based on renewable energy. Performance of the directly-irradiated fluidized gas heater (50 mm-ID × 100 mm high) with silicone carbide particles has been determined for the application of exhaust steam reuse in the low- and medium temperature processes. The minimum fluidization velocity (U_{mf}) of SiC is 0.0054 m/s, where the solar receiver was operated for keeping the fluidization state. The bed temperature shows a maximum value of about 200 °C around 0.013–0.021 m/s of gas velocity. It is considered that a high gas temperature is obtained in the vicinity of the minimum bubbling velocity where small bubbles are formed. The produced heat energy increases up to 18 W with increasing gas velocity. The optimum condition in this study is around 0.050 m/s. The energy efficiency was calculated to be 14%. A possible improvement of the gas heater has been proposed based on the experimental results.

Keywords Solar energy · Steam reuse · Fluidized bed gas heater

1 Introduction

All too often, low-pressure waste steam and flash steam in the industrial plant are simply released to atmosphere instead of being reused. This can be an unhealthy practice, since losing steam often means a loss of useable energy and water resource. Although various ways have been proposed, additional investment and energy should be required and the methods focus on the energy recovery, not on water resource. To decrease water consumption in the processes, the exhaust steam reuse by upgrading steam quality could be a better idea. Due to serious environmental impact from

S. W. Kim (✉) · S. H. Park
School of Chemical and Material Engineering, Korea National University of Transportation, Chungju-si, Chungbuk 27469, Republic of Korea
e-mail: kswcfb@ut.ac.kr

R. Sun and L. Fei (eds.), *Sustainable Development of Water and Environment*, Environmental Science and Engineering,
https://doi.org/10.1007/978-3-030-16729-5_8

the consumption of huge amount of energy and water for the steam production in industrial processes, the industries have been looking for new systems based on renewable energy. Among all forms of renewable energy, solar energy attracts the most attention as a promising option to be applied in the processes (Jia et al. 2018). Solar heat for industrial processes (SHIP) is recognized as the most potential one among solar heating and cooling applications, because a variety of industrial processes require huge amount of thermal energy, which makes the industrial sectors a promising market for solar thermal applications. However, the SHIP still needs to reduce installation and operating costs and increase the efficiency to be competitive with other methods as already shown in the case of the concentrated solar power technology (Ma et al. 2015).

Temperatures of the processes are ranging from low and medium less than 250 °C to high. The low and medium temperature processes present a high share of heat demand in the mining, food, pulp and paper, machinery and equipment manufacturing sectors (Jia et al. 2018). The solar thermal energy might be suitable for the low- and medium temperature processes, considering the cost, efficiency and temperatures obtainable in a solar heating. In the SHIP system, the solar energy receivers require the development of geometric shapes, materials, heat-transfer fluids and processes related with solar irradiance and absorption, heat loss and reliability (Ho 2016). The direct heating on the fluid is advantageous in the heat transfer including minimization of the heat loss.

The fluidization of solid particles in a solar receiver has been proposed for several decades, and early 1980s by Flamant (1982). More recently, Zhang et al. (2015) reported a good heat transfer between air and silicon carbide (SiC) particle in quartz tube where fluidized particles are vertically irradiated by heliostat system to receive more sunlight, despite the possibility of heat loss.

Challenges still be in the development of a suitable window for the het receiver and the development of a solid–gas suspension system that maintains a uniform particle concentration and temperature within the fluidized bed receiver (Ho 2016). The performance in the gas heater is related with fluidization behavior of the particle in the bed. The previous studies (Flamant 1982; Zhang et al. 2015) used coarse particles as bed materials to get high mass flux of gas because the fine particles are easily carried over to outlet of the receiver. However, the coarse particles have relative low gas-solid contacting efficiency and area per volume, indicating low particle-to-gas heat transfer and resulting low performance of gas heater.

In this study, performance of the directly-irradiated fluidized gas heater with fine particle has been determined for the application of exhaust steam reuse in the low- and medium temperature processes. A possible improvement of the gas heater has been proposed based on the experimental results.

2 Experimental

The system mainly consists of a solar light receiver and a fluidized bed gas heater. The solar light receiver system is composed of the first reflective mirror, Fresnel lens, the second reflective mirror and focal lens as in Fig. 1. The effective diameter of the Fresnel lens (Edmund optics) with transmission of 92% is 0.457 m. The solar mirror (model 1100, 3M) of film type has 93% of reflectance. Experiments were carried out in a fluidized bed unit made of Pyrex glass column as shown in Fig. 2. It consisted of a main column (50 mm-ID × 100 mm high). The column diameter was expanded to 110 mm to reduce elutriation of particles. The top surface was made of quartz plate to get high transparency. A sintered plate as distributor was used to inject air for fluidization. Fluidizing air was introduced into the column using a mass flow meter (RK1150, Kojima instrument). Two pressure taps were located at the wall of the inlet and outlet of column to measure pressure drops for obtaining the information of solid holdup. 5 K-type thermocouples are used to measure the inlet air temperature, outlet air temperature and fluidized bed bulk temperature. Silicon carbide (F220, Showa Denko) was used as bed material for heat transfer to air. The average particle diameter is 0.052 mm and the bulk density is 1373 kg/m^3. Bed materials of 120 g were loaded and the static bed height was 45 mm considering solar focus on the bed surface. The solar radiation is concentrated by the Fresnel lens and directed on to the fluidized bed of the SiC particles at given gas velocity. The gas velocity was varied 0.00–0.06 m/s.

3 Results and Discussion

From the engineering view point, the minimum fluidization velocity (U_{mf}) is a key indicator of the overall behavior of a fluidized bed (Whitcombe et al. 2002). To determine the reference gas velocity for the operating conditions in the solar receiver, the U_{mf} was measured from the pressure drop-versus-velocity diagram (Kunii and Levenspiel 1991) as in Fig. 2.

The pressure drop across the bed is approximately proportional to gas velocity in the fixed bed, and the pressure drop reaches a static pressure of the bed, indicating the fluidized bed. The U_{mf} of SiC in the study is 0.0054 m/s. The first bubble is observed on the bed surface with further increase of gas velocity. The gas velocity is called the minimum bubbling velocity (U_{mb}), another key indicator of the fluidized bed. The U_{mb} of SiC was 0.0118 m/s. From the results, the solar receiver was operated at gas velocity over 0.0054 m/s for keeping the fluidization state.

Timely variation of temperatures at bed and freeboard above bed surface in the solar receiver is shown in Fig. 3. Gas velocity is 0.009 m/s and the inlet temperature of air is 19 °C. The bed temperature rises to approximately 145 °C within 20 min. The difference between bed and freeboard (outlet) temperatures was small. The solar thermal energy receiving system uses SiC particles as a heat transfer medium to

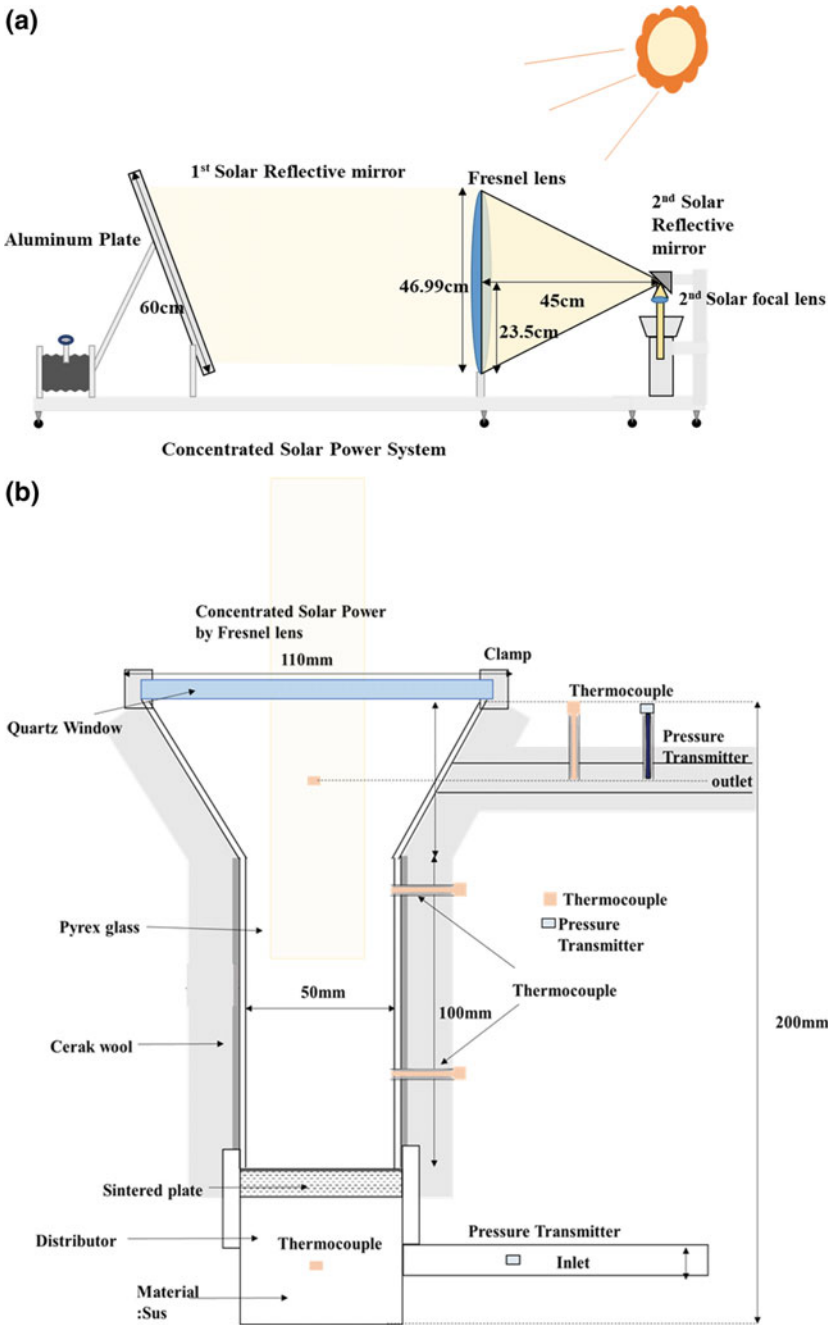

Fig. 1 Experimental apparatus: **a** solar light receiver system, **b** solar heat gas heater system

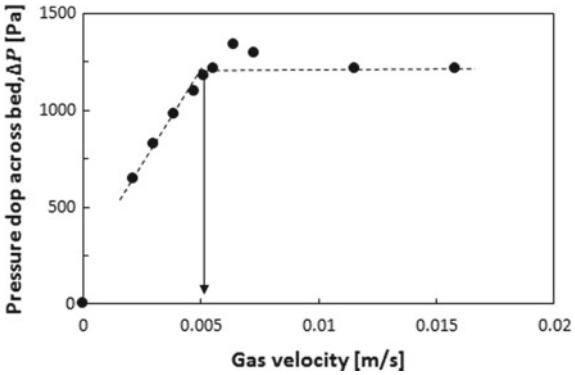

Fig. 2 Pressure drop-versus-velocity diagram

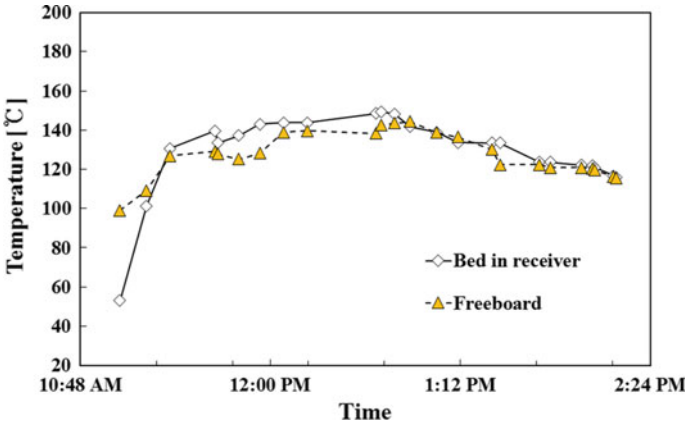

Fig. 3 Timely variation of temperatures in the solar receiver ($U_g = 0.009$ m/s)

directly absorb incident solar radiation. The heated particles on the bed surface go down to the bed center region, and contact with the air. The heat receiving system can achieve the heat and raise the bed temperature quickly in the fluidized bed with fast renewal of bed surface as heat receiving area. However, the temperature has timely variation depending on weather condition such as partly clouds.

Effect of gas velocity on temperatures in the solar heat receiver system is shown in Fig. 4. The bed temperature shows a maximum value of about 200 °C around 0.013–0.021 m/s of gas velocity. The temperature slowly goes down with increasing of gas velocity. Interestingly, the gas velocity in maximum temperature range is just above U_{mb}. Above the U_{mb}, part of the gas in the fluidized bed goes through the bed as bubbles (Kunii and Levenspiel 1991). The part increases with gas velocity due to increasing bubble size. Actually, the bubble behavior is positive for the solid-gas heat transfer due to better mixing of the fluidized bed. The gas in the bubble has a resistance in heat transfer from hot particles (Kim and Kim 2013). Due to

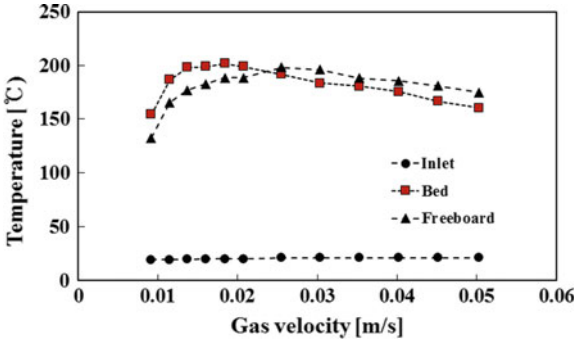

Fig. 4 Effect of gas velocity on temperatures in solar heat receiver

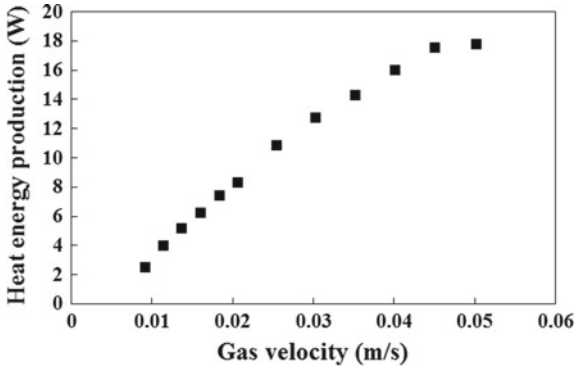

Fig. 5 Effect of gas velocity on heat energy production in solar heat receiver

the opposing effects of the bubbles on the heat transfer, it is considered that a high temperature is obtained in the vicinity of U_{mb} where small bubbles are formed.

Effect of gas velocity on heat energy production from solar heat receiver is shown in Fig. 5. The heat energy is calculated by Eq. (1) as.

$$\dot{Q}_{gas} = \rho_g * \dot{V} * \overline{c_{pg}} * \left(T_{freeboard} - T_{g,in}\right) \tag{1}$$

The produced heat energy increases up to 18 W with increasing gas velocity. Although the outlet gas temperature slightly decreased, the total produced energy is proportional to the gas mass flow rate, indicating there is optimum operating condition considering outlet temperature and gas mass flow rate. The optimum condition in this study is around 0.050 m/s. However, the energy efficiency (heat energy production/solar power in atmosphere) in this system was calculated to be 14%.

Finally, the results in the study indicate additional improvement of the system is required to increase the energy efficiency. The system insulation around gas inlet parts such as gas distributor and inlet pipe should be strengthened. Also, solar light receiving efficiency could be improved by enlarging light-bed material contacting area and minimizing the reflection of the light to the system (Gomez-Garcia et al. 2017).

4 Conclusion

Performance of the directly-irradiated fluidized gas heater with fine particle has been determined for the application of steam supply in the low- and medium temperature processes. The U_{mf} of SiC in the study is 0.0054 m/s. the solar receiver was operated at gas velocity over 0.0054 m/s for keeping the fluidization state. The bed temperature shows a maximum value of about 200 °C around 0.013–0.021 m/s of gas velocity. It is considered that a high gas temperature is obtained in the vicinity of U_{mb} where small bubbles are formed. The produced heat energy increases up to 18 W with increasing gas velocity. The optimum condition in this study is around 0.050 m/s. However, the energy efficiency in this system was calculated to be 14%. A possible improvement of the gas heater has been proposed based on the experimental results.

Acknowledgements This research was supported by Basic Science Research Program through the National Research Foundation of Korea (NRF) funded by the Ministry of Education (NRF-2017R1D1A3B030299 17).

References

Flamant G (1982) Theoretical and experimental-study of radiant-heat transfer in a solar fluidized-bed receiver. AIChE J 28:529–535

Gomez-Garcia F, Gauthier D, Flamant G (2017) Design and performance of a multistage fluidised bed heat exchanger for particle-receiver solar power plants with storage. Appl Energy 190:510–523

Ho C (2016) A review of high-temperature particle receivers for concentrating solar power. Appl Therm Eng 109:958–969

Jia T, Huang J, Li R, He P, Dai Y (2018) Status and prospect of solar heat for industrial processes in China. Renew Sustain Energy Rev 90:475–489

Kim SW, Kim SD (2013) Heat transfer characteristics in a pressurized fluidized bed of fine particles with immersed horizontal tube bundle. Int J Heat Mass Transfer 64:269–277

Kunii D, Levenspiel O (1991) Fluidization engineering, 2nd edn. Butterworth-Heinemann, US, pp 71–72

Ma Z, Mehos M, Glatzmaier G, Sakadjian BB (2015) Development of a concentrating solar power system using fluidized-bed technology for thermal energy conversion and solid particles for thermal energy storage. Energy Procedia 69:1349–1359

Whitcombe JM, Agranovski IE, Braddock RD (2002) Impact of metal ridging on the fluidization characteristics of FCC catalyst. Chem Eng Technol 25:981–987

Zhang YN, Bai FW, Zhang XL, Wang FZ, Wang ZF (2015) Experimental study of a single quartz tube solid particle air receiver. In: International conference on concentrating solar power and chemical energy systems, Solarpaces 2014, vol 69, pp 600–607

Review on Hydrodynamic Behavior of Continuous Flow Reactors for Water Treatment by Electron Beam

Rui Ding, Chen Xie, Ziwu Fan and Zeyu Mao

Abstract Water pollution is one of the most significant environmental issues in China and the world. Electron beam (EB) treatment of water, which is a new technology for water treatment, provides a new way to remove the pollutants that can't be degraded by traditional water treatment technology. For the past few decades, the biological and chemical effect of electron beam (EB) on wastewater has been studied a lot. Comparatively less attention has been paid on the hydrodynamic behavior of the flow reactors for water treatment by electron beam (EB reactors). The hydrodynamic behavior of EB reactor is crucially important for EB treatment efficiency. In this paper, EB reactors were analyzed and compared, the advantages and disadvantages of different kinds of EB reactors were briefly reviewed. Previous studies on EB reactors mainly focus on the experimental study on velocity, depth and mean absorbed dose of the flow formed by EB reactors, ignoring the detailed hydrodynamics of the EB reactor and its effect on the absorbed dose distribution. Further research area on EB reactors was proposed. Computational fluid dynamic (CFD) method should be used to study the velocity, depth and density distribution of the flow formed by EB reactors. The Monte Carlo method, integrated with the CFD simulation result, should be used to study the absorbed dose distribution of EB reactors and therefore optimize the EB reactors to make the absorbed dose evenly distributed.

Keywords Electron beam water treatment · Hydrodynamics behavior of EB reactors · Absorbed dose distribution · CFD · Monte Carlo method

1 Introduction

Water pollution is one of the most significant environmental issues in China and the world (Han et al. 2016; Wang and Yang 2016). Electron beam (EB) treatment of

R. Ding (✉) · C. Xie · Z. Fan
Nanjing Hydraulic Research Institute, 210029 Nanjing, China
e-mail: dingrui@nhri.cn

Z. Mao
Tsinghua University, 100084 Beijing, China

R. Sun and L. Fei (eds.), *Sustainable Development of Water and Environment*, Environmental Science and Engineering,
https://doi.org/10.1007/978-3-030-16729-5_9

water, which is a new technology for water treatment, provides a new way to remove the pollutants that can't be degraded by traditional water treatment technology (Wang and Chu 2016). When water is exposed to electron beam, the predominant products of the water radiolysis reaction are the oxidizing hydroxyl radical OH*, the reducing hydrated electron e_{aq}^{-} and the hydrogen radical H* (Spinks and Woods 1990; Jan et al. 2015), all of which are highly reactive transient species that are responsible for the various effects of EB water treatment including the reduction of pathogens, the oxidation of hazardous organic pollutants, the destruction of molecular structures of targeted pollutants, and the elimination of odor nuisance (Wang and Wang 2007; Abdou et al. 2011).

For the past few decades, a lot of researches have been conducted to study the biological and chemical effect of electron beam on different kinds of contaminants in water (Getoff 2002; Skowron et al. 2014; Lee et al. 2015). Comparatively less attention has been paid on the behavior of the flow reactor for EB water treatment (Mahendra et al. 2010, 2011; Ding et al. 2017).

Structures, device and containers that could conduct water treatment are all called water treatment reactors. The main carrier for Mass and energy transfer of the water treatment reactor is water. The hydrodynamic behavior of a reactor directly affects the mixing process of the flow, which restricts the treatment efficiency of the reactor. Research on biological or chemical reaction kinetics of water treatment are wide and profound, but study on the fluid dynamics and mass transfer of the water treatment reactor is relatively weak. The hydrodynamic behavior of the reactor need a further study to solve the technical problems of reactor configuration design and to improve the flow condition and efficiency of the reactor.

The continuous flow reactors for electron beam treatment of water (EB reactors) are systems that expose flowing water to electron beam. The hydrodynamic behavior of the flow presented to electron beam and the characteristic of the electron beam prominently affects the EB treatment efficiency. As a result, it is necessary to study the hydrodynamic behavior of the EB reactors, which has a scientific significance for the water treatment process.

In this paper, existing EB reactors were analyzed and compared, and the advantages and disadvantages of different kinds of EB reactors were briefly reviewed. Further research area on EB reactor was proposed.

2 Characteristic of Different Kinds of EB Reactors

Different kinds of EB reactors were proposed to dispose different kinds of wastewater and to adopt different kinds of treatment method. EB reactors could be generally divided into four types based on the difference in the form of flow, which specifically are water fall EB reactors, spraying EB reactors, nozzle jet EB reactors and up-flow EB reactors. Four kinds of EB reactors were shown in Figs. 1, 2, 3 and 4 and their brief characteristic was shown in Table 1.

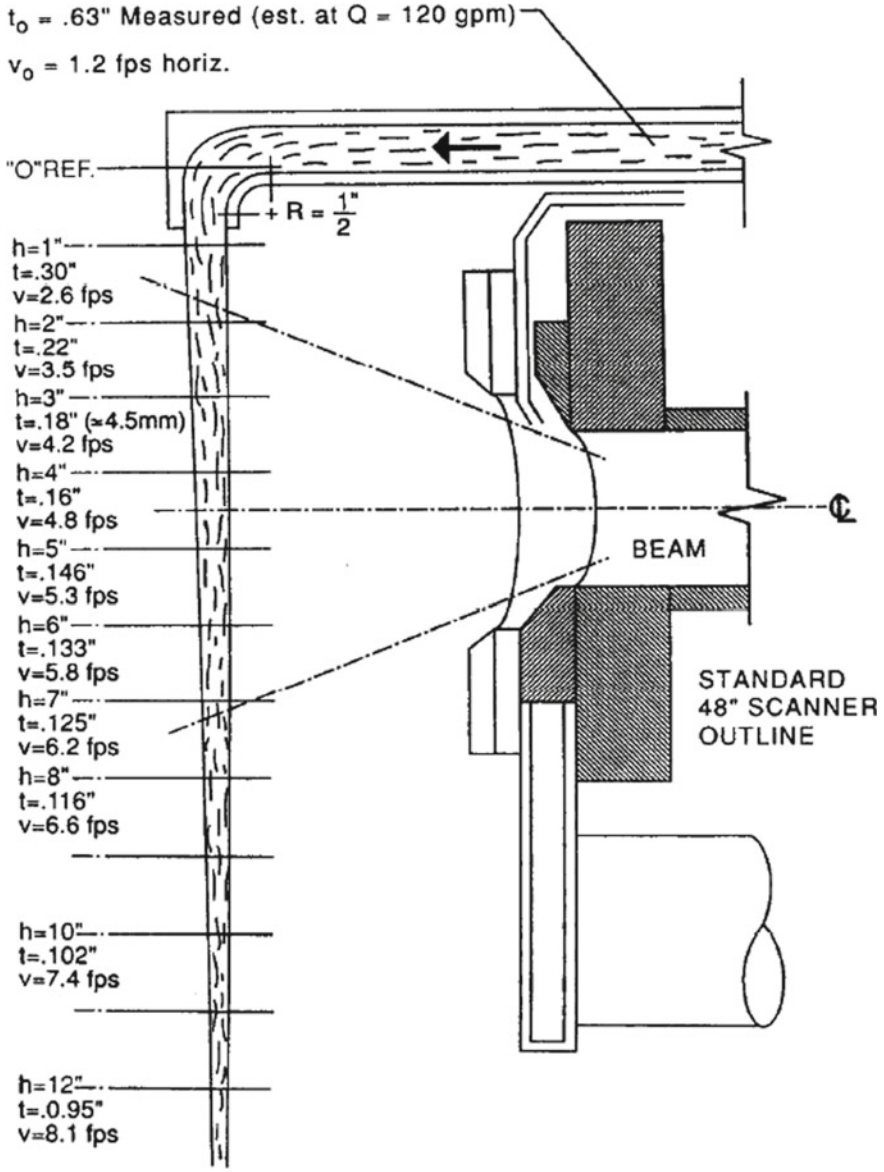

Fig. 1 The water fall EB reactor

Table 1 Introduction and comparison of four different kinds of EB reactors

Type of the reactor	Water fall EB reactors	Spraying EB reactors	Nozzle jet EB reactors	Up-flow EB reactors
Country	USA	Russia	Russia, Korea, China	Brazil
Citation	Cleland et al. (1984), Kurucz et al. (1995), Trump et al. (1984), Waite et al. (1989)	Gehringer et al. (1995), Pikaev et al. (1997, 2001), Pikaev 2002, 2000), Podzorova et al. (1998)	Han et al. (1997, 2002, 2005, 2012)	Duarte et al. (2002), Rela et al. (2000), Sampa et al. (1995)
Treatment object	Municipal sewage sludge, contaminated groundwater	Municipal wastewater	Textile dyeing wastewater	Drinking water and wastewater
Treatment method	Electron beam	Electron beam and ozone treatment	Electron beam and biological treatment	Electron beam
EB energy and power	1.5 meV, 75 kW	0.3 meV, 15 kW	1 meV, 400 kW	1.5 meV, 60 kW
Hydraulic behavior (velocity, thickness and concentration of the flow)	Flow is about 0.38 cm thick and velocity is 1.6 m/s during radiation. Variation in thickness is less than 10%. Allowing flow rate range is 230–610 L/min	Density of the aerosol flow is 0.02–0.05 g/cm^3. Diameter of droplets is 50–180 μm. Thickness of the aerosol flow is 9 cm. velocity is 9.65 m/s	Thin and wide jet flow is formed. The width of the jet flow is about 1.5 m. The velocity of the flow is about 3–4 m/s	Three kinds of up-flow EB reactors were studied from the view of hydrodynamic and mean absorbed dose, and the third one was chosen
Absorbed dose	Use calorimetry to measure mean absorbed dose. The efficiency of energy transfer is 65%	Dosimetry was conducted with cellulose triacetate films	Absorbed dose was measured by dichromate dosimeter	Use calorimetry to measure mean absorbed dose. The maximum efficiency of energy transfer is 75%
Required dose (kGy)	4	1.3	1–2	2
Max treatment amount (m^3/d)	654	500	10,000	1,680
Cost ($/m^3)	2		0.3	1.2

(continued)

Table 1 (continued)

Type of the reactor	Water fall EB reactors	Spraying EB reactors	Nozzle jet EB reactors	Up-flow EB reactors
Main advantage	Thin flow is appropriate for electron beam. Water fall is suitable for sludge for its high viscosity	Synergistic effects of EB and ozone reducing the required dose and the cost of water treatment	Large treatment amount. EB and biological treatment improve the treatment efficiency	Large treatment amount, better closed system, high energy transfer efficiency
Main disadvantage	Beyond the flow rate of 610 L/min, water splashes onto the scanner window	Small treatment amount. Lack of study on the hydrodynamic of the aerosol flow	The depth of the flow is very low, about 4–6 mm, the high uniformity of the flow ejected from the reactor is hard to achieve	Residence time of flow in the middle is longer than that of flow in the side-wall of the reactor, causing the dose distribution uneven

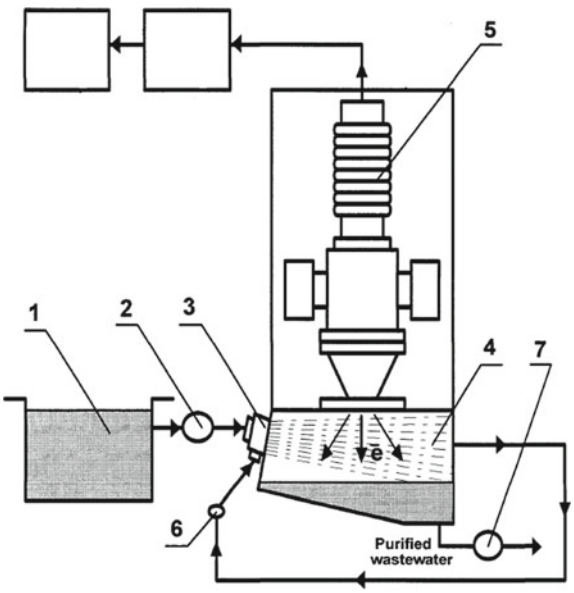

Fig. 2 The spraying EB reactor, (In Fig. 2, (1) is reservoir of wastewater intake, (2) is electric pump unit for wastewater moving, (3) is sprayer unit (it contains four sprayers) for production of the aerosol, (4) is irradiation chamber, (5) is electron accelerator, (6) is turboblower, and (7) is electric pump unit for purified wastewater removal.)

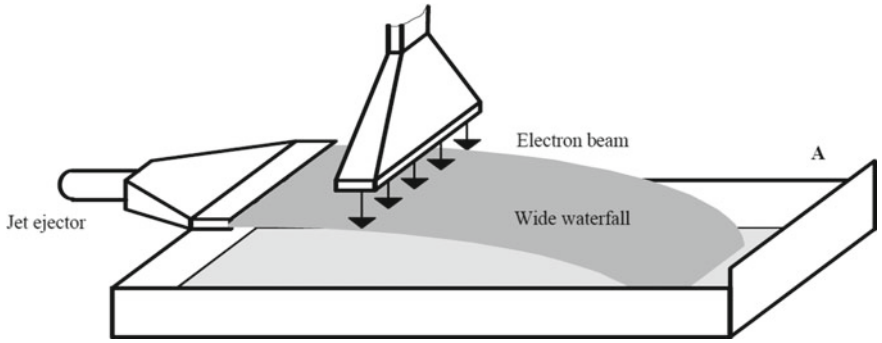

Fig. 3 The nozzle jet EB rector (Chmielewski 2009)

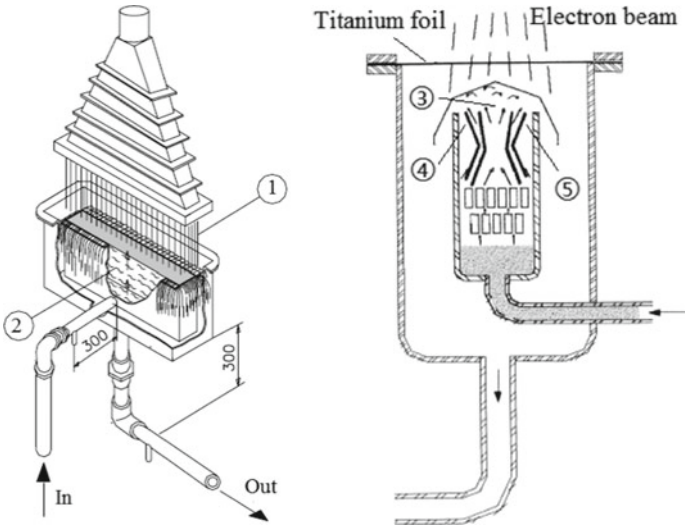

Fig. 4 Up-flow EB reactors (① is electron beam, ② is upward water, ③ is water in the middle of the reactor, ④ and ⑤ is water near the side wall of the reactor.) (Rela et al. 2000; Duarte et al. 2002)

The water fall EB reactor was shown in Fig. 1 (Kurucz et al. 1995). Thin and wide falling flow, formed by water fall EB reactors, is presented to electron beam. Water fall EB reactors are suitable for high viscosity liquid, sludge for example.

The spraying EB reactor was shown in Fig. 2, where irradiated air containing ozone can circulate through the irradiation chamber (Pikaev et al. 1997). Spraying EB reactors take the advantage of synergistic effects of electron beam and ozone treatment to reduce the requirement of absorbed dose and therefore reduce the cost of water treatment. The water and ozone was sprayed in the form of aerosol flow.

The nozzle jet EB reactor is shown in Fig. 3 (Chmielewski 2009). Wastewater was ejected horizontally from the nozzle jet EB reactor, forming the shape of the thin and

wide jet flow irradiated by the electron beam above. The flow formed by the nozzle jet EB reactor is very similar with the waterfall flow formed by the waterfall reactor.

The Up-flow EB reactors are shown is Fig. 4 (Rela et al. 2000; Duarte et al. 2002). Wastewater flows upwards through the up-flow EB reactor and then overflows the edge of the side wall of the reactor, during which irradiated by the electron beam above. There is a titanium foil window at the top of the up-flow EB reactor, allowing the reactor working as a closed system, avoiding the spread of gaseous by-products to the environment (Rela et al. 2000).

3 Absorbed Dose of Water Flow

Absorbed dose describes the amount of energy deposited in material exposed to electron beam, causing the biological and chemical effect of radiation. Absorbed dose can be defined as the amount of energy absorbed divided by the mass of material irradiated (Wang and Wang 2007), which could be expressed as follows:

$$D = \mathrm{d}E/\mathrm{d}m \tag{1}$$

where D is absorbed dose in Gray, 1 Gy = 1 J/kg, E is the amount of energy deposited in material in Joule, and m is the mass of material in kilogram.

The treatment efficiency of EB reactors is mainly determined by the uniformity of absorbed dose distribution of the flow. The more uniform distribution of the absorbed dose, the higher efficiency of EB reactors.

The relationship between the absorbed dose D in kilogray and the electron energy deposition D_e in the practical units is expressed by the following equation (Cleland et al. 2002):

$$D = 6.0 D_e I t / A \tag{2}$$

where I is the electron beam current intercepted by the material in milliamper, T is the treatment time in minute and A is the area of the material in square meter. Values of D_e are given in practical units of MeV per gram per square centimeter or MeV square centimeter per gram. The values of D and D_e must be specified at a particular depth in the material.

The electron beam was emitted in a plane and distributed evenly within the scan area. When electron beam is emitted vertically to homogeneous material, electron energy deposition D_e distributes evenly along horizontal direction, and the distribution of electron energy deposition D_e along penetration depth direction is shown in Fig. 5 (Kurucz et al. 1995). Curves in Fig. 5 shows the variation of electron energy deposition per incident electron per unit thickness vs. depth in pure water for electron energies from 0.5 to 2.0 meV, where R_{opt} (optimum penetration depth) is the equal-entrance, equal-exit parameter (IAEA 2011). For mid-energy (0.5–5 meV)

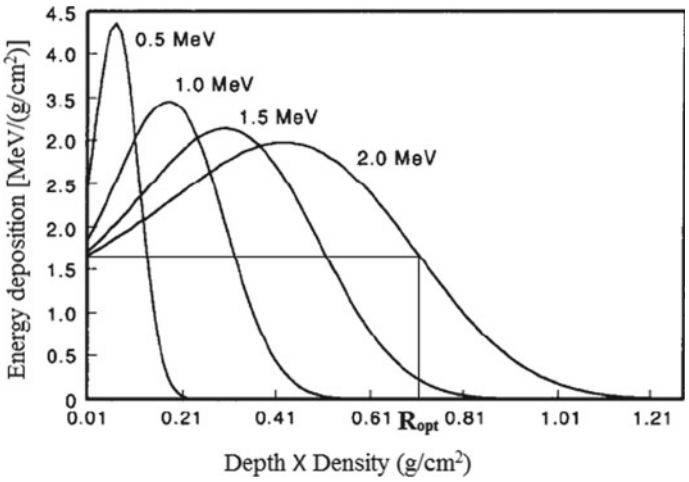

Fig. 5 Electron energy deposition versus depth X density in water

electron accelerators, it is common to express electron beam penetration on the basis of equal-entrance, equal-exit exposure in unit density material (IAEA 2011). As a result, it would be the best to make the thickness of the irradiated material equal to the optimum penetration depth R_{opt}.

As can be seen from Fig. 5, electron energy deposition D_e is related to electron energy E, the penetration depth h and material density ρ, which could be expressed in the following equation:

$$D_e = D_e(E, h, \rho) \tag{3}$$

Equation (2) is appropriate for homogeneous solid material. With regard to the flowing water, because of the complexity of water flow motion, it is necessary to take water elements as research units to study their motion characteristic and absorbed dose. Water elements irradiated by electron beam are shown in Fig. 6. A water element is made up of fluid particles and has a certain volume and quality. The absorbed dose of a water element could be calculate by studying its motion characteristic during irradiation. Absorbed dose distribution of the flow could be calculated by studying sufficient amount of water elements.

For EB reactors, besides the motion of water elements along x direction, there may also be velocity of water elements along y direction, causing the depth of a water element varying with time. Besides that, aerosol flow formed by the spraying EB reactor would make the density of water elements varying with time. Meanwhile, the electron energy deposition D_e is related to the penetration depth h and material density ρ. Therefore, the electron energy deposition in a water element would vary with time.

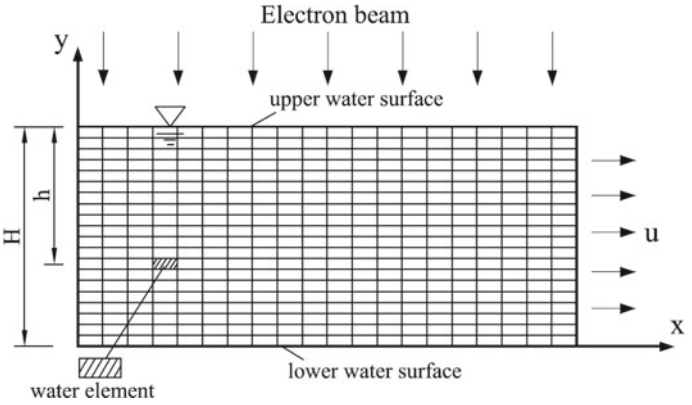

Fig. 6 Water elements irradiated by electron beam, (h is depth of the water element, H is the thickness of the flow)

According to Eqs. (2) and (3), absorbed dose of a water element could be expressed as:

$$D = \int_0^t 6.0 D_e \frac{I}{A} \mathrm{d}t = \int_0^t 6.0 D_e(E, h, \rho) \frac{I}{A} \mathrm{d}t \tag{4}$$

The electron beam current intercepted by material could be assumed evenly distributed. The energy of electrons emitted by electron accelerator is identical. And the area of water element could be assumed equally. Then, Eq. (4) becomes:

$$D = \int_0^t 6.0 D_e(E, h, \rho) \frac{I}{A} \mathrm{d}t = 6.0 \frac{I}{A} \int_0^t D_e(E, h, \rho) \mathrm{d}t \tag{5}$$

According to Eq. (5), the absorbed dose of a water element is mainly determined by its depth, density and residence time in electron beam. And the residence time of a water element is mainly determined by its velocity. As a result, the uniformity of absorbed dose distribution of the flow is mainly determined by velocity, depth (or thickness) and density distribution of the flow. In order to improve the uniformity of absorbed dose distribution of the flow and therefore improve the efficiency of the EB reactors, it's quite essential to study the hydrodynamic of EB reactors, including the velocity, depth (or thickness) and density distribution of the flow.

4 Hydrodynamic Behavior of EB Reactors

The hydrodynamic behavior of the waterfall and nozzle jet EB reactors are very similar. Both of them are thin, wide and fast moving flow, which fulfill the requirement of low penetration depth in water of electron beam. The waterfall flow is about 0.38 cm thick and velocity is 1.6 m/s during radiation. Variation in thickness is less than 10%. However, when the flow rate exceed 610 L/min (878 m^3/d), the water would splash onto the scanner window (Kurucz et al. 1995), which limits the treatment amount for EB reactors. This phenomenon indicate that besides the vertical velocity, horizontal flow velocity exist in the falling water, causing some part of water moving horizontally and therefore splash onto the scanner window. Hence, it's essential to study the hydrodynamic behavior of the water fall reactor to optimize the reactor.

For the nozzle jet EB reactor, thin and wide jet flow is formed. The treatment amount of the reactor could reach 10,000 m^3/d, while the width of the jet flow is about 1.5 m, and the velocity of the flow is about 3 m/s (Han et al. 2002, 2005, 2012). Author of this paper optimized the configuration of the nozzle jet EB reactor by a computational fluid dynamic method (Ding et al. 2017). Three key configuration parameters that affect the hydrodynamic behavior of the EB reactor were got from the simulation result, which were flow velocity of the reactor inlet, length of the horizontal contraction part, improvement of the bend part configuration. The optimal reactor configuration parameters were as follows: flow velocity of the reactor inlet is 0.76 m/s, length of the horizontal contraction part is 0.45 m, the configuration of the bend part should along the flow velocity direction. The hydrodynamic conditions of the optimal reactor was greatly improved, and a nozzle jet reactor of 2,000 m^3/d treatment amount is built.

The water and ozone was combined in the spraying EB reactors, and sprayed in the form of aerosol flow. The concentration of aerosol flow is decreasing along the flow direction, and the thickness of the aerosol flow is increasing along the flow direction. The velocity and thickness distribution of the flow under electron beam has a significant influence on the absorbed dose distribution which determined the EB treatment efficiency. However, there are very few studies on the velocity and thickness distribution of the aerosol flow which needs a further study.

As wastewater flows upwards through the up-flow EB reactor, shown in Fig. 4, the hydraulic residence time of flow in the middle of the reactor is longer than that of the flow near the side wall of the reactor, which might cause the absorbed dose distribution non-uniform, affecting the EB treatment efficiency. Hydraulic residence time distribution is mainly determined by the flow velocity distribution. As a result, it's necessary to study the hydrodynamic behavior of the up-flow EB reactor so as to study the residence time and absorbed dose distribution of the flow.

5 Research Prospect of EB Reactors

From the above analysis, it could be seen that study on EB reactors should focus on the study of absorbed dose distribution of the flow and therefore optimization of the EB reactors by making the absorbed dose evenly distributed as much as possible. Study on absorbed dose distribution of water flow is an inter-discipline composed of some different fields, including fluid mechanics and electron energy deposition in material. Currently there are very few researches on the hydrodynamic behavior of EB reactors. Previous studies mostly simply measure the velocity and thickness of the flow by experiment, lacking of studies on the flow velocity distribution, which has a significant effect on the residence time distribution of water elements in electron beam.

Calorimetry and different kinds of dosimeter were usually used in previous studies to measure mean absorbed dose of the water flow. There was hardly any research published on the absorbed dose distribution of water flow in EB reactors. That maybe because it's very difficult to obtain the absorbed dose distribution of water by experiment for continuous flow of EB reactors.

For the past few years, with the rapid development of computing technology, computational fluid dynamics (CFD) has been greatly and widely developed in many fields, especially in the field of reactors for water treatment, such as chlorine contact tanks (Angeloudis et al. 2014), ultraviolet reactors (Devia-Orjuela et al. 2018) and photocatalytic reactors (Boyjoo et al. 2013). Many researchers use CFD method to study the hydrodynamic behavior of different types of reactors, and therefore optimize the reactors to improve the treatment efficiency (Wols et al. 2011). However, there is very less paper published on the hydrodynamic behavior of EB reactors by CFD method, which should be conducted to study the velocity, depth and density distribution of the flow in EB reactors.

On the other hand, with the rapid development of computing technology, Monte Carlo method has been widely used in the field of calculation of particle energy deposition. For the uniformity of absorbed dose distribution of electron beam, Monte Carlo method is widely used in the field of radiotherapy treatment (Andreo 2018) and food irradiation (Kim et al. 2007). However, there was hardly any paper published on the dose distribution of water flow in EB reactors by Monte Carlo method, which should be studied to improve the uniformity of the absorbed dose distribution of the water flow.

5.1 Water Fall and Nozzle Jet EB Reactors

The jet flow formed by the nozzle jet EB reactor is very similar with the waterfall flow formed by the waterfall EB reactor, both of which are thin, wide and fast moving flow. Meanwhile, it would be the best to make the thickness of the irradiated material equal to the optimum penetration depth R_{opt}. As a result, the thickness of the thin and wide flow should be evenly distributed and equals to the optimum penetration depth R_{opt}.

When the thickness of the flow is evenly distributed, the distribution of electron energy deposition D_e along electron penetration depth direction is shown in Fig. 5, and electron energy deposition D_e distributes evenly along flow direction and flow width direction. For water fall and nozzle jet EB reactors, the velocity along flow thickness direction is small enough to ignore the motion of water element along flow thickness direction. As a result, the depth of a water element is identical during the irradiation process. According to Eq. (3), the electron energy deposition in the water element is identical during the irradiation process, and Eq. (5) becomes:

$$D = 6.0\frac{I}{A}\int_0^t D_e(E, h, \rho)\mathrm{d}t = 6.0\frac{I}{A}D_e(E, h, \rho)\cdot t \tag{6}$$

According to Eq. (6), in order to make the absorbed dose of the water flow distributed evenly along flow direction and flow width direction, the residence time of the water elements in electron beam as well as the thickness of the flow should be uniformly distributed, which means the velocity distribution of the flow should be uniform, in other words, the velocity along flow movement direction should be identical and there should be no velocity along flow width direction. Therefore, the hydrodynamic behavior of the water fall and nozzle jet EB reactors should be studied to make the velocity and thickness distribution of the flow uniform and therefore to improve the EB treatment efficiency.

CFD is a valid method to study and optimize the hydrodynamic behavior of EB reactors. Studying and optimization of water fall and nozzle jet EB reactors by CFD method should include following steps: (1) Built a three dimensional numerical flow model for the primary design EB reactor based on the previous study and the hydrodynamic objective of the EB reactor which is the velocity and thickness of the flow evenly distributed, (2) Calculate and analyze the flow field of the EB reactor, (3) Optimize the structure and size of the EB reactor based on the analysis of the flow field of the reactor to make the velocity distribution of the flow near the outlet of the reactor uniform, (4) Built a three dimensional numerical flow model of the reactor optimized by step (3), (5) Repeat the step (2) to step (4) continuously until get the promising result of the flow field of the EB reactor.

Author of this paper has already optimized the configuration of the nozzle jet EB reactor by a computational fluid dynamic method (Ding et al. 2017), greatly improving the hydrodynamic conditions of the reactor. But the uniformity of the absorbed dose distribution of the flow hasn't been studied, which directly determined the EB treatment efficiency.

5.2 Spraying EB Reactors

The wastewater and ozone was sprayed in the form of aerosol flow from the spraying EB reactor. The density of aerosol flow is decreasing along the flow direction, and

the thickness of the aerosol flow is increasing along the flow direction. Meanwhile, electron energy deposition in water D_e is related to the thickness and density of the flow. As a result, the varying of the thickness and density of the aerosol flow along flow direction would lead to the change of distribution of the electron energy deposition in water D_e and therefore change the absorbed dose distribution of the flow.

Hence, it's necessary to study the hydrodynamic behavior of the aerosol flow. Air-liquid two phase flow model could be used to study the velocity, thickness and density distribution of the aerosol flow along flow direction. Based on the result of the hydrodynamic study, the absorbed dose distribution of the aerosol flow could be calculated by Monte Carlo method. The spraying EB reactor could be optimized based on the Monte Carlo result to make the dose distribution uniform.

5.3 Up-Flow EB Reactors

The flow depth of the up-flow EB reactor is quite large, shown in Fig. 4, much bigger than the maximum penetration depth of electrons. So, the vast majority of the electron beam energy is deposited in the water flow, which is also verified by calorimetry that the energy transfer efficiency is 75% (Rela et al. 2000). However, the hydraulic residence time of the flow in the middle of the up-flow EB reactor is longer than that of the flow near the side wall of the reactor, which might cause the absorbed dose distribution non-uniform, affecting the EB treatment efficiency.

Water elements under electron beam would move along the horizontal and vertical direction. So the depth of a water element would change during radiation. The electron energy deposition in the water element would also changes with its depth varying. In addition, the residence time of the flow in the middle of the up-flow EB reactor is longer than that of the flow near the side wall of the reactor, which means that there are differences in residence time of different water elements. Both the depth and residence time of a water element in the up-flow EB reactor is related to the path of the water element. Therefore, according to Eq. (5), the absorbed dose of a water element is closely related to its trajectory in the flow.

CFD integrated with Monte Carlo method should be used to study the absorbed dose distribution of the up-flow EB reactor. Lagrangian method of fluid mechanics should be used to track the path of sufficient number of water elements to obtain the depth and velocity distribution of the water elements during irradiation. Once the depth distribution of a water element during irradiation is obtained, electron energy deposition in the water element during irradiation could be calculated by Monte Carlo method. Meanwhile, once the velocity and path of a water element is obtained, the residence time of the water element could be get. Then the absorbed dose of the water element could be obtained by Eq. (5). By studying sufficient quantity of water elements, absorbed dose distribution of the water flow in the up-flow EB reactor could be got.

6 Conclusions

Different kinds of EB reactors are categorized and introduced in this paper. The advantages and disadvantages of different kinds of EB reactors are analyzed from the perspective of fluid dynamics and the uniformity of absorbed dose distribution. Previous studies on EB reactors ignored the detailed hydrodynamic behavior of the EB reactors, including the velocity, thickness and density distribution of the flow, as well as their effects on the absorbed dose distribution. Further research areas of different types of EB reactors were proposed.

The research objective of water fall reactors and nozzle jet reactors is to make the thickness and velocity of the thin flow formed by the EB reactor evenly distributed. CFD method should be used to study the hydrodynamic behavior of the EB reactor and therefore optimize the EB reactor to achieve the objective. Study on spraying reactors should focus on the velocity, thickness and density distribution of the aerosol flow, as well as the influence of the varying thickness and density of the aerosol flow on absorbed dose distribution. Study on up-flow EB reactors should focus on tracking the path of water elements in complex hydrodynamic condition by Lagrangian method. CFD method integrated with Monte Carlo method should be used to study the absorbed dose distribution of the up-flow EB reactor and thus optimize the EB reactor.

Acknowledgements This study is financially supported by the National Key Research and Development Program of China (No. 2016YFC0401500), 7th sub-topic (No. 2016YFC0401507).

References

Abdou LAW et al (2011) Comparative study between the efficiency of electron beam and gamma irradiation for treatment of dye solutions. Chem Eng J 168(2):752–758

Andreo P (2018) Monte Carlo simulations in radiotherapy dosimetry. Radiat Oncol 13(1):121

Angeloudis A, Stoesser T, Falconer RA (2014) Predicting the disinfection efficiency range in chlorine contact tanks through a CFD-based approach. Water Res 60:118–129

Boyjoo Y, Ang M, Pareek V (2013) Some aspects of photocatalytic reactor modeling using computational fluid dynamics. Chem Eng Sci 101:764–784

Chmielewski AG (2009) Electron beam processing—what are the limits. International topical meeting on nuclear research applications and utilization of accelerators

Cleland MR, Fernald RA, Maloof SR (1984) Electron beam process for the treatment of wastes and economic feasibility of the process. Radiat Phys Chem 24:179

Cleland M, Galloway R, Genin F et al (2002) The use of dose and charge distributions in electron beam processing. Radiat Phys Chem 63(3):729–733

Devia-Orjuela JS, Betancourt-Buitrago LA, Machuca-Martinez F (2018) CFD modeling of a UV-A LED baffled flat-plate photoreactor for environment applications: a mining wastewater case. Env Sci Pollut Res Int

Ding R, Mao Z, Wang J (2017) CFD simulation and optimization of the water treatment reactor by electron beam. China Env Sci 37(3):980–988

Duarte CL, Sampa MHO, Rela PR et al (2002) Advanced oxidation process by electron-beam-irradiation-induced decomposition of pollutants in industrial effluents. Radiat Phys Chem 63(3):647–651

Gehringer P, Eschweiler H, Fiedler H (1995) Ozone-electron beam treatment for groundwater remediation. Radiat Phys Chem 46(4):1075–1078

Getoff N (2002) Factors influencing the efficiency of radiation-induced degradation of water pollutants. Radiat Phys Chem 65(4–5):437–446

Han B, Kim DK, Pikaev AK (1997) Research activities of Samsung heavy industries in the conservation of the environment. In: Radiation technology for the conservation of the environment, proceedings of the symposium held in Zakopane, Poland, 8–12 September 1997. IAEA, Vienna, pp. 339–347

Han B, Ko J, Kim J, et al (2002) Combined electron-beam and biological treatment of dyeing complex wastewater. Pilot plant experiments. Radiat Phys Chem 64(1):53–59

Han B, Kim J, Kim Y et al (2005) Electron beam treatment of textile dyeing wastewater: operation of pilot plant and industrial plant construction. Water Sci Technol 52(10–11):317–324

Han B, Jin KK, Kim Y et al (2012) Operation of industrial-scale electron beam wastewater treatment plant. Radiat Phys Chem 81(81):1475–1478

Han D, Currell MJ, Cao G (2016) Deep challenges for China's war on water pollution. Environ Pollut 218:1222–1233

IAEA (2011) Industrial radiation processing with electron beams and X-rays. Int Atomic Energy Agency 1 May 2011–Revision 6:5–6

Jan S, Kamili AN, Parween T et al (2015) Feasibility of radiation technology for wastewater treatment. Desalin Water Treatment 55(8):2053–2068

Kim J et al (2007) 3-D dose distributions for optimum radiation treatment planning of complex foods. J Food Eng 79(1):312–321

Kurucz CN, Waite TD, Cooper WJ (1995) The Miami electron beam research facility: a large scale wastewater treatment application. Radiat Phys Chem 45(2):299–308

Lee O et al (2015) A comparative study of disinfection efficiency and regrowth control of microorganism in secondary wastewater effluent using UV, ozone, and ionizing irradiation process. J Hazard Mater 295:201–208

Mahendra AK, Sashi KGN, Sanyal A et al (2010) Design optimization of sludge hygenization research irradiator. Int J Emerg Multidiscip Fluid Sci 2(1):59–71

Mahendra AK, Sanyal A, Gouthaman G (2011) Simulation and optimization of sludge hygienization research irradiator. Comput Fluids 46(1):333–340

Pikaev AK (2000) Current status of the application of ionizing radiation to environmental protection: III. Sewage sludge, gaseous and solid systems (A review). High Energy Chem 34(3):129–140

Pikaev AK (2002) New data on electron-beam purification of wastewater. Radiat Phys Chem 65(65):515–526

Pikaev AK, Podzorova EA, Bakhtin OA (1997) Combined electron-beam and ozone treatment of wastewater in the aerosol flow. Radiat Phys Chem 49(1):155–157

Pikaev AK, Podrozova EA, Bakhtin OM, Lysenko SL, Belyshev VA (2001) Electron beam technology for purification of municipal wastewater in the aerosol flow. IAEA-TECDOC-1225, IAEA, Vienna, Austria, pp 45–55

Podzorova EA, Pikaev AK, Belyshev VA et al (1998) New data of electron-beam treatment of municipal wastewater in the aerosol flow. Radiat Phys Chem 52(52):361–364

Rela PR, Sampa MHO, Duarte CL et al (2000) Development of an up-flow irradiation device for electron beam wastewater treatment. Radiat Phys Chem 57(3):657–660

Sampa MHO, Somessari ES, Lug OAB (1995) The use of electron beam accelerator for the treatment of drinking water and wastewater in Brazil. Radiat Phys Chem 46(4–6): 1143–1146

Skowron K, Paluszak Z, Olszewska H et al (2014) Effectiveness of high energy electron beam against spore forming bacteria and viruses in slurry. Radiat Phys Chem 101(31):36–40

Spinks JWT, Woods RJ (1990) An introduction to radiation chemistry. Radiat Res 124(3):403–408

Trump J, Merill E, Wright K (1984) Disinfection of sewage wastewater and sludge by electron treatment. Radiat Phys Chem 24:55

Waite T, Kurucz C, Cooper W, Narbaitz R, Greenfield J (1989) Disinfection of wastewater effluents with electron radiation. In: Proceedings of the 1989 specialty conference on environmental engineering, ASCE, 619

Wang J, Chu L (2016) Irradiation treatment of pharmaceutical and personal care products (PPCPs) in water and wastewater: an overview. Radiat Phys Chem 125:56–64

Wang J, Wang J (2007) Application of radiation technology to sewage sludge processing: A review. J Hazard Mater 143(s1–s2):2–7

Wang Q, Yang Z (2016) Industrial water pollution, water environment treatment, and health risks in China. Environ Pollut 218:358–365

Wols BA et al (2011) A systematic approach for the design of UV reactors using computational fluid dynamics. American Institute of Chemical Engineers. AIChE J 57(1):193

Environmental Impacts of the Selected Building Structures

Adriana Estokova, Alena Paulikova and Eva Singovszka

Abstract Environmental assessment of buildings and materials' impacts is of great importance because of reduction of the negative influence of construction sector to the environment. The paper presents a study of the environmental evaluation of the vertical structures made of brick, aerated concrete and reinforced concrete as core wall materials. Two types of the insulation materials were considered whereas the material composition of the walls was designed to ensure the same thermal performance of the structure. For each material composition, the following environmental indicators were calculated per 1 m^2 of the structure: the primary energy (PEI), the global warming potential (GWP) and the acidification potential (AP). The calculation was based on the unit data originating from a selected Life cycle analysis (LCA) data-base. Multi-criterial analysis was applied to identify the most appropriate composition when considering also the physical parameters of the walls. The findings revealed that the most environmentally sound wall composition was represented by aerated concrete insulated by graphite polystyrene.

Keywords Buildings · Environmental assessment · GWP

1 Introduction

The environmental assessment of building materials, buildings, processes and technologies in construction sector is becoming an indispensable tool for effective reducing the negative impacts of the construction to the environment.

A. Estokova (✉) · E. Singovszka
Faculty of Civil Engineering, Technical University of Kosice, Vysokoskolska 4, 04200 Kosice, Slovakia
e-mail: adriana.estokova@tuke.sk

A. Paulikova
Faculty of Materials Science and Technology in Trnava, Slovak University of Technology in Bratislava, Jana Bottu 25, 91724 Trnava, Slovakia

R. Sun and L. Fei (eds.), *Sustainable Development of Water and Environment*, Environmental Science and Engineering,
https://doi.org/10.1007/978-3-030-16729-5_10

Research on environmental impact assessment of buildings has been taking place for a long time (Asif et al. 2007; Abanda et al. 2014; Mitterpach and Štefko 2016; Keun et al. 2015; Pujadas-Gispert et al. 2018). However, the assessment methods are still not completely harmonised even though they are based on LCA approach. Various methods offer various results classified in different categories. In buildings research, the greatest attention is still devoted to the energy demands of buildings and materials, their global warming potentials (GWP), and acidification potentials (AP). Sartori and Hestnes (2007) reported that the embodied energy in materials varied between 9 and 46% of the overall energy used over the building's lifetime when dealing with low energy consumption buildings. The findings revealed that the environmental load of the buildings or particular constructions could be decreased by a selection of the building materials with the environmentally sound properties (Estokova and Porhincak 2015). According to (Thormark 2006), embodied energy in conventional buildings can be reduced by approximately 10–15% through proper selection of building materials with low environmental impacts.

This paper aims to compare the vertical constructions of various compositions in order to find the environmentally optimal composition provided that the functional properties are preserved and thermal performance of house envelope is the same for all materials alternatives.

2 Materials and Methods

2.1 Vertical Structures

The vertical structures with three types of the load materials have been investigated: Type A was represented by the brick walls, Type B included the aerated concrete and Type C the reinforced concrete blocks. On the basis of how often individual building materials are used in family houses construction, a number of variants were selected from individual load-bearing materials. Type A involved 96 wall variants, Type B 52, and Type C only 8 alternatives. All the structures were insulated by expanded polystyrene boards (EPS) or mineral insulation. A combination of various thicknesses of the core materials and the insulations was investigated. However, the primary aim was to compare the structures with the same thermal performance expressed by the value of the heat transfer coefficient U = 0.2 W/(m^2 K). Therefore, the overall thicknesses of the structures analysed differed as well. All other components of the structures were designed to be identical including internal and external plasters.

2.2 Environmental Assessment

The function unit for the environmental analysis was set to the unit area (1 m^2) of the structure with the same thermal performance. For each material composition of the vertical structure, the following environmental indicators were calculated: the

primary energy (PEI), the global warming potential (GWP) and the acidification potential (AP). The calculations were made using a simple calculation tool in MS Excel multiplying the LCA unit values for the individual building materials by their masses (Eqs. 1–3). The LCA unit values of materials have been taken from the IBO database (Waltjen et al. 2009) while taking into account the mandatory boundaries in the EPD assessment from cradle to gate (ISO EN 15804:2012). Global warming potential of analysed building materials was calculated considering the data for 100-year time horizon.

$$\mathrm{PEI} = \sum_{i} m_i \cdot \mathrm{PEI}_i, \ (\mathrm{MJ}) \tag{1}$$

$$\mathrm{GWP} = \sum_{i} m_i \cdot \mathrm{GWP}_i, \ \left(\mathrm{kg\ CO_2eq}\right) \tag{2}$$

$$\mathrm{AP} = \sum_{i} m_i \cdot \mathrm{AP}_i, \ \left(\mathrm{kg\ SO_2eq}\right) \tag{3}$$

where m_i is weight of the individual building material and PEI_i, GWP_i, and AP_i represent the unit value of that material per 1 kg for primary energy, global warming potential, and acidification potential, respectively. The overall environmental load of structures was expressed in $\mathrm{MJ/m^2}$ for the PEI, in kg $\mathrm{CO_2eq/m^2}$ for GWP, and in kg $\mathrm{SO_2eq/m^2}$ for AP indicators.

2.3 Multi-criterial Evaluation

The multi-criteria analysis was used to determine the order of material alternatives of individual constructions based on the analysis of a higher number of criteria, including environmental parameters (primary energy (PEI), global warming potential (GWP) and the acidification potential (AP)), and technical parameters (number of layers, thickness, weight and interior surface temperature).

To select an optimal alternative of wall composition, the weighted sum approach (WSA) method, as a part of the MCA7 software, was used. The weighted sum method is based on the principle of maximizing the effect with respect to the evaluator's ideas. The method is based on the linear function of the utility on a scale from 0 to 1. The worst variant had the value of 0, the best had the value of 1 and all the others were within this interval (Korviny 2010). The alternative that achieved the highest utility value was determined to be the best. Other wall alternatives were arranged according to the decreasing value of the utility.

For the purpose of setting weights of analysed parameters in this article, subjective weighing was used, while a paired comparison method was used by means of the Fuller triangle. When calculating the weights using the Fuller triangle, the individual criteria were ranked by creating a pair of criteria, each pair being present in the set only once. The authors then marked, in each pair, the criterion they considered

Table 1 Designed scales for the multi-criteria analysis of vertical structures

Variant	Layers	Thickness	Weight	PEI	GWP	AP	θ_{si}
MV 1	15	45	35	–	–	–	5
MV 2	–	–	–	45	35	20	–
MV 3	20	25	15	9	8	5	4
MV 4	5	9	8	25	20	15	4

important. The calculation became simpler because it enabled dividing 100% of the weight between the individual criteria without having to consider all the parameters simultaneously. The weight of the individual criteria was calculated according to Eq. (4) (Linkov and Moberg 2012).

$$v_i = \frac{n_i}{N} \tag{4}$$

where n_i represents the number of markings of importance for a given criteria, and N is the total number of marks.

Four variants of weighing (Table 1) were considered for the multi-criteria analysis of the vertical structures. The scale values have been chosen as per subjective consideration by the authors.

In the MV1 variant, only the technical parameters were included in the analysis; the environmental criteria were not considered at all. The thickness of the structure was given the highest importance, followed by the number of material layers, the weight and the internal surface temperature. This approach represents a conventional evaluation of the wall alternatives.

The MV2 variant considered only the environmental parameters; the thermal and physical parameters were not considered. In this variant, PEI was considered the most important, followed by GWP and then AP.

In the MV3 variant, all analysed parameters were considered, with the highest importance being assigned to the conventional criteria, in particular, thickness, number of layers and weight, PEI and GWP. Lower significance was assigned to the surface temperature and the acidification. Even the weighting process itself contains the elements of subjectivity.

For the MV4 variant, all analysed parameters were considered as well; however, the highest emphasis was placed on two environmental criteria (PEI, GWP, and AP), followed by the conventional thickness. A lower significance was associated with weight, number of layers and surface temperature of the structure. The Fuller triangle method was used to set the weights similar to MV3. These preferences are expressed in priorities or weights and indicate trade-offs between the criteria.

3 Results and Discussion

The environmental parameters were calculated in the range 649.95–1754.01 MJ/m^2 for PEI, 51.74–131.53 kg CO_2eq/m^2 for GWP, and 0.15–0.62 kg SO_2eq/m^2 for AP as presented in Fig. 1. The calculated values are similar with the results found by other authors who analysed the environmental properties of building materials in various building constructions (Gustavsson and Joelsson 2010; Abd Rashid and Yusoff 2015; Vilcekova et al. 2015).

The lowest PEI value (649.9 MJ/m^2) was calculated for the wall made of 300-mm thick aerated concrete with insulation of graphite polystyrene. The highest PEI value was calculated for the wall made of reinforced concrete insulated by mineral wool (1754 MJ/m^2). A high PEI up to 1421 MJ/m^2 was achieved for the brick wall (300 mm) with mineral wool insulation.

The same trend was observed regarding the amount of embodied CO_2 and SO_2 emissions. The lowest value of GWP (51.7 kg CO_2eq/m^2) and AP (0.15 kg SO_2eq/m^2) were associated with the 300-mm thick aerated concrete wall with the graphite EPS, while the highest value to the reinforced concrete wall with mineral insulation (GWP = 131.5 kg CO_2eq/m^2; AP = 0.62 kg SO_2eq). The brick wall load varied,

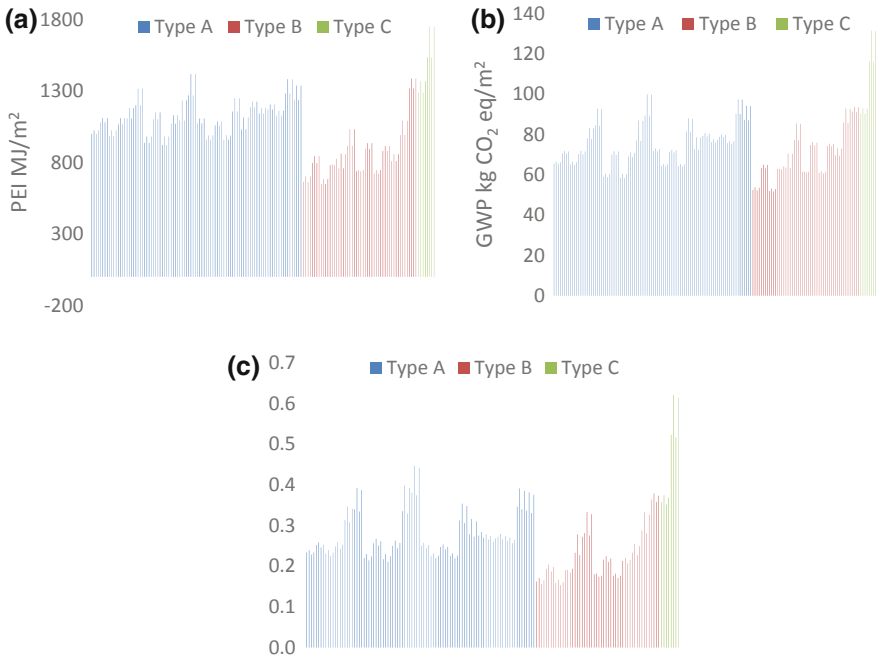

Fig. 1 Primary energy (**a**), Global warming potential (**b**), and Acidification potential (**c**) of the evaluated structures

Table 2 Summary of technical and environmental parameters of the vertical structures

	No. of layers	Thickness (mm)	Weight (kg/m^2)	PEI (MJ/m^2)	GWP (kg CO_2 eq/m^2)	AP (kg SO_2 eq/m^2)	θ_{si} (°C)
Minimum	6.00	383.00	153.96	649.95	51.74	0.1532	18.24
Maximum	7.00	553.00	553.06	1754.01	131.53	0.6205	18.33
Mean	6.08	474.03	320.33	1058.16	75.17	0.2734	18.29
Median	6.00	473.00	341.21	1074.21	72.74	0.2556	18.28

Table 3 List of the most and least suitable structures, considering only conventional technical parameters

	The best alternatives		The worst alternatives	
	No. of structure	Value	No. of structure	Value
MV1	B4	0.948	A93	0.303
	B2	0.948	A75	0.299
	B8	0.916	A73	0.299
	B6	0.916	A91	0.296
	A35	0.827	A89	0.296

Table 4 List of the most and least suitable structures considering only environmental parameters

	The best alternatives		The worst alternatives	
	No. of structure	Value	No. of structure	Value
MV2	B11	1.000	A46	0.349
	B9	0.996	C7	0.201
	B3	0.990	C5	0.197
	B1	0.987	C8	0.004
	B12	0.978	C6	0.000

having the worst GWP (99.9 kg CO_2eq/m^2) and AP (0.44 kg SO_2eq/m^2) values for the 300 mm brick wall with mineral wool.

Based on the above results, it can be stated that the most environmentally suitable material composition is assigned to the material group represented by aerated concrete insulated by graphite polystyrene. The numerical comparison of the individual variables in the form of minimum and maximum values as well as the average values is given in Table 2.

Tables 3, 4 and 5 show the ranking of the five best and five worst construction compositions for individual weighting variants (MV1–MV4) based on the multi-criteria analysis of all construction compositions. Compositions are listed in order from the most appropriate to the least appropriate wall alternatives.

For the MV1 variant, where the suitability of the material compositions of the constructions was assessed only from the point of view of the conventional requirements, and the environmental parameter was assigned zero importance, the material alternative B4 (aerated concrete 300 mm, EPS 80 mm) was identified as the best

Table 5 List of the most and least suitable structures, considering both environmental and technical parameters

	The best alternatives		The worst alternatives	
	No. of structure	Value	No. of structure	Value
MV3	B4	0.955	A95	0.354
	B2	0.954	A93	0.353
	B8	0.903	A90	0.344
	B6	0.903	A91	0.339
	B25	0.851	A89	0.338
MV4	B9	0.879	C3	0.361
	B6	0.877	A92	0.356
	B2	0.869	A90	0.341
	B10	0.868	C6	0.268
	B4	0.867	C4	0.266

composition. This wall composition was assigned a small thickness, low weight and better surface structure temperature in comparison to the other structures. This alternative was followed by other aerated concrete structures with the EPS of various thicknesses. Only one alternative of Type A, based on 300-mm brick with 120-mm graphite EPS (A35) was labelled as another optimal variant.

If only environmental criteria were to be considered in the MV2 analysis, the vertical wall made of 300-mm aerated concrete and 70-mm EPSg (B11) would be considered the best option, which would mean a composition with minimum values of the environmental indicators PEI, GWP and AP. Similarly, other constructions of aerated concrete and graphite polystyrene (B9, B12), or ordinary polystyrene (B3 and B1) of various thicknesses were identified as environmentally suitable as well. By contrast, the material alternatives with reinforced concrete and mineral wool (180–200 mm) were found to be the least environmentally suitable compositions (C5-C8). In these compositions, the highest values of embodied CO_2 and SO_2 emissions, and primary energy were recorded. The brick construction A46 (brick 300 mm + mineral wool 150 mm) was designated as inappropriate as well.

For the MV3 variant, which represents a combination of conventional and environmental criteria with more significant attention given to technical parameters, the calculations identified the thickest aerated concrete blocks with EPS insulation (B2, B4, B6, and B8) as the most appropriate wall compositions. These are walls with relatively low thickness, lower weight, better thermo-technological parameters and lower negative impact on the environment. The thicker aerated concrete blocks of 375 mm and EPS thermal insulation were also found to be suitable (B25). The brick structures 440 mm with mineral insulation (80–90 mm) (A89-A91, A93 and A95) were identified as the least appropriate structures. These material alternatives were relatively thick but heavy and had considerable impact on the environment.

The wall made of 300-mm thick aerated concrete with 70-mm thick graphite polystyrene insulation (B9) was identified as the most appropriate one in the MV4

variant. MV4 analysis considered a combination of conventional and environmental criteria, with more importance being given to the environmental parameters. The material alternatives B6, B2, B10, and B4 can also be considered as optimal. By contrast, the least suitable compositions, based on the MV4 analysis, have been identified as the walls made of reinforced concrete with the mineral wool insulation (200 mm)—C3-C6. These walls exhibited high weight and their impacts on the environment has been considerably negative (high values of PEI, GWP and AP). Compositions A90 and A92 (440 mm of brick and 90 mm of mineral wool) were similarly labelled as less optimal, parallel to the wall (320 mm reinforced concrete wall, 180 mm mineral wool).

Comparing the results of the multi-criteria analysis, there is no fundamental difference between the material compositions of the most suitable wall alternatives from the environmental and technical perspective. The Type B wall compositions, made of aerated concrete, have been proved the best performance followed by Type A, made of brick. The worst environmental performance was identified for the Type C, wall compositions made of reinforced concrete. Regarding the insulation materials, the better environmental parameters were associated with the polystyrene thermal insulation, both ordinary EPS and graphite polystyrene EPSg. The walls with the mineral insulation (rock wool) reached the higher negative environmental impacts.

4 Conclusion

The paper presents the analysis of the environmental performance of the vertical structures made of the conventionally used masonry materials in the region of the Central Europe. The simplified multi-criterial analysis was used to identify the optimal constructions regarding their environmental impacts when considering also their technical parameters.

The order of the individual materials according to the best achieved score is as follows: aerated concrete > brick > reinforced concrete. The structures with the aerated concrete were identified as the best even when considering only environmental parameters. The findings revealed that, the analysed vertical structures with the mineral insulation contributed to the negative environmental impacts of the constructions more than those of the same materials but with the polystyrene insulation. Nevertheless, more research is needed to conclude a definite conclusion.

Acknowledgements This research was funded by VEGA—Scientific Grant Agency of the Ministry of Education, Science, Research and Sport of the Slovak Republic and the Slovak Academy of Sciences, grant number 1/0648/17.

References

Abanda FH, Nkeng GE, Tah JHM, Ohanjah ENF, Manijia MB (2014) Embodied energy and CO_2 analysis of mud-brick and cement-block houses. Energy 2(1):18–40

Abd Rashid AF, Yusoff S (2015) A review of life cycle assessment method for building industry. Renew Sustain Energy Rev 45:244–248

Asif M, Muneer T, Kelley R (2007) Life cycle assessment: a case study of a dwelling home in Scotland. Build Environ 42:1391–1394

Estokova A, Porhincak M (2015) Environmental analysis of two building material alternatives in structures with the aim of sustainable construction. Clean Techn Environ Policy 17:75–83

Gustavsson L, Joelsson A (2010) Life cycle primary energy analysis of residential buildings. Energ Build 42:210–220

ISO EN 15804:2012+A1:2013 Sustainability of construction works. Environmental product declarations. Core rules for the product category of construction products

Keun HY, Tae HK, Seung JR (2015) Analysis of lifecycle CO_2 reduction performance for long-life apartment house. Env. Progress Sust Energ 34(2):555–556

Korviny P (2010) MCA7, v 2.6. Software, manual

Linkov I, Moberg E (2012) Multi-criteria decision analysis: environmental applications and case studies, 1st edn. CRC Press, Boca Raton

Mitterpach J, Štefko J (2016) An environmental impact of a wooden and brick house by the LCA Method. Key Eng Mat 688:204–209

Pujadas-Gispert E, Sanjuan-Delmás D, Josa A (2018) Environmental analysis of building shallow foundations: the influence of prefabrication, typology, and structural design codes. J Clean Prod 186:407–417

Sartori I, Hestnes AG (2007) Energy use in the life-cycle of conventional and low-energy buildings: a review article. Energ Build 39:249–257

Thormark C (2006) The effect of material choice on the total energy need and recycling potential of a building. Build Environ 41:1019–1026

Vilcekova S, Culakova M, Kridlova-Burdova E, Katunska J (2015) Energy and environmental evaluation of non-transparent constructions of building envelope for wooden houses. Energies 8:11047–11075

Waltjen T, Pokorny W, Zegler T, Torghele K, Mötzl H, Bauer B, Boogmann P (2009) Details for passive houses: A catalogue of ecologically rated constructions, 3rd edn. Springer, Wien

Analysis of Haze Pollution Based on Principal Component Analysis in Jinan City

Haoqiang Zhao and Fang Luo

Abstract With the rapid development of economy, the quality of atmospheric environment is gradually getting worse, and the frequent occurrence of haze weather has seriously affected people's lives. Taking Jinan City as the research object, this paper adopts the method of principal component analysis, and selects 13 indexes such as regional gross product, secondary industry proportion, motor vehicle ownership, central heating area, etc. Based on the data from 2007 to 2016, this paper analyzes the haze pollution situation in Jinan City. The results show that from 2007 to 2015, the haze pollution situation in Jinan City showed an upward trend. In 2015, the haze pollution in Jinan City reached its peak. After that, the haze pollution change showed a downward trend until 2016, and the atmospheric environment gradually improved. Two principal components were extracted from the results of principal component analysis. Among them, the socioeconomic factors with variance contribution rate of 65% contributed the most to the haze pollution in Jinan City, followed by the natural environment factors.

Keywords Haze pollution · Principal component analysis · Jinan city

1 Introduction

With the rapid development of economy, frequent environmental problems and frequent haze weather have seriously affected the production and life of the people. According to the definition of haze by the China National Meteorological Administration's "Ground Meteorological Observation Code", fog refers to a large number of small droplets of water suspended in the air, usually milky white, making the

H. Zhao · F. Luo (✉)
School of Water Conservancy and Environment, University of Jinan, 250022 Jinan, China
e-mail: stu_luof@ujn.edu.cn

H. Zhao
Institute of Tibetan Plateau Research, Chinese Academy of Sciences, 100101 Beijing, China

University of Chinese Academy of Sciences, 100049 Beijing, China

R. Sun and L. Fei (eds.), *Sustainable Development of Water and Environment*, Environmental Science and Engineering,
https://doi.org/10.1007/978-3-030-16729-5_11

horizontal visibility of the atmosphere less than 1.0 km; Haze refers to the weather phenomenon in which a large number of extremely small dust particles are evenly suspended in the atmosphere, causing the horizontal visibility of the atmosphere to be less than 10 km (China Meteorological Administration 2003).

Research on the mechanism of haze occurrence and its impact on the environment has been the focus of domestic and foreign scholars. Yin et al. studied the meteorological observations of Jinan City from 1961 to 2013 and found that the number of fog days in the city has generally fluctuated and decreased with the years, and the number of haze days has shown a trend of "increase, decrease and increase" with the years (Yin et al. 2014). Studies of haze in Malaysia, such as Latif, have found that peat fires caused by traditional agricultural production methods in the peat area in Malaysia are the main source of atmospheric pollutants (Latif et al. 2018). Davis conducted a simulation study of the smoke incident in London and found that the main causes of the smoke incident in London were dust and coal pollution, and indirectly caused by the accumulation of pollutants in the atmosphere (Davis 2002). Hu proposed that the unscientific energy consumption structure, uncontrolled industrial exhaust emissions, the continuous increase in the number of motor vehicles, and the large amount of building dust brought about by the urbanization process are the economic reasons for the continuous deterioration of haze weather (Hu 2013). Rong and Feng used two statistical methods to make empirical analysis of haze pollution. The results showed that the proportion of secondary industry, urban area, and vehicle ownership contributed greatly to haze, among which the number of motor vehicles had the greatest impact (Rong and Feng 2015). Kang et al. analyzed the haze weather in Seoul and pointed out that SO_4^{2-}, NO_3^-, NH_4^+, and organic matter are the two components with the highest content in PM2.5, and their contribution to reduced visibility is the most obvious (Kang et al. 2013). According to studies on the relationship between economic development and environmental pollution, Quah et al. found that Singapore's economic losses caused by haze weather in 1999 alone accounted for more than 4% of GDP in that year (Quah and Boon 2003). Dong and Tai have proposed to improve and optimize the urban energy structure, vigorously promote the development of new energy industries, and improve the level of urban fuel cleaning to solve the problem of haze pollution in Chinese cities effectively (Dong and Tai 2014).

2 Materials and Methods

2.1 Research Area

Jinan City is the capital of Shandong Province, located in the central and western part of Shandong Province, at the intersection of the hilly area in the central and southern part and the alluvial plain in the northwest part of Shandong Province. In recent years, with the acceleration of urbanization in Jinan City, haze weather frequently appears.

The terrain is high in the south and low in the north in Jinan City. High-pressure cold cyclones blow from the north to the south, which is not conducive to the diffusion of pollutants and further aggravates the influence of haze. Haze weather has become a problem that can not be ignored in the development of Jinan City.

2.2 Methods

In this paper, principal component analysis (PCA) is adopted to reduce dimensionality of evaluation indexes with certain correlation, so that they can be recombined into a group of new unrelated comprehensive evaluation indexes to replace the original indexes, so that they can retain as much information as possible contained in the original variables, and improve the accuracy of the comprehensive evaluation results.

2.3 Index Selection

The formation of haze weather is not only affected by pollution sources, but also has a great deal to do with local meteorological conditions. Referring to the research results of other scholars (Liu 2011; Gong et al. 2017; Cheng 2016; Wu et al. 2007; Ren et al. 2017) and combining with the specific situation of Jinan City, 13 indicators related to the formation of haze pollution were selected (Table 1).

Table 1 Haze pollution index of Jinan City

Haze pollution index	Variable name
GDP ($100 million)	GDP
Population density (person/square kilometer)	POP
Proportion of secondary industry (%)	SI
Energy consumption per 10,000 yuan of GDP (tons of standard coal/ 10,000 yuan)	EC
Central heating area (10,000 square meters)	HA
Building construction area (square kilometers)	CA
Number of civil motor vehicles (10,000)	CAR
Green coverage area (km^2)	GA
SO_2 annual discharge (ton)	SO2
Annual emission of smoke and dust (tons)	DE
Ammonia nitrogen emission (ton)	NE
Annual precipitation (mm)	P
Annual average wind speed (0.1 m/s)	WS

2.4 Data Source

The data in this paper are mainly from the standard annual economic, urban construction and social development data in the statistical yearbook of shandong province from 2007 to 2016, and the meteorological data of Jinan City in the daily data set of China's surface climatic data from 2007 to 2016.

3 Results

SPSS22.0 was used for principal component analysis, and 13 indexes were formed into a comprehensive evaluation index system of haze pollution. The correlation coefficient matrix of each index is calculated for the normalized data. According to the correlation coefficient matrix, the characteristic values and the contribution rate and cumulative contribution rate of each principal component are calculated. The calculation results are shown in Table 2.

As can be seen from Table 2, the eigenvalues of the first two principal components are greater than 1, and their cumulative variance contribution rate reaches 89.57%, so the two principal components are extracted. The degree of correlation between the extracted principal component and the original variable index is represented by the loading value of the factor. The higher the loading value of the factor, the more information that the factor covers the index. The principal components are independent of each other and can represent a class of components independently of other factors. Table 3 shows the principal factor loading matrix after orthogonal rotation.

Table 2 Total variance explained

Component	Initial eigenvalues			Extraction sums of squared loadings		
	Total	% of variance	Cumulative %	Total	% of variance	Cumulative %
1	8.554	65.8	65.801	8.554	65.801	65.8
2	3.09	23.77	89.57	3.09	23.769	89.57
3	0.809	6.223	95.79			
4	0.357	2.748	98.54			
5	0.102	0.787	99.327			
6	0.06	0.459	99.786			
7	0.016	0.126	99.912			
8	0.01	0.076	99.988			
9	0.002	0.012	100			

Table 3 Component matrix after rotation

Variable	F_1	F_2
GDP	0.9886	0.0827
POP	0.9823	0.0547
SI	−0.9813	0.0346
EC	−0.9829	−0.1075
HA	0.9895	−0.0722
CA	0.9879	0.0889
CAR	0.9943	−0.0061
GA	0.9790	−0.1705
SO_2	−0.2307	0.9076
DE	0.4536	0.7052
NE	0.0445	0.9403
P	−0.0107	−0.8912
WS	0.7029	0.2260

Table 4 Score

Variable	F_1	F_2
GDP	0.34	0.01
POP	0.34	−0.01
SI	−0.33	0.06
EC	−0.34	−0.02
HA	0.34	−0.08
CA	0.34	0.01
CAR	0.34	−0.04
GA	0.33	−0.13
SO2	−0.06	0.52
DE	0.17	0.38
NE	0.04	0.53
P	−0.02	−0.51
WS	0.25	0.1

It can be seen from Table 3 that: (1) F1, the first principal component, is heavily loaded on GDP, POP, SI, EC, HA, CA, CAR and GA, among which GDP, SI and EC reflect the level of regional economic development; POP, CA and GA reflect the status of urban development. HA and CAR reflect the living standard of residents. Therefore, the first principal component can be named "socio-economic factor". (2) the second principal component F2 has a large load on SO_2, DE, NE and P, reflecting the natural environment of the region. The score coefficients of the first two principal components on 13 indicators are shown in Table 4.

Table 5 2007–2016 Comprehensive score of haze pollution of Jinan City

Year	F_1	F_2	F
2016	4.406	−3.652	2.268
2015	3.795	1.333	3.141
2014	2.778	1.704	2.493
2013	0.831	0.177	0.657
2012	0.005	1.292	0.346
2011	−0.532	2.204	0.194
2010	−1.695	−1.568	−1.661
2009	−2.520	−0.637	−2.021
2008	−3.156	−0.372	−2.417
2007	−3.911	−0.482	−3.001

Table 4 shows that the expressions of the two principal components are:

$$\begin{aligned} F_1 = {} & 0.34\mathrm{GDP} + 0.34\mathrm{POP} - 0.33\mathrm{SI} - 0.34\mathrm{EC} \\ & + 0.34\mathrm{HA} + 0.34\mathrm{CA} + 0.34\mathrm{CAR} + 0.33\mathrm{GA} - 0.06\mathrm{SO_2} \\ & + 0.17\mathrm{DE} + 0.04\mathrm{NE} - 0.02\mathrm{P} + 0.25\mathrm{WS} \end{aligned} \tag{1}$$

$$\begin{aligned} F_2 = {} & 0.01\mathrm{GDP} - 0.01\mathrm{POP} + 0.06\mathrm{SI} - 0.02\mathrm{EC} - 0.08\mathrm{HA} \\ & + 0.01\mathrm{CA} - 0.04\mathrm{CAR} - 0.13\mathrm{GA} + 0.52\mathrm{SO_2} \\ & + 0.38\mathrm{DE} + 0.53\mathrm{NE} - 0.51\mathrm{P} + 0.1\mathrm{WS} \end{aligned} \tag{2}$$

The higher the variance contribution rate, the more important the principal component is. Since the original index can be basically replaced by the first two principal components, the coefficient of the index in the comprehensive scoring model can be regarded as the weighted contribution of the variance of the two principal components. Thus, the comprehensive score model of haze pollution in Jinan city can be obtained as follows:

$$\begin{aligned} F = {} & 0.25\mathrm{GDP} + 0.25\mathrm{POP} - 0.23\mathrm{SI} - 0.25\mathrm{EC} + 0.23\mathrm{HA} \\ & + 0.25\mathrm{CA} + 0.24\mathrm{CAR} + 0.21\mathrm{GA} + 0.1\mathrm{SO_2} \\ & + 0.23\mathrm{DE} + 0.17\mathrm{NE} - 0.15\mathrm{P} + 0.21\mathrm{WS} \end{aligned} \tag{3}$$

Therefore, comprehensive evaluation results of haze pollution in Jinan from 2007 to 2016 can be obtained, as shown in Table 5 and Fig. 1.

According to the comprehensive evaluation results of principal component analysis, it can be seen that from 2007 to 2015, the change of haze pollution in Jinan showed an upward trend, and from 2015 to 2016, the change of haze pollution showed a downward trend. This means that the atmospheric environment has been getting

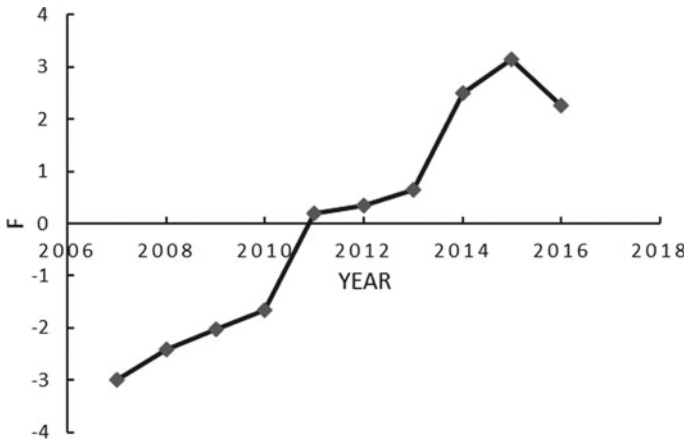

Fig. 1 2007–2016 Comprehensive score of haze pollution of Jinan City

worse from 2007 to 2015, when the haze pollution in Jinan City reached its peak, and then the environment gradually improved.

4 Discussion

Haze weather has its complexity, both the impact of the natural environment, but also the impact of social and economic development. The pollutant discharge caused by human activities exceeding the environmental carrying capacity is the internal cause of haze formation. The aerodynamic condition that hinders the diffusion of pollutants is the external cause of haze weather. The combined effect of internal and external factors finally leads to haze pollution.

4.1 Regional Economic Development

Grossman and Kreuger concluded that the environment is also polluted before it is improved in the process of economic development (Grossman and Alan 1995). From the above analysis, it can be seen that the information contained in the first principal component mainly comes from socio-economic aspects. The score coefficients of the three indicators in the comprehensive score model are the first, the third and the sixth, respectively. The changes of these three indicators have an important impact on the haze pollution in Jinan city.

4.2 Urbanization Process

The variables reflecting urbanization process in the first principal component are population density, building construction area and urban green coverage area. In 2016, the population per unit area of Jinan was 884.54 people/km^2, more than 6 times the national average. Excessive population load will increase urban infrastructure construction, consumption and industrial output, and the increase of urban population and the expansion of urban area will directly increase the emission of smog-related pollutants (Zhang and Han 2018). The construction area of houses ranks the second place in the comprehensive evaluation system of haze pollution in Jinan city, which shows a strong positive correlation with the formation of haze pollution in Jinan city (Liu 2015).

4.3 Terrain

The formation of haze is not only related to the emission of pollution sources exceeding the environmental carrying capacity, but also closely related to the regional natural environment. The occurrence of haze weather in Jinan is largely related to the topography of Jinan and the regional natural environment. Jinan topography is a basin. Affected by the topography, the air pressure field is weak and there is a strong inversion layer over Jinan. The polluted air is difficult to diffuse, which to some extent aggravates the air pollution.

5 Conclusion

The haze pollution in Jinan has been alleviated since 2015, but overall it is still at a high level. Haze pollution is still a problem that cannot be ignored in the economic development of Jinan City.

5.1 Change the Pattern of Economic Development

On the one hand, we need to promote green and low-carbon industrial development, and achieve sustainable economic development in the region by strictly controlling industries with high pollution and emissions, eliminating outdated production capacity, and developing energy-saving and water-saving technologies. On the other hand, we should accelerate the pace of industrial upgrading and upgrading and optimize the industrial structure of this region. Therefore, it is necessary to give full play to the dual role of the “visible hand” of the government and the “invisible hand” of the

market, encourage enterprises to make independent innovation, reasonably combine the new composition of the three industries, increase the proportion of the tertiary industry in the national economy, and finally achieve sustainable development of regional economy.

5.2 Improve the Structure of Energy Consumption

First, we need to adjust the energy mix, vigorously support high-tech industries, and rectify existing high-polluting enterprises within a certain period of time. For the high pollution enterprises that must exist, they should also move downwind from the urban areas to the suburbs. Second, we need to increase the proportion of clean energy sources such as solar energy and natural gas, strictly control total coal consumption in the region and accelerate the development of new energy sources. Third, we need to step up the upgrading and upgrading of coal-fired heating boilers in winter, strengthen coal quality testing and emission supervision, increase the implementation of "coal for natural gas" and "coal for electric power", vigorously develop clean energy, increase the exploitation of natural gas, and increase the scale of imported natural gas. Fourth, we will strengthen regulation and ban the use of coal by retail investors in profit-making small coal stoves, open-air burning and barbecues. Optimizing the energy consumption structure is a slow process, and the change of the energy structure is not changeable, but also requires the guidance of policies and the cooperation of enterprises and industries.

5.3 Control Vehicle Exhaust Emissions and Advocate Green Travel

In order to control the exhaust emission and growth rate of urban motor vehicles, in addition to mandatory management measures such as purchase restriction and driving restriction, we can also vigorously promote new energy vehicles and hybrid electric vehicles. Give new energy vehicles from the development, production, purchase to use more preferential policies. Secondly, private cars should be guided to "replace oil with gas" and use natural gas, solar energy and other clean energy to reduce the emission of fine particles in exhaust gas. In addition, according to the old and new degree of the car, the use of energy types, the use of the life of the car and the displacement of the car emissions and other taxes. Finally, we should establish the policy of priority development of public transportation, adhere to the priority development of public transportation, and advocate green modes of travel.

References

Cheng L (2016) Investigation of air quality status under the new normal and analysis of countermeasures—taking Jinan city as an example. Shanxi Agric Econ (12):49

China Meteorological Administration (2003) Specifications for ground meteorological observation. Beijing: meteorological publishing house

Davis DL (2002) A look back at the London smog of 1952 and the half century since. Environ Health Perspect 110(12):A734

Dong Y, Tai B (2014) Analysis on causes and treatment measures of urban haze pollution. J Qilu Normal Univ 29(4):113–119

Gong A, Liu X, Dai X (2017) Analysis on the causes and influencing factors of haze in chengdu. Environ Impact Assess 39(1):93–96

Grossman GM, Alan K (1995) Economic growth and the environment. Q J Econ 110(2):353–357

Hu M (2013) Economic analysis of haze. Econ Res Guide (16):13–15

Kang E, Han J, Lee M et al (2013) Chemical characteristics of size-resolved aerosols from Asian dust and haze episode in Seoul metropolitan city. Atmos Res 127(6):34–46

Latif MT, Othman M, Idris N et al (2018) Impact of regional haze towards air quality in Malaysia: a review. Atmos Environ (3):1127–1140

Liu T (2011) Research on influencing factors of industrial structure change in Shandong province based on principal component analysis. J Shandong Univ (philosophy and social science edition) (3):107–112

Liu H (2015) Influence of construction on haze weather and Suggestions on prevention and control. Brick Tile (04):53–56

Quah E, Boon TL (2003) The economic cost of particulate air pollution on health in Singapore. J Asian Econ 14(1):73–90

Ren P, Li X, Sheng R (2017) Analysis on causes and countermeasures of haze weather. Environ Dev 29(08):200–202

Rong FS, Feng K (2015) Factors influencing haze and countermeasures based on statistical analysis. J Xiamen Univ 54(1):114–121

Wu Q, Li B, Ding L (2007) Evaluation of economic development potential of urban areas in Jiangsu province based on principal component a nalysis. Value Eng (9):25–27

Yin C, Yu L, Zhang Y (2014) Analysis of haze characteristics in Jinan city. Population Resour Environ China 24(S3):68–70

Zhang Y, Han Y (2018) Influence of population factors on haze pollution—empirical analysis based on provincial panel data. World Surv (1):9–16

Comprehensive Evaluation of Oil Sorbent Based on AHP Method

Guohua Luan, Shengli Chu, Xin Li and Guangbo Ma

Abstract In order to make a comprehensive assessment of adsorption performance for oil sorbent, a three-level indicator system is set up, which consists of three second class indicators, namely static adsorption property, spot operation property, energy saving and environment protection property and nine third class indicators like oil absorption rate, water absorption rate, oil-holding rate and so on. According to the five class evaluation principle, the score comparison table, can be derived based on the test results of oil sorbent. Weights for indexes at every level are calculated with analytic hierarchy process. Through the above-mentioned evaluation methods, eight alternative oil sorbents are sorted, which offers scientific decision-making basis for enterprise enterprise.

Keywords Oil sorbent · Analytic hierarchy process · Comprehensive evaluation method

1 Introduction

The oil spill to rivers or sea is a great threat to the water environment, and could cause devastating disasters to the local ecological environment and fishery resources (Feng 2010; Guan and Han 2010; Bao et al. 2015; Liu et al. 2015; Pan and Huo 2009). The processing methods of oil spill can be categorized into biological, chemical

G. Luan (✉) · S. Chu · X. Li
CNPC Research Institute of Safety & Environment Technology, Block A12, CNPC Petroleum Technology Park, Xishantun, Beijing City, Shahe Town, Changping District, China
e-mail: luanguohua@cnpc.com.cn

S. Chu
e-mail: chushengli@cnpc.com.cn

X. Li
e-mail: lixin630205@163.com

G. Ma
China National Petroleum Corporation, Jidong Oilfield Branch, Caofeidian District 116, Tangshan City, Hebei Province, China

R. Sun and L. Fei (eds.), *Sustainable Development of Water and Environment*, Environmental Science and Engineering,
https://doi.org/10.1007/978-3-030-16729-5_12

and physical (Li et al. 2016; Liao et al. 2012). Among them, the physisorption is the main method because of its quick effect, large handing capacity and strong adaptability. As a common adsorption material, oil sorbent has the characteristics of high oil absorption rate, good hydrophobic property and low price. It is widely used in the oil spill emergency practice (Liao et al. 2012; Jiang et al. 2015; Lan et al. 2015; Sun et al. 2015; Xiao et al. 2005). Both in china and abroad, the current standards put forward the performance indexes such as oil absorption rate, water absorption, oil holding rate, breakage and settlement, and so on (JT/T 2004; Q/SY 1712; F716-2009 2006; Zhao et al. 2016). The difficulties for enterprises emergency preparedness are how to consider comprehensively the effect of each index on the sorbent's performance, and then evaluate and select the optimum sorbent based on the test results of. The standard for performance evaluation index system and the three levels for suction linoleum performance are developed based on fully drawing on existing linoleum performance index and expert judgement. The weight of each index is derived through analytic hierarchy process (AHP). Combined with the test results based on performance indicators, a comprehensive evaluation can then be carried out. The linoleum performance evaluation index system, AHP weights and linoleum performance standard that this paper presenting is for the evaluation for enterprises decision-making in emergency linoleum optimization.

2 Performance Evaluation Index of Oil Sorben

A number of key performance indicators for the performance of oil sorbent are proposed in some occupation, such as the occupation standard of American Society of Testing Materials (ASTM), Standard Test Methods for Sorbent Performance of Absorbents, Chinese transportation occupation standard sorbent and standard for petroleum enterprises performance requirements for oil spill emergency products part second: sorbent (JT/T 2004; Q/SY 1712; F716-2009 2006; Zhao et al. 2016). At present, both domestic and international standards have adopted 2 indexes of

Table 1 Standard for evaluating the performance of suction linoleum

Serial No.	Standard code	Standard hierarchy	Index setting	
1	F 716-2009	Foreign industry standards	Oil absorbency water absorption	–
2	JT/T 560-2004	Industry standard		Oil retention, breakage, solubility, sedimentation, strength, usability, combustibility
3	Q/SY 1712.3-2014	Manufacturer's standard		

oil absorbency and water absorption rate, while Chinese industry and related enterprises standards specified 7 assessments including oil-holding capacity, breakage, solubility, settleability, strength, usability and combustibility (Table 1).

3 Evaluation of Oil Sorbent Based on AHP Method

3.1 Introduction to AHP Method

As mentioned above, the performance index of the sorbent is influenced by many factors, such as oil absorption ratio, water absorption, oil retention, breakage, solubility and settleability and so on. Analytic hierarchy process (AHP) is a subjective weight assignment method to deal with/handle the multi factor and multi index system. The AHP method was put forward by T. L. Saaty in 70s, which has been widely used in many factors such as safety assessment, risk assessment, drilling evaluation and so on. The basic steps of the AHP method to assign the weights of the hierarchy indexes are as follows: the establishment of the hierarchy, the construction of the judgment matrix, the weight calculation and the consistency test (Guo et al. 2008; Deng et al. 2012; Yang et al. 2006; Luan et al. 2014; Wu et al. 2013).

3.2 I Construction of Evaluation Index System

As mentioned above, the performance index of the sorbent is related to many indexes such as oil absorption ratio, water absorption, oil retention, breakage, solubility and settleability and so on. After a comprehensive classification of the performance indicators, we divide the linoleum performance evaluation system into 3 levels, with linoleum comprehensive performance as the first level; Three indexes, namely static adsorption properties, field operation and energy saving and environmental protection performance, are developed at the second level, while at the third level, nine indicators are established. The comprehensive evaluation for the performance index of the sorbent is shown in Table 3.

3.3 Scoring Method and Weight Calculation

3.3.1 Scoring Method

According to the aforementioned industry and enterprise standards, the design of linoleum comprehensive performance of third indicators with the total score of 5 points, divided into 5 levels as excellent, good, general, poor pass. The corresponding

Table 2 Comparison table of the performance index of the sorbent

Evaluation index	Grade				
	5 (excellent)	4 (good)	3 (commonly)	2 (pass mark)	1 (poor)
Oil absorbency	≥15	≥10, <15	≥8, <10	≥6, <8	<6
Water absorbency	≤5%	<5%, ≤10%	<10%, ≤15%	–	>15%
Oil holding capacity	≥90%	≥80%, <90%	≥70%, <80%	≥60%, <70%	<60%
Breakage	Maintain the prototype after 12 h	–	–	–	Can not maintain the prototype after 12 h of oscillation
Settling property	Float on the water after 12 h of oscillation	–	–	–	Can not float on the water after 12 h of oscillation
Solubility	No dissolution and deformation in the oil	–	–	–	Dissolution and deformation occurred in the oil
Strength	No tear occurred after 3 min of hammer test	–	–	–	Tear occurred after 3 min of hammer test
Usability	Can be used more than 10 times	–	–	–	Can be used less than 5 times
Combustibility	Combustion treatment without pollution	–	–	–	Combustion treatment with pollution

evaluation methods are shown in Table 2. The score of the test results is given according to the score table.

3.3.2 Weight of Top Class

According to AHP, we invited the experts to sort the importance of each level of performance indicators, construction hierarchy judgment matrix, using MATLAB 7 software to calculate the maximum characteristics of each judgment matrix eigenvalues and eigenvectors, and to check the consistency of judgement matrix. The

Table 3 The calculation results of the comprehensive performance index and the weight of the sorbent

Serial number	First grade index	Second grade index	Second level weight	Third grade index	Third level weigh
1	Comprehensive performance of sorbent	Static adsorption performance	0.7306	Oil absorbency	0.7172
2				Water absorption	0.0881
3				Oil holding rate	0.1947
4		Field performance	0.18839	Damage property	0.1654
5				Solubility	0.0482
6				Settling property	0.6208
7				Strength property	0.1656
8		Energy saving and environmental protection performance	0.0810	Usability	0.1667
9				Combustibility	0.8333

calculation results of the weight value of the performance index for the comprehensive performance of the sorbent are shown in Table 3.

4 Examples of Application of Sorbent

Company L is a large petrochemical enterprises adjacent to the river, which there is a risk of oil leakage of water pollution incidents in it, the company needs to buy a batch of linoleum as emergency supplies of oil spill, the 8 existing suppliers to provide samples of linoleum (Z1-Z8) available. Company L tests the use of the sample performance according to the above industry, enterprise standards, the test results are shown in Table 4.

As shown in the above table, there are obvious differences in the performance test results of the 8 kinds of sorbent on the spot, which can not be applied to the company. In order to ensure the matching work is scientific and reasonable, based on the application of the above-mentioned “linoleum evaluation method based on AHP” to comprehensive performance the linoleum overall evaluation, comprehensive performance results of linoleum are shown in Fig. 1.

As shown above, the test 8 linoleum sample comprehensive performance scores have significant differences, including Z4, Z1, Z8 three kinds of linoleum rank-

Table 4 Evaluation of the performance index of the sample of the sorbent

Serial number	Performance index	Z1	Z2	Z3	Z4	Z5	Z6	Z7	Z8
1	Oil absorbency	5	4	3	5	4	4	3	5
2	Water absorption	4	4	3	5	4	5	5	4
3	Oil holding rate	3	3	5	4	4	4	5	4
4	Damage property	5	5	1	5	5	5	5	5
5	Solubility	5	1	1	1	5	5	5	1
6	Settling property	5	5	1	5	5	1	5	5
7	Strength property	1	1	5	5	5	1	1	1
8	Usability	5	5	5	5	1	5	5	5
9	Combustibility	5	5	1	5	5	5	1	5

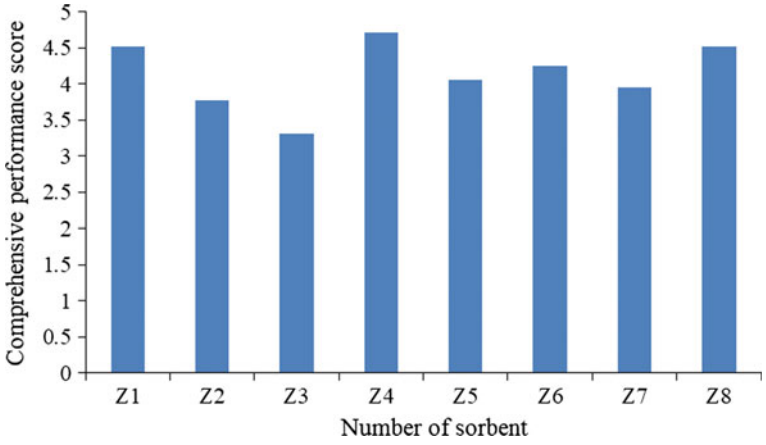

Fig. 1 Calculation results of comprehensive performance of sorbent

ing more forward, which is recommended as a priority with linoleum. Other types of asphalt sorbent score ranking is relatively backward, is not recommended as a priority with the suction pad. The above established linoleum performance index hierarchy, and each index test results into the score, the score results were weighted superposition, the final calculation of comprehensive performance ranking is obtained, and provide a scientific basis for the selection of linoleum products.

5 Conclusion

This paper established a three-level indicator system for the comprehensive evaluation of the performance of sorbent, within which three second-level indicators of static adsorption performance, field performance, energy saving and environmental

protection performance, and nine test indexes "including oil absorbency, water absorption and oil holding rate" are adopted. Based on the five-level judgment principle, a score table for test results of the performance index of the sorbent is given. Application of hierarchical analysis, calculation of the weight of indicators at all levels. By applying the methodology of AHP based oil sorbents overall performance evaluation, a comprehensively evaluation of the performance for 12 alternative solutions can be derived, which can provide a scientific basis for the selection of sorbent in enterprises.

References

Bao M, Pi Y, Sun P et al (2015) Research progress on "deepwater horizon" Oil Spill of Gulf of Mexico. Period Ocean Univ China 01:55–62

Deng X, Li J, Zeng H et al (2012) Research on computation methods of AHP wight vector and its applications. Math Pract Theory 42(7):93–101

F716-2009 (2006) Standard test methods for sorbent performance of absorbents. ASTM, USA

Feng Y (2010) Lessons learned from the emergency response to the July 16 Oil Spill Incident in Dalian. China Marit Saf 12:17–18

Guan Y, Han J (2010) Review of the cleaning action taken at sea after the July 16 Oil Spill Incident in Dalian and some suggestions related thereof. China Marit Saf 12:19–21

Guo J, Zhang Z, Sun Q (2008) Study and applications of analytic hierarchy process. China Saf Sci J 18(5):148–152

Jiang X, Lanzhujun, Zhu B et al (2015) Oil absorptive properties and application research of oil sorbent. China Water Transp 4:322–324

JT/T 560-2004 (2004) Sorbents for ship. Water Resources and Electric Power Press, Beijing, p 8

Lan Z-J, Zhu B-K, Jiang X-T (2015) Analysis of oil adsorbing effect of oil sorbent on diesel and its application. J Green Sci Technol 6:176–178

Li F, Duan L, Luan G et al (2016) Research of oil absorption materials based natural organic fiber of cotton linter. New Chem Mater 02:111–113

Liao G, Ma Y, Gao Z (2012) Enlightenment on Oil Spill Incident in Gulf of Mexico to oil spill pollution control management of deep sea in our country. Ocean Dev Manag 5:70–76

Liu P, Li B, Zheng X (2015) Application of environment sensitivity technology in leakage of long-distance pipelines. Petrochem Ind Technol 4:97–98

Luan G, Pei Y, Wu D et al (2014) The AHP-FUZZY method for an integrated emergency drills assessment in industrial production. Math Pract Theory 10:98–103

Pan D, Huo Y (2009) Risk analysis on oil and gas leakage accident in offshore oil & gas field engineer. Mar Environ Sci 28(4):426–429

Q/SY 1712.2-2014 (2014) Performance technology requirements of products used for oil spill response-the second part: oil sorbent. Petroleum Industry Press, Beijing

Sun W, Zhang Y, Pu Z et al (2015) Discussion on technology of oil spill emergency response in port. Environ Eng S1:971–974+984

Wu D, Pei Y, Luan G et al (2013) Assessment on emergency drills of oil depot based on AHP-Fuzzy method. J Saf Sci Technol 07:130–133

Xiao H, Shen B-X, Chen X-Z (2005) Investment on crude oil spills adsorbing effect of melt-blown polypropylene fabric (MBPP). Oil Gas Storage Transp 24(5):24–27

Yang W, Shi X, Yu C (2006) Impact assessment of spilled oil pollution from ship based on AHP method. Shipp Manag 05:13–16

Zhao Y, Hou J, Sun L (2016) Differences in technical standards for oil spill responses at home and abroad. Oil-Gas Storage Transp 10:1083–1086+1091

Part III
Water Resource and Water Environmental

An Optimal Design of Groundwater-Environment Remediation Scheme in Chengdu Plain, China: A Case Study of Huaikou Landfill

Adam Khalifa Mohamed, Liu Dan, Song Kai, Abubakr Hassan, Basheer A. Elubid and Elsiddig Aldaw

Abstract A 3D model was constructed to optimize the remediation scheme of groundwater environment which was contaminated through leaching from the municipal solid waste landfill. Based on groundwater sampling test results, potassium permanganate index (COD_{Mn}) was selected as a pollution indicator with high concentration. Two scenarios were predicted in this study. Scenario 1 is assigned for the combination of a horizontal landfill barrier covers by high-density polyethylene (HDPE) and monitored natural recovery (MNR). Scenario 2 is resulted from the combination of horizontal and vertical barrier technology and pumping treatment (P-T). The results showed that the leachate could be well controlled by Scenario 2. Applying of Scenario 2 plays an important role of restoring the quality of groundwater to its nature after 2000 days as compared to Scenario 1, which needs more than 6000 days. The usefulness of anti-seepage measures regarding leachate control in landfill has been put forwarded, and findings could be applied according to the evaluation of actual contamination sites. This study will provide a scientific basis to utilize the groundwater resources sustainably in the study area.

Keywords Groundwater quality · Huaikou landfill · Remedial alternatives · Visual modflow

1 Introduction

Recently, with the advance of societal development and the improved quality of human life, many serious problems that have posed threats to human health and environment have emerged (Zhu et al. 2014; Mohamed et al. 2018). Among them,

A. K. Mohamed · L. Dan · S. Kai (✉) · A. Hassan · B. A. Elubid · E. Aldaw
Faculty of Geosciences and Environmental Engineering, Southwest Jiaotong University, Chengdu, China
e-mail: songkailw@163.com

A. K. Mohamed · E. Aldaw
Faculty of Water and Environmental Engineering, Sudan University of Science and Technology, Khartoum, Sudan

R. Sun and L. Fei (eds.), *Sustainable Development of Water and Environment*, Environmental Science and Engineering,
https://doi.org/10.1007/978-3-030-16729-5_13

groundwater pollution caused by landfills worldwide due to rapid expansions of urban, industrial and commercial activities prompted by rapid population growth (Han et al. 2016; Li et al. 2014). The dump is the most common approach for deposal of wastes in China (Zhang et al. 2016) which is determined as one of the leading threats to groundwater resources due to the leakage of leachate (Han et al. 2016; Maiti et al. 2016). Therefore, for the protection of water resources in landfills area, the pollution of the landfill into groundwater needs to be forecasted and controlled. Also, some measures of prevention and protection should be provided (Zhang et al. 2016).

In general, selection of a fit groundwater treatment alternative of a landfill should be based on the solid waste characterization and the surrounding natural environment. Then the alternatives should be examined through internal or field experiments (An et al. 2013). However, this procedure will often be costly and takes an extended period. In order to select suitable alternatives for groundwater treatment in landfills and significantly reduce the time and cost, numerical simulation has been used by Visual Modflow.

In recent years, the impact of a landfill on groundwater has given rise to several studies using Visual Modflow because it is widely used in the simulation of pollutants transport and fate (Rona et al. 2018). Most of these studies focused on the assessment of the extent of contaminants migration and prediction for each of the concentrations of nitrate (NO_3^-), chromium (Cr^{6+}), arsenic (As), chloride (Cl^-) and others (An et al. 2013; us Saba et al. 2016; Ma et al. 2012; Zhang et al. 2007). However, less attention has been considered about pollutants transport in aquifers by numerical modeling on potassium permanganate index (COD_{Mn}). Therefore, in this research, the Huaikou landfill Northeast of the Chengdu plain, China was selected to evaluate the efficiency of two kinds of groundwater remedial alternatives based on the simulation results. Groundwater flow and solute transport model have been established for simulating the transport and fate of COD_{Mn} concentration in the groundwater to be the major target of pollution in the study area. The evaluation results will assist in drafting a control plan for unregulated landfill leachate-contaminated groundwater in the future.

2 Materials and Method

2.1 Site Description

The Huaikou landfill located in the eastern part of Huaikou town on the left bank of Minjiang River, China. It is mainly used to fill the compacted informal domestic garbage. The operation of the site started in May 2014 and stopped operation in 2017. The garbage covers an area of approximately 3336 m^2, a landfill thickness of 6.0 m. The landfill volume of 18,000 ton, and a piling point service population of 11,500 people, which receives 6.0 tons of residues per day. The climatic condition of the area is subtropical monsoon with four distinct seasons. The average annual

temperature of the area is 16.6 °C, and the annual relative humidity is 80%. Rainfall is the main recharge source with an annual average of about 924.6 mm. Groundwater from the Quaternary Unconsolidated Sediments is the primary source of drinking water, irrigation and industrial use in the study area. The open dumping of municipal solid waste (MSW) on the land and discharge of the sewage into groundwater in this area is commonly responsible for groundwater quality deterioration and water-borne diseases. Therefore, it is necessary to carry out comprehensive monitoring of the groundwater pollution sources and taking further pollution reduction measures.

2.2 Selection of Pollution Indicator

To investigate and evaluate the possible influence of the leachate on groundwater samples, groundwater samples data were collected from five observation points piezometers (ZK1, ZK2, ZK3, ZK4 and ZK5) situated at the groundwater outflow from the landfill and three observation point (J1, J2 and J3) situated at the inflow of groundwater to the landfill. By collecting and analyzing these samples in the study site, contrasting the primary pollutants of the leachate, and referring to Class III of the groundwater quality standard (GB/T14848-2017), the results indicated that contaminants had leached and contaminated the water-table aquifer. These pollutants are mainly including organic pollution, inorganic pollution and heavy metal pollution. The organic pollution is mainly COD_{Mn}, the inorganic pollution includes nitrate, nitrite, ammonia nitrogen and fluoride; heavy metal pollution including iron and lead. Among these pollutants, it was found that COD_{Mn} was the most critical contaminant which has exceeded the standard several times. So, this contaminant was taken to predict its dynamics in this study.

2.3 Visual Modflow

Visual Modflow is extensively used in various groundwater contamination transport simulations and to predict the impacts of different management plans on the transport of pollutant in the variably saturated heterogeneous subject to a variety of boundary conditions (Ma et al. 2012). In the study area, the landfill body is the major contamination source for groundwater pollution. The computer module MODFLOW-2000 (Harbaugh 2005) has been applied for simulating the groundwater flow and the computer module MT3DMS (Zheng and Patrick Wang 1999) was run to simulate the solute transport in the contaminated aquifer system. Boundary condition was considered to be a constant concentration of COD_{Mn} in the model domain.

Table 1 The essential parameters values of the model

Model parameter	Value
Length of model domain in x-direction (m)	4100
Length of model domain in y-direction (m)	3800
Dimension of one grid cell (m)	50 * 50
Recharge	138 mm/a
Hydraulic conductivity (K_x and K_y in m/s)	$8.5 * 10^{-7}$
Hydraulic conductivity (K_z in m/s)	$8.5 * 10^{-8}$
Specific yield (Sy)	0.1
Effective porosity	0.1
Total porosity	0.15
Specific storage (Ss/m)	$1.0 * 10^{-7}$
D_L longitudinal dispersion	0.467
D_T Ratio of longitudinal dispersion to transverse dispersion	$1/10 D_L$

2.4 Generalization of the Aquifer Structure and Parameterization

The available data for Quaternary loose sedimentary was analyzed to evolve a groundwater flow regime in the study area using the hydrogeological database. According to this hydrogeological information, a one-layer model has been created. The investigation of geological field revealed that the thickness of the aquifer ranges from 35 to 40 m. The lithologic composition of the underlying bedrock of the aquifer is dominated by mudstone. The groundwater flows from the northeast to the south and is finally discharged to the Minjiang River. In the simulation process of pollutant transport, the aquifer has been assumed to be isotropic and homogeneous. The hydraulic head was brought from the water head between the river and the adjacent water-table aquifer. In the same vein, the aquifer was closely related to the surface waters around and it was mainly determined through vertical permeability coefficient. The detailed hydrogeologic characterization of the study area was carried out in order to assign the essential parameters for modeling. These parameters include hydraulic conductivities, specific storage, dispersion coefficient, effective porosity, total porosity and others as shown in Table 1.

2.5 Boundary Conditions

Modflow divides the computing units into three main categories: fixed head units, invalid units, and variable head units. In the simulation area, the Lijiang River lies on the west side of the landfill which is considered as a river boundary. The northern and

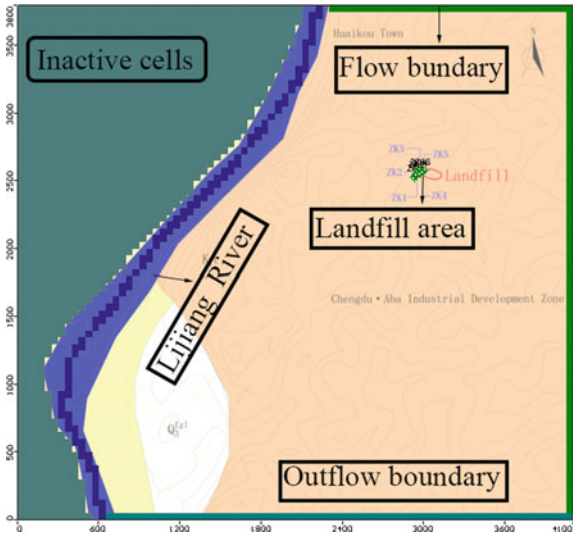

Fig. 1 Boundary conditions in the model domain

eastern sides are upstream of groundwater runoff direction of the study area which was considered as the hydrological flow boundary. The south side is downstream of the simulation area and is set to the outflow boundary. Figure 1 shows the boundary conditions of the study area.

2.6 Groundwater Flow and MT3DMS Contaminant Transport

The model of groundwater flow and solute transport was created using Visual Modflow. The method of finite difference discretization was implemented to divide the simulation region of 17.28 km^2, and it is assumed to be a rectangular shape with 50×50 m grids generated. Meanwhile, in the simulation process of pollutant transport, the aquifer has been assumed to be isotropic and homogeneous. The scope and boundary of the groundwater flow model were compatible with the solute transport model. In this study, the characteristics of boundary's were treated through the COD_{Mn} concentration range. The effects of temperature and water density on the hydrodynamic fields were neglected in the simulation process. The parameters of the model were determined precisely as a conservative type. Accordingly, the simulation process was based on the assumption that the pollutant source was seen as a continuous point source and the entire landfill as the source scope. Hence, the results of the model were used to assess the possible "best" scenario to stop the migration of COD_{Mn} from the landfill. Groundwater data observed in 2014 were utilized as the initial conditions of the model.

3 Results and Discussion

3.1 Model Calibration and Verification

In the study area, the model has been calibrated for the steady-state conditions of groundwater flow and solute transport model. Various hydraulic parameters and configuration were introduced during the calibration process. The groundwater quality result at 2014 was used as an initial concentration in the calibration and validation of steady-state model as well as all values of parameters which were used in flow model and MT3D model without any change. The calibration results were evaluated through the appropriate curve between observed and calculated hydraulic heads data of groundwater flow model and achieved by a trial-and-error method, as well as COD_{Mn} concentration of solute transport model. The initial value of COD_{Mn} was set to the lowest detected value of 0.97 mg/L. From the calibration process, the hydrogeologic parameters as in (Table 1) were acceptable due to the calculated values of hydraulic heads of the flow field with root-mean-squared (RMS) error of the simulated water level is 0.33 m. Also, the concentration of COD_{Mn} in the groundwater samples (ZK1 to ZK5) was found fully compatible with the observed values that are within the 95% confidence interval. Therefore, the trend prediction analysis based on the groundwater flow and solute transport field indicates good and acceptable calibration result. Figure 2 is shown the results of groundwater flow of the simulation area.

Figure 3 shows the current situation of solute transport field of the simulation area. According to the results in Fig. 3, the current situation of groundwater contamination in the study is caused by infiltration and leaching of household litter without measures which resulted in pollution of the surrounding groundwater environment. The

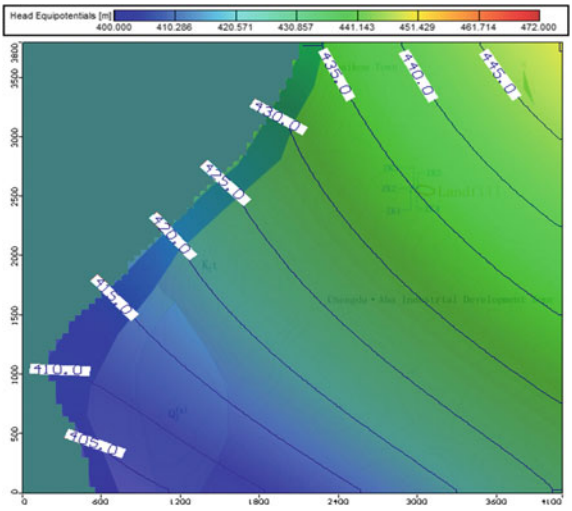

Fig. 2 Groundwater flow field results of the simulation area

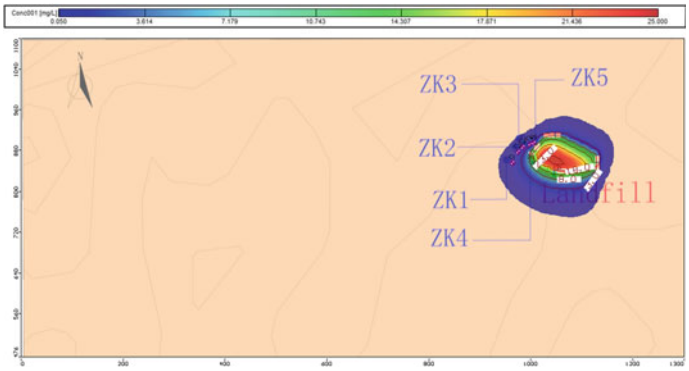

Fig. 3 COD_{Mn} concentration after steady state calibration at 2014

maximum contribution of COD_{Mn} is 23 mg/L which caused the groundwater in the downstream range has exceeded the standard of groundwater quality (GB/T14848-2017). So, it was necessary to predict the migration of COD_{Mn} concentration of different periods to restore the quality of the groundwater environment in the study area.

3.2 Modeling Predictions of Remediation Scenarios

The calibrated model was run to predict two scenarios up to 20 years to increase the environmental quality of groundwater and prevent further migration of COD_{Mn} into the groundwater aquifer. Scenario 1: landfill coverage only by the high-density polyethylene (HDPE) geomembrane to minimize the amount of leachate produced and to rely on the ability of groundwater to self-purification which makes its surrounding environment recover naturally. Scenario 2: the groundwater environmental protection and restoration measures of this scenario are mainly concentrated in three aspects; (1) Closure of the site to reduce the amount of leachate produced; (2) Preventing the diffusion and migration of pollution plumes by curtain wall and (3) Drilling of sewage collection wells in the curtain wall to extract contaminated groundwater in order to accelerate the restoration of groundwater environment. Figure 4 depicts the proposed groundwater remediation technology of Huaikou landfill and the simulation results for different periods (300, 1000, 2000 and 6000 days) of COD_{Mn} concentration for both scenarios are shown in Fig. 5.

According to the results of the comparative prediction of the two models in (Fig. 5), the periods of 300 and 1000 days for both scenarios showed that the concentration of COD_{Mn} is still above the allowable limit (3.0 mg/L) of Chinese groundwater quality standard (GB/T14848-2017). But Scenario 2 showed that after 2000 days of closure, COD_{Mn} concentration was essentially recovered from maximum value of 23 mg/L

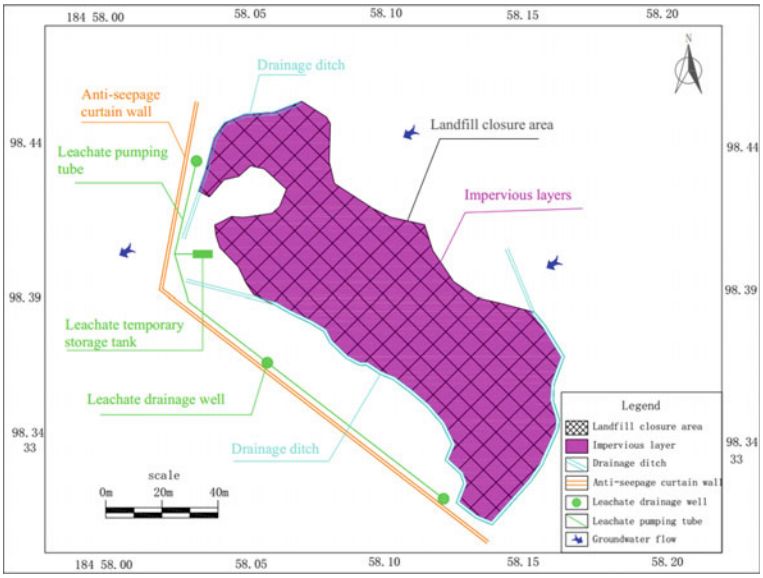

Fig. 4 Groundwater remediation technology of Huaikou landfill

to the permissible limit of (GB/T14848-2017) standard. While Scenario 1 showed that the groundwater environment could be recovered after the landfill was simply covered for more than 6000 days. Therefore, Scenario 2 is considered more effective to prevent and control the migration of pollutants compared to Scenario 1.

In summary, the groundwater environment has been affected by the temporary dumping point of the garbage, resulting in groundwater pollution around the downstream area. Its worth mentioning that Scenario 2 is very costly, but we recommend to be applied in the garbage storage area because the downstream area has many groundwater supply wells, which are considered the primary source of drinking water for the local residents. In order to protect the groundwater environment and restore its quality when scenario 2 is applied, we suggest the following measures:

1. Adoption of advanced and reliable technology with reasonable economic cost in order to cover the field system to reduce the amount of leachate produced. According to the Technical Regulations for the Closure of Domestic Waste Landfill Sites (CJJ112-2007) of China, a complete closure system must be established for the landfill which includes the primary layer (permeability system), drainage layer, and vegetation layer. The top surface slope of the garbage dump should not be less than 5%. When the slope of the hill is greater than 10%, the stepped slope should be adopted. Also, the slope of the hill between the steps should not be greater than 1:3, and the step width is less than 2 m.
2. Set up drainage ditch for implementing rainwater and sewage diversion to reduce rain entering the garbage storage area and reduce the amount of leachate production.

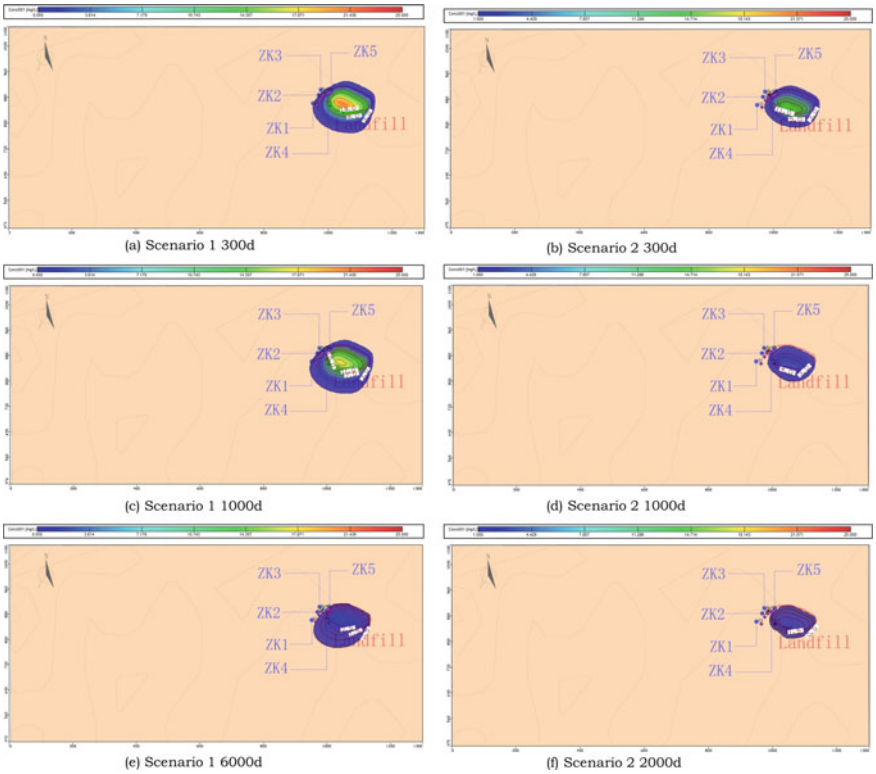

Fig. 5 The predicted results for different periods of CODMn concentration of Scenario 1 and 2

3. Set up the leachate drainage and collection system as well as the leachate drainage well near the curtain wall designed to resist the migration of pollution in the downstream direction. Then, use the water pump periodically to pump the leachate in the well, which should be collected and transported regularly by suction trucks.
4. Set up the anti-seepage curtain wall system and use it to penetrate the bedrock in order to prevent the landfill leachate from infiltrating into the lower Minjiang River from the groundwater channel and polluting the Lijiang River basin.

4 Conclusions

A hydrogeological model was performed by utilizing Visual Modflow to study the effect of COD_{Mn} concentration on groundwater of Huaikou landfill. All the available geological and hydrological data were used for the preparation and validation of the numerical model. Within the boundaries of the current research paper and study area, it can be inferred that:

1. The landfill pollutes the groundwater aquifer due to COD_{Mn} leaching.
2. The best treatment action to prevent COD_{Mn} leachate from the landfill into the aquifer is to apply scenario 2, and our study highly recommended its implementation.
3. The results of simulation correspond to the actual transport characteristics of pollutants, which provide the quantitative basis for predicting contaminant migration and landfills control to groundwater in Huaikou area.
4. Finally, the study would give a scientific basis to use the groundwater resources sustainably in the study area.

References

An D, Jiang Y, Xi B, Ma Z, Yang Y, Yang Q, Li M, Zhang J, Bai S, Jiang L (2013) Analysis for remedial alternatives of unregulated municipal solid waste landfills leachate-contaminated groundwater. Front Earth Sci 7(3):310–319

Han Z, Ma H, Shi G, He L, Wei L, Shi Q (2016) A review of groundwater contamination near municipal solid waste landfill sites in China. Sci Total Environ 569:1255–1264

Harbaugh AW (2005) MODFLOW-2005, the US Geological Survey modular groundwater model: the ground-water flow process. US Department of the Interior, US Geological Survey Reston, VA

Li Y, Li J, Deng C (2014) Occurrence, characteristics and leakage of polybrominated diphenyl ethers in leachate from municipal solid waste landfills in China. Environ Pollut 184:94–100

Ma ZF, An D, Jiang YH, Xi BD, Li DL, Zhang JB, Yang Y (2012) Simulation on contamination forecast and control of groundwater in a certain hazardous waste landfill. Huan jing ke xue= Huanjing kexue 33(1):64–70

Maiti SK, De S, Hazra T, Debsarkar A, Dutta A (2016) Characterization of leachate and its impact on surface and groundwater quality of a closed dumpsite—a case study at Dhapa, Kolkata, India. Procedia Environ Sci 35:391–399

Mohamed AK, Liu D, Mohamed MAA, Song K (2018) Groundwater quality assessment of the quaternary unconsolidated sedimentary basin near the pi river using fuzzy evaluation technique. Appl Water Sci 8(2):65

Rona M, Lev O, Gvirtzman H (2018) Optimal remediation scheme for a wastewater recharge site: Contaminants fate and transport model. Groundwater 56(6):871–880

us Saba N, Umar R, Ahmed S (2016) Assessment of groundwater quality of major industrial city of Central Ganga plain, Western Uttar Pradesh, India through mass transport modeling using chloride as contaminant. Groundw Sustain Dev 2:154–168

Zhang C-Y, Ma L-N, Zhang S, Li Z-H, Yin M-Y, Zhang Y (2007) The application of visual modflow to the simulation of groundwater nitrate contamination in Shijiazhuang. Acta Geoscientia Sinica 28(6):561

Zhang B, Li G, Cheng P, Yeh T-CJ, Hong M (2016) Landfill risk assessment on groundwater based on vulnerability and pollution index. Water Resour Manag 30(4):1465–1480

Zheng C, Patrick Wang P (1999) Mt3dms: a modular three-dimensional multispecies transport model for simulation of advection, dispersion, and chemical reactions of contaminants in groundwater systems; documentation and user's guide. Technical report, Alabama Univ University

Zhu H-N, Yuan X-Z, Liang J, Yin J, Jiang H-W, Huang H-J et al (2014) Integrated evaluation system under randomness and fuzziness for groundwater contamination risk assessment in a little town, Central China. J Cent South Univ 21(3):1044–1050

Transboundary Water Management of the Indus River: A Repetitive Cycle

Jessica M. Williams

Abstract The Indus River plays an important role in both India and Pakistan's food and energy security through irrigation and hydropower. Despite the presence of an international agreement, the Indus Water Treaty, tensions between the two states over the river have persisted since partition. As such, the Indus has come to be governed along nationalistic and technocratic lines, with little coordination or cooperation between the two dominant riparian countries. This approach has resulted infrastructure construction and engineers being prioritised over environmental or social considerations on both sides of the border. By taking a discourse based approach, the transboundary water governance of the Indus River is unpacked to demonstrate how actors in both India and Pakistan utilise discursive tactics to maintain this policy approach. As such, discourse is shown to be 'stuck' in a state termed as discourse inertia. This inertia prevents the introduction of new actors and management approaches into the discourse, allowing both states to seek to control the river through an infrastructure-orientated and technocratic approach. Such an approach tends to results in negative social and environmental externalities as well as increased regional tensions.

Keywords Indus river · Discourse · Water management · Transboundary water

1 Introduction

The Indus River has a turbulent history, which continues to influence riparian relations. Resource scarcities and climate change have the potential to exacerbate the already tense and sensitive issue of transboundary water governance. The discourse employed by decision makers regarding the river is considered informative in understanding the present situation, particularly in regards to the approaches undertaken by both India and Pakistan towards managing the Indus River. Persistent tensions result

J. M. Williams (✉)
The University of Hong Kong, Pokfulam, Hong Kong
e-mail: jw89@hku.hk

R. Sun and L. Fei (eds.), *Sustainable Development of Water and Environment*, Environmental Science and Engineering,
https://doi.org/10.1007/978-3-030-16729-5_14

in genuine cooperative efforts being stymied and prevalence of water management approaches that focus on nationalism and security, to the detriment of environmental and social considerations.

Discourse change can be indicative of policy change (Jørgensen and Phillips 2002), yet the discourse employed by decision makers regarding the Indus River appears to be 'stuck' in a situation termed as 'discourse inertia'. Recognition of the way that discourse is employed by the Indus countries in relation to the management and governance of the river is important in opening up discussion on how to break this inertia, ease tensions and introduce more sustainable water management practices.

The Indus River originates in the northern Himalayas and is shared by China, Afghanistan, India and Pakistan. India and Pakistan dominate the basin, from a geographical and resource perspective as well as from a political one. From 1859, the British developed the Indus into the world's largest continuous irrigation system. Partition split this system, leaving the headwaters in India and the majority of the irrigation structures in Pakistan. The Indus Water Treaty (IWT) was signed in 1960 with the aim to resolve the dispute that arose from this split.

The IWT apportions the three western rivers of the Indus—the Jhelum, Chenab and Indus to Pakistan and the eastern rivers—the Ravi, Beas and Sutlej to India. India is allowed limited use of the western rivers for domestic, non-consumptive and agricultural purposes as well as generating hydropower, subject to treaty specifications and unlimited use of the eastern rivers. There are currently no formal water governance agreements between the other riparian states. The Indus countries are all engaged developing dams for storage and hydropower on the basin. However, the basin is particularly susceptible to the impacts of climate change and already suffering from water shortages caused by over-extraction for irrigation, (Food and Agriculture Organisation of the United Nations 2011) increasing the urgency for greater coordination and the sustainable management of the river.

2 Methodology: Discourse and the Indus River

While institutional and governance approaches have made a significant contribution to the study of water governance issues, it is argued that the incorporation of the ideational dimension in such studies is beneficial. The predominance of positivist and neo-positivist approaches in international relations and political studies often results in the discursive dimension being under-developed (Fischer 1998; Phillips et al. 2004). A discourse-centric approach is, therefore, undertaken in exploring the dynamics of water governance on the Indus River.

Discourse consists of the group of ideas, concepts and categories, which are produced, reproduced and evolved through interactions. In this way, social and physical relations are given meaning (Jägerskog 2002; Mirumachi 2002). When discourses become unquestioned and dominant they are described as sanctioned (Phillips et al. 2004). The assumptions contained within the sanctioned discourse constrain the

options available for policy makers and so indicate policy outcomes (Dayton 2000; Gerlak and Schmeier 2014).

Change in the sanction discourse may signal policy change and can occur when it is confronted by exogenous events or crises. Similarly, change may be incentivised through pressure from foreign governments or financial/donor institutions. Change may also be intentionally sort by actors through discursive strategies such as constructing narratives, counter-narratives, exclusion strategies and the deployment of normative power. How successful actors are in effecting change depends on their power, position and resources, and the level of change sought (Leipold and Winkel 2013). However, changes in the sanctioned discourse may be superficial. Co-opting elements, particularly normative concepts, from another discourse may give the appearance of change, but the core beliefs and assumptions remain unchanged (Christoff 2013).

Discursive change may also be avoided by shifting issues up or down the political agenda by using depoliticising or securitising discursive acts (Zeitoun et al. 2011). This can place the issue out of the remit of certain groups while making others responsible. Technical language is often used to depoliticising policy processes, which places responsibility with engineers and technocrats, resulting in ostensibly neutral policy outcomes (Shore and Wright 1997). Policies that become highly politicised are securitised and treated as high priority issues, constituting an issue of state sovereignty and national interest. This allows exceptional measures to be mobilised and removes the issue from debate at lower political levels (Buzan et al. 1998; Allan and Mirumachi 2010). Threats do not have to be in existence or real for securitisation to occur (Mirumachi 2002; Stritzel 2007).

Understandings of change/stasis dynamics within policy is often incomplete due to the role of ideas and discourse being overlooked. The concept of discourse inertia is utilised to focus attention on resistance to change, the relationship between discourse and institutions and factors exogenous to institutions. This is done by expanding on discursive institutionalism (Schmidt 2006, 2011) and the discursive institutional spiral (Den Besten et al. 2014).

Discursive institutionalism introduces discourse into institutional theories through recognising the discourse that actors partake in when generating, deliberating and/or legitimating ideas concerning political action within the institutional context. Ideas are created through interactions and these are encapsulated within institutions. An institutional change may occur when the ideas and discourses that actors hold regarding that institution change. Discourses are shaped by the institutional context, which determines where discourses matter (Schmidt 2006). Ideas are distinguished based on their impact on policy change. Ideas are categorised based on if they are ones of policy, policy programme or public philosophy (Schmidt 2011).

Policy ideas are more changeable and have less of an impact on policy than policy programme or public philosophical ideas. Policy programme ideas define the problems for policies to solve. These are underlined by public philosophical ideas, which appeal to deeper values and principles of knowledge and society. When these ideas change, it is considered revolutionary (Schmidt 2011). When applied to discourse, narratives at the everyday level are considered more fluid and changeable,

while those that are institutionalised are more resistant to change. Discourses that become privileged, those which contain fundamental ideas, beliefs and interests, will resist change.

Discourse inertia aids explanation of how and why certain narratives, and so policies, are maintained, even when they may not be the most appropriate. Inertia is considered to be the persistent promotion and dominance of a perception of reality, which results in certain narratives and elements of discourse being continuously reproduced. Discourses that are sanctioned are believed to be more likely to display inertia due to path dependent tendencies and powerful entrenched interests.

Even when discourse inertia is present, discourse must be continually reinforced and reproduced. When actors' discourse becomes sanctioned, they fiercely defend this dominance. This continuously reinforces and embeds the sanctioned discourse, which can result in certain narratives reaching an ideational status by becoming entrenched in institutional, politically and social practices. These narratives are considered to be privileged, they are taken for granted and self-reinforcing and so prone to discourse inertia. Over these privileged narratives, more shallow ones can work to achieve an objective or align with an outside interest. These narratives are more easily manipulated as they are more fluid and flexible.

Discourse inertia conceptualises how a discourse may resist pressure for change. It is illustrated through extending Den Besten et al. (2014) discursive-institutional spiral. The discursive-institutional spiral depicts how discourses evolve through interactions between actors, their ideas, subject areas and institutional initiatives. These interactions form a spiral, the loops of which start with institutionalisation. This catalyses discussion and debate and brings in new actors. As actors become more involved, the more likely they will introduce new ideas and concepts. This expansion of ideas and actors results in institutionalisation and the discourse narrowing, this then begins the next loop of the spiral. Power is evident in the spiral through the exclusion or inclusion of actors or ideas in the discursive institutional process (Den Besten et al. 2014).

When discourse inertia occurs, a process similar to institutional path-dependency is present within the spiral. This restricts the entry of new actors and ideas into the discourse, which narrows the spiral and limits the evolution and expansion of discourses. Discursive elements that become institutionalised may be reinforced along subsequent spirals and act to exclude other elements and actors. The ability of new actors to access the discourse is further reduced, which restricts the introduction of alternative ideas.

2.1 The Indus River Case Study

India and Pakistan account for the majority of the discussion on the Indus and their current water discourses can be traced to British India. The British initially justified and legitimised their rule through legal language. This started to change from 1890 when science was layered over the legal language to further legitimise colonial

presence. The state's dominance was justified through appeals to notions of impartiality and detached ruling, forming a strong notion of state authority. This invoked the state's ability to command waterways and alter landscapes through science and technology. The dominant vision of environmental control linked with the growing professionalization of water engineering emerged from this conception (Gilmartin 2015).

The construction of the extensive irrigation system by the British is evidence of this move to control nature. It resulted in civil engineers and bureaucrats displacing local irrigators and community approaches as well as the displacement of traditional water practices with the control of floods and natural river regimes. This approach persists in modern India and removes alternative management practices while establishing infrastructure as the only feasible option (D'Souza 2008).

Engineering the Indus in this manner meant that the basin and its network of irrigation structures were perceived as a technical whole. It was held that water needed to be moved from areas of abundance to those of deficit. Maximising the amount of land under irrigation, rather than efficiency, was the main intent. Therefore, the system was deliberately built to embody water scarcity. As a result, a large proportion of the population came to be dependent on the system (Gilmartin 2015).

At partition it was suggested that India and Pakistan maintain the integrity of the irrigation system by running it as a unit. However, this was met with hostility (Gilmartin 2015). Instead, a Standstill Agreement was signed by the chief engineers of east and west Punjab in 1947. This maintained the existing arrangement while a solution was sought, however, on expiry, no resolution had been reached. In 1948 East Punjab shut off water from several of the canals into Pakistan (Akhtar 2010). The act illustrated to Pakistan how ideas of nation were connected to the basin (Gilmartin 2015) and embedded a sense of vulnerability. The incident threated Pakistan's food security and pressured acceptance of India's terms. This resulted in another agreement, the 1949 Delhi Agreement, but the issue persisted (Akhtar 2010).

In India, the Prime Minister, Nehru, famously liked dams to 'temples of new India' at the Bhakra-Nangal inauguration in 1954. This association of dams with religion and modernity invokes a higher morality. It also links back to pre-colonial perspectives regarding the sanctity of water reservoirs. In such a way, dams became symbolic of a higher moral purpose and representative of the way towards development through the control of nature (Gilmartin 2015; Morrison 2010).

As the Bhakra Nangal project was a point of contention in an unresolved dispute between Punjab and Sindh, the completion of the dam was only possible through India asserting a full legal claim over the river. The realisation of the project and emphasis on the dam for Indian development essentially dismissed Sindh's concerns and asserted Indian claim to full use of the river's water. Therefore, Nehru's discourse paints a unified picture based on a higher morality of Indus development but at the same time, contains a narrow nationalistic territoriality by denying downstream rights. As a result, an issue of India versus Pakistan was created. Pakistan's response was to engage in building a string of water diversion projects aimed at preventing similar incidents. Nationalistic rhetoric accompanied these projects and actions where hailed as patriotic. In contrast, in negotiations Pakistan constantly evoked its moral

right to continue using water from east Punjab's rivers based on its historical use (Gilmartin 2015).

The Indus negotiations occurred during the Cold War so there was a risk of escalation. The western international community feared instability would allow communist influences to take hold of the region and sought involvement. Therefore, in 1952 the World Bank (WB) became involved in negotiations. Notably, David Lilenthal, the founder of the Tennessee Valley Authority, was prominent in mediation. He initially pushed for the integrated management of the basin, believing this to be possible if politics were removed and the issue treated as technical (Akhter 2015). However, both states were frantically engaged in a process of nation building. Taking the watershed as the scale for management would blur the distinction between the states. By 1954 it was evident this approach was not feasible. During negotiations, Lilenthal ignored the Kabul River, Afghanistan and China (Haines 2014). This allowed for discursive simplification, which privileged certain actors and scales over others (Fox and Sneddon 2007).

Lilenthal perceived the problem to be technical rather than political or religious. Consequently, he looked to replace politicians with engineers and those with technical expertise in negotiations. This aligned with South Asia's history of holding engineers in esteem and so they came to play a prominent role in negotiations. Their utility was in their ability to effect technological change but engineers were also linked through their professional and personal histories. This gave them a way of transcending political differences as well as a shared language. Both of which were vital to the realisation of the IWT as it allowed negations to progress without involving issues of sovereignty or territoriality (Haines 2014).

Despite their shared backgrounds and professions, the engineers worked separately to draw up basin plans, which predictably, favoured their own national interests. Neither sides plan was accepted so the WB drew up its own blueprint dividing the basin on geographic lines, which formed the basis of the IWT. The willingness of those involved to prioritise technical actors during the process further embedded the group's position and allowed engineers to expand their authority to the international level. This was accompanied naturalising the belief about the objectivity of experts in decision making (Haines 2014). In 1960, the IWT was signed by India, Pakistan and the WB.

Since its signing, the IWT has been invoked to mediate several disputes. The most recent is the Kishanganga and Ratle dispute. The Kishanganga dispute involves an Indian hydropower project that diverts water from the Kishanganga to the Jhelum River. Pakistan has plans to build a hydropower station downstream, which also relies on diverting water from the Kishanganga River. Both countries began construction of their projects with the intent to claim 'prior appropriation' and 'existing use' of the river's water (Uprety and Salman 2011; Briscoe 2014).

As per the IWT's dispute resolution proceedings, Pakistan submitted the case to the Court of Appeal (CoA) in 2010. A partial award was handed out in 2013, which allowed India to continue with its construction. This decision was based on the Indian plant being run-of-the-river and India demonstrating a high degree of certainty when it started construction in 2004–2006. The Court also ruled that India should

construct and operate the project in a way that maintains minimum environmental flows to Pakistan (Uprety and Salman 2011; Briscoe 2014). This recognition of the environment is significant as it is not accounted for within the IWT (Grover 2014). It may, therefore, represent an attempt to shift discourse towards greater environmental sensitivity.

The dispute continues in the form of the Kishanganga and Ratle disputes, which concerns design and technical features of the Indian project. Pakistan's objections are framed technically and based on a literal reading of the IWT. This is done to avoid becoming tangled in emotive issues associated with the Indus. There is also a lack of common understanding between the two countries as to the issue being debated. Pakistan is concerned with the cumulative storage capacity of Indian projects, which India has refused to recognise as a legitimate concern (Mustafa 2010). This denies it space in the official discourse. The dispute is on-going, with bilateral talks making little headway.

2.2 Document Selection and Analysis

Discourse analysis was conducted to explore the governance and management of the Indus River. There is no standardised approach for discourse analysis (Gill 2000) and so analysis is informed by the discussed conceptual elements. Detailed readings of the documents were undertaken and these were then coded into broad categories based on water governance or management. This allowed the privileged discourses to be identified, which indicates if these discourses change over time.

Analysis was concerned with locating each state's privileged discourse regarding the management of the Indus River from the past five years (2012–2017). This

Table 1 Types of documents analysed regarding the Indus River

Country	Source	Type of document
India	Ministry of Water Resource, River Development and Ganga Rejuvenation	Annual report
		Ebooks
		National policy
		Organisation reports
	Ministry of External Affairs	Question and answer sessions
		Speech transcripts
		Press release
Pakistan	Water and Power Development Authority	Research papers
		Annual reports
		National policy
	National Assembly	Question and answer sessions
	Press Information Department	Press releases

includes consideration of discursive mechanisms such as framing, co-optation and narratives in dissecting how actors argued their stance. Once analysis has occurred, it can be combined with the historical background, detailed above, to determine if discourse change has occurred/is occurring.

Documents for discourse analysis are located from recent state sources. These documents are likely to uphold the states' sanctioned discourse and so reflect the dominant approach to water resources management of the Indus. These include those concerning the Indus and the IWT, which includes statements to the WB and other international organisations (Table 1).

3 Analysis

Analysis reveals that infrastructure, notably dams, dominates the Indus discourse. Indian and Pakistani discussions are mostly bilateral, with Afghanistan and China often being overlooked in the debate. However, there are exceptions, mostly when a countries dam project comes under discussion.

In India and Pakistan dams are linked to state development, control and modernity. Concepts with normative value from ecological modernisation and sustainability based discourses have been used to justify projects. Nationally, India's water policy is worded to align with IWRM and good water governance. It emphasises the need to promote the 'integrated and sustainable development and management' of water (CWC 2017). Focus is on the Central Water Commission's Dam and Rehabilitation and Improvement Programme, despite there being a significant number of new hydropower and irrigation projects under construction or consideration (Ministry of Water Resources 2016a). Pakistan's Water and Power Development Authority report titled "Integrated Water Resources Management in Pakistan" (Sufi et al., n.d.) uses IWRM to justify the need to build reservoirs to increase supply.

Discourse at the transboundary level differs. Statements from India stress plans to "accelerate development" of water projects for "optimal usage of water allocated to India" under the IWT (Ministry of Water Resources 2016b) (28). In Pakistan, international discourse holds dams to be of 'national importance' thanks to their energy generating and storage capabilities (Press Information Department 2017). Subsequently, the transboundary level is dominated by development and sovereignty narratives.

In Pakistan, the Indus is a sensitive and politicised topic. The role of the government and Indus Water Commissioner in ensuring Pakistan's rights under the IWT has been questioned on several occasions along with accusations of them being in league with India (Gishkori 2014; Ahmed 2012; National Assembly Secretariat 2017a, b). While accusations of this ilk remain at the lower political levels, they do demonstrate national discontent and mistrust towards India and potentially the government. The government's discourse may thus be influenced when handling differences under the IWT and may make it more likely to call on international mechanisms for their resolution.

India and Pakistan appear to be competing for geopolitical influence in Afghanistan. India is framing itself as a benevolent 'partner' to Afghani development. It emphasise how India has aided Afghanistan and refers to Pakistan as a destabilising influence. This allows India to contrast itself in opposition to Pakistan which, positions itself favourably (Ministry of External Affairs 2016a). India's actions concern Pakistan as it sees itself as being surrounded by hostile influences, which strengthens the narrative that India seeks to keep Pakistan weak. Pakistan is seeking joint cooperation on the Kunar River (National Assembly Secretariat 2014), which could be an attempt at exercising its strategic influence. It also allows it insider information into the project, allowing it ensure its downstream rights while benefitting from exported hydropower.

In Pakistan, water discourses emphasise the nation's growing scarcity and energy shortages. The situation is likened to a 'crisis' and as 'critical', blamed for keeping "large proportions of the population impoverished" (Clarke and Chaudhry 2014) (ES-28). The solution to build infrastructure, "[t]o improve the situation it is dire need of time to construct storage facilities and improve flood regulation" (Ahmad et al. 2012) (74), "WAPDA has been vigilantly looking after the water scarcity issue in the country…There are several other small, medium and large multipurpose projects which are at different stages of execution" (National Assembly Secretariat 2004) (30) and "Pakistan is facing water shortages which are going to get worse with every passing year…immediate construction of storage dams, not for power alone but for water storage is essential" (National Assembly Secretariat 2017a) (13).

Hydropower and storage dams are positioned by Pakistan as the solution to issues spanning from droughts and floods to socio-economic development and human health. Urgency is instilled through neo-Malthusian narratives of limits and scarcity, which justify prioritising projects. Even WAPDA's IWRM document presents storage as the answer to water issues. Following, any threat to the Indus River's water supply conflicts with this solution and so is an issue of national survival, becoming highly politicised.

Indian infrastructure projects appear to revive the Indus debate in Pakistan. The media in Pakistan often accuses India of violating the IWT, despite prominent actors, within Pakistan and abroad, stating that this is not the case (Mustafa 2017). In 2014, The Minister for Water and Power stated that India does "not have the any capability to control or misuse…the western rivers" and that "Pakistan is receiving almost the same volume of water in all three western rivers as we were receiving at the time of signing of the Treaty in 1960" (National Assembly Secretariat 2014) (24). However, in 2016, the same minister stated that "it is a fact that India is not fully abiding by the provisions of the Indus Water Treaty 1960 in its true letter and spirit…The design of these [Indian run-of-the-river] plants [under construction] are mostly in violation of the design criteria specified by the Indus Water Treaty 1960." The design provides "the potential for using higher than the Treaty permitted control for India's own advantage and to Pakistan's harm" (National Assembly Secretariat 2016) (2). Therefore, Pakistan's official stance towards Indian actions is prone to inconsistencies. Changes in rhetoric are likely to be reflective of changes in the levels of tension between the two states.

Narratives from India generally dismiss Pakistan's concerns and tend to question if a dispute is actually present. Before the Kishanganga case was submitted to the CoA, the Indian Minister of State for Water Resources stated that it had been explained to Pakistan that the project complied with the IWT and so the 'stage of a difference/dispute has not arisen'. The issue, therefore, should remain at the commission level (Press Information Bureau 2009). In the recent Kishanganga and Ratle situation, India holds the issue to be a 'difference' rather than a 'dispute' and so pushes for additional consultation and to resolve the issue bilaterally (Ministry of External Affairs 2016b, 2017a). Indian narratives aim to maintain bilateralism and refuse to recognise the issues at the higher dispute levels. The balance of power is tilted in India's favour and discussions at the bilateral level draw out the procedure, which allows construction to continue.

The Uri terror attacks in September 2016 intensified the Kishanganga and Ratle case. Indian responses included threats to scrap the IWT. The Indian Prime Minister Narendra Modi stated that "blood and water cannot flow together" and the intent to fast track hydropower projects to harness India's full allocation of the western rivers under the IWT (Rediff 2016) (1). The issue is complicated by both sides submitting requests to the WB for different dispute resolution proceedings under the IWT. Pakistan requested the CoA procedure while India, for the appointment of a neutral expert (NE). The timeline of proceedings is also confused; India claims it submitted its request on the 4th October 2016, which was followed by Pakistan's request on the 27th October (Ministry of External Affairs 2016b). While, Pakistan holds that it informed India on the 19th August 2016 of its intent to request a CoA and that on the 27th September 2016, it requested the WB to appoint the Court's Judges (Press Information Department 2016a). The countries may be competing for the high ground by presenting the other's submission as appearing to undermine the IWT's dispute resolution mechanisms, while increasing the legitimacy of their own action.

The WB initially began both proceeding simultaneously but then announced a pause to protect the IWT. This basically handed the issue back to India and Pakistan by asking them to find a resolution within the remits of the IWT. This essentially denies a core element of the IWT's dispute resolution capacity by withholding resource to a CoA or NE. The success of the IWT hinges on its ability to mediate securitised discourse and prevent conflict. If the Bank proceeded with concurrent requests, issues of hierarchy become involved that could undermine the IWT. However, by halting proceedings, the WB's neutral role may be questioned as India has refused to halt construction.

India responded unfavourably to the WB's initial pursuit of concurrent proceedings. The Minister of External Affairs stated that the India Government 'strongly protests' to the WB's decision and has 'grave concerns' that the workability of the IWT will be called into question (Ministry of External Affairs 2016b). He warned that India 'cannot be a party to actions which are not in accordance with the IWT' (Ministry of External Affairs 2016c) (4). This narrative positions the WB and, indirectly, Pakistan as threats to the survival of the IWT. Legal rhetoric is utilised as justification and Indian statements may indicate that it will stop complying with

proceedings. As the other actors are framed as acting outside the legal bounds of the IWT, India's actions are legitimised. This may have exerted pressure on the WB and contributed to its decision to halt proceedings.

Conversely, the decision to pause proceedings was received negatively by Pakistan. The Finance Minister declared that the decision 'seriously prejudices' Pakistan's interests and rights under the IWT. The WB is accused of denying Pakistan a competent forum to address its grievances. The rhetoric is starting to show disillusionment with the IWT and its procedures. This may be why Pakistan continually states the WB's legal obligations and frames the establishment of a CoA as the only way to resolve the dispute (Press Information Department 2016b, 2017). The Prime Minister of Pakistan recently conveyed that he hoped the WB will play a lead role in the resolution of the dispute through the establishment of a CoA (Press Information Department 2017). Pakistani narratives in this area frequently stress the role of the WB and the need to adhere to the IWT. This may be due to the perception of vulnerability that persists in Pakistan causing it to use international mechanisms to hold India accountable.

India has claimed that it is Pakistan who is violating the IWT as they 'rushed' to a third party forum instead of attempting to reach an amicable resolution (Ministry of External Affairs 2016d). Pakistan is downstream, which strengthens this shift in blame as it is unusual for the lower riparian to be able to deliberately harm the upper state. This positions Pakistan as using the IWT against India and strengthens Indian claims that they are acting within the treaty by delegitimising Pakistan's accusations.

India's water relations and discourse in the region tend to prefer bilateralism. This is as despite it being the most powerful basin state, aside from China, it is an upstream and downstream riparian on several transboundary rivers. Multilateral discourse would, therefore, shift the power balance and limit India's influence. Multilateralism enables countries to form a bloc to increase their influence through combined pressure. India's bilateral approach is being challenged, particularly by China and its actions towards Pakistan. Notably, India is wary of the China–Pakistan Economic Corridor arm of China's Belt and Road strategy (Ministry of External Affairs 2017b). The Indian Government has repeatedly informed China that it is concerned with their activities in Pakistan; particularly those that involve Pakistan occupied Kashmir, and asked them to cease. The involvement of a disputed region, Kashmir, invokes issues of sovereignty. Despite such issues of national interest, Indian official narratives rarely escalate to securitisation in regards to China.

4 Discussion and Conclusions

The Indus River's history is influential in shaping how the river is perceived, discussed and managed. The British suppressed local water management practices with the introduction and cultivation of a technocratic and engineering approach. They privileged engineers as well as linked infrastructure and technological constrictions with modernity and progress. This approach was carried forward at partition and

was further institutionalised by the discourse of nation building and dam projects. Indian and Pakistani discourse both linked political legitimacy and nationalism to large dam projects. The IWT was made a reality through engineers communicating using technocratic language, which institutionalised the technical approach in the treaty.

Rather than evolving to incorporate more cooperative, environmentally or socially sustainable water management approaches, discourse seems to be in a state of discourse inertia. The technocratic and infrastructure orientated approach is maintained by actors. This is often done by shifting issues across the political levels, moving from technical narratives through to politicised and securitised ones, before then being de-securitised by technical narratives. Therefore, little actual change is occurring in how the Indus is perceived and governed. Technocratic and neo-Malthusian narratives advocate infrastructure projects, which ignite nationalist and sovereignty concerns. This results in heightened rhetoric. Communication is only able to occur through institutionalised technical narratives and the IWT.

Therefore, the debate only allows for technical or politicised/securitised nationalistic narratives that revolve around infrastructure. This is problematic as such an approach ignores or subverts issues such as climate change or local livelihoods and concerns (Mirumachi 2002; Earle et al. 2015). Hydraulic infrastructure also interferes with the river's hydrology and so impact ecosystem services and flow regimes (Räsänen et al. 2017). This could further exacerbate tensions between India and Pakistan as both sides look to optimise their share of benefits from the Indus.

The actors maintaining these narratives primarily comprise of engineers, bureaucrats and security departments. Discourse is predominantly bilateral. This appears to be deliberately enforced by India as bilateralism allows it to take advantage of the favourable balance of powers in the basin. Nationalistic and territorial notions are often used to frame issues concerning the Indus. Consequently, discourse is frequently politicised and securitised. This leaves little space for civil society, NGOs or academics. The dominance of technical and legal jargon compounds this situation. Due to its role as third party to the IWT, the WB is in a unique position as it can join the debate, but only when formally requested to by India or Pakistan and its role is mostly procedural. The dominant actors tend to come from powerful government water management bodies, which have long histories tied to nation building. The ability to draw on nationalistic sentiments allows these groups to dominate the discourse and perpetuate actions congruent to their interests.

Despite there being a range of cooperative institutions, including SAWI and ICIMOD, they generally are not involved at the transboundary discursive level. Also, while there are a host of narratives suggesting improvements for the management of the Indus or on resolving Indian–Pakistani differences, at the transboundary level the IWT and associated institutions dominate. As such, discussion is limited and the agenda tightly controlled, which reinforces embedded discourses.

There are areas where greater cooperation and sustainable management can be sought. Of note, is the Kishanganga partial award for its inclusion of environmental flows. This seems to be the only time at the transboundary level that the environment is given space in the discourse. It sets a precedent for including environmental issues,

which are absent from the IWT. It may provide a path for environmental narratives to expand upon, however, this will be dependent on an influential actor with access to the debate taking up the rhetoric. Without strong backing, it seems unlikely that environmental narratives can gain ground against the technical and security/sovereign storylines that dominate.

National perceptions of vulnerability or sovereignty stemming from the basin's history have resulted in access to the debate being tightly controlled and predominately technical narratives that are prone to politicisation or securitisation. Technical narratives can be traced back to British India. They comprised the neutral language for water negotiations when sovereignty and security narratives arose at partition. The basin countries hold dams as essential to national interests, but construction causes political narratives at the transboundary level to emerge. This escalates the discourse towards securitisation. The debate is narrowed when technical discourses are employed, which de-securitises the issue or allows meaningful discussion. Discourse appears trapped within this process of securitisation/descuritisation surrounding infrastructure and so is held as being in a state of discourse inertia. This prevents more environmentally sensitive and sustainable management approaches from entering the agenda. Instead, focus remains on hydraulic infrastructure construction, which results in negative social and environmental externalities.

Acknowledgements The author would like the thank P. Hills, K. Joe-Laidler, and W. Law for input and guidance on the project. J. M. Williams was supported by a University of Hong Kong studentship.

References

Ahmad I, Sufi AB, Hamid S, Gulrez W (2012) Construction of large and medium dams for sustainable irrigated agriculture and environmental protection. World Environment Day, June 2012, WAPDA, Pakistan, pp 61–75

Ahmed K (2012) Target: Jamaat Ali Shah. The Express Tribune, 2 Dec 2012

Akhtar DS (2010) Emerging challenges to Indus Waters Treaty. Reg Stud 28(4):3–66

Akhter M (2015) The hydropolitical cold war: the Indus Waters Treaty and state formation in Pakistan. Political Geogr 46:65–75

Allan JA, Mirumachi N (2010) Why negotiate? Asymmetric endowments, asymmetric power and the invisible nexus of water, trade and power that brings apparent water security. In: Earle A, Jägerskog A, Öjendal J (eds) Transboundary water management: principles and practice. Earthscan, London, pp 13–26

Briscoe J (2014) Peace, not war on the Indus. The Hindu, 31 Dec 2014

Buzan B, Waever O, De Wilde J (1998) Security: a new framework for analysis. Lynne Rienner Publishers, Boulder

Christoff P (2013) Globalization and the environment. Rowman & Littlefield Publishers, Lanham

Clarke M, Chaudhry AA (2014) Strategic sectoral environmental and social assessment of the Indus Basin, vol I: main report, final. Ministry of Water and Power Government of Pakistan, SMEC, EGC

CWC (2017) Central Water Commission—an apex organization in water resources development in India. http://cwc.nic.in. Last accessed 4 Jan 2018

Dayton BW (2000) Policy frames, policy making and the global climate change discourse. In: Addams H, Proops J (eds) Social discourse and environmental policy. Edward Elgar, UK, pp 71–99
Den Besten JW, Arts B, Verkooijen P (2014) The evolution of REDD+: an analysis of discursive-institutional dynamics. Environ Sci Policy 35:40–48
D'Souza R (2008) Framing India's hydraulic crisis: the politics of the modern large dam. Mon Rev 60(3):112
Earle A, Cascão AE, Hansson S, Jägerskog A, Swain A, Öjendal J (2015) Transboundary water management and the climate change debate. Routledge, London, UK
Fischer F (1998) Beyond empiricism: policy inquiry in post positivist perspective. Policy Stud J 26:129–146
Food and Agriculture Organisation of the United Nations (2011) Indus Basin. Aquastat. http://www.fao.org/nr/water/aquastat/basins/indus/index.stm. Last accessed 25 Apr 2016
Fox CA, Sneddon C (2007) Transboundary river basin agreements in the Mekong and Zambezi basins: enhancing environmental security or securitizing the environment? Int Environ Agreements Polit Law Econ 7(3):237–261
Gerlak AK, Schmeier S (2014) Climate change and transboundary waters: a study of discourse in the mekong river commission. J Environ Dev 23(3):358–386
Gill R (2000) Discourse analysis. In: Bauer MW, Gaskell G (eds) Qualitative researching with text. Image and sound: a practical handbook. Sage, Cheltenham, UK
Gilmartin D (2015) Blood and water: the Indus river basin in modern history. University of California Press, California
Gishkori Z (2014) Pakistan's water rights: senate panel wants ex-Indus water commissioner arrested. The Express Tribune, 1 Oct 2014
Grover PK (2014) Impact of verdict on Kishanganga project. Hindustantimes, 28 Jan 2014
Haines D (2014) (Inter)nationalist rivers? Cooperative development in David Lilienthal's plan for the Indus Basin, 1951. Water Hist 6:133–151
Jägerskog A (2002) The sanctioned discourse—a crucial factor for understanding water policy in the Jordan river basin. Occasional paper No. 41, Department for Water and Environmental Studies, Linköping University
Jørgensen M, Phillips L (2002) Discourse analysis: as theory and method. Sage, Thousand Oaks
Leipold S, Winkel G (2013) Actor-centred approaches of policy change discursive agency: towards an actor-centred analysis of political discourses. Paper prepared for the 1st international conference on public policy (ICPP 2013) June 26–28, France
Ministry of External Affairs (2016a) Visit of Prime Minister to Afghanistan (June 4, 2016). Government of India, New Delhi, 2 June 2016. https://bit.ly/2CNcgyq. Last accessed 10 Oct 2017
Ministry of External Affairs (2016b) Question No. 3673 Indus Water Treaty. Government of India, 7 Dec 2016. https://bit.ly/2FbkaTM. Last accessed 10 Jan 2018
Ministry of External Affairs (2016c) Official spokesperson's response to a query on Kishanganga matter at the World Bank. Government of India, 10 Nov 2016. https://bit.ly/2SAW7lk. Last accessed 9 Nov 2017
Ministry of External Affairs (2016d) Official spokesperson's response to a question on inter governmental water negotiations between India and Pakistan. Government of India, 16 July 2016. https://bit.ly/2F6EneC. Last accessed 9th Nov 2017
Ministry of External Affairs (2017a) Question No. 3209 support of USA on Indus Water Treaty. Government of India, 30 Mar 2017. https://bit.ly/2R6tfV7. Last accessed 10 Jan 2018
Ministry of External Affairs (2017b) Official spokesperson's response to a query on participation of India in OBOR/BRI forum. Government of India, New Delhi, 13 May 2017. https://bit.ly/2SyZDN1. Last accessed 11 Nov 2017
Ministry of Water Resources (2016a) River development and Ganga rejuvenation. Annual report 2015–2016. Central Water Commission, New Delhi

Ministry of Water Resources (2016b) River development and Ganga rejuvenation, winning with water. [ebook] The Government of India, New Delhi. http://mowr.gov.in/ebook-2016–17/mobile/index.html#p=1. Last accessed 5 Jan 2018
Mirumachi N (2002) Transboundary water politics in the developing world. Routledge, New York
Morrison KD (2010) Dharmic projects, imperial reservoirs, and new temples of India: an historical perspective of dams in India. Conserv Soc 8(3):182–195
Mustafa D (2010) Hydropolitics in Pakistan's Indus Basin. US Institute of Peace, Washington
Mustafa D (2017) Time for calmer hydro-diplomacy. Daily Times, 23 April 2017
National Assembly Secretariat (2004) National Assembly Secretariat questions for oral answers and their replies (9th session). Government of Pakistan, 26 Feb 2004. https://bit.ly/2R8aQr1. Last accessed 20 Oct 2017
National Assembly Secretariat (2014) National Assembly Secretariat questions for oral answers and their replies (9th session). Government of Pakistan, 26 Feb 2014. https://bit.ly/2R8aQr1. Last accessed 20 Oct 2017
National Assembly Secretariat (2016) National Assembly Secretariat questions for oral answers and their replies (34th Session). Government of Pakistan, 15 Aug 2016. https://bit.ly/2s9N5Qt. Last accessed 21 Oct 2017
National Assembly Secretariat (2017a) National Assembly Secretariat questions for oral answers and their replies (39th session). Government of Pakistan, 1 Feb 2017. https://bit.ly/2TpOyh9. Last accessed 21 Oct 2017
National Assembly Secretariat (2017b) National Assembly Secretariat questions for oral answers and their replies (39th session). Government of Pakistan, 21 April 2017. https://bit.ly/2CNcfdQ%20pdf. Last accessed 21 Oct 2017
Phillips N, Lawrence TB, Hardy C (2004) Discourse and institutions. Acad Manage Rev 29(4):635–652
Press Information Bureau (2009) Kishanganga hydro-electric project. The Government of India, 6 Aug 2009. https://bit.ly/2Svti9W. Last accessed 5 Nov 2017
Press Information Department (2016a) PR No. 221 Islamabad: Sept 27, 2016. Government of Pakistan, 27 Sept 2016. https://bit.ly/2SzkyiT. Last accessed 19 Oct 2017
Press Information Department (2016b) PR No. 271 U.S. Secretary of State John Kerry telephone call to the Finance Minister Senator Muhammad Ishaq Dar Islamabad: Dec 30, 2016. Government of Pakistan, 30 Dec 2016. http://www.pid.gov.pk/pid_old/?p=32231. Last accessed 19 Oct 2017
Press Information Department (2017) PR No. 244 MS. Kristalina, I. Georgieva, Chief Executive Officer (IBRD/IDA), World Bank Group Called on the Prime Minister Muhammad Nawaz Sharif Islamabad: Jan 26, 2017. Government of Pakistan. http://www.pid.gov.pk/pid_old/?p=33723. Last accessed 19 Oct 2017
Räsänen TA, Someth P, Lauri H, Koponen J, Sarkkula J, Kummu M (2017) Observed river discharge changes due to hydropower operations in the Upper Mekong Basin. J Hydrol 545:28–41
Rediff (2016) Blood and water cannot flow together: PM Modi on Indus Water Treaty. Rediff News, 26 Sept 2016
Schmidt VA (2006) Give peace a chance: reconciling four (not three) "New Institutionalisms". Paper prepared for presentation for the annual meetings of the american political science association, Philadelphia, Aug 31–Sept 3
Schmidt VA (2011) Speaking of change: why discourse is key to the dynamics of policy transformation. Crit Policy Stud 5(2):106–126
Shore C, Wright S (1997) Policy: a new field of anthropology. In: Shore C, Wright S (eds) Anthropology of policy: critical perspectives on governance and power, 1st edn. Routledge, London, pp 3–39
Stritzel H (2007) Towards a theory of securitisation: Copenhagen and beyond. Eur J Int Relat 13(3):357–383
Sufi AB, Hussain Z, Sultan SJ, Tariq I (n.d.) Integrated resources management in Pakistan. WAPDA, Pakistan

Uprety K, Salman MAS (2011) Legal aspects of sharing and management of transboundary waters in South Asia: preventing conflicts and promoting cooperation. Hydrol Sci J 56(4):641–661
Zeitoun M, Mirumachi N, Warner J (2011) Transboundary water interaction II: the influence of 'Soft' power. Int Environ Agreements 11(2):159–178

Restoration of Groundwater Over-Exploitation Area Based on MODFLOW in North Weifang, Shandong Province, China

Weijie Diao, Yong Zhao, Jiaqi Zhai, Fan He and Jing Yin

Abstract With rapid socio-economic developments, significant exploitation of groundwater has emerged as a serious environmental concern. In order to alleviate groundwater over-exploitation and determine a reasonable mining layout, a groundwater numerical simulation model was used in this study for the years 2014 to 2023. Simulations were conducted for various scenarios, including current conditions, agricultural water saving, groundwater replacement, and a comprehensive scenario. The results showed that under the current mining scenario, the groundwater level in the entire area decreased with a water budget of -0.45×10^8 m^3/a. Agricultural water saving can raise the groundwater level in most areas and groundwater replacement can efficiently control the drawdown funnels. However, the effect of a single measure is not comprehensive. Therefore, a utilisation coefficient of irrigation water at 0.7 and a 100% replacement of groundwater sources was established as a comprehensive scenario which resulted in groundwater level recovery and the disappearance of drawdown funnels by the end of 2023. Additionally, the groundwater flow returned to its natural direction from south to north and the northern water level was simulated to be higher than 0 m which would effectively prevent seawater intrusion. The conclusion can provide a reasonable reference for other areas facing similar challenges.

Keywords Groundwater over-exploitation · Numerical simulation · Restoration of groundwater · South to north water transfer project · Visual MODFLOW

1 Introduction

Groundwater resources play an important role in determining social and economic growth in many countries (Zektser et al. 2005; Konikow and Kendy 2005). However, with ever increasing water demands and limited surface water resources,

W. Diao · Y. Zhao (✉) · J. Zhai · F. He · J. Yin
State Key Laboratory of Simulation and Regulation of Water Cycle in River Basin, China Institute of Water Resources and Hydropower Research (IWHR), 100038 Beijing, China
e-mail: zhaoyong@iwhr.com

R. Sun and L. Fei (eds.), *Sustainable Development of Water and Environment*, Environmental Science and Engineering,
https://doi.org/10.1007/978-3-030-16729-5_15

massive groundwater resources are exploited. Groundwater over-exploitation areas are formed when the exploitation of groundwater over the years is greater than the recharge (Bromley et al. 2001; Camp et al. 2010). Such over-exploitation not only lowers the groundwater level but also results in ecological and environmental problems such as seawater intrusion and land subsidence (Pei 2018). Therefore, it is important to control groundwater over-exploitation areas (Huo et al. 2007; Lin et al. 2015).

In the past decades, much attention has been paid to restoration of groundwater system to alleviate groundwater over-exploitation and assist in the recovery of groundwater levels (Hu et al. 2010; Nam and Ooka 2010; Seo et al. 2014). The exploitation of groundwater mainly results from operation of pump wells and, therefore, closing such wells is a direct way for restoring groundwater level. In China's Zhangye Oasis, the degree of groundwater level recovery varies according to the reduction of exploitation; a decrement of up to 30% of the current conditions will result in a maximum groundwater level rise of 10 m after 10 years (Chen et al. 2016). Additionally, as for confined aquifer, since the early 1960s, artificial injection of groundwater has been proposed as an important measure for restoring confined aquifers and this method has been successfully adopted in numerous locations (Donovan et al. 2002; Han 2003; Phien-Wej et al. 1998; Tu et al. 2011). A study in Jordan (Abdulla 2010) compared different artificial recharge options (low, moderate, and high) with no recharge scenario for a period of 27 years. The results show that groundwater level in different areas ranged from 1.5 to 20 m under a high recharge scenario, indicating the need for management of groundwater resources in arid and semi-arid areas.

Although a simple reduction in the extraction of groundwater can raise the groundwater levels, it cannot fundamentally address the water supply and demand contradiction. The artificial recharge of groundwater can effectively conserve the groundwater system. However, several factors, such as water quality and economic feasibility, need to be considered. Presently, in the context of sustainable development, conservation of groundwater and its resources is an inevitable choice and groundwater replacement is an optimal scheme to alleviate over-exploitation of such resources. Several studies have indicated groundwater replacement to be an effective method for addressing the problem of over-exploitation of groundwater resources (Garcíagil et al. 2015; Mossmark et al. 2008).

In order to determine the dynamic changes to groundwater levels under different schemes, numerical models have been established using several software programs such as MODFLOW (Mcdonald and Harbaugh 1988), FELFLOW (DierschHJG 2005), and GMS (Group 2006). Additionally, Visual MODFLOW has been developed by integrating PEST and MT3D and has been utilised in several studies to analyse groundwater levels and water budgets (Zume and Tarhule 2008; Ayvaz 2009; Xu et al. 2012; Mohtashami et al. 2017; Iwasaki et al. 2014; Jang et al. 2016).

In this study, north Weifang in China, which exhibits the typical features of most groundwater over-exploitation areas, such as groundwater level decline and seawater intrusion, was selected as the study area. Moreover, it is also a water receiving area which makes it further suitable for conducting this study. To address the over-exploitation of ground water and determine the optimal groundwater restoration lay-

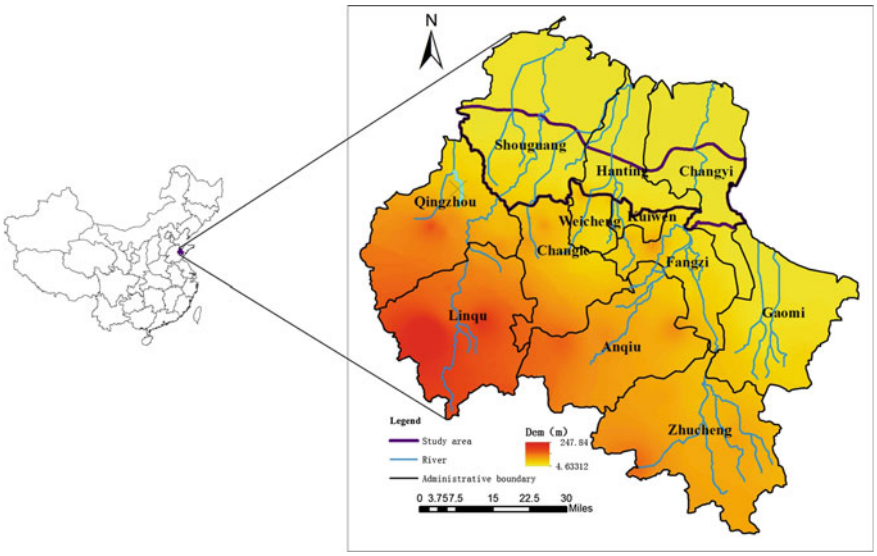

Fig. 1 Overview of the study area

out, Visual MODFLOW software was utilised to predict the groundwater flow after 10 years and the water budget under different scenarios were compared and analysed. Finally, make sure that the combination of agricultural water saving and replacement of groundwater sources as the proper restore scenario, which will provide a scientific reference in other over-exploitation area.

2 Methods and Data

2.1 Study Area

Over-exploitation of groundwater is mainly concentrated in three areas in north of Weifang, i.e. Shouguang, Hanting, and Changyi. These regions cover a total area of 2101.96 km^2. As shown in Fig. 1. According to the water resources bulletin statistics, the groundwater exploitation in 2013 was 2.51×10^8 m^3 which accounted for 58% of the total water supply. The consumption for agricultural activities and daily water usage by the residents were 1.43×10^8 m^3 and 0.51×10^8 m^3, accounting for 57 and 20% of the total groundwater consumption, respectively.

Based on the data from 17 boreholes, two hydrogeological profiles were drawn for the study area. As shown in Fig. 2. The aquifer system in the study area was divided into two parts, the southern piedmont alluvial plain which is a part of the

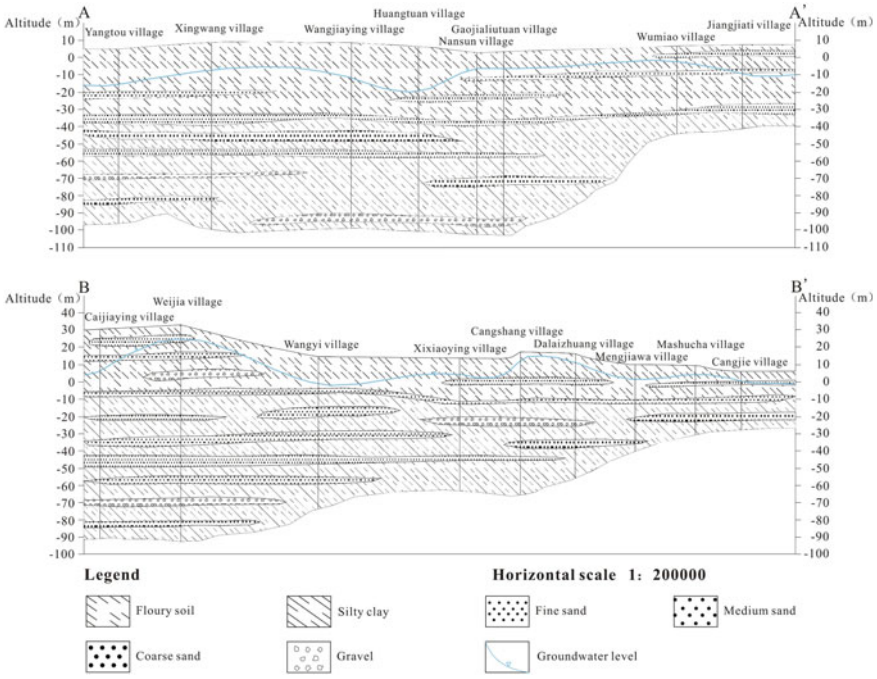

Fig. 2 Hydrogeological profiles of sections A and B

single-layer phreatic aquifer, the other part is the multi-layer complex aquifer in the northern flood plain which is complex in lithology.

2.2 Method

According to the hydrogeological conditions of the study area, a two-dimensional groundwater numerical simulation model was established by using Visual MODFLOW software. Its horizontal direction was defined as a two-dimensional grid structure while its vertical direction was defined as a phreatic aquifer. Based on the conceptual model, the mathematical model is established as follows:

$$\begin{cases} \frac{\partial}{\partial x}\left[k_x(h-b)\frac{\partial h}{\partial x}\right]+\frac{\partial}{\partial y}\left[k_y(h-b)\frac{\partial h}{\partial y}\right]+\frac{\partial}{\partial z}\left[k_z(h-b)\frac{\partial h}{\partial z}\right]+\varepsilon=\mu\frac{\partial h}{\partial t},(x,y,z)\in\Omega \\ h(x,y,z,t)|_{t=0}=h_0(x,y,z),(x,y,z)\in\Omega \\ h(x,y,z,t)|_{\Gamma 1}=h_1(x,y,z),(x,y,z)\in\Gamma_1 \\ k_n\frac{\partial h}{\partial n}|_{\Gamma 2}=q(x,y,z,t),(x,y,z,t)\in\Gamma_2 \end{cases} \tag{1}$$

Where Ω is the domain of the simulated scope, Γ_1 and Γ_2 are the boundaries of the first boundary and the second boundary, n is the direction of the outer normal line of the second boundary, μ is the specific yield, h_0 (x, y, z) represents the initial conditions, i.e. the initial head distribution (m), h_1 (x, y, z) indicates the first type boundary conditions (m), q (x, y, z) represents the second type boundary conditions with inflow being negative and outflow being positive (m^3/day), h is the groundwater level (m), b is the elevation of phreatic aquifer baseboard (m), k is the permeation coefficient of the aquifer (m/day), and ε denotes the source/sink factors of groundwater, i.e. the intensities of vertical water pumping and of percolation recharge per unit area (m/day).

A series of statistical indexes, such as the root mean square error (RMSE), the relative error (RE), the error at the end of the year (E), and the correlation coefficient (R^2) Were used to judge the simulation precision of the model. R^2 measures the degree to which two variables are linearly related. RMSE and RE provide different types of information about the predictive capabilities of the model. E represents the deflected degree at the simulated period. RMSE, RE, E, and R^2 are defined as follows:

$$RMSE = \sqrt{\frac{1}{N}\sum_{i=1}^{n}(S_i - O_i)^2} \tag{2}$$

$$RE = \frac{1}{N}\sum_{i=1}^{N}\left(\frac{|S_i - O_i|}{\max(O_i) - \min(O_i)}\right) \times 100\% \tag{3}$$

$$E = |S_i - O_i| \tag{4}$$

$$R^2 = \frac{\left[\sum_{1}^{N}\left(S_i - \overline{S}\right)\left(O_i - \overline{O}\right)\right]^2}{\sum_{i=1}^{N}\left(S_i - \overline{S}\right)^2 \sum_{1}^{N}\left(O_i - \overline{O}\right)^2} \tag{5}$$

where N is the number of observations, O_i and S_i are the i-th values of observed and simulated data, respectively, $\overline{S}$ and $\overline{O}$ are the averages of the data arrays of S_i and O_i, respectively.

3 Results and Discussion

In order to improve the reliability of the model simulation results, it is necessary to simulate the transient flow. To estimate transient flow, data from the 36 observation wells were also used for model calibration (2011–2012) and validation (2013). Each month was a stress period and each stress period was divided into six time-steps. The hydrogeological and the boundary conditions were assigned according to the

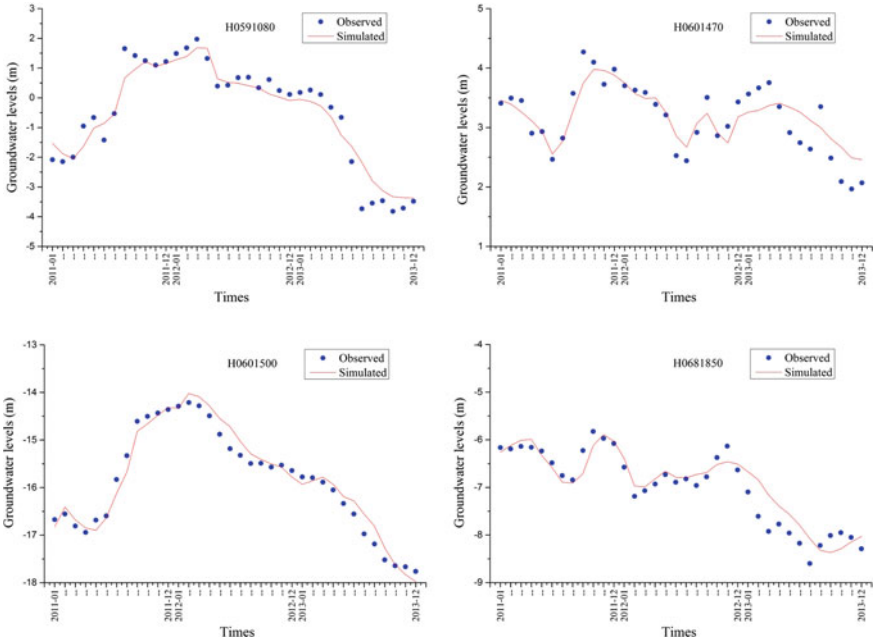

Fig. 3 Comparison of simulated and observed groundwater levels for four monitoring wells from 2011 to 2013

actual conditions. Figure 3 indicates a comparison between the measured levels and the simulated levels for four observation wells.

It is believed that when the RMSE of the model is less than 1 m, a correlation coefficient greater than 0.9 conforms to the requirement of model accuracy. The results for model precision are presented in Table 1. The model calibration (2011–2012) index values are as follows: RMSE = 0.17–0.56 m, RE = 4.84–20.63%, E = 0.14–0.73 m, and $R^2 = 0.99$, while those for model variation (2013) are the following: RMSE = 0.22–0.87 m, RE = 5.45–30.38%, E = 0.19–1.25 m, and $R^2 = 0.98$. The accuracy of the validation period was slightly lower than the calibration period and could be attributed to the lack of actual data for groundwater exploitation in some areas.

In this study, three basic scenarios, i.e. water saving, groundwater replacement, and the comprehensive scheme were considered. The current condition represents the basic scheme to compare groundwater remediation under different scenarios (Table 2).

Table 1 Statistical indexes for model calibration and validation

Observation well	Calibration (2011–2012)			Validation (2013)		
	RMSE	RE (%)	E	RMSE	RE (%)	E
H0591020	0.33	20.63	0.42	0.61	26.95	0.74
H0591030	0.42	15.79	0.21	0.39	14.83	0.18
H0591080	0.37	4.99	0.29	0.61	8.69	0.50
H0601440	0.56	26.41	0.63	0.87	30.38	1.25
H0601470	0.20	6.99	0.16	0.41	17.10	0.39
H0601500	0.20	4.84	0.17	0.22	5.45	0.19
H0681840	0.22	7.53	0.38	0.35	9.33	0.51
H0681850	0.17	5.52	0.14	0.44	15.26	0.40
H0681880	0.49	19.37	0.73	0.58	21.52	0.92
H0681940	0.27	10.24	0.25	0.48	15.27	0.37

Table 2 Simulation scenarios of groundwater in over-exploitation area of north Weifang

Simulation scenarios	Description
Scenario A	Current condition
Scenario B1	Improving effective water utilisation coefficient to 0.6
Scenario B2	Improving effective water utilisation coefficient to 0.7
Scenario B3	Improving effective water utilisation coefficient to 0.8
Scenario C1	Using external transfer water to replace groundwater sources to 50% of the current condition
Scenario C2	Using external transfer water to replace groundwater sources to 75% of the current condition
Scenario C3	Using external transfer water to replace groundwater sources to 100% of the current condition
Scenario D	Improving effective water utilisation coefficient to 0.7 and using external transfer water to replace groundwater sources to 100% of the current condition

3.1 Current Conditions

Figure 4a shows the groundwater contour map for 2023. The results indicate that the groundwater flow field was largely consistent with the previous results of steady flow. Additionally, the groundwater level showed a significant downward trend due to excessive exploitation. In particular, for most areas, groundwater exploitation was entered evenly in the model, therefore, no apparent drawdown funnel was observed. The groundwater level was found to decline at a rate of 0.3–0.4 m/a. However, in the groundwater source areas, the groundwater level is likely to decline at a rate of 0.6–1 m/a due to concentrated mining of the wells. The maximum groundwater depth in the centre of the funnel is likely to reach 50 m.

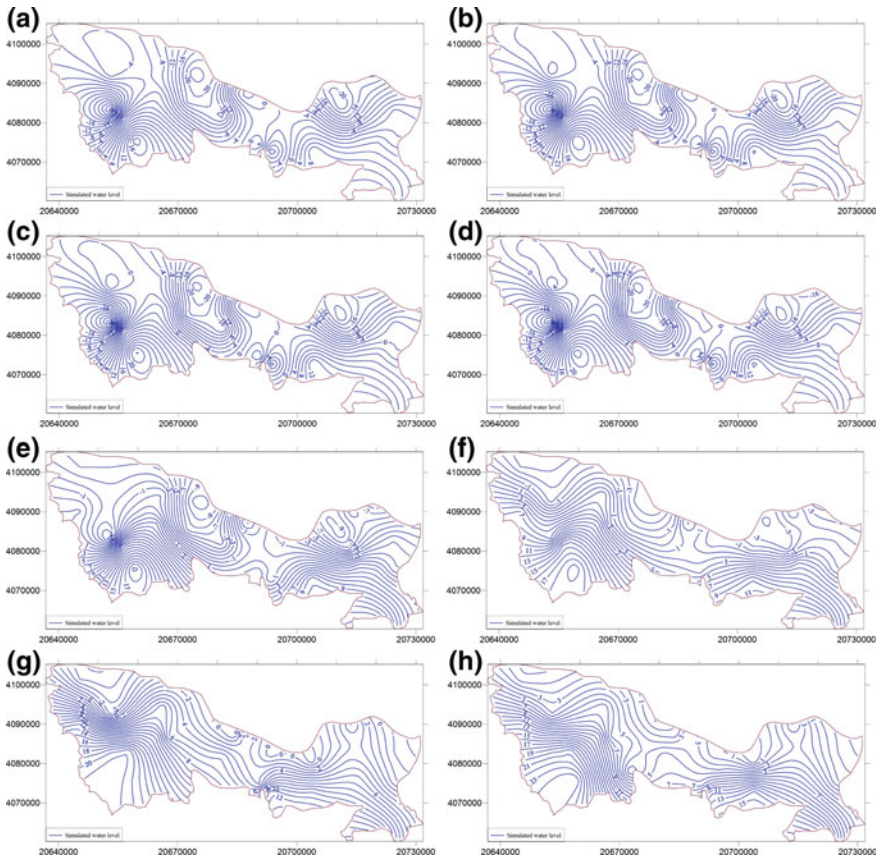

Fig. 4 Groundwater contour map under different scenarios after 10 years

According to the water budget, the average groundwater budget was -0.494×10^8 m^3/a which was slightly higher than the previous results. Therefore, it is urgent to definite reasonable groundwater exploitation mitigation measures for the study area.

3.2 Scenarios B1–3: Different Utilisation Coefficients

As indicated in Fig. 4b, c, d, in comparison to scenario A, groundwater level in most areas will rise. Shouguang, an agriculturally developed area, uses 1.37×10^8 m^3/a as irrigation water, of which groundwater contributes 1.16×10^8 m^3/a. With continuous improvement of the utilisation coefficient, compared to the other two regions, the groundwater level was shown to increase and the largest water level increase was to

8 m. The rise of the groundwater level in Hanting was estimated between 2 and 4 m, while in most areas of Changyi, the trend of groundwater level showed an initial rise followed by a decline. This trend could be attributed to surface water irrigation in Changyi where only a small volume of groundwater is used for irrigation. Therefore, the increase in the coefficient resulted in a decrease in groundwater exploitation, and consequent a rise in the groundwater level. However, with continuous improvement of the coefficient resulted in is almost no irrigation return recharge. Moreover, the decrease of groundwater exploitation was less than the return recharge, therefore, the groundwater level was shown to drop. In the vicinity of several groundwater sources, regardless of the utilisation coefficient changes, the variation of the groundwater level was always small and a drawdown funnel was obvious. Therefore, although agricultural irrigation was the main consumer of water in the study area, it was not the direct cause of the drawdown funnel.

As shown in Fig. 4, the groundwater budgets under the scenarios B1-3 were -0.334×10^8 m^3/a, -0.265×10^8 m^3/a, and -0.269×10^8 m^3/a, respectively. In general, agricultural water savings were beneficial to groundwater safety. However, because the study area is not dependent only on groundwater irrigation, there are several areas where surface water is used for irrigation and the rise of utilisation coefficient will affect the volume of return recharge. For example, the utilisation coefficient of scenario B2 is 0.7 and groundwater budget is -0.265×10^8 m^3 when the utilisation coefficient is increased to 0.8, the budget is -0.269×10^8 m^3 which is less than that observed for a utilisation coefficient of 0.7.

3.3 Scenarios C1–3: Different Replacement of Groundwater Source

In order to govern the groundwater drawdown funnel, three scenarios were designed in accordance with the South to North Water Diversion Project. As shown in Fig. 4e, f, g, compared to scenario A, groundwater level in the drawdown funnel area is likely to increase significantly through replacement of groundwater and the greater the replacement, the more the rising of the groundwater level. The maximum rise of the water level in the funnel centre was 35 m and the area of the drawdown funnel was shown to obviously reduce. When the replacement water reached 100%, as indicated in Fig. 4g, there was almost no drawdown funnel in the study area and the groundwater flow returned to the natural state from south to north. But in most areas, the trend of groundwater level decline in most areas is still not solved. In summary, the concentrated exploitation of groundwater was found to be the main reason for the drawdown funnel and agricultural irrigation was the main reason for the decline in groundwater levels across large areas.

Water budget shows that when the replacement of water sources comes to 75% of current exploitation, the total water budget of the groundwater system achieves balance. However, it is evident from the flow field that there is still a small part of the

drawdown funnel in the study area considering the external transfer water was 0.6×10^8 m^3 and could not be completely replaced. Therefore, with regards to repairing the drawdown funnel, the optimal replacement proportion was estimated to be 100%.

3.4 Scenario D: Comprehensive Scheme

In order to achieve the comprehensive management of the entire over-exploitation area, the optimal utilisation coefficient is 0.7 and the optimal replacement of water is 100%. It is evident from Fig. 4h that there is no drawdown funnel in the study area and the groundwater level in the north is higher than the sea level. Additionally, the flow of water is from south to north and eventually into the Laizhou Bay. Under such scenario, the problem of overexploitation of groundwater can be alleviated and the invasion of sea water will be effectively controlled.

4 Conclusion

In this study, Visual MODFLOW was used to simulate the dynamic changes of groundwater. After calibration and validation, the model was used to predict dynamic changes of groundwater from 2014 to 2023 in the over-exploitation area of Weifang.

Under the current mining scenarios, the groundwater level showed different degrees of decline. In particular, the decline in most areas was estimated at a rate of 0.3–0.4 m/a and the decrease in groundwater sources ranged from 0.6–1 m/a. The maximum water depth was calculated to reach 50 m, therefore, it is important to alleviate the over-exploitation of groundwater resources. In order to restore the groundwater system, first agricultural water savings were simulated. However, from the simulation results, the utilisation coefficient of B2 was found to be less than the utilisation coefficient of B3, while the water budget of B2 was more than the water budget of B3. Therefore, a higher utilisation coefficient is not always more conducive to the restoration of groundwater system. The second simulation was based on groundwater replacement. The results indicate that the groundwater system realises balance when the replacement is 75% of the current water sources and the more the replacement water is, the better the drawdown funnel repair effect. Thus, the combination of B2 and C3 is suggested as a comprehensive plan to effectively control the over-exploitation area. These results not only provide a scientific basis for groundwater restoration in study area but also for other similar areas.

References

Abdulla FA (2010) Artificial groundwater recharge to a semi-arid basin: case study of Mujib aquifer. Jordan Environ Earth Sci 60(4):845–859

Ayvaz MT (2009) Application of harmony search algorithm to the solution of groundwater management models. Adv Water Resour 32(6):916–924

Bromley J, Cruces J, Acreman M, Martínez L, Llamas MR (2001) Problems of sustainable groundwater management in an area of over-exploitation: The upper Guadiana catchment, Central Spain. Int J Water Resour Dev 17(3):379–396

Camp MV, Radfar M, Walraevens K (2010) Assessment of groundwater storage depletion by over-exploitation using simple indicators in an irrigated closed aquifer basin in Iran. Agric Water Manage 97(11):1876–1886

Chen S, Yang W, Huo Z, Huang G (2016) Groundwater simulation for efficient water resources management in Zhangye Oasis. Northwest China Environ Earth Sci 75(8):647

DierschHJG (2005) WASY Software FEFLOW ® -Reference Manual

Donovan DJ, Katzer T, Brothers K, Cole E, Johnson M (2002) Cost-Benefit Analysis of Artificial Recharge in Las Vegas Valley, Nevada. J Water Resour Plann Manage 128(5):356–365

Garcíagil A, Vázquezsuñé E, Sáncheznavarro JÁ, Mateo Lázaro J (2015) Recovery of energetically overexploited urban aquifers using surface water. J Hydrol 531:602–611

Group SS (2006) Groundwater modeling system (GMS). John Wiley & Sons, Ltd

Han Z (2003) Groundwater resources protection and aquifer recovery in China. Environ Geol 44(1):106–111

Hu YK, Moiwo JP, Yang YH, Han SM, Yang YM (2010) Agricultural water-saving and sustainable groundwater management in Shijiazhuang irrigation district, North China Plain. J Hydrol 393(3–4):219–232

Huo ZL, Feng SY, Kang SZ, Cen SJ, Ma Y (2007) Simulation of effects of agricultural activities on groundwater level by combining FEFLOW and GIS. N Z J Agric Res 50(5):839–846

Iwasaki Y, Nakamura K, Horino H, Kawashima S (2014) Assessment of factors influencing groundwater-level change using groundwater flow simulation, considering vertical infiltration from rice-planted and crop-rotated paddy fields in Japan. Hydrogeol J 22(8):1841–1855

Jang CS, Chen CF, Liang CP, Chen JS (2016) Combining groundwater quality analysis and a numerical flow simulation for spatially establishing utilization strategies for groundwater and surface water in the Pingtung Plain. J Hydrol 533(1):541–556

Konikow LF, Kendy E (2005) Groundwater depletion: a global problem. Hydrogeol J 13(1):317–320

Lin Z, Lin W, Pengfei L (2015) Analysis of shallow-groundwater dynamic responses to water supply change in the Haihe River plain. Biochemistry 368(1):373–378

Mcdonald MG, Harbaugh AW (1988) A modular three-dimensional finite-difference ground-water flow model p 387–389

Mohtashami A, Akbarpour A, Mollazadeh M (2017) Development of two dimensional groundwater flow simulation model using meshless method based on MLS approximation function in unconfined aquifer in transient state. J Hydroinformatics 19(5)

Mossmark F, Hultberg H, Ericsson LO (2008) Recovery from groundwater extraction in a small catchment area with crystalline bedrock and thin soil cover in Sweden. Sci Total Environ 404(2–3):253

Nam Y, Ooka R (2010) Numerical simulation of ground heat and water transfer for groundwater heat pump system based on real-scale experiment. Energy Build 42(1):69–75

Phien-Wej N, Giao PH, Nutalaya P (1998) Field experiment of artificial recharge through a well with reference to land subsidence control. Eng Geol 50(50):187–201

Seo JP, Cho W, Cheong TS (2014) Development of priority setting process for the small stream restoration projects using multi criteria decision analysis. J Hydroinformatics 17(2):211

Tu YC, Ting CS, Tsai HT, Chen JW, Lee CH (2011) Dynamic analysis of the infiltration rate of artificial recharge of groundwater: a case study of Wanglong Lake, Pingtung. Taiwan Environ Earth Sci 63(1):77–85

Xu X, Huang G, Zhan H, Qu Z, Huang Q (2012) Integration of SWAP and MODFLOW-2000 for modeling groundwater dynamics in shallow water table areas. J Hydrol 412(1):170–181
Yao J, Ren Y, Wei S, Pei, W (2018) Assessing the complex adaptability of regional water security systems based on a unified co-evolutionary model. J Hydroinformatics
Zektser S, Loáiciga HA, Wolf JT (2005) Environmental impacts of groundwater overdraft: selected case studies in the southwestern United States. Environ Geol 47(3):396–404
Zume J, Tarhule A (2008) Simulating the impacts of groundwater pumping on stream–aquifer dynamics in semiarid northwestern Oklahoma. USA Hydrogeol J 16(4):797–810

Stability Analysis During Excavation of Low-Permeability Rock Surrounding an Underground Water Sealed Cavern

Guotao Ma, Zhiming Chao, Meng Wang, Jiangbo Wei, Hengyang Hu and Yao Zhang

Abstract This paper establishes a solution for describing the mechanical behavior of low-permeability rock considering fluid-solid coupling. The proposed model is applied in numerical method to explore the stability of underground water sealed cave by considering the hydro-mechanics of low-permeability rock during excavation. This paper draws the following findings: Fluid seepage causes the increasing of the displacement of caverns, especially for the displacement at the bottom of caverns. Fluid seepage causes the reduction of stress in surrounding rock around water sealed caverns during excavation, whereas the plastic strains of surrounding rock increase due to the effect of fluid seepage.

Keywords Low-permeability rock · Hydro-mechanics · Underground water sealed carven · FEM

G. Ma
The Faculty of Geoscience and Environmental Engineering, Southwest Jiaotong University, Chengdu 610000, Sichuan, China

G. Ma · Z. Chao (✉) · M. Wang · Y. Zhang
The School of Engineering, University of Warwick, Coventry CV4 7DA, UK
e-mail: Z.chao@warwick.ac.uk

G. Ma · Z. Chao · M. Wang
Chengdu Derek Super-Computational Technology Co., Ltd., Chengdu 610000, Sichuan, China

M. Wang
MOE Key Laboratory Deep Underground Science and Engineering, Sichuan University, Chengdu 610000, Sichuan, China

J. Wei
Xian University of Science and Technology, Xian 710000, Shanxi, China

H. Hu
Southwest Subsidiary Company of China Airport Construction Group Corporation, Chengdu 610202, Sichuan, China

R. Sun and L. Fei (eds.), *Sustainable Development of Water and Environment*, Environmental Science and Engineering,
https://doi.org/10.1007/978-3-030-16729-5_16

1 Introduction

With the rapid development of the world economy, the demand for energy such as oil and natural gas is increasing. A safe and stable energy supply is an important guarantee for the sustained and healthy development of the economy. The construction of underground water sealed oil and gas caverns is undoubtedly a preferential energy reserve method. Compared with the over-ground reservoir, the underground carven has the advantages of small occupation of land, high safety and etc. Underground oil and gas storage caverns are usually built in hard and complete low-permeability rock mass with stable lithology, stable natural water table and shallow depth. The mechanical properties of this type of rock has significant impacts on the safety of underground water sealed caverns.

Underground water sealed caverns utilize water-sealing LPR to store petroleum and liquefied petroleum (Duan et al. 2017). The seepage field of LPR has crucial impacts on the safety of underground water sealed caverns (Luo and Wang 2011). However, current research about the stability of underground water sealed caverns mainly adopt the theory of groundwater dynamics, which does not reflect the effect of surrounding rock deformation (Kim et al. 2013; Zhou et al. 2015; Lee et al. 2013). Hence, it is necessary to research the stability of LPR surrounding underground water sealed caverns by adopting hydromechanical method.

Finite Element Method (FEM) is an effective approach to explore the behaviours of the surrounding rock mass and the stability of the underground water sealed caverns (Run-jian et al. 2009; Ma et al. 2016; Wolkersdorfer 2008). However, currently, the research about the application of FEM in the stability analysis of the LPR surrounding underground water sealed cavern is rare. This is because it is difficult to measure the permeability and porosity of LPR and determine the interaction relationship between the stress field and the seepage field of LPR in FEM numerical models to describe the mechanical responses of LPR considering hydromechanics. The mechanical responses of LPR considering hydromechanics is considerably different from that of LPR without considering hydromechanics. Thus, it is worthy to conduct research about the stability analysis of the LPR surrounding underground water sealed caverns considering hydromechanics.

In addition, the change of the stress and seepage fields and the geometry of the LPR surrounding underground water sealed caverns induced by the excavation of underground water sealed caverns causes relatively large influence on the stability of underground water sealed caverns (Ming 1992). Therefore, it is significant to investigate the stability of the underground water sealed caverns during excavation.

This paper establishes numerical models to replicate the mechanical behavior of LPR considering hydromechanics and conduct the stability analysis of LPR surrounding underground water sealed caverns during excavation.

2 Modelling

2.1 Seepage Theory

In the FEM model, the seepage analysis adopts the Forchheimer seepage law (Papanastasiou and Durban 2018).

$$k = \frac{k_{liq}}{(1 + \theta\sqrt{Vw \cdot Vw})} ks \tag{1}$$

where, k is the permeability coefficient, k_{liq} is the absolute permeability, and is the function of the porosity, k_s is the fully saturated permeability, θ is a velocity coefficient that relate to the void ratio, Vw is the fluid velocity.

The fluid flow continual equation (Eq. 1) is then obtained based on the mass conservation equation (Eq. 2) (Belmokhtar et al. 2018):

$$-\left(\frac{\partial v}{\partial x} + \frac{\partial v}{\partial y} + \frac{\partial v}{\partial z}\right) = S\frac{\partial h}{\partial t_1} \tag{2}$$

where, t_1 is time, v is velocity, S is water storage rate, h is water head.

Assuming that the seepage is stable, namely s = 0, the continual equation of the stable seepage is deduced as Eq. 3.

$$\frac{\partial v}{\partial x} + \frac{\partial v}{\partial y} + \frac{\partial v}{\partial z} = 0 \tag{3}$$

The stable seepage equation (Eq. 4) is then proposed as follow

$$\frac{\partial}{\partial x}\left(k_x\frac{\partial h}{\partial x}\right) + \frac{\partial}{\partial y}\left(k_y\frac{\partial h}{\partial y}\right) + \frac{\partial}{\partial z}\left(k_z\frac{\partial h}{\partial z}\right) = 0 \tag{4}$$

where, k_x, k_y and k_z are the permeability coefficients of LPR in x, y and z axis directions respectively.

When the permeability coefficient is isotropic, the Laplace Equation (Eq. 5) is as shown in the following equation (Zhao et al. 2018).

$$\frac{\partial^2 h}{\partial x^2} + \frac{\partial^2 h}{\partial y^2} + \frac{\partial^2 h}{\partial z^2} = 0 \tag{5}$$

For the two-dimensional seepage, Eq. 5 can be rewritten as

$$\frac{\partial^2 h}{\partial x^2} + \frac{\partial^2 h}{\partial y^2} = 0 \tag{6}$$

Hence, Eq. 4 is transformed as

$$\frac{\partial}{\partial x}\left(k_x \frac{\partial h}{\partial x}\right) + \frac{\partial}{\partial y}\left(k_y \frac{\partial h}{\partial y}\right) = 0 \tag{7}$$

2.2 Hydromechanical Theory

2.2.1 The Effect of the Seepage Field on the Stress Field

In the FEM model, the seepage field changes the permeate body force thus affecting the distribution of the stress field. Under two-dimensional seepage condition, the permeate body force is in direct proportion to the hydraulic gradient, as shown in Eq. 8 (Jianjun et al. 2002):

$$\begin{Bmatrix} f_x \\ f_y \end{Bmatrix} = \begin{Bmatrix} -r_w \frac{\delta h}{\delta y} \\ -r_w \frac{\delta h}{\delta y} \end{Bmatrix} = \begin{Bmatrix} r_w \ J_x \\ r_w \ J_y \end{Bmatrix} f = \sqrt{f_x + f_y} \tag{8}$$

where, f is the body force generated by seepage, r_w is the unit weight of water, fx and fy are the component forces of seepage body force in x and y direction, respectively, Jx and Jy are the hydraulic gradient of the element in x and y directions, respectively.

Equations 9 and 10 can transform the permeate volume strength of elements to equivalent nodal load when the numerical method is adopted to calculate the stress filed.

$$\{F_s\} = \int_{\Omega} [N]^T \begin{Bmatrix} f_x \\ f_y \end{Bmatrix} dxdy \tag{9}$$

where, $\{F_s\}$ is the equivalent nodal force generated by the seepage body force, $[N]$ is the element shape function.

$$\{\Delta F_s\} = \int_{\Omega} [N]^T \begin{Bmatrix} f_x \\ f_y \end{Bmatrix} dxdy \tag{10}$$

where, $\{\Delta F_s\}$ is the equivalent nodal force generated by the increment of the seepage body force.

Therefore, the mathematical model (Eq. 11) of the stress field considering the effect of the seepage field is attained:

$$\begin{cases} [k_{liq}]\{\Delta\delta\} = \{\Delta F\} + \{\Delta F_s\}, (x, y) \in \Omega \\ \{\delta\} = \{\delta_0\}, (x, y) \in S_u \\ \sigma_{ij} n_j = T, (x, y) \in S_a \end{cases} \tag{11}$$

where, $\{\Delta F\}$ is nodal load increment, δ is displacement, $\Delta\delta$ is displacement increment, S_u is the determined displacement boundary conditions, S_a is the determined stress boundary conditions.

2.2.2 The Effect of the Stress Field on the Seepage Field

In the FEM model, the effect of the stress filed on the seepage filed is mainly about affecting the porosity of material thus affecting the permeability coefficient of material. Since the volumetric strain is determined by the stress field and the volumetric strain determines the permeability of material, the two-dimensional stable seepage mathematical model considering the effect of the stress field is attained, as shown in Eq. 12.

$$\begin{cases} \frac{\partial}{\partial x}[k_{liq}(\phi)]\frac{\partial h}{\partial x} + \frac{\partial}{\partial y}[k_{liq}(\phi)]\frac{\partial H}{\partial y} = 0, (x, y) \in \Omega \\ H(x, y) = H_1(x, y), (x, y) \in \Gamma_1 \\ k_{liq}(\phi)\frac{\partial H}{\partial n_2} = q_1(x, y), (x, y) \in \Gamma_2 \\ H(x, y) = y, k_{liq}(\phi)\frac{\partial H}{\partial n_3} = 0, (x, y) \in \Gamma_3 \end{cases} \tag{12}$$

where, ϕ is porosity, q_1 is flow, Γ_1 is the boundary conditions with determined water head, Γ_2 is the boundary conditions with determined flow, Γ_3 is the mixed boundary conditions, namely $h + \frac{\partial h}{\partial t_1}\alpha_1 = \beta_1$, α_1 and β_1 are constants.

Hence, the key of determining the effect of the stress field on the seepage filed in the proposed FEM model is to determine the relationship between the porosity and the permeability of LPR. The LPR gas permeability experiment is then conducted to determine the relationship between permeability and porosity of LPR.

The relationship between the permeability and the porosity of LPR is determined by the LPR gas permeability experiment that was conducted by Chao et al. (2017), and the relationship between the porosity and the permeability of LPR is attained, as shown in Eq. 13.

$$k_{liq} = 0.313\phi^2 \tag{13}$$

Equation 13 is then introduced into Eq. 12. The effect of the stress field on the seepage filed is determined. Equation 12 can be rewritten as

$$\begin{cases} \frac{\partial}{\partial x}[0.313\phi^2]\frac{\partial H}{\partial x} + \frac{\partial}{\partial y}[0.313\phi^2]\frac{\partial H}{\partial y} = 0, (x, y) \in \Omega \\ H(x, y) = H_1(x, y), (x, y) \in \Gamma_1 \\ 0.313\phi^2\frac{\partial H}{\partial n_2} = q(x, y), (x, y) \in \Gamma_2 \\ H(x, y) = y, 0.313\phi^2\frac{\partial H}{\partial n_3} = 0, (x, y) \in \Gamma_3 \end{cases} \tag{14}$$

The seepage field and stress filed coupling mathematical model (Eq. 15) is attained by combining the mathematical models of the two fields:

$$\begin{cases} [K]\{\Delta\delta\} = \{\Delta F\} + \{\Delta F_s\} \\ [0.313\phi^2]\{H\} + \{f\} = 0 \\ k = 0.313\phi^2 \end{cases} \tag{15}$$

where, $\{f\}$ is the water head distribution function of the seepage field.

3 Numerical Analysis

3.1 The Brief Description of the Numerical Model

Underground water sealed caverns adopt the airtightness of water-bearing LPR to conduct the storage of petroleum and liquefied petroleum gas. In order to replicate the sealed effect, the underground water sealed caverns are mainly placed under the ground water level, and the water curtain system is placed above the roof of caverns to guarantee the sealed effect (Shi and Liu 2010). This makes the underground water sealed caverns to be surrounded by water during construction and operation periods. The interaction between the stress field and the seepage filed causes relatively large influence on the stability of surrounding LPR. Therefore, the hydromechanics of LPR should be considered in the stability analysis of the underground water sealed caverns during excavation per (Fan and Xiaoliang 2012).

The Abaqus software is used to conduct FEM numerical simulation to analyse the stability of underground water sealed caverns during excavation. The stability of underground water sealed caverns during excavation considering and without considering fluid-solid coupling are both analysed. The numerical results can provide suggestions for the excavation and the operation of LPR surrounding underground water sealed caverns.

The designed usage of the underground water sealed caverns is 50 years. The designed cavern span is 20 m, and the designed cavern height is 30 m. The cross section is stalk dome shape. The water curtain tunnel is placed at 30 m above the caverns. The stratum of the cavern site is low-permeability sandstone. The layout of the caverns is shown in Fig. 1.

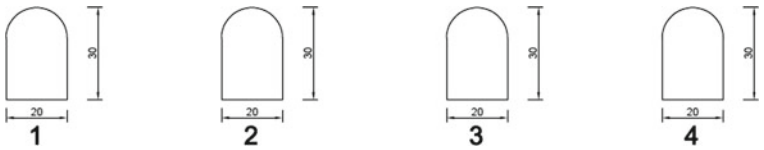

Fig. 1 The schematic diagram of the water sealed caverns

3.2 The Numerical Model and Bounding Conditions

In order to simplify, the geometry of the FEM model is simplified to a two-dimension model. The model is composed of four main caverns, and the size of the four main caverns are the same. The rock layers are mainly constituted by the low-permeability sandstone. The underground water level is set to 50 m. The numerical model contains 21,110 elements and 31,500 nodes. In order to guarantee the calculating accuracy, the fine meshes are adopted in the FEM model. The constitutive model in this FEM model adopts the porous media elasticity model and the modified Drucker–Prager model to describe the mechanical behavior of LPR. The material parameters of the numerical model adopt the parameters listed in Table 1.

The boundary conditions are set as: the horizontal displacement in of the left and right sides of the model is restricted, and the vertical displacement at the bottom of the model is also restricted.

The seepage boundary conditions are set as: the bottom, left and right boundaries of the model are set as impermeable boundaries, and the top boundary of the model is set as free permeation boundary where the pore pressure of it is set as 0. After cavern excavation, the pore pressure of the boundaries of the caverns is set as 0, and the bottom boundary of the water curtain tunnel is 0 water head boundary. The mesh of the numerical model is shown in Fig. 2.

In order to analyses the effect of seepage on the deformation of the surrounding LPR, the monitoring points are placed along the boundaries of caverns, as shown in Fig. 3. The initial stress field is shown in Fig. 4.

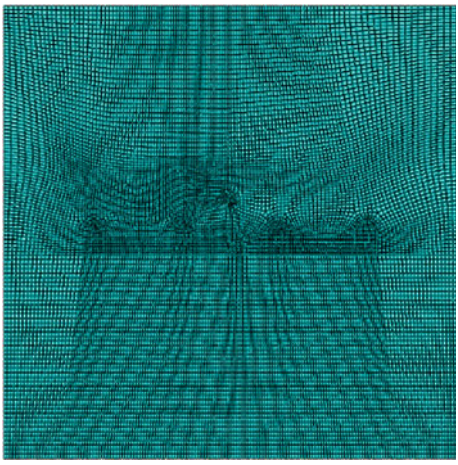

Fig. 2 The mesh of the numerical model

Table 1 The parameters of the numerical model

Log bulk modulus (GPa)	Poisson's ratio	Cohesion (MPa)	Friction angle (°)	Cap eccentricity	Initial yield surfaces position	Transition surface position	Flow stress ratio	Initial porosity (%)	Initial permeability (m^2)	Density (kg/m^3)
5.505	0.25	2.67	31.6	2	0	0.02	0.79	6.6	1.4E−016	2460

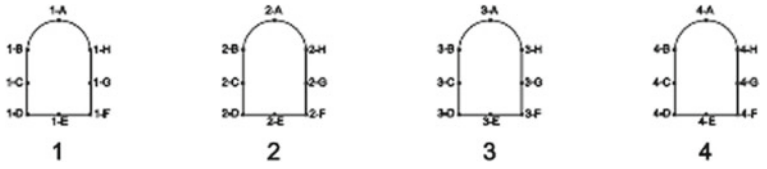

Fig. 3 The monitoring points around caverns

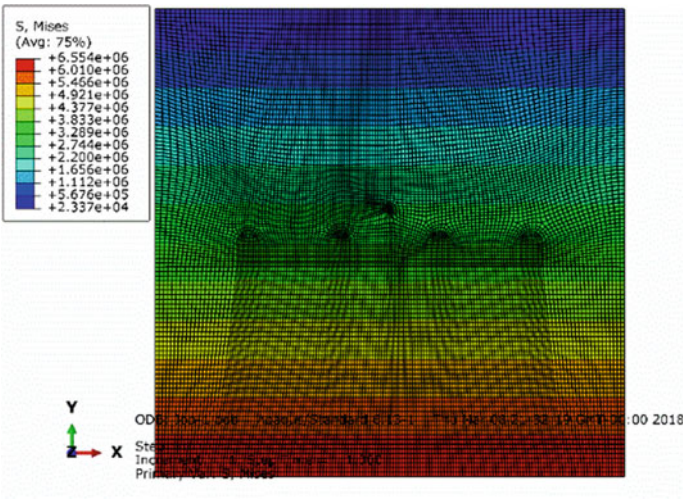

Fig. 4 The initial stress field

3.3 The Analysis of Numerical Simulation Results in Non-seepage Condition

3.3.1 Displacement Field Features

According to Fig. 5, the displacements caused by cavern excavation are mainly concentrated on the vaults and bottoms of the caverns. The deformations of the vaults of the caverns are mainly vertical sedimentation, and the deformation of the bottoms of the caverns are principally vertical.

3.3.2 Stress Field Features

The distributions of Mises stress, maximum principle stress and minimum principle stress are shown in Fig. 6. The secondary adjustment of stress field of the caverns is caused by excavation. The total stress is mainly concentrated on the flank walls of the caverns due to stress concentration. In the aspect of the maximum principle stress,

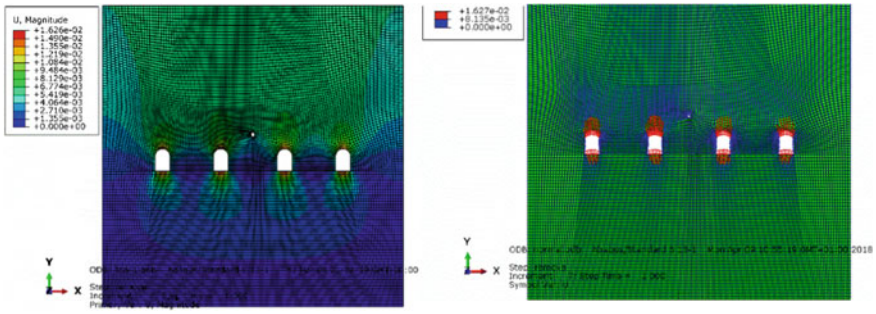

(a) The total displacement diagram (b) the total displacement vector diagram

Fig. 5 The displacement field

the tensile stress concentration district is located around the bottoms of the caverns with a maximum value of 0.25 MPa. The compressive stress concentration districts are located around the flank walls and vaults of the caverns with a maximum value of 0.91 MPa. According to Fig. 6c, the minimum principle stress in the surrounding area of the caverns is mainly compressive stress, and the compressive stress concentration districts are located around the flank walls of the caverns.

3.3.3 Plastic Zone Features

The plastic zone of surrounding LPR is as shown in Fig. 7, only quite minor part of the surrounding LPR undergoes plastic deformation, and the plastic zones are mainly located at the bottom flank walls of the caverns.

3.4 The Analysis of Numerical Simulation Results in Seepage Condition

3.4.1 Displacement Field Features

According to Fig. 8, the displacements caused by cavern excavation are mainly concentrated on the vaults and flank walls of the caverns. The deformation of the vaults of the caverns is mainly vertical, and the deformation of the flank walls of the caverns is principally horizontal. There is minor vertical displacement at the bottoms of the caverns.

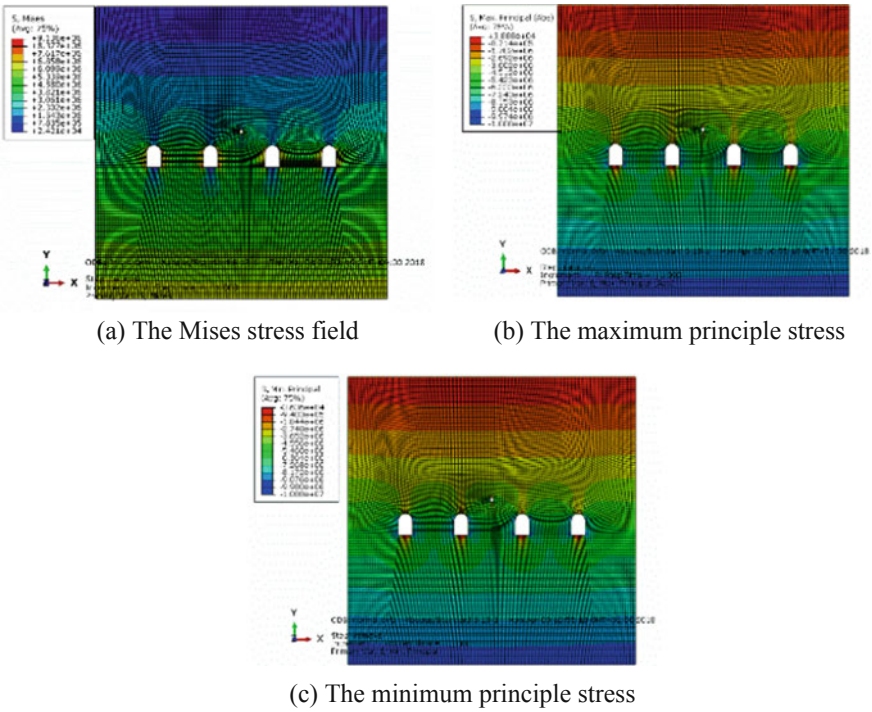

(a) The Mises stress field

(b) The maximum principle stress

(c) The minimum principle stress

Fig. 6 The stress field

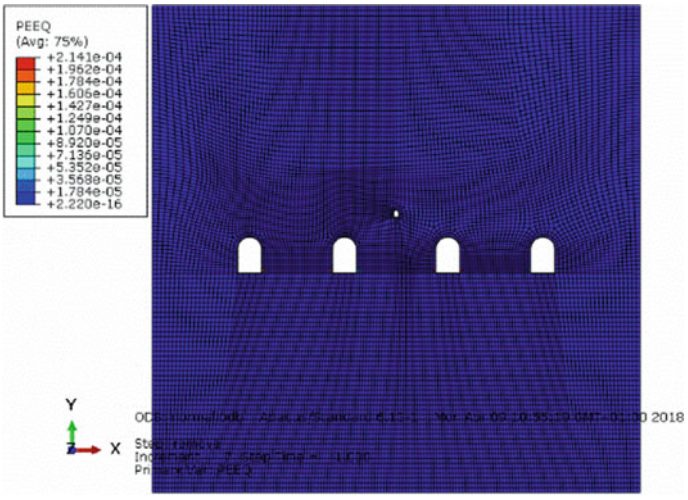

Fig. 7 The distribution of the plastic zone

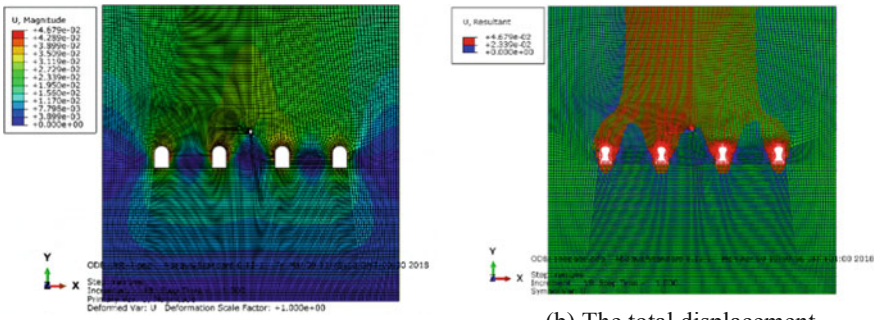

(a) The total displacement diagram

(b) The total displacement vector diagram

Fig. 8 The displacement field

3.4.2 Stress Field Features

The distribution of Mises stress, maximum principle stress and minimum principle stress are plotted in Fig. 9. The secondary adjustment of the stress field of the caverns is caused by excavation. The total stress is mainly concentrated between the caverns with a maximum stress of 7.9 MPa. In the aspect of the maximum principle stress, the tensile stress concentration district is located on the flank walls of the caverns, and the maximum value is 0.23 MPa. The compressive stress concentration districts are located at the vaults and bottoms of the caverns with the maximum value of 0.048 MPa. For the surrounding LPR between caverns, compressive stress is dominant with a maximum value of 3.2 MPa. According to Fig. 9c, the principle stress in the surrounding area of the caverns is mainly compressive stress.

3.4.3 Plastic Zone Features

The calculated plastic zone of surrounding LPR is as shown in Fig. 10. The plastic zones are mainly located on the flank walls of the caverns. It is noted that the plastic zones are connected in this case.

3.5 The Numerical Simulation Results Under Seepage and Non-seepage Conditions

3.5.1 Displacement Field

According to Figs. 5 and 8, the displacement of monitoring points a, b, h in seepage condition is lower than that without seepage after excavation. Then, the displacement

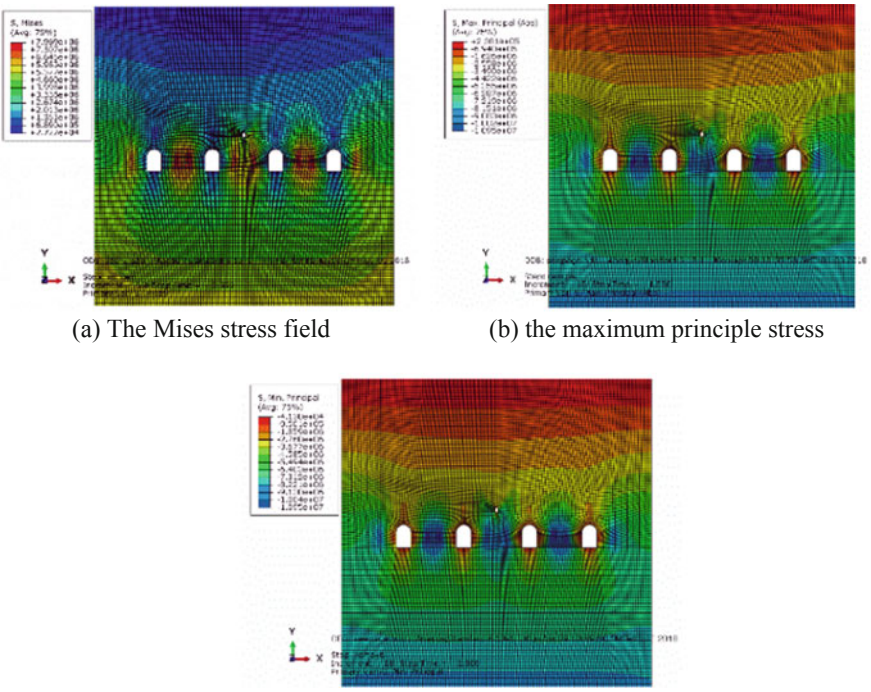

(a) The Mises stress field (b) the maximum principle stress

(c) the minimum principle stress

Fig. 9 The stress field

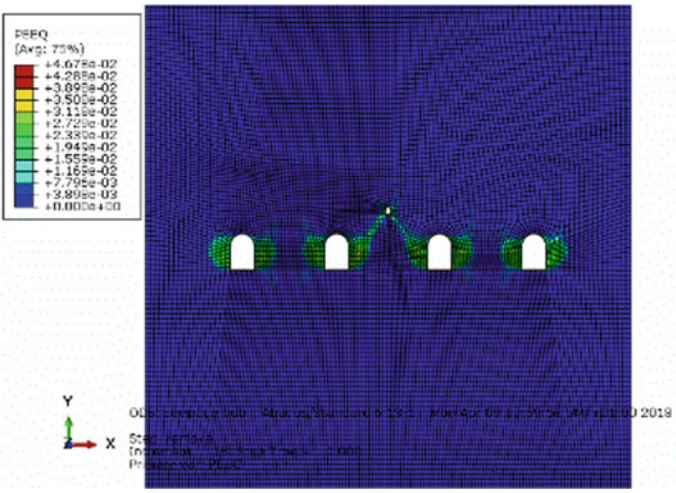

Fig. 10 The distribution of the plastic zone

in these monitoring points rapidly increases and overtakes that in without seepage condition. However, for monitoring points c, d, e, f and g under seepage condition, is the displacements are always larger than that in non-seepage condition. This shows that, in general, seepage causes the increasing of the displacement of caverns.

3.5.2 Stress Field

According to Figs. 6a and 9a, the Mises stresses at monitoring points a and e under seepage condition are similar with that under non-seepage condition, but the Mises stress at other monitoring points under seepage condition are generally lower than that under non-seepage condition. This means that seepage causes the decrease of Mises stress at the two flanks of caverns, and the effect of seepage on the Mises stress at the top and bottom of caverns is minor.

According to Figs. 6b and 9b, the maximum principle stress of monitoring points a, c, e and g under seepage condition is almost the same with that under non-seepage condition, while for monitoring points b, d, f and h the maximum principle stress under seepage condition is slightly larger than that under non-seepage condition. This indicates that seepage causes the increase of maximum principle stress in the vertexes of caverns.

According to Figs. 6c and 9c, the minimum principle stress of monitoring points a and e under seepage condition is almost the same with that under non-seepage condition, while for monitoring points b, c, d, g and h the minimum principle stress under seepage condition is larger than that under non-seepage condition. This indicates that seepage causes the increase of maximum principle stress at the two flanks of caverns.

3.5.3 Equivalent Plastic Strain (PEEQ)

According to Figs. 7 and 10, the PEEQ under seepage condition is larger than that under non-seepage condition, and the PEEQ in seepage condition increases from the top of caverns to the bottom of the caverns. This indicates that seepage causes the increase of the PEEQ, especially for the surrounding LPR at the bottom of caverns.

4 Conclusions

This paper establishes FEM numerical models to simulate the mechanical responses of LPR considering hydromechanics and research the stability of underground water sealed caverns during excavation considering hydromechanics. The following conclusions are attained

1. Seepage causes the increasing of the displacement of caverns, especially for the displacement at the bottom of caverns.
2. Fluid seepage causes the decrease of Mises stress, maximum stress and minimum stress at the two flanks of caverns. The effect of seepage on the Mises stress, maximum stress and minimum stress at the top and bottom of caverns is minor.
3. Fluid seepage causes the increase of displacement and PEEQ of caverns, especially for the displacement at the bottom of caverns. Therefore, fluid seepage causes the diminishing of the stability of underground water sealed cave during excavation period.

References

Belmokhtar M, Delage P, Ghabezloo S, Conil N (2018) Drained triaxial tests in low-permeability shales: application to the Callovo-Oxfordian claystone. Rock Mech Rock Eng 1–15

Chao Z, Wang H, Xu W, Jia C,Fang Y (2017) Gas Klinkenberg effect of low-permeability rocks with different degrees of water saturation. Chin J Geotech Eng 39(12):2287–2295

Duan S-Q, Feng X-T, Jiang Q, Liu G-F, Pei S-F, Fan Y-L (2017) In situ observation of failure mechanisms controlled by rock masses with weak interlayer zones in large underground cavern excavations under high geostress. Rock Mech Rock Eng 50:2465–2493

Fan ZBLWF, Xiaoliang WBC (2012) Numerical ssimulation for fluid-solid coupling charateristics in surrounding rock of underground water-sealed oil storage based. J Eng Geol 5:020

Jianjun L, Xiangui L, Yareng H, Shengzong Z (2002) Study of fluid-solid coupling flow in low permeablable oil reservoir. Chin J Rock Mechan Eng 1:018

Kim H-M, Rutqvist J, Jeong J-H, Choi B-H, Ryu D-W, Song W-K (2013) Characterizing excavation damaged zone and stability of pressurized lined rock caverns for underground compressed air energy storage. Rock Mech Rock Eng 46:1113–1124

Lee J, Min K-B, Rutqvist J (2013) Probabilistic analysis of fracture reactivation associated with deep underground CO_2 injection. Rock Mech Rock Eng 46:801–820

Luo JA, Wang L (2011) High-temperature mechanical properties of mudstone in the process of underground coal gasification. Rock Mech Rock Eng 44:749

Ma K, Tang C, Wang L, Tang D, Zhuang D, Zhang Q, Zhao J (2016) Stability analysis of underground oil storage caverns by an integrated numerical and microseismic monitoring approach. Tunn Undergr Space Technol 54:81–91

Ming X (1992) 3-D elastoplastic fem analysis of implicit cylindric anchor bar element for underground opening. Chin J Geotech Eng 5:002

Papanastasiou P, Durban D (2018) The influence of crack-face normal and shear stress loading on hydraulic fracture-tip singular plastic fields. Rock Mech Rock Eng 1–13

Run-Jian W, Guo-Min L, Yan-Hui D, Ming L, Xiao-Juan Q (2009) Analysis of seepage simulation of underground water sealed caverns in Jinzhou. J Yangtze River Sci Res Inst 10:024

Shi H-B, Liu B-G (2010) Design and seepage discharge analysis of artificial water curtains for water sealed underground petroleum storage caverns in rock. Chin J Geotech Eng 32:130

Wolkersdorfer C (2008) Water management at abandoned flooded underground mines: fundamentals, tracer tests, modelling, water treatment. Springer Science & Business Media

Zhao X, Huang B, Wang Z (2018) Experimental investigation on the basic law of directional hydraulic fracturing controlled by dense linear multi-hole drilling. Rock Mech Rock Eng 1–16

Zhou S-W, Xia C-C, Du S-G, Zhang P-Y, Zhou Y (2015) An analytical solution for mechanical responses induced by temperature and air pressure in a lined rock cavern for underground compressed air energy storage. Rock Mech Rock Eng 48:749–770

Design of a Humidification-Dehumidification Seawater Desalination System Combined with Solar Chimneys

Fei Cao, Heng Zhang, Qingjun Liu, Tian Yang and Tianyu Zhu

Abstract A new humidification-dehumidification seawater desalination system combined with the solar chimney is proposed in the present study. The proposed system consists of the solar collectors, two-tower solar chimney updraft wind system and the sea water condensers. Mathematical models are built to analyze the solar collector, the chimney and the condensers respectively. The performance of the system is simulated. The monthly fresh water generation is calculated. It is found from the study that, the system with the similar dimension of the Spanish solar chimney power plant prototype can averagely generate fresh water of 1.51 kg/h, when the average solar radiation is 598.66 MJ/m^2.

Keywords Sea water desalination · Humidification · Dehumidification · Solar chimney · Solar energy

1 Introduction

Solar sea water desalination is one of the most effective methods to solve the water shortage in China. Solar humidification and dehumidification is a kind of active solar distillation desalination method with small scale, distributed arrangement, low investment and less maintenance. It is of high significance to the locations such as the inland rural areas, coastal islands, ocean vessels and defense front reef, etc. Sievers and Lienhard V analyzed the steam flow and condensation characteristics in two kinds of condensers, plate type and flat fin circular tube type, by means of numerical simulation, and pointed out the different laws of the enhancement of heat transfer in the humidification-dehumidification seawater desalination and the condenser in a HVAC system (Sievers and Lienhard 2013, 2015). Chehayeb et al. analyzed the solar humidification-dehumidification thermodynamic process by using Enthalpy-Pinch-Point method, and found the variation law of parameters such as airflow temperature and

F. Cao (✉) · H. Zhang · Q. Liu · T. Yang · T. Zhu
College of Mechanical and Electrical Engineering, Hohai University, Jiangsu 213022, China
e-mail: fcao@hhu.edu.cn

R. Sun and L. Fei (eds.), *Sustainable Development of Water and Environment*, Environmental Science and Engineering,
https://doi.org/10.1007/978-3-030-16729-5_17

velocity with the recovery of latent heat series in different systems (Chehayeb et al. 2014). Kabeel built a solar humidification—dehumidification desalination device and reported the fresh water production rate can be up to 23 kg/h when the evaporator inlet temperature reaches 90 °C (Gu 2013). Kabeel and El-Said carried out the experiment and simulation study of a small solar humidification-dehumidification desalination device by doping Al_2O_3 nanoparticles in seawater. Their fresh water production rate was 41.8 kg/day (Chang et al. 2014).

In 2005, Wang and Zhu proposed to introduce the solar chimney into the seawater desalination system. The seawater was heated through the greenhouse effect, under which the evaporated moisture was obtained (Zhu 2005; Wang et al. 2006). Zuo et al. established a small solar chimney desalination experimental device with a solar collector area of 1.45 m^2, which can produce both electricity and fresh water. The maximum fresh water productivity reached 174.3 g/(h m^2) (Zuo et al. 2012).

In the present study, a new solar chimney humidification-dehumidification seawater desalination (SCHDHSD) system is proposed. Schematic of the SCHDHSD system is shown in Fig. 1. As shown in Fig. 1, the system is composed of five main parts: an inner chimney, an outer chimney, a sloped solar collector, a horizontal collector and a condenser. The fresh seawater flows along the sloped plate and evaporates inside the sloped solar collector. Ambient air enters into the system from the sloped and the horizontal solar collectors respectively. The updraft airflow from the horizontal solar collector enters the inner chimney. The wet airflow from the sloped solar collector enters the gas between the inner and outer chimney. The hot air inside the inner and outer chimney mixes with the moist air inside the inner and outer chim-

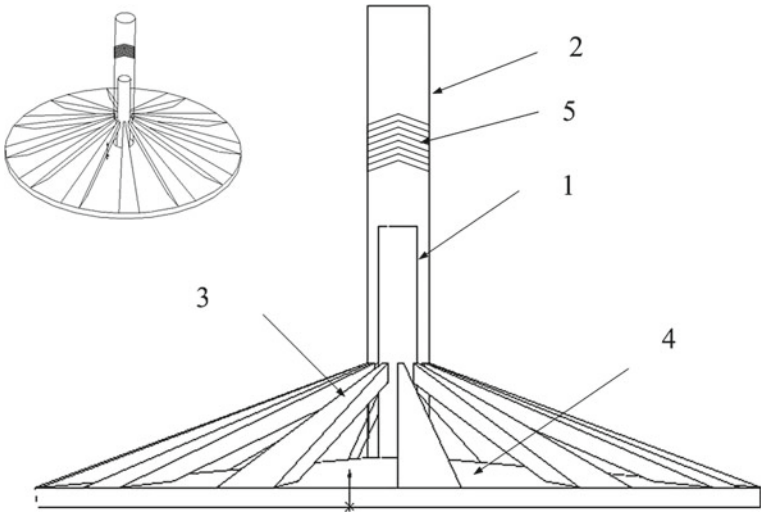

Fig. 1 Schematic of the solar chimney humidification-dehumidification seawater desalination system (1—inner chimney, 2—outer chimney, 3—sloped solar collector, 4—horizontal solar collector, 5—condenser)

ney and condenses into fresh water through the condenser, and the remaining air is discharged from the exit of the outer chimney.

2 Mathematical Model

2.1 Solar Collector

There are six assumptions used in simulation and they are: (1) steady state conditions, (2) the airflow speed at the collector inlet is ignored, (3) The sloped solar collectors are central symmetry with the chimney and each one absorbs the same solar radiation, (4) no evaporation or condensation takes place under the collector, (5) the vertical temperature profile of the collector air is constant, and (6) energy loss from the airflow to the ambient air at the collector inlet is ignored.

Horizontal solar collector

Continuity equation:

$$\frac{\partial \rho}{\partial t} + \frac{1}{r}\frac{\partial}{\partial r}(\rho r v_r) = 0 \tag{1}$$

Momentum equation:

$$\frac{\partial}{\partial t}(\rho v_r) + \rho v_r \frac{\partial v_r}{\partial r} = -\frac{\partial p}{\partial r} + \mu\left[\frac{\partial}{\partial r}\left(\frac{1}{r}\frac{\partial}{\partial r}(r v_r)\right)\right] \tag{2}$$

Energy equation:

$$\frac{\partial}{\partial t}\left(\rho c_p T\right) + \frac{\partial}{\partial r}\left(c_p \rho v_r T\right) = \frac{\partial S_\Phi}{\partial t} \tag{3}$$

Sloped solar collector

The momentum equation of the sloped solar collector can be revised as:

$$\frac{\partial}{\partial t}(\rho v_{r'}) + \rho v_{r'} \frac{\partial v_{r'}}{\partial r'} = -\frac{\partial p}{\partial r'} - \rho g_{r'} + \mu\left[\frac{\partial}{\partial r'}\left(\frac{1}{r'}\frac{\partial}{\partial r'}(r v_{r'})\right)\right] \tag{4}$$

2.2 Chimney

The model described below is based on the following simplified assumptions: (1) Boussinesq approximation is assumed to be valid, (2) energy loss through the chim-

ney wall is ignored, (3) energy loss at the connection section of the inner and outer chimneys is ignored and (4) turbulence after the turbine is ignored.

Continuity equation:

$$\frac{\partial \rho}{\partial t} + \frac{\partial}{\partial z}(\rho v_z) = 0 \tag{5}$$

Momentum equation:

$$\frac{\partial}{\partial t}(\rho v_z) + \rho v_z \frac{\partial v_z}{\partial z} = -\frac{\partial p}{\partial z} - \rho g_z + \mu \frac{\partial^2 v_z}{\partial z^2} \tag{6}$$

Energy equation:

$$\frac{\partial}{\partial t}\left(c_p \rho T\right) + \frac{\partial}{\partial z}\left(c_p \rho v_z T\right) = 0 \tag{7}$$

2.3 Evaporation and Condensation

Four assumptions are used to calculate the fresh water productivity: (1) the air humidity is zero from the inlets of the horizontal and the sloped solar collectors; (2) the solar energy in the horizontal solar collector heat the airflow; (3) the solar energy in the sloped solar collector is used to heat the seawater, the collector cover and the sloped plate and the rest energy ΔH is used to generate the moist airflow; and (4) the air humidity at the outlet of the condenser is zero.

According to the assumption, the next equation can be obtained:

$$\Delta H = S_2 - Q_w - Q_c - Q_f - Q_a \tag{8}$$

And the evaporated seawater and the generated fresh water can be obtained according to the following equation:

$$m_f = m_e = \frac{Q_w}{\Delta H} \tag{9}$$

3 Results and Discussion

3.1 System Performance

A SCHDHSD system with the same size as the Spanish solar chimney power plant prototype (Haaf 1984) was studied with solar radiation of 900 W/m^2 and ambient

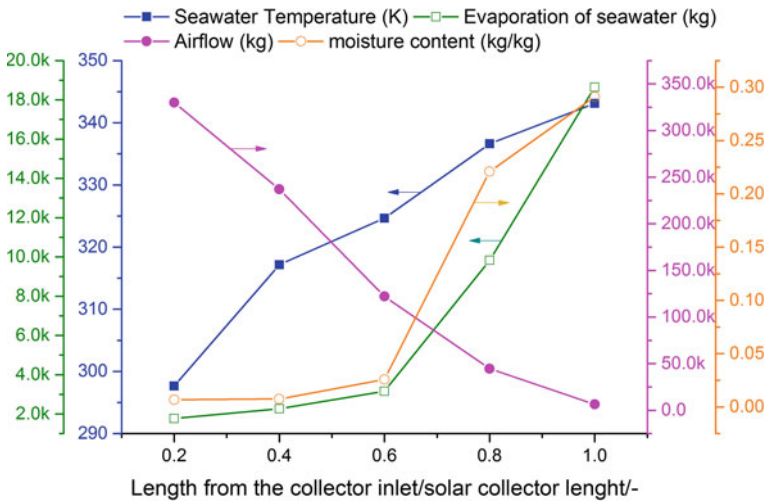

Fig. 2 Tendencies of sea water temperature, evaporated seawater, airflow and moisture content of the SCHDHSD system from the collector inlet to its outlet

temperature of 293 K. Performance of the SCHDHSD system is calculated according to the built mathematical model. The results are shown in Fig. 2. It can be seen from Fig. 2 that: (1) the sea water temperature increases gradually, with the highest temperature in the solar collector reaches 57 K, (2) The airflow decreases due to the decrease of the cross-section area as shown in Fig. 1, (3) the moisture content gradually increases from the collector inlet to the outlet, and (4) the evaporated seawater increases sharply along the solar collector.

3.2 Transient Performance Analysis

The transient performance of a SCHDHSD system is then simulated using the meteorological condition of Lanzhou as a case study. The solar radiation, ambient temperature and humidity in each month is shown in Table 1.

The thermal efficiency of the SCHDHSD system in each month is shown in Fig. 3. It is found from the figure that the highest thermal efficiency locates in June, which reaches 58%.

The fresh water productivity of the SCHDHSD system in each month is shown in Fig. 4. It is found from the figure that the highest fresh water productivity locates in June, which reaches 1.51 kg/h. And the lowest fresh water productivity in January can be over 1.0 kg/h. The annually average fresh water productivity is 1.32 kg/h.

Table 1 Meteorological condition of Lanzhou City

Month	Solar radiation (MJ/m^2)	Ambient temperature (°C)	Ambient humidity (%)
1	234.13	0.9	52
2	304.46	5.8	50
3	433.10	12.6	41
4	511.67	19.6	39
5	604.66	23.8	48
6	598.66	27.3	54
7	589.45	28.8	62
8	542.93	28.0	62
9	423.75	22.0	73
10	333.29	16.8	66
11	241.25	9.0	64
12	207.82	1.9	59

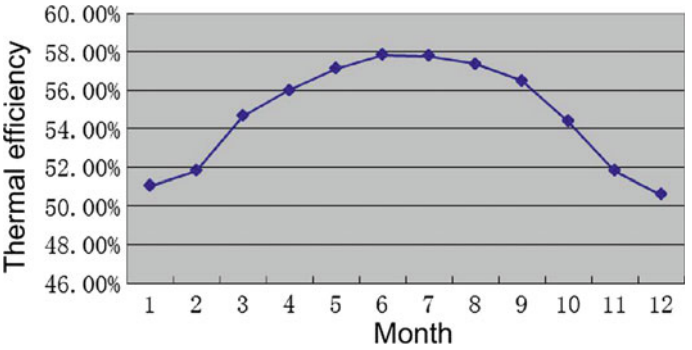

Fig. 3 Thermal efficiency of the SCHDHSD system throughout the year

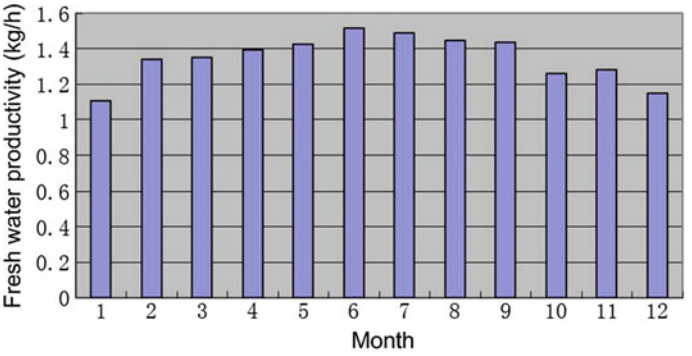

Fig. 4 Fresh water productivity of the SCHDHSD system throughout the year

4 Conclusions

Solar water desalination is an effective method to solve the shortage of fresh water resources. In this paper, a new SCHDHSD is proposed. A mathematical model is established to analyze the performance of the system. Monthly fresh water productivity is simulated by taking Lanzhou as a case study and the Spanish solar chimney power plant as the configuration. The following conclusions are obtained in this study:

(1) The sea water temperature increases gradually, with the highest temperature in the solar collector reaches 57 K. But the airflow decreases due to the decrease of the cross-section area, which leads to the rise of moisture content from the collector inlet to the outlet.
(2) Highest thermal efficiency locates in June, which reaches 58%.
(3) The maximum fresh water productivity of the system was 1.51 kg/h and the average fresh water productivity was 1.32 kg/h.

Acknowledgements This research was funded by the National Natural Science Foundation of China (No.: 51506043), the Fundamental Research Funds for the Central Universities (Grant No.: 2019B21914) and the "Dayu Scholar" foundation of Hohai University.

References

Chang ZH, Zheng HF et al (2014) Experimental investigation of a novel multi-effect solar desalination system based on humidification-dehumidification process. Renew Energy 69:253–259

Chehayeb KM, Narayan GP et al (2014) Use of multiple extractions and injections to thermodynamically balance the humidification dehumidification desalination system. Int J Heat Mass Transf 68:422–434

Gu F (2013) Research on humidification-dehumidification solar water desalination technology. Jiangsu University, Zhenjiang

Haaf W (1984) Solar chimneys, part II: preliminary test results from the Manzanares pilot plant. Int J Solar Energy 2(2):141–161

Sievers M, Lienhard VJH (2013) Design of flat-plate dehumidifiers for humidification-dehumidification desalination systems. Heat Transf Eng 34(7):1–19

Sievers M, Lienhard VJH (2015) Design of plate-fin tube dehumidifiers for humidification–dehumidification desalination systems. Heat Transf Eng 36(3):223–243

Wang YP, Wang JH et al (2006) The study of sea desalination and hot wind electric power integrated system by solar chimney. Acta Energiae Solaris Sinica 27:731–736 (in Chinese)

Zhu L (2005) A systematic study on economic comprehensive utilization of seawater by solar chimney. Tianjin Univresity, Tianjin

Zuo L, Yuan Y et al (2012) Experimental research on solar chimneys integrated with seawater desalination under practical weather condition. Desalination 298:22–33

Effects of Emergent Hydrophytes on the Water Restoration of Wuliangsu Lake in Inner Mongolia

Mangmang Gou, Xiaoqing Xu, Xing Li and Rong Ren

Abstract In order to study the ability of emergent hydrophytes on the water restoration of Wuliangsu Lake in Inner Mongolia by chemical oxygen demand (COD), nitrogen and phosphorus, three macrophytes species (*Typha latifolia* L., *Zizania latifolia* Turcz. and *Iris pseudacorus* L.) were treated with various concentrations of TN/TP/COD (T1: 2.0/0.4/40 mg L^{-1}, T2: 4.0/0.8/80 mg L^{-1} and T3: 320/60/8 mg L^{-1}). The results showed that planting emergent hydrophytes were more effective at reducing concentrations of COD, total nitrogen (TN) and total phosphorus (TP) than unplanted. Under the same treatment, the removal of TN was the best after planting *Zizania latifolia* Turcz., and the removal of TP was the best after planting *Iris pseudacorus* L. The removal effect of COD on each planting emergent hydrophytes were about 50%. However, the difference between treatments is not significant.

Keywords Water restoration · *Typha latifolia* L. · *Zizania latifolia* Turcz. · *Iris pseudacorus* L. · Wuliangsu lake

Lake water pollution is a very serious water environment problem facing the world, which seriously jeopardizes human health and living environment and is extremely harmful. China is a country with severe water shortage, and the problem of lake water resources has been very prominent (Peng et al. 2018). Wuliangsu Lake is located in the western part of the Inner Mongolia Autonomous Region of China. It is the most typical eutrophication-very algae-type lake in the arid regions of Inner Mongolia (Li et al. 2011). The deterioration of water quality has caused water blooms and

M. Gou
Water Conservancy and Civil Engineering Department, Inner Mongolia Technical College of Mechanics and Electrics, Hohhot 010070, China

X. Xu (✉) · X. Li
Inner Mongolia Engineering Research Center for Water-Saving Agriculture, Inner Mongolia Normal University, Hohhot 010022, China
e-mail: 913234212@qq.com

R. Ren
Inner Mongolia Hohhot Vocational College, Hohhot 010051, China

R. Sun and L. Fei (eds.), *Sustainable Development of Water and Environment*, Environmental Science and Engineering,
https://doi.org/10.1007/978-3-030-16729-5_18

occur from time to time. After the blooms, the toxins produced by the algae will be released into the water body. The drinking water safety of surrounding residents is greatly threatened, which has seriously affected the health of the people. The earliest, German scholar Kichuth proposed that planting aquatic plants can affect the water environment in the 1970s. He proposed the theory of the root zone method, which has attracted the attention of environmental scholars all over the world (Junli 2004). Thereafter, Governments are paying increasing attention to water pollution problems. The idea that plants have a role in sewage purification is widely recognized by scholars (Mulderij et al. 2005). Constructed wetland is a new type of sewage ecological treatment technology. It has the advantages of low investment, low energy consumption and optimized ecological environment. It has been widely used for treating eutrophic lakes. At the same time, emergent hydrophytes play an important role in the purification of sewage. The key measures to restore and rebuild constructed wetlands are that how to choose the right water plant (Cao et al. 2018; Gao et al. 2017). Recent studies have shown that reed planting can alleviate eutrophication of water bodies in the water purification of Wuliangsu Lake (Wei et al. 2016). However, the research results on the water purification ability of the emergent plants in Wuliangsu Lake are rarely reported. Experimental research on the variation of water quality parameters was carried out during the growth period of emergent plants. The purpose is to provide new ideas and important references to control eutrophication of Wuliangsu Lake.

1 Materials and Methods

1.1 Test Area

Wuliangsuhai is located in the Urad Front Banner of Bayannaoer City, Inner Mongolia Autonomous Region. It is the eighth largest freshwater lake in China. It is the most typical eutrophicated shallow grass-algae lake in the arid zone of Inner Mongolia. It is also the largest natural wetland at the same latitude on Earth. It not only plays an important role in water conservation, water storage and water transfer in the middle and upper reaches of the Yellow River, but also plays a key role in regulating ecosystem balance and protecting the ecological environment.

In recent years, the water environment problem is very serious, mainly reflected in the following aspects: 1. Abnormal algae growth and reproduction. 2. The process of lake swamping is intensifying. 3. The eutrophication of lake waters continues to increase and water quality continues to deteriorate. 4. The water level and water depth are continuously decreasing. 5. The quantity and quality of species resources are declining. 6. Tourism development is hindered and restricts the development of regional economy.

Table 1 Artificial simulation water quality

Levels	V Level	Inferior V_1	Inferior V_2
Treatments	T1	T2	T3
COD	40	80	160
TP	0.4	0.8	1.6
TN	2.0	4.0	8.0

1.2 Test Materials

Three macrophytes species (*Typha latifolia* L., *Zizania latifolia* Turcz. and *Iris pseudacorus* L.) are collected from a water body ecological landscape cultivation company. Picking healthy plants and taking robust growth and the size suitable as a test material. Suitability culture is carried out for 30 days after rinsing. The test was carried out in a flower pot. Flower pot diameter is 45 cm and height is 30 cm. In the experiment, the sediment (taken from Wuliangsu Lake) was used as the substrate and the thickness is 25 cm. After the eutrophication of Wuliangsu Lake is considered comprehensively, the test water quality is matched including 3 levels, and specifically shown in Table 1.

1.3 Test Design

The test was carried out at a constructed wetland test site. The trial was conducted from May to September. Planting density for each barrel is 4 strains of *Typha latifolia* L., 6 strains of *Zizania latifolia* Turcz. and 4 strains of *Iris pseudacorus* L. Taking each plant as a treatment, and each treatment is set to 3 repetitions. Replenish water is done every 7 days and the amount of replenishment water is 10 L. Effective water depth is 20 cm. Sewage before replenishment water is collected, and each collection is 100 mL. Water quality indicators (CODcr, TP, TN) were taken on the day of water withdrawal. The removal rate is calculated as $R = 100(Ci - C0)/Ci \times 100\%$. Among them Ci is the water quality before planting, and C0 is the water quality after planting.

1.4 Index Detection

The water quality is determined by the method in the Water and Wastewater Monitoring and Analysis Method (Fourth Edition, Supplemental Edition, 2002). TN is oxidized by potassium persulfate-ultraviolet spectrophotometry. TP is oxidized by molybdenum antimony anti-spectrophotometry. CODcr is oxidized by potassium dichromate.

1.5 Data Analysis

The test data was applied to Excel 2007, and statistical analysis and analysis of variance were performed using SAS 9.0 software.

2 Results and Analysis

As can be seen from the figure, the three kinds of emergent hydrophytes had significant effects on the restoration of water bodies.

2.1 Comparison of Purification Effects of TN and TP in Different Growth Stages

From the perspective of the entire growth period (Figs. 1 and 2), compared with the pre-plant water quality, the removal rate of TN and TP increased significantly with the growth of the three kinds of emergent hydrophytes. Compared with the initial stage of planting, the removal rate was higher in August–October, the TN removal rate was 27–45%. The TP removal rate was 34–53%, with the highest in September and the removal rate exceeding 30%. From the perspective of sewage concentration, as the concentration of sewage increases the removal rate first increases and then decreases. From the perspective of emergent hydrophytes, *Zizania latifolia* Turcz. had the best removal effect on TN, with a removal rate of up to 47%, followed by *Typha latifolia* L. and *Iris pseudacorus* L. However, *Iris pseudacorus* L. had the best removal effect on TP, and the removal rate was as high as 57%. As the plant growth and density enhancement, the ability of total nitrogen and total phosphorus in water were reduced.

2.2 Comparison of Purification Effects of COD in Different Growth Stages

From the perspective of the entire growth period (Fig. 3), compared with pre-plant water quality the removal rate of COD was significantly increased. Compared with early planting, the removal rate was higher in August–October, and the COD removal rate was 54–59%. From the perspective of sewage concentration, with increasing concentration of waste, COD removal efficiency was also increased. In terms of plant species, the removal rate of COD in the same concentration was not significant ($P < 0.05$).

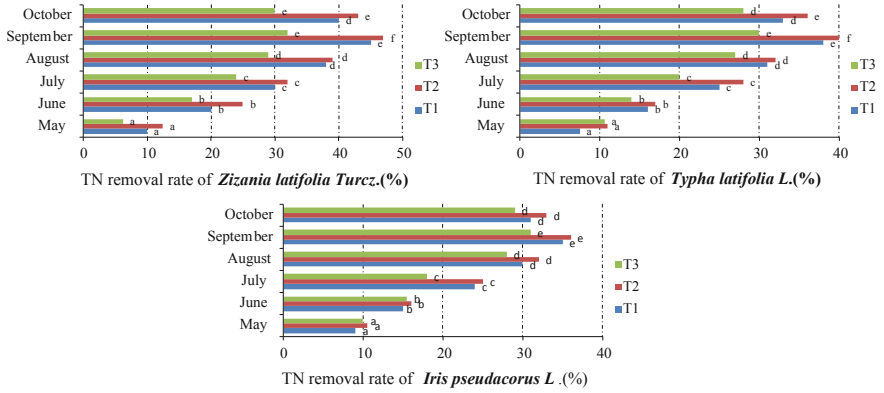

Fig. 1 Purification effects of TN of three emergent hydrophytes

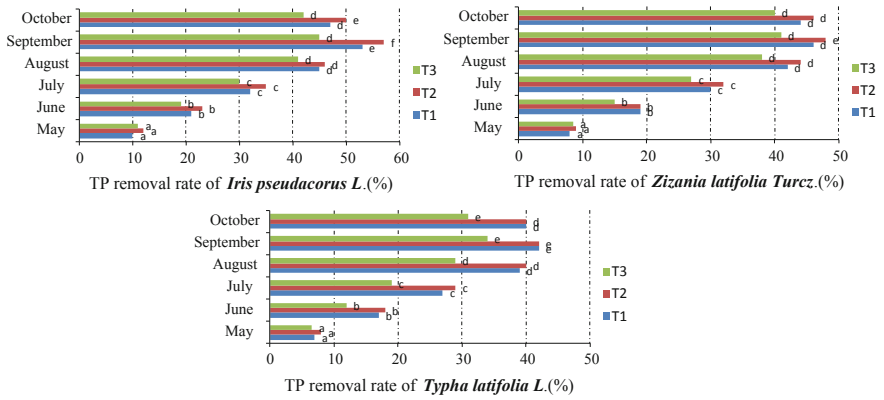

Fig. 2 Purification effects of TP of three emergent hydrophytes

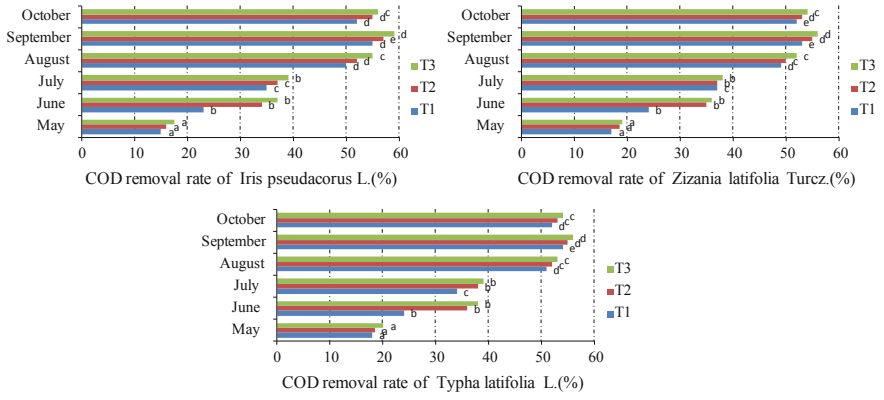

Fig. 3 Purification effects of COD of three emergent hydrophytes

3 Conclusions and Discussion

Today, water pollution problems in lakes and rivers are becoming more and more serious, which seriously affect human health and living environment. The results show the following points on studying the aquatic plants to control the eutrophication of water bodies. On the one hand, emergent plants can remove nitrogen, phosphorus and other pollutants through absorption. On the other hand, the emergent plants accelerate the decomposition of pollutants by releasing oxygen and secretions from the plant roots. It can be seen that they play an important role in purifying water quality. In this study, water quality monitoring was carried out for the whole growth period of plant growth. The results showed that the water purification effect was the highest during the plant growth period, and the removal rates of TN, TP and COD were 47, 57 and 59% respectively. The water purification effect was more significant. The results of this study are consistent with the results of Dornelas et al. (2009) and Zhao et al. (2016). Different plant species have differences in nutrient absorption capacity, root growth distribution and biomass, resulting in different purification effects. *Zizania latifolia* Turcz. is a perennial aquatic plant with characteristics of strong root development and activity.

Li et al. (2010) found that root structure of *Zizania latifolia* Turcz. can transport more oxygen and nutrients, which is beneficial to the formation of ammonia-oxidizing bacteria, reducing the accumulation of nitrogen in water, and achieving the effect of purifying water. This is the same as the results of this study. The results of this study show that the effect of removing TP from *Iris pseudacorus* L. is the best. This is similar to the conclusion of Yuan (2017). Regular harvesting of plants can transfer and remove nitrogen and phosphorus from some water bodies to achieve removal TN and TP. The effect of plants on water purification is affected by various factors such as sewage load, residence time, water quality concentration and wetland type. In this study, three levels of sewage concentrations were designed. With the increase of concentration, the removal effect of TN and TP decreased. Plants have a significant effect at a certain sewage concentration. However, when the concentration of pollutants is higher, the removal effect will decrease. The reason is mainly because plant growth is stressed in adversity. This is similar to the results of Ling et al. (2012).

Acknowledgments Fund Project: 1. 2018 Inner Mongolia Science and Technology Project (KCBJ2018008); 2. 2017 Inner Mongolia Technical College of Mechanics & Electrics Science Fund (NJDZJZR1701).

References

Cao K, Ding H, Deng C (2018) Purification effects of wetland aquatic plants on eutrophic water. J Biol (6):29–32

Dornelas M, Moonen AC, Magurran AE et al (2009) Species abundance distributions reveal environmental heterogeneity in modified landscapes. J Appl Ecol 46(3):666–672

Gao Y, Chen T, Zhang Y et al (2017) Eutrophicated water quality improvement by combination of different organisms. Chin J Environ Eng 11(6):3556–3563

Junli K (2004) Feasibility study on constructed wetland ecology system in waste water reuse. Environ Sanitation Eng (2):114–117

Li EH, Li W, Wang XL et al (2010) Experiment of emergent macrophytes growing in contaminated sludge: implication for sediment purification and lake restoration. Ecol Eng 36(4):427–434

Li X, Yang Q, Gou M (2011) Temporal and spatial distribution of water quality in Lake Wuliangsuhai, Inner Mongolia. Ecol Environ Sci 20(8–9):1301–1306

Ling Z, Yang J, Yu G et al (2012) Study on the effect of sewage concentration on treatment efficiency of artificial wetland of plateau lake. J Hydroelectric Eng 31(5):133–153

Mulderij G, Mooij WM, Smolders AJP et al (2005) Allelopathy inhibition of phytoplankton by exudates from Stratiotes aloides. Aquat Bot 82(4):284–296

Peng W, Liu X, Wang Y et al (2018) Review and prospect of progress in water environment and water ecology research. Shuili Xuebao 49(9):1055–1067

Wei J, Wang L, Liu D et al (2016) On the decomposition dynamics and nutrient release of Phragmites australis litter in Wuliangsu Lake. J Saf Environ 16(5):364–370

Yuan J, Dong L, Yang J et al (2017) Study on purification effect of nitrogen and phosphorus in eutrophic river water by six emerged plants. Environ Sci Manage 42(4):75–83

Zhao Y, Tian Y, Huang D et al (2016) The seasonal variation performance of vertical subsurface flow constructed wetlands with four plants under different influent C/N ratios. Acta Sci Circumst 36(1):193–200

Application Status on Hydrological Detention Efficiency of Urban Green Space in China

Xi Wang, Xiaoyan Cao and Tiemao Shi

Abstract With the acceleration of China's urbanization process, the expanding city scale has caused serious damage to the urban water system and natural water processes, which has led to the increasingly serious urban rainfall flood disasters. Developed countries have more experience in urban diseases, so the research on urban stormwater management and utilization has been Relatively well. For the study of the impact mechanism of green land demurrage, foreign countries have a relatively complete theoretical system and a large number of case practice tests. These rich practical experiences can be used as a reference for China. However, combined with China's special national conditions and regional characteristics, we still need to carry out deeper and more local research. While domestic research on green land rain and flood detention is concentrated in water conservancy, plant protection and other disciplines, lacking different environmental characteristics for the city, In the perspective of macro-planning, the quantitative calculation of green space depletion efficiency capacity based on factors such as soil conditions, vegetation types, rainfall conditions.Urban green space is the main natural carrier of the rain stagnant. It is the main part of the construction of the sponge city. However, the currently attention of urban green space planning more focus on the ecological function such as oxygen release. It is relatively insufficient on the evaluation and planning studies on the efficacy of green area rainwater stagnation. By establishing the quantitative relationship between the characteristics of rainfall, runoff, soil, vegetation and other factors and the stagnant capacity of green space rainwater, the comprehensive impact mechanism is evaluated, and the artificial measures of rainwater control are combined to adjust the spatial pattern of urban green space, which is to improve the green storage efficiency. The use of indispensable content is also an inevitable development trend in the application of rainwater flood management in future urban green space depletion efficiency.

X. Wang · T. Shi (✉)
Shenyang Jianzhu University, Hunnan Shenyang 110168, China
e-mail: tiemaos@sjzu.edu.cn

X. Cao
University of Science and Technology LiaoNing, Hunnan Shenyang 110168, China

R. Sun and L. Fei (eds.), *Sustainable Development of Water and Environment*, Environmental Science and Engineering,
https://doi.org/10.1007/978-3-030-16729-5_19

Keywords Urban green space · Hydrological regulation function · Quantitative research progress

1 Current Status of China's Stormwater Management

1.1 Severe Hydrological Circulation Disorder

In recent years, frequent droughts and floods in China have occurred frequently, and 2/3 of the country's land area is threatened by floods. According to the statistics of the Urban Flood Control and Countermeasures Research Group, the average annual economic loss of flood disasters reached 145.78 billion in 2011–2017, and even reached 316.8 billion yuan in 2013. In 2016, 261 cities across the country experienced different levels of storms and floods. Taking Beijing as an example, the 2012.7.21 torrential rain disaster caused 79 deaths. The traffic in the whole city was paralyzed, and the mountainous areas in the suburbs were seriously affected. The city directly lost more than 15 billion yuan (Fig. 1).

On the other hand, the annual average urban water shortage in the country is 6 billion cubic meters. The per capita water resources of 11 provinces and cities are lower than the internationally recognized heavy water shortage line. These provinces and cities have frequent floods and water supply and demand conflicts. It also aggravated the burden of groundwater. The direct and indirect losses caused by over-exploitation of land subsidence to the Yangtze River Delta region have reached 315 billion yuan. The groundwater level in Beijing has dropped from an average of 12 m in 1999 to an average of 24 m in 2010, and a subsidence area of 2650 km has been formed.

Causes of flood disasters. The causes of the frequent floods in cities today are very complex, and we need to conduct scientific analysis and evaluation. According to domestic and foreign literature studies, there are mainly the following aspects:

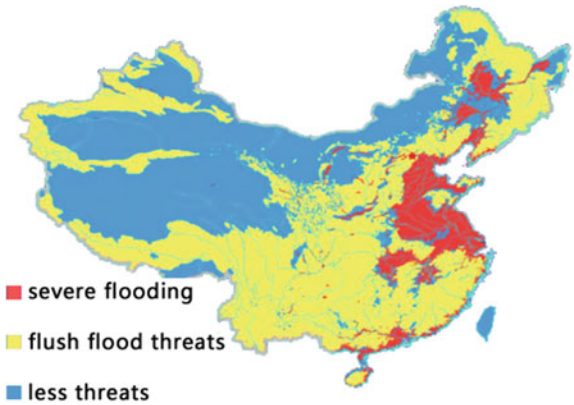

Fig. 1 National flood risk distribution. *Source* China Sponge City Conference (2018)

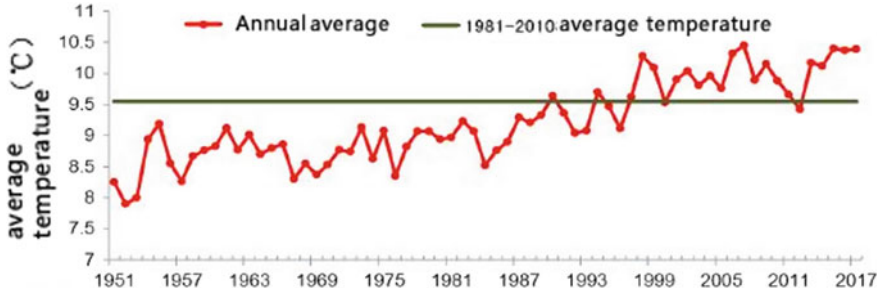

Fig. 2 National average temperature trend, 2018 China Sponge City Conference (2018)

The influence of special geographical location, climatic conditions and topographical features in China. Affected by the Pacific Water Vapor and the Indian Ocean Water Vapor, there are very large differences in climate zones in China, and the characteristics of the monsoon are prominent. The annual average rainfall varies greatly in different regions, and the hydrological changes are obvious, which is likely to cause flood disasters. This is an objective natural condition that cannot be ignored (Fig. 2).

Global warming and tropical cyclones are increasing. The 2017 WMC Global Climate Status Statement states that, 2017 is one of the warmest three years in the world, with a global average temperature of 0.46 ± 0.1 °C higher than the 1981–2010 average, and about 1.1 ± 0.1 °C above the pre-industrial level. In the past 100 years (1919–2010), China's surface temperature has risen by 0.9–1.5 °C, and the surface temperature of land has risen by 1.38 °C in the past 60 years, higher than the global average. In 2018, many places in China continued to have a high temperature of over 40 °C, while the temperature in the Arctic reached 32 °C. Global warming, on the one hand, leads to an increase in the hydrological cycle and an increase in ocean evaporation, and on the other hand leads to an increase in the water content of the atmosphere itself. At the same time, the temperature rise causes the atmospheric water holding capacity to increase, and more water vapor is needed, so that the atmosphere can be saturated, thereby forming rainfall conditions, and once rainfall occurs, the rainfall intensity will be greater. The damp and warm atmosphere is less stable and is also prone to rainstorms.

With China's entry into rapid urbanization development stage, the urban heat island and rain Island phenomenon is growing. From 36.3% in 2000 to 58.5% in 2017, the statistics show that the frequency of heavy rains in the Yangtze River Delta is significantly higher than that in the suburbs. Compared with 1961–1980, the increase in the number of rainstorm days in urban and suburban areas of Suzhou is 30.0 and 18.0%, Nanjing was 22.5 and 11.0% respectively, and Ningbo City achieved a significant comparison of 32 and 2%.

The influence of special geographical location, climatic conditions and topographical features in China. Affected by the Pacific Water Vapor and the Indian Ocean Water Vapor, there are very large differences in climate zones in China, and

the characteristics of the monsoon are prominent. The annual average rainfall varies greatly in different regions, and the hydrological changes are obvious, which is likely to cause flood disasters. This is an objective natural condition that cannot be ignored. Exploring the reasons for its significant contrast, along with the deepening of urbanization, the urban population expansion and industrial development have largely changed the original hydrological conditions of the land, and the gradually increasing urban soot has become a catalyst, which in turn has produced The "rain island effect" and "heat island effect" further contributed to the increase in urban rainfall. The increasing area of urban roads and plazas has led to an increase in the impervious surface and dense surface of the underlying surface, reducing the chance of rainwater runoff infiltration and the ability of the soil to absorb water. The surface has a weaker ability to accumulate rainwater and a larger runoff coefficient. Under the premise of the same rainfall level and intensity, the flood peak flow in the surface runoff process is seriously increased due to the rapid convergence of the runoff, and the final rainwater process shows a sharp increase trend.

Urban development has squeezed the flood storage space on a large scale. Unreasonable urban expansion has greatly reduced the amount of cultivated land and forest land, and also eroded natural rivers, wetlands and riverside forests, which has attenuated and fragmented waters, resulting in greatly reduced capacity for natural resources to accommodate and reduce rainwater. Taking the torrential rain that suffered in Wuhan in 2016 as an example, in the 1950s, there were 127 lakes in the Taihu Lake Basin. Today there are only 38 lakes. The lake area dropped sharply by 106 km^2 between 1987 and 2013, a decrease of 30%. The ecological resources were severely damaged, and the urban development of Tianhu Land eventually caused a strong counterattack from nature.

With China's entry into rapid urbanization development stage, the urban heat island and rain Island phenomenon is growing. From 36.3% in 2000 to 58.5% in 2017, the statistics show that the frequency of heavy rains in the Yangtze River Delta is significantly higher than that in the suburbs. Compared with 1961–1980, the increase in the number of rainstorm days in urban and suburban areas of Suzhou is 30.0 and 18.0%, Nanjing was 22.5 and 11.0% respectively, and Ningbo City achieved a significant comparison of 32 and 2%.

Disordered development of the city. Underground facilities such as parking lots and sunken overpasses are likely to cause rainwater to accumulate. Urbanization construction over-exploited groundwater, and land subsidence caused the sinking of subgrades, buildings, and underground pipelines, which became the cause of urban flooding.

Urban drainage standards are generally low. The construction of urban drainage infrastructure in China started late. Due to the aging of facilities, the unreasonable drainage system and the low design standards, the drainage capacity of infrastructure is far behind urban development. As urban population, buildings, and traffic density continue to increase, the cost and difficulty of infrastructure expansion increases, and the expansion space is also very limited. According to the survey of the Ministry of Housing and Urban-Rural Development, more than 70% of urban drainage system construction in China has a design rainstorm return period of less than one year,

and 90% of the key areas in the old city area are even lower than the lower limit specified in the regulations. At present, the design standards for drainage systems in Beijing are once in 1–2 years. Under normal circumstances, they can only withstand 36 mm of rain per hour. Exceeding this standard is bound to cause urban disasters. In February 2014, the "Outdoor Drainage Design Code" newly issued by the Ministry of Housing and Urban-Rural Development significantly improved the drainage design standards. However, due to the funding problems and the difficulty of the current situation, the results were still slow.

Urban emergency management system urgently needs improvement. China's current stormwater safety management still lacks sufficient scientific guidance. The Ministry of Housing and Urban-Rural Department's water conservancy departments and other departments have their own rights and ambiguities, resulting in serious shortage of urban flood emergency plans. At the same time, nowadays, intelligent technology applications are still in the process of exploration. It is extremely urgent to use scientific and technological means to provide emergency management mode.

For these reasons a comprehensive hydrological conditions led to the whole city and gradually into a vicious circle, showing a serious lack of water at the same time has stimulated serious obstacle to the phenomenon of rain will flood.

1.2 Disadvantages of Current Stormwater Management Model

The traditional way for cities to cope with floods is to build a drainage network and build concrete dams in the waterfront. Through the underground pipe network, the rainwater will be discharged into the receiving water bodies such as flood rivers and lakes as soon as possible. This not only increases the pressure on the downstream areas to withstand floods, but also increases the possibility of flood disasters in these areas, and at the same time, due to the planning of some local cities. The water level of the flood discharge channel is high. When the water rises during the rainy season, the difference between the water level and the rainwater drainage outlet is small, which affects the drainage of the pipe network. Therefore, once there is heavy rain, the drainage of the pipe network will be difficult to bear, and the rainwater will be retained or even inverted.

This way of relying solely on infrastructure to eliminate or passively defend against rain and flood, although it has a certain effect in a short period of time, in the long run, it destroys the ability of natural drainage systems such as natural surface and wetland tidal flats to cope with rain and flood, which makes the effects of surface seepage and retention of flood storage are greatly reduced. At the same time, this way of eliminating rainwater as soon as possible also wastes a lot of water resources, which is contrary to the reality of water shortage in many cities, and does not treat rainwater as a valuable resource. The infrastructure has the only goal of drainage and flood control, and the functional benefits are very limited. Ultimately, it will lead to

a vicious circle, that is, to build a larger and more underground pipe network and a higher concrete dam. China's traditional rainwater management model has been unable to cope with the increasingly serious disasters and needs to be fundamentally transformed.

1.3 The Lack of Current Urban Green Space Planning

The traditional way for cities to cope with floods is to build a drainage network and build concrete dams in the waterfront. Through the underground pipe network, the rainwater will be discharged into the receiving water bodies such as flood rivers and lakes as soon as possible. This not only increases the pressure on the downstream areas to withstand floods, but also increases the possibility of flood disasters in these areas, and at the same time, due to the planning of some local cities. The water level of the flood discharge channel is high. When the water rises during the rainy season, the difference between the water level and the rainwater drainage outlet is small, which affects the drainage of the pipe network. Therefore, once there is heavy rain, the drainage of the pipe network will be difficult to bear, and the rainwater will be retained or even inverted.

This way of relying solely on infrastructure to eliminate or passively defend against rain and flood, although it has a certain effect in a short period of time, in the long run, it destroys the ability of natural drainage systems such as natural surface and wetland tidal flats to cope with rain and flood, which makes The effects of surface seepage and retention of flood storage are greatly reduced. At the same time, this way of eliminating rainwater as soon as possible also wastes a lot of water resources, which is contrary to the reality of water shortage in many cities, and does not treat rainwater as a valuable resource. The infrastructure has the only goal of drainage and flood control, and the functional benefits are very limited. Ultimately, it will lead to a vicious circle, that is, to build a larger and more underground pipe network and a higher concrete dam. China's traditional rainwater management model has been unable to cope with the increasingly serious disasters and needs to be fundamentally transformed.

Within the urban environment, urban green space can effectively repair the natural water cycle, increase the connection between surface water and atmospheric precipitation and groundwater environment. Green space, as the main part of urban soft natural cushion surface, plays a positive role in alleviating urban flood disaster, regulating and storing rainwater runoff, and reducing peak flow rate, etc. Scientifically and quantitatively applying the stagnation efficiency of urban green space, fully excavating and giving full play to its regulating role in the process of runoff generation and confluence, repairing and bridging the natural hydrological cycle process, and reasonably coordinating the functional relationship between the artificial water cycle system can effectively alleviate the obstacle of urban water cycle.

However, the current urban green space system planning generally starts from the Angle of shaping urban form, focusing on the construction of spatial pattern with

several axes, several belts, several changes and several rings, and takes green space planning as a means to express the aesthetics of urban form. However, in the face of some increasingly serious resources and ecological environment problems, such as water resource shortage and waste, habitat fragmentation, disorderly expansion of built-up areas, urban heat island effect, etc., this planning method has certain limitations. Due to the lack of detailed consideration of natural ecological processes, such as the process of surface runoff confluence, flood process, etc., most of them do not have specific plans for rain and flood management for natural hydrological processes.

At the present stage, due to the lack of in-depth research on the mechanism of the effect of hysteretic storage efficiency and the need to improve the pertinence of the simulation prediction model, there is still a bias in the quantitative evaluation of the degree of hysteretic storage efficiency. However, the construction of sponge city has just started, and it focuses on the research and application of low-impact development (LID) measures. The research on green space pattern optimization based on the quantitative evaluation of stagnation efficiency is relatively weak, and the prototype observation quantity is insufficient. The construction of sponge green space system still needs further systematic and scientific in-depth research.

This paper summarizes and sorts out the research progress on the application of urban green space's hysteretic storage efficiency in stormwater management, analyzes the development trend of future research on urban green space's hysteretic storage efficiency, and provides new ideas for maximizing the effect of urban green space on stormwater management.

2 Research Trends of Stormwater Management Models

Studies related to urban stormwater management mode are mainly reflected in best management practices (BMPs) in the United States, low impact development (LID) [6], water-sensitive urban design (WSUD) in Australia and sustainable drainage systems (SUDS) in the United Kingdom. Low-impact development is developed on the basis of BMPs. The difference is that the best management practices program takes terminal treatment before development, and the main purpose is to reduce the peak rainstorm flow (Gilroy and Mc Cuen 2009). Fletcher et al. (2015) pointed out that the planning method combining LID and GI pays more attention to the needs of macro planning and its development (Fig. 3).

It has become an important means to effectively control urban flood disaster by using models to simulate rainfall surface runoff process. Examples include the US environmental protection agency's stormwater management model (SWMM), the usgs's diffused stormwater runoff model (dr3m-uqal), the UK's Info Works CS model and the highway research institute model (TRRL). Kiruna, Northern Sweden (2018) USES the SWMM model to integrate topography, drainage systems and future climate data and simulate runoff. I-tree software can simulate basic data such as soil type, terrain, rainfall, evaporation and soil cover of the area, which

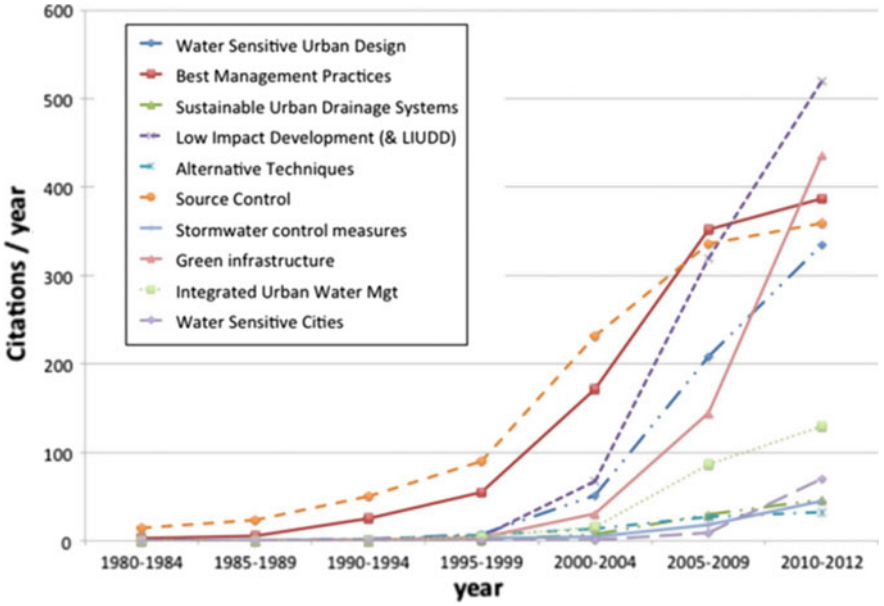

Fig. 3 Development of terminology related to urban stormwater management in the world from 1980 to 2012. *Source* Fletcher et al. (2015)

is more effective than traditional CIT or random sampling (Song 2014). Coccolo et al. (2018) used Citysim model to quantitatively analyze the influence of evapotranspiration of different vegetation materials on urban energy balance. Nice et al. (2018) discussed a microscale model vtuf-3d (Vegetated Temperatures of Urban Facets) in which vegetation cooling was simulated, and analyzed the characteristics of important physiological processes of plants. Graca et al. adopted the I-tree Eco v5 simulation tool to quantitatively analyze the flood detention regulation function of different types of urban green space and its impact on ecological services. Zhang Dongdong et al. used hydrological model to simulate the dynamics of rain-flood risk space-time. Jiao et al. assessed the potential risk of rain and flood in Changsha city through the coupling model of GIS and SCS in 2017.

In general, at the present stage, foreign research on urban stormwater management and utilization has been relatively complete, and there are rich practical experience for reference. Although some progress has been made in the management and utilization of rain-flood in China, it is difficult to play an obvious role in alleviating the whole urban waterlogging problem in China due to its late start. Therefore, the rain-flood problem should be appropriately solved according to China's national conditions and regional characteristics.

3 Application Progress of Urban Green Space Stagnation Efficiency

Different green space structure and environment have different stagnation efficiency. Domestic scholars have relatively more studies on the stagnation efficiency of vegetation and soil. Wang Aijuan et al. believed that developed plant roots could loosen soil and increase soil water storage capacity. Assuming a daily rainfall of 10–25 mm, 15–40% can be intercepted by the canopy, with a small part of evaporation and most of infiltration on the understory of the forest. Plant canopy has an obvious interception effect on rainfall, and dead branches and leaves covered by the ground can promote the infiltration of rainwater. Trunk runoff in rainy days is related to the size of the tree, the structure of the canopy and the branch Angle of the trunk. The area, slope, vegetation composition, soil characteristics and other factors of green space will all have an impact on the rainwater harvesting effect of garden green space, among which the selection of vegetation type plays an important role in the storage and consumption of soil moisture.

At the present stage, there is a lack of quantitative research on the hysteretic efficiency of green land according to different environmental characteristics of cities and taking into account factors such as soil conditions, vegetation types, rainfall conditions and hydrological cycle characteristics. These parts still need further exploration.

The research of urban green space pattern on rain and flood control has been discussed. Foreign researchers have found that in urban areas without vegetation, about 60% of rainfall is discharged into urban sewers in the form of surface runoff. When studying residential green space, it is found that a 10% increase in coverage can reduce 4.9% of surface runoff. Zoulia and Kaini et al. proposed the infrastructure with low impact of green development. The reasonable layout of decentralized layout combined with internal connectivity can generate longer hydrological process path than the centralized layout, resulting in lower peak flow and longer flood peak delay. Auffret found that there was A positive correlation between forest soil water content and vegetation three-dimensional green volume density, especially in the downstream areas of basin. Proper site design, selection of dominant tree species, accurate positioning of key greening zones, improvement of species richness and planting density of plant communities, reduction of water footprint by plants through biological filtration, and maximum improvement of water resource utilization and conversion rate all contribute to urban flood control. Auffret et al. studied and proposed that the decentralized layout mode of green rain-flood facilities combined with a good hydrological connector can better reduce and delay the flood peak flow. Kim and Park discussed the impact of space configuration of specific green infrastructure on surface runoff scale, quantity, connection path and edge shape; Green ecological hubs and corridors can effectively provide empirical basis for rainwater runoff management. When the rainfall is small, the decentralized layout of green stormwater facilities is conducive to reducing surface runoff.

References

Coccolo S, Kaempf J, Mauree D, Scartezzini JL (2018) Cooling potential of greening in the urban environment, a step further towards practice. Sustain Cities Soc 38:543–559

Fletcher TD, Shuster W, Hunt WF et al (2015) SUDS, LID, BMPs, WSUD and more—the evolution and application of terminology surrounding urban drainage. Urban Water J 12(7):525–542

Gilroy KL, Mccuen RH (2009) Spatio-temporal effects of low impact development practices. J Hydrol 367(3–4):228–236

Jiao S, Zhang X, Xu Y (2017) A review of Chinese land suitability assessment from the rainfall-waterlogging perspective: evidence from the Su Yu Yuan area. J Cleaner Prod 144:100–106

Nicea KA, Couttsa AM, Tapper NJ (2018) Development of the VTUF-3D v1.0 urban micro-climate model to support assessment of urban vegetation influences on human thermal comfort. Urban Climate (Available online)

Song C, Porter A, Foster JS (2014) iTree: efficiently discovering high-coverage configurations using interaction trees. IEEE Trans Software Eng 40(3):251–265

Response of Ecological Water Supply Service to Land Cover Change in the Source Area of the Yellow River

Aihong Gai, Liping Di, Junmei Tang, Liying Guo and Huihui Kang

Abstract In this paper, the InVEST model was applied to simulate the quantity of water supply of the source area of the Yellow River, China based on land use data of 1990, 2000 and 2010 extracted from the Landsat TM imageries. The CA-Markov model was then used to simulate the land cover in 2020, and the water supply in 2020 was predicted based on land cover of 2020. The results suggested that the primary land cover type of the source area of the Yellow River was grassland from 1990 to 2000, and the land cover changed mainly from higher ecological level to lower one at a rapid speed in the early stage. But from 2000 to 2010, the decline of vegetation area slowed greatly, which indicated a change from degradation to recovery. The rank of water supply capacities per unit area of different land cover types were shrub, construction land, high coverage grassland, middle coverage grassland, bare land, forest land, low coverage grassland, cultivated land, and wetland. The distribution of the water supply capacity was from the high-value zone in Southeast Ruoergai and Hongyuan County to the low-value area in the Northwest of Qumalai, Chengduo and Maduo county. The supply quantity of water source in the source area of the Yellow River showed an increasing trend from 1990 to 2010, and the ecological water supply capacity of the region was predicted to increase in 2020, and showed higher increase trend in Southeast and lower trend in Northwest.

This project was support by Discipline Construction Fund Project of Gansu Agricultural University (GAU-XKJS-2018-216). This project was support by Funds for China Scholarship Council (No. 201508625049).

A. Gai (✉) · H. Kang
College of Resources and Environmental Sciences, Gansu Agricultural University, 730070 Lanzhou, China
e-mail: gaiah@gsau.edu.cn; agai@gmu.edu

A. Gai · L. Di · J. Tang · L. Guo
Center for Spatial Information Science and System, George Mason University, Fairfax, VA 22030, USA

L. Guo
Chinese Academy of Sciences, Beijing 100101, China

R. Sun and L. Fei (eds.), *Sustainable Development of Water and Environment*, Environmental Science and Engineering,
https://doi.org/10.1007/978-3-030-16729-5_20

Keywords Land GIS & RS technology · Modeling · Land cover change · Water supply · The source area of the yellow river

1 Introduction

Land use change is a direct reflection of human economic and social development on the use of land resources, and is the main content of global environmental change and sustainable development research (Aihong Gai and Guozhang Cen 2015). With the rapid development of ecosystem service research in recent years, changes in water supply services and their impact mechanisms have begun to receive attention (Shimei Li 2010), because of their importance to the ecosystem.

The Yellow River is China's second largest river and the most important source of water for supply in the north and northwest China. Changes in the water resources of the source area of the Yellow River will directly lead to changes in the ecological, hydrological and socio-economic aspects of the whole basin (Ying Wang 2013). Some scholars believe that the decline in ecosystem water supply capacity may be the main factor leading to reduced runoff (Gengxu Wang 2009). However, it is still unclear how the water supply service of Huangyuan District's ecosystem has changed (Tao Pan 2013). At present, many scholars have begun to use models such as CA-Markov, GUMBO, and InVEST models, to predict land use cover change trends, study ecosystem functions and their changing processes, and their interactions (Zhiming Li 2017). Based on the InVEST model, this paper conducted a simulation assessment of the water supply in the source regions of the Yellow River in 1990, 2000, and 2010. The CA-Markov model was used to simulate the land cover of 2020 and to provide a basis to discuss the effects of land cover change on water supply. The model is used to provide scientific basis for the ecological protection and construction of the source region of the Yellow River.

2 Materials and Methods

2.1 Overview of the Study Area

The source area of the Yellow River is located at the junction of Qinghai, Gansu, and Sichuan provinces. The source area lies between the Yellow River mainstream Tangnaihai hydrological station and Heyuan, between 32° 09′–36° 07′N and 95° 53′–103° 24′E. The source area has an area of 121,900 km^2. It's altitude is between 2902 and 6070 m, which belongs to plateau lakes and marsh landforms. It's topography changes smoothly, showing strong erosion of the mountainous landforms, weakly eroded plateau low hilly landforms, then lake basins and valleys (see Fig. 1).

Fig. 1 The location map in the source region of Yellow River

The study area has a semi-arid-semi-humid climate with high temperature. The annual average rainfall is between 320.0 and 750.5 mm. The source area has a variety of natural environments and the alpine vegetation is widely distributed.

2.2 Data Sources and Processing

The main data required for this study include land cover data, climate data, and soil data. The land cover data (1990, 2000 and 2010, spatial resolution of 1 km) come from the Chinese Academy of Sciences Resource and Environment Data Center. According to Liu Jiyuan's China Land Use Classification System (Jiyuan Liu 2018), the classification was carried out based on the research content and the actual conditions in the source region of the Yellow River (Table 1).

The climate data is from the China Meteorological Science Data Sharing Service (http://cdc.cma.gov.cn). Digital elevation model (DEM) data originated from the Resource and Environment Data Center of the Chinese Academy of Sciences with a spatial resolution of 1 km. Soil data is the result of the second national census data. The normalized vegetation index (NDVI) was derived from the MODIS synthetic product of the geospatial data cloud (http://www.gscloud.cn/) with a time scale of months and a spatial resolution of 1 km.

Table 1 Land cover types in the source region of Yellow River

Item	Land classification code and name		
Code	1	2	3
Name	Cropland	Forestland	High coverage grassland
Code	4	5	6
Name	Middle coverage grassland	Low coverage grassland	Wetland
Code	7	8	9
Name	Construction land	Shrub	Bare land

2.3 Research Methods

Land cover condition index and transfer matrix. Quantitative analysis of the status of different land cover types in different periods in 1990, 2000 and 2010 was performed, and their transfer routes and ranges were analyzed to characterize the ecosystem of the Yellow River source region Status and direction of change (Quanqin Shao 2010). Based on previous research methods, the study determined the four types of ecosystems, including forest land, high-coverage grassland, wetland and shrubland, to calculate the land cover condition index:

$$Z = \left(\sum_{i}^{n} C_i / A \right) \times 100\%$$

In the formula: C_i represents the area of a covering type; A denotes the total area of the study area.

Water supply. InVEST model was jointly developed by Stanford University, University of Minnesota, TNC and WWF to provide a comprehensive evaluation model for ecosystem services that can be used to quantify multiple ecosystem services (Heather Tallis 2015). The evapotranspiration part is based on the approximation algorithm proposed by Baopu Fu (1981) and Yongqiang Zhang (2004) based on the Budyko curve (Yifeng Li 2013). The specific algorithm is as follows:

$$Y_{xj} = (1 - AET_{xj}/P_x) \times P_x$$

$$AET_{xj}/P_x = (1 + W_x + R_{xj})/\left[1 + W_x + (1/R_{xj})\right]$$

$$W_x = Z \times (AWC_x/P_x)$$

$$R_{xj} = (k_{xj} \times ET_o)/P_x$$

where Y_{xj} is the annual water supply on cell x in landscape type j; AET_{xj}/P_x is the ratio of actual evapotranspiration to precipitation. The Zhang coefficient, R_{xj} is the Budyko Drying Index on cell X in the landscape type, defined as the ratio of potential evapotranspiration to precipitation; W_x is the ratio of annual water demand and precipitation of vegetation; Z is a constant, typically 5.

CA-Markov model and prediction method. The advantages of the CA-Markov model combine the time dimension analysis of the Markov model and the advantages of the CA model in spatial dimension analysis. The specific forecasting process is as follows:

(1) Using year 2000 as the starting point of the forecast, the data of land use distribution in 2000 is the initial state, and the area of transition between land use types in 1990–2000 is used as the element of the Markov state transition probability matrix. (2) Establishment of Suitability Atlas: Applying MCE to integrate different criteria, obtain the suitability maps of different land types, merge them into a suitable atlas, and participate in the prediction of land use changes. (3) Parameter setting: This paper uses year 2000 as the starting point of forecasting time and sets 5×5 cell filters to predict the spatial distribution of land use in 2010. When the prediction accuracy is better, with 2010 as the starting year, the spatial distribution of land use in 2020 is forecasted.

3 Results and Analysis

3.1 Analysis of Land Cover Structure in the Study Area

The type of land cover in the source region of the Yellow River is dominated by grassland, and the area of high, medium and low coverage grassland is larger, accounting for more than half of the total area of the study area. From 1990 to 2010, the area of forest land, medium coverage grassland, low coverage grassland and shrubland showed a decreasing trend. The forest land area decreased from 1263 km^2 in 1990 to 1236 km^2 in 2000. The area of the middle coverage grassland continued to decrease in 2010, but the rate of reduction slowed compared to that of 1990–2000. The area of low coverage grassland in 1990 was 29,754 km^2. By the year 2000, it had decreased by 345 km^2, accounting for a 0.28% reduction. By 2010, the area of low coverage grassland had decreased by another 200 km^2. From 1990 to 2000, the shrub area decreased by 73 km^2, accounting for a 0.75% decline. In 2010, compared with 2000, it only decreased by 12 km^2, accounting for 0.12% decrease. In 1990, the area of high coverage grassland in the source region of the Yellow River accounted for 14.55% of total land area. In 2000, the proportion of the area increased slightly, accounting for 17.59%, and by 2010, the area decreased by 390 km^2, a decrease of 1.81%. From 1990 to 2010, the area of cropland, wetland, and bare land increased. The area of cropland increased by 53 km^2, an increase of 11.60%; Compared with 1990, the wetland area increased by 330 km^2 in 2000 compared with that in 1990, which was

Table 2 Land cover condition of 1990–2010 in the source region of Yellow River

Code	1990		2000		2010	
	Area (km^2)	Proportion	Area (km^2)	Proportion	Area (km^2)	Proportion
1	457	0.37	463	0.38	510	0.41
2	1263	1.03	1236	1.01	1231	1
3	17,869	14.55	21,605	17.59	21,215	17.27
4	40,939	33.34	37,300	30.37	37,203	30.29
5	29,754	24.23	29,409	23.95	29,209	23.78
6	8120	6.61	8450	6.88	8502	6.92
7	9774	7.96	9701	7.9	9689	7.89
S	68	0.06	66	0.05	85	0.07
9	14,564	11.86	14,575	11.87	15,169	12.35

4.70% in 2010; from 1990 to 2010, the bare land increased first and then decreased; The area of cropland and construction land in the study area is the least. From 1990 to 2010, it showed a trend of decreasing first and then increasing (see Table 2).

3.2 The Spatial and Temporal Differences in the Change of Water Supply

The InVEST water supply model was used to assess the different water supply levels for the three phases of the study area in 1990, 2000, and 2010 (see Fig. 2). From the three different water supply spatial distribution maps, it can be seen that the ecological water supply in the study area is declining from the southeast to the northwest.

The high value areas for water supply in 1990 were mainly distributed in Ruoergai, Aba, Maqu, and the southeastern parts of Jiuji County in the southeastern part of the study area. Low water supply areas were located in the northern part of Qumalai and Xinghai County in the northwestern part of the study area. In 2000, the high value areas for water supply in the study area expanded slightly compared with 1990, mainly in the southern part of the study area, in the southern part of the Dagi County, and in the southern part of the Jiuji, Maqu, Aba, and Hongyuan counties. It has also increased in the northwestern part of Qumalai and Maduo County, northeast of Xinghai County and northwest of Tongde County. By 2010, the water supply function high value areas expanded to the middle of the source areas, but the main distribution areas were still in the southern part of the study area, including the Aba, Hongyuan, and Jiuji counties, and the low water supply area. In the study area, northeast of Qumalai, Maduo, Xinghai, and northwest of Zoige County. The average water supply of the Yellow River source areas in 1990, 2000, and 2010 was estimated at 126.78, 186.15, and 228.25 mm, respectively. In 1990, the total water supply in the source area was 1.51×10^7 t, and in 2000 it increased to 2.26×10^7 t. By 2010,

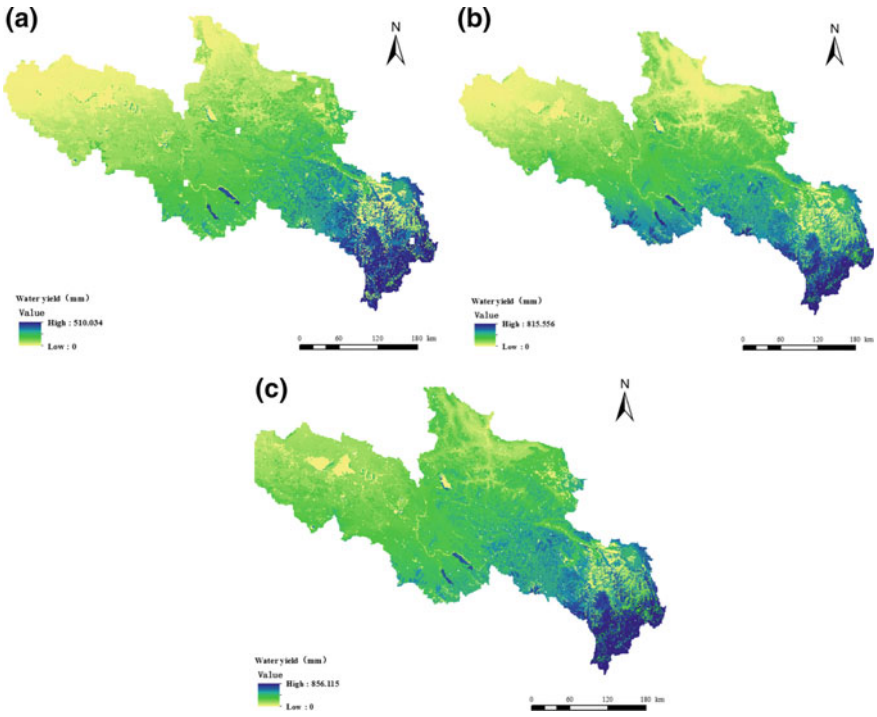

Fig. 2 water supply spatial distribution map of the source region of Yellow River (**a** is water supply map in 1990, **b** is water supply map in 2000, **c** is water supply map in 2010)

the total water supply was 2.7×10^7 t. It can be seen that in the last 20 years, the total water supply in the source area of the Yellow River is growing.

3.3 The Zoning Statistics of Land-Cover Types in the Source Region of the Yellow River Are Compared

By comparing the average water supply of each land type, we found that the water supply of different types of land cover varies in different periods. In 1990, the supply of water for construction land was the highest, which was 250.91 mm. By 2000, the water supply decreased by 47.82 mm. In 2010, the water supply for construction land increased by 87.62 mm. The average water supply of cropland increased from 45.75 mm in 1990 to 89.74 mm in 2000. By 2010, the average water supply increased by 47.26 mm. The average supply of water to the shrublands was also high. It was 223.11 mm in 1990 and increased by 17.16 mm in 2000. In 2010, the water supply increased to 301.69 mm. The supply of water with high coverage grassland in the source area in 1990 was 185.35 mm. In 2000, the water supply increased by 81.23 mm.

In 2010, the water supply increased by 32.28 mm. The average water supply of middle coverage grasslands increased from 133.98 mm in 1990 to 165.68 mm in 2000 and increased by 74.49 mm by 2010; The average water supply of low coverage grassland in 1990 was 107.37 mm, and the increase range from 1990 to 2000 and 2000 to 2010 were 80.19 mm and 23.26 mm, respectively. In 1990, the average supply of water in wetlands was 52.32 mm, which increased by 51.84 mm during 1990–2000. The increase in water supply during the period from 2000 to 2010 slowed to 34.10 mm. The average water supply for bare land continued to increase during the period 1990–2010.

Overall, the average supply of water in high coverage grassland, low coverage grassland, and bare land in the source region of the Yellow River has changed significantly. The average water supply for high-coverage grassland has increased by 113.51 mm, followed by low-coverage grassland (103.46 mm) and bare land (103.36 mm).

By 2010, the average water supply of shrublands was the highest, at 301.69 mm, followed by high-coverage grassland and construction land, at 298.87 and 290.70 mm, respectively; the average water supply of cropland is the lowest, at 93.01 mm.

In the spatial variation of water supply from 1990 to 2000, we see that the main trend of water supply changes is increasing, and from southeast to northwest a trend of increasing to decreasing. The area with reduction more than 152 mm is mainly in the northwest and north. The area where the supply of water changes by more than 160 mm is mainly located in the southeast of the study area. From the spatial change of water supply in 2000–2010, we see that the overall water supply capacity of the Yellow River source area has increased, but the water increasing trend is not significant. The 2000–2010 period compared with 1990–2000 shows a relatively large increase. Areas with an increase in water supply greater than 80 mm are mainly distributed in the northwest, northeast, and southeastern regions of the study area, including Hongyuan, Tongde, Zeku, and Qumalai. Areas where the reduction in water supply exceeds 30 mm are concentrated in Da Ri and other counties in the southwest of the study area (see Fig. 3).

3.4 CA-Markov Model Predicts Coverage Data

The CA-Markov model was used to simulate the land cover of the Yellow River source area in 2010. The simulation results were compared with the 2010 land cover data. After the Kappa coefficient test, the accuracy was 88%, indicating a good quality prediction result. It is basically in line with reality, based on which the land cover data of the study area in 2020 is predicted (see Table 3).

In 2020, the land-use cover structure shows that grassland is still the main cover type of the study area, accounting for 71.31% of the study area. Among them, the middle coverage grassland has the largest area, and the high coverage grassland has

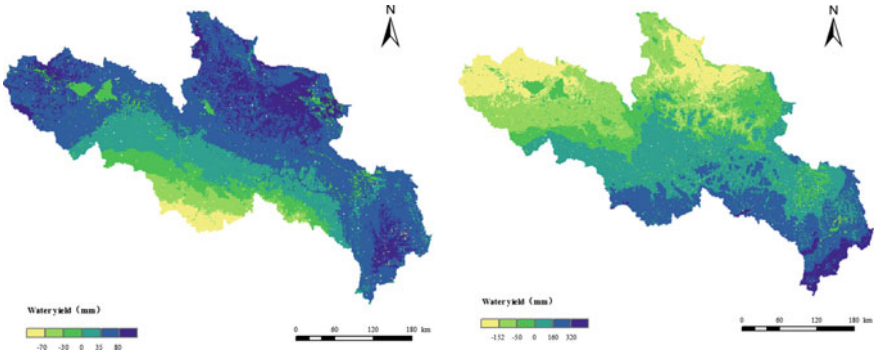

Fig. 3 Spatial distribution of water supply variation in 1990–2000 and 2000–2010

Table 3 Land cover condition of 2020 in the source region of Yellow River

Type	Area (km^2)	Proportion (%)
Cropland	510	0.41
Forestland	1240	1.00
High coverage grassland	21,635	17.61
Middle coverage grassland	26,764	29.90
Low coverage grassland	29,265	23.80
Wetland	8571	6.93
Shrub	9701	7.89
Construction land	71	0.06
Bare land	15,173	12.35

the smallest proportion of the grassland area. The next largest area is bare land, followed by shrublands and wetlands and construction land last.

According to the land cover situation in 2010, we see that by 2020, the coverage of various types of land in the source region of the Yellow River will increase or decrease, but the overall development is in a good direction. Among them, the croplands remain unchanged, and the areas of forest land, high-coverage grassland, low-coverage grassland, wetland and shrublands will have all increased to varying degrees. The area of low-coverage grassland will have increased by 56 km^2, the area of wetland will have increased by 69 km^2, and the area covered by high coverage will increase. The area of grassland will increase by 420 km^2 with an increase of 1.98%; the area of middle coverage grassland will decrease by 438 km^2, and the reduction ratio 1.18%. The area of construction land will decrease slightly, and the area of bare land will increase slightly, but the range of change is not significant.

Table 4 Water supply per unit area of different cover types in different periods in the source region of Yellow River (unit: 10^2 t)

	1990	2000	2010	Average
Cropland	0.44	0.36	0.46	0.42
Forestland	0.85	1.16	1.68	1.23
High coverage grassland	1.80	2.75	3.3	2.62
Middle coverage grassland	1.30	1.67	2.07	1.68
Low coverage grassland	0.10	0.18	2.06	0.78
Wetland	0.10	0.32	0.49	0.30
Shrub	2.20	2.82	3.47	2.83
Construction land	2.47	1.81	3.62	2.63
Bare land	0.76	1.30	1.90	1.33

3.5 Land Cover Change and Water Supply Function

It can be seen that from 1990 to 2010, the amount of water supply per unit area of different types of cover has increased or decreased over time. Combined with the average value of the three phases of water supply, it can be seen that the supply of water per unit area of shrubs is the highest, followed by construction land and high coverage grasslands (see Table 4).

Judging from the impact of land cover change in different counties on water supply, the sources of water supply in the southern Yellow River source areas, such as Hongyuan and Da Ri, are higher than those in Tongde and Zeku counties in the north. Changes in water supply show a trend of decreasing from southeast to northwest, gradually increasing and decreasing the water supply of each county in different periods.

From 1990 to 2000, the supply of water in Tongde, Zoige, Qumalai and other counties has decreased, indicating that the water supply function has declined. Combined with changes in land cover, it can be seen that the grassland area in Tongde County increased by 19 km^2, and the wetland area increased by 4 km^2. Water supply in the counties of Aba, Hongyuan, Maqu, Maduo, and Dayis increased significantly, and forest land area in Aba County decreased. The grassland area has decreased by 15 km^2, and the bare land area has increased by 8 km^2. Maduo County Forestland decreased by 8 km^2, shrubland area decreased by 10 km^2, and high and low coverage grassland area decreased, but middle coverage grassland area increased. Bare land area is relatively reduced, resulting in a small increase in water supply; Dari forestland, low coverage grassland and wetland area reduced 104 km^2.

From 2000 to 2010, the supply of water in Zoige, Malang and Xinghai counties all increased, but the increase was relatively small, and the water supply function

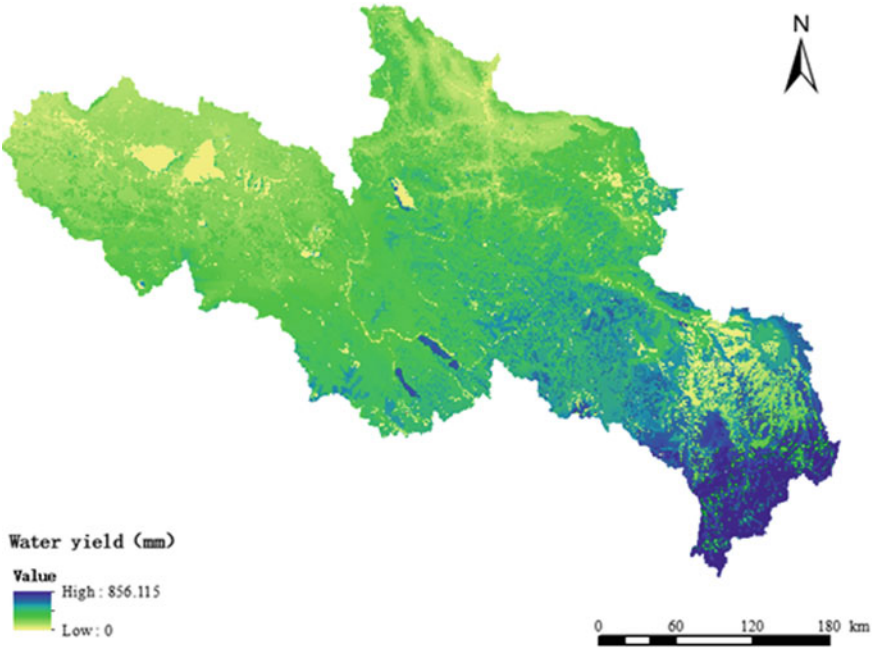

Fig. 4 Spatial distribution of water yield in the source region of the Yellow River in 2020

was improved. The area of high coverage grasslands and wetlands in Zoige County was reduced by 117 and 30 km^2 respectively. The area of forestland and grassland in Hongyuan County has been reduced by 5 and 80 km^2 respectively, and the area of bare land has increased. The area of cropland in Tongde County has decreased by 17 km^2. Due to the large amount of water consumed by cropland, the water supply has increased, and the water supply in Daxian County has increased. With some reductions, combined with changes in land cover, it was found that the area of low and middle coverage grassland increased by 14 km^2, and that of high coverage grassland also increased by 89 km^2.

Using the InVEST model to evaluate the source water supply service in the source area in 2020, it can be seen that the high value area of water supply function is still distributed in the northwest of Aba, Hongyuan, and Maqu counties in the source area, and the low supply value area is distributed in the source in the northwest direction of Qumalai County, the northwest of Maduo County, the junction of eastern Zoige County and Maqu County, etc. (see Fig. 4). The distribution of water supply in the study area in 2020 is forecast to be basically the same as in 2010, but the total water supply will increase slightly from 2010, reaching 2.77×10^7 t, of which the water supply of cropland, high coverage grassland, middle coverage grassland and shrubs will increase, but forestland, low coverage grasslands, wetlands, construction land, and bare land will have reduced water supplies.

4 Conclusion and Discussion

(1) The state of land cover and ecosystems in the source area of the Yellow River from 1990 to 2010 experienced first a period of degradation, and then a period of recovery. During the period 1990–2000, the area of forestland, high coverage grassland, middle coverage grassland, and low coverage grassland showed a decreasing trend and the changes were more severe. In the later period of recovery, the wetland area in the study area increased. The area reduction rate of the remaining cover types is greatly reduced. Based on the changes in land cover during the three phases, the CA-Markov model was used to simulate the land cover of the Yellow River source region in 2020. It was found that the forest land, high coverage grassland, low coverage grassland, wetland, bare land and shrublands of the study area is on the rise, the area of construction land is reduced, and the area of cropland remains unchanged.

(2) The areas with high water supply functions in 1990, 2000, and 2010 were located in the southeastern cities of Zoige and Hongyuan, while the low-value areas were located in the northwestern Qumalai, Chengdo, and Maduo counties, but the overall supply function of water resources of the study area in 1990 was low. By the year 2000, the area of low-value areas expanded, mainly in the northwestern and northern regions of the study area, including Xinghai and Tongde. In 2010, the area of high water supply was expanded to the northwestern direction of the study area, such as Malang, and the overall water supply function was greatly increased.

(3) From 1990 to 2010, the water source supply function in the source region of the Yellow River reflected a decrease from the southeast to the northwest, and the decrease in the spatial variation of water supply from 1990 to 2000 was mainly distributed in the northwest and north of the study area; The increased area is mainly located in the southeast of the study area. The scope of increase in water supply from 2000 to 2010 is slightly different from that of 1990 to 2000. The scope is mainly concentrated in Tongde, Zeku and other counties in the northwest, northeast, and southeast corners of the study area, while the water supply is reduced. It is concentrated in Da Ri, etc., in the southwest of the study area.

(4) The water supply capacity per unit area under different cover types in the source area of the Yellow River was in this order, from highest to lowest: shrublands > construction land > high coverage grassland > middle coverage grassland > bare land > forestland > low coverage grassland > cropland > wetland. The construction land area supply of water per unit area is very large because most of them have not been effectively utilized and have become runoff or underground pipeline networks. At the same time, forestland has great water evapotranspiration. Forestland per unit area can lose more water than cropland and low coverage grassland. Therefore, the supply of water per unit area of forest land is small.

(5) The high value-added water supply service areas in 2020 are still distributed in the northwestern parts of Aba, Hongyuan, and Maqu counties in the source area, while Qumalai County and Maduo County, which provide low-function areas, are distributed in the northwest direction of the source area. In the northwestern part of the county, at the junction of Ruoergai County and Maqu County in the east, the supply of water sources will have increased, and the water supply function slightly enhanced, showing a state of high water supply in the southeast and in the northwest. The supply of water to cropland, high coverage grassland, middle coverage grassland and shrublands will increase, while the supply of water to forestland, low coverage grassland, wetland, construction land, and bare land will decrease.
(6) Increased supply of water to cropland and grasslands is beneficial for food production and ecosystem productivity. Reduced supply of water to construction land and bare land and wetlands is also good news, since it will result in reduced erosion and run-off. Future land use planning should consider how to increase water supply to forest land and low coverage grasslands, to improve the health of these ecosystems.

References

Aihong Gai F, Guozhang Cen S (2015) Evaluate on land use/cover change and land ecological security in Qingyang city, 1st edn. China Meteorological Press, Beijing

Baopu F (1981) On the calculation of evaporation from soil. Acta Meteorol Sinica 39(2):226–236

Gengxu Wang F (2009) Hydrologic effect of ecosystem responses to climatic change in the source regions of Yangtze River and Yellow River. Adv Clim Change Res 5(4):202–208

Jiyuan Liu F (2018) Spatio-temporal patterns and characteristics of land-use change in China during 2010–2015. Acta Geogr Sin 73(5):789–802

Quanqin Shao F (2010) The characteristics of land cover and macroscopical ecology changes in the source region of three rivers on Qinghai. Geogr Res 29(8):1439–1451

Shimei Li F (2010) Flow process of water conservation service of forest ecosystem. J Nat Resour 25(4):585–593

Tallis H (2015) Mitigation for one & all: an integrated framework for mitigation of development impacts on biodiversity and ecosystem services. Environ Impact Assess Rev 55(2015):21–34

Tao Pan F (2013) Spatiotemporal variation of water source supply service in Three Rivers Source Area of China based on InVEST model. Chin J Appl Ecol 24(1):183–189

Yifeng Li F (2013) Effects of land use change on ecosystem services, a case study in Miyun reservoir watershed. Acta Ecol Sin 33(3):0726–0736

Ying Wang F (2013) Eco-environment changes and countermeasures in the Yellow River source region. J Arid Meteorol 31(3):550–557

Zhang Y (2004) Water and heat transfer mechanics in the soil-plant-atmosphere continuum and regional evapotranspiration mode. J Grad Sch Chin Acad Sci 21(4):562–567

Zhiming Li F (2017) Change and prediction of the land use in Harbin city based on CA-Markov model. Chin J Agric Resour Reg Plann 38(12):41–48

River Structure and Spatial Pattern Along Jiulongjiang Watershed

Rong Sun, Yarong Zheng and Fuguo Chen

Abstract The 1923 km long Jiulongjiang River is located at the southwest of Fujian Province, China. It is one of the typical climate zone representative of humid subtropical monsoon in the similar latitude. Based on Geographic Information System and the spatial relationships, natural and social environments in Jiulongjiang river watershed, the river structure and the spatial pattern of Jiulongjiang River were studied. The results showed: (1) A seven hierarchy established in Jiulongjiang watershed, with first order rivers contributing up to 50% of the watershed. (2) River orders and lengths changed among ecological function regions. (3) Altitude change range, average elevation, slope change range and average slope decreased with steam orders. (4) Along river orders, the population density and gross domestic products changed, which was the higher river orders and the bigger population densities and gross domestic products. Combining parameters, such as height, slope, population, gross domestic products and hierarchy of river with field investigation, results showed that the river nets exhibited typical spatial differential features, which was related to the natural factors and affected by the social factors. This meant that Hierarchical Management Strategy should be applied to river management.

Keywords Jiulongjiang river · Natural factors · River hierarchical · Social factors · Spatial pattern

1 Introduction

The river eco-system is the key factor for basin study and management. Vannote et al. (1980) found that rivers from the catchment area in their source, and then converge into bigger current, creating a unique and integral continuum, which is the

R. Sun · Y. Zheng
College of Chemical Engineering, Huaqiao University, Xiamen 361021, Fujian, China

F. Chen (✉)
SPIC Yuanda Environmental Protection Catalyst Co., Ltd., Chongqing 401336, Nan'an, China
e-mail: 61228976@qq.com

R. Sun and L. Fei (eds.), *Sustainable Development of Water and Environment*, Environmental Science and Engineering,
https://doi.org/10.1007/978-3-030-16729-5_21

River Continuum Concept. Its landscape, which is formed by the drainage network, structurally, runs through the whole mountainous region. The network consists of rivers that can bring water, organic matters and organisms along the rivers (Yuan et al. 2007). The river system had been regarded as an integrated system and had been studied on internationally science from the 1940s. The recent studies are focused on the eco-process, anthropogenic disturbance and its mechanism in the basin (Sun et al. 2014, 2017). Horton and Strahler (data) put forward the Horton's law of the river system, which was based on their observation and experiment. It is especially useful that we use the Hierarchical System of Rivers, which was established by Strahler as an indicator for rivers, reaches, basins and small basins (Merot et al. 2009). After the 1990s, with the application of GIS (Geographic Information System), the dimension and accuracy within the analysis of the basins' structure gains further progresses (Puente and Castillo 1996; Grave and Davy 1997). Wang et al. (2002) analyzed the dimensional characteristics of the Qinhuai River with GIS, Zhang et al. (2002) made model analysis on the catchment area in the mountainous region of northeastern China, Yuan et al. (2007) analyzed the influences of urbanization on the structure of rivers throughout analyzing the hydrographic net of Shanghai. Since rivers have their ways of being affected by their regional factors like geological and climatic parameters, different river structures do affect the converging and flooding procedure (Rui 2004), as well as the hydrographic net and water quality (Han et al. 2004). Thus, it is necessary enhancing the study on the structures of different basins aiming at a more efficient way of protecting and exploiting the river resources (Dong 2009). With the increasing environmental problems and complexities of rivers, after the 20th century, both China and others regions are attaching importance to the river management based on the opinion of Basins. In 1933, the United States issued the Tennessee River Basin Management Bureau law. In 1984, France issued the Water Law. England established the Thames Water Authority in 1974, and here in China, Taihu river basin management regulations was proclaimed in 2011, which made it clear that the domestic river had gradually transited from the water to a more integrated grade-basin. Jiulongjiang basin locates in the southeastern part of Fujian province, processing an integrated small basin geographic structure, is one of the places that well preserve its natural vegetation with subtropical monsoon climate compared to those on the same latitude. The analysis on river hierarchy system and spatial patterns of the rivers provides the basic materials for discussing the interrelationship and interaction between rivers and the integrated basin management, which has great significance maintaining the sustainable development of the river ecosystem.

2 Methods

2.1 Study Area

Jiulongjiang River locates at southeastern of Fujian province, the second largest river in the province, which was consisted of the Beixi river sources from Meihuashan mountain and the Xixi river sources from Banliao mountain. The length of the northern tributary is 274 km with an average gradient of 2.4% and an average annual discharge of 281.4 m^3/s and that of the Xixi river is 166 km with an average gradient of 3.1% and an average annual discharge of 117 m^3/s. The middle mountain, low mountain, high hills, plain and hill area in the basin distributes in order, the ridge runs towards both northeast (NE) and north-north-east (NNE) with mountains and valleys; the basin covers the southern subtropics and the mid-subtropics, undergoing a subtropical marine monsoon climate with an average annual temperature ranges from 19.9 to 21.1 °C, and an average annual precipitation of 1400–1800 mm (Deng et al. 2013). The vegetation composition in the basin was complicated, and showed an obvious feature of transitivity. The natural vegetation mainly consisted of subtropical evergreen forests, mixed coniferous broad leaved forests and coniferous forests, and, so far, being occupied by artificial secondary forests and artificial fruit woods (Hong et al. 2008). In the end of 2005, the main districts in the basin: Longyan, Zhangzhou, and Xiamen have a total population of 8.9742 million and a regional Gross domestic products (GDP) growth of 202.074 billion RMB. The ratios of the population and GDP are 25.93 and 30.76% compared to the total population and GDP of Fujian province.

2.2 Data Sources

The 1:10,000 geological maps were used as the basic layer, the DEM (Digital Elevation Model) and slope were created with ARC/INFO. The Normalized Difference Vegetation Index (NDVI) was projected utilizing the CBERS (China Brazil Earth Resource Satellite) data of July, 2008. The hierarchical drainage net was divided into different buffering zones accordingly in order to study different covering situations, the principles of setting up the buffering zones were 100 meter's area on both side of the grade 1 stream, 200 meter's area on both side of the grade 2 stream, the rest can be done in the same way … 700 meter's area for the grade 7 stream. The NDVI of each stream was extracted afterwards generating the covering situations of every river from grade 1 to grade 7. The geological and hydrographic data got from the Fujian natural geographical atlas.

2.3 Natural Environment and Social Environmental Factor

The ecological function zones of Jiulongjiang basin was differentiated based on the ecological function zoning of Fujian province in the book Fujian natural geographical atlas (Atlas of Fujian, China 2009). The natural environmental factors were represented by the latitude, gradient; the social environmental factors were represented by the population density and the GDP in the basin. Based on the geomorphic characteristics couple with the distribution of the forest vegetation and human disturbance, the basin was divided into: plain terrain and areas below (≤250 m), low hilly terrain (250 ~ ≤500 m), high hilly terrain (500 ~ ≤750 m), low mountain landform (750 ~ ≤1000 m), mid-mountain landform (>1000 m) based on the elevation, and are divided into gentle slope (≤5°), slope (5 ~ ≤15°), abrupt slope (15 ~ ≤25°), steep slope (15 ~ ≤35°) and risky slope (>35°) based on gradient. The population density and GDP density were differentiated under the spatialized population data of a 1 km^2 grid in 2003 and GDP data under the ARC/INFO, the categories are:

The population densities were classified into that ≤250 people/km^2, 250 ~ ≤500 people/km^2, 500 ~ ≤750 people/km^2, 750 ~ ≤1000 people/km^2, >1000 people/km^2, and GDP were those ≤2.5×10^6 RMB/km^2, 2.5×10^6 ~ ≤5.0×10^6 RMB/km^2, 5.0×10^6 ~ ≤7.5×10^6 RMB/km^2, 7.5×10^6 ~ ≤1.0×10^7 RMB/km^2 和 > 10^7 RMB/km^2, then extract the river distributions in different grades of elevations, gradients, population densities and GDP densities from the ArcGIS system.

3 Results

3.1 Spatial Pattern of the Jiulongjiang River

On the basis of the landform, gradient, exposure and their relationship and the characteristics of current couple with the ARC/INFO hydrographic analytical module, we can get the hierarchy system of the Jiulongjiang basin. There are 7 hierarchies in the basin in which the grade 1 stream took over 50% of both the rivers' quantities and the total length, reaching a drainage density of 0.259 km/km^2. With the increasing of stream grade, the quantities and lengths of rivers showed a trend of decreasing, the grade 7 stream forms from the converging of the northern stream and the western stream at the estuary. Because of the existence of estuarine islands, the river was divided into the northern port, middle port and the southern port where the southern stream went into the sea (Table 1).

Table 1 River properties along river orders in Jiulongjiang river

River orders	Number	Percentage (%)	Length (km)	Density (km km^{-2})	Bifurcation ratio
First	2181	75.00	3846	0.259	3.97
Second	550	19.50	1854	0.125	3.97
Third	139	4.10	1047	0.070	4.21
Fourth	33	1.00	556	0.037	4.71
Fifth	7	0.30	184	0.012	3.50
Sixth	2	0.13	157	0.010	2.00
Seventh	–	0.07	22	0.001	–
Total	2913	100.00	7666	0.515	–

3.2 Regional Differentiation of the Distribution of the Rivers

The quantities and length of rivers of different grades were calculated by extracting the conformation of different ecological function zones based on the ecological function zones of the Jiulongjiang basin (Table 2). We can conclude from chart 2 that the differentiation of quantities and length of rivers in its ecological function zone varies a lot. What took the first and second place in both quantity and length were tea and fruits producing areas and soil conserving areas, mountain land water conserving and forestry ecological function zones. The last two of them are mountain land natural ecological recovering and soil erosion controlling zones, culture heritage protecting and eco-touring zone.

3.3 Spatial Pattern of Rivers Under the Distribution of Natural Environmental Factors

Elevation. The distribution of river changed with elevation (Table 3; Fig. 1a). Both the river quantities and the length of rivers were lower than that in other areas in the two areas higher than 750 m. Take an overlook at the quantities, areas between 250 and 500 m had the largest, and at altitude-grade, between 500 and 750 m, occupied the longest rivers.

Gradient. The distribution of rivers with 5 gradient grades were listed in Table 4 (Fig. 1b). It was showed that areas that contains the largest number of rivers are those with a gradient less than 15° while the number of rivers in those areas with a gradient greater than 35° are less than that of the other ones.

Table 2 Spatial pattern of river structure in different ecological functional in Jiulongjiang river

Ecological function area	First		Second		Third		Fourth	
	Number	Length	Number	Length	Number	Length	Number	Length
Fruit tea production and soil conservation ecological area	670	1014.8	164	496.2	49	231.3	18	223.3
Urban ecological function area	165	291.2	48	132.5	13	77.8	2	44.3
Valley basin of agricultural ecological function area	81	144.1	20	101.8	4	28.1	1	31.9
Water conservation and biodiversity protection function area	265	491.0	74	270.0	25	156.0	5	71.4
Basin valley upland agriculture and soil conservation ecological function area	261	402.3	69	163.2	13	125.0	6	11.0
Mountain water conservation and forestry ecological function area	582	1078.3	137	511.8	37	323.4	9	13.3
Maintenance of water conservation and restoration of the natural ecological mountain ecological function areas	77	98.4	28	43.8	7	22.2		
Restoration and maintenance of natural ecological mountain and control of soil erosion ecological function area	39	37.3	11	9.6	1	0.5		
Mountain in highland agriculture	65	86.1	20	66.0	8	38.4	1	11.4
Protection of cultural heritage and tourism ecological function area	38	64.1	4	12.6	1	27.1	1	2.9
Drinking water catchment protected ecological function area	55	102.3	23	54.9	6	22.2	1	7.1
Center city ecological function area	61	77.3	31	57.4	16	33.5	4	13.3

(continued)

Table 2 (continued)

Ecological function area	Fifth		Sixth		Seventh		Total number	Total length
	Number	Length	Number	Length	Number	Length		
Fruit tea production and soil conservation ecological area	3	76.1	1	77.7			**905**	**2119.4**
Urban ecological function area			1	25.9	3	64.0	232	635.7
Valley basin of agricultural ecological function area	3	49.8	1	25.9			110	381.6
Water conservation and biodiversity protection function area	3	34.0					**372**	**1022.4**
Basin valley upland agriculture and soil conservation ecological function area							349	701.5
Mountain water conservation and forestry ecological function area	3	19.5	1	47.0			**769**	**1993.3**
Maintenance of water conservation and restoration of the natural ecological mountain ecological function areas							112	164.4
Restoration and maintenance of natural ecological mountain and control of soil erosion ecological function area							51	47.4
Mountain in highland agriculture							94	201.9
Protection of cultural heritage and tourism ecological function area							44	106.7
Drinking water catchment protected ecological function area							85	186.5
Center city ecological function area	1	8.4	2	19.4			115	209.3

Note The river length unit: km

Table 3 Spatial pattern of river structure in different elevational grade in Jiulongjiang river

Altitude (m)	First		Second		Third		Fourth		Fifth		Sixth		Seventh		Total number	Total length
	Number	Length	Number	Length	Number	Length	Number	Length	Number	Length	Number	Length	Number	Length		
≤250	716	852.4	213	399.1	67	227.5	22	151.4	6	76.8	2	196.0	3	64.0	**1029**	**1967.2**
250 ~ ≤500	968	917.7	273	545.9	69	269.4	18	286.6	4	106.9					**1332**	**2126.5**
500 ~ ≤750	868	1039.1	186	635.8	43	401.9	4	117.8							**1101**	**2194.6**
750 ~ ≤1000	442	790.8	68	237.1	10	148.1									520	1176
>1000	82	228.2	5	35.9											87	264.1

Note The river length unit: km

Table 4 Spatial pattern of river structure in different slope grade in Jiulongjiang river

Slope	First		Second		Third		Fourth		Fifth		Sixth		Seventh		Total number	Total length
	Number	Length	Number	Length	Number	Length	Number	Length	Number	Length	Number	Length	Number	Length		
≤5°	2146	986.5	550	654.5	139	419.2	33	299.8	7	130.6	2	152.9	3	62.1	**2880**	**2705.6**
5 ~ ≤15°	1876	1324.0	450	557.7	117	272.2	27	115.5	6	27.0	2	25.2	3	2.0	**2481**	**2323.6**
15 ~ ≤25°	934	1051.6	216	430.0	61	231.8	18	90.4	4	14.3	1	12.7			1234	1830.8
25 ~ ≤35°	232	390.5	45	166.8	20	105.2	10	38.7	2	7.0	1	5.6			310	713.8
>35°	37	70.4	5	32.76	1	18.5	3	11.2	1	4.8					47	137.66

Note The river length unit: km

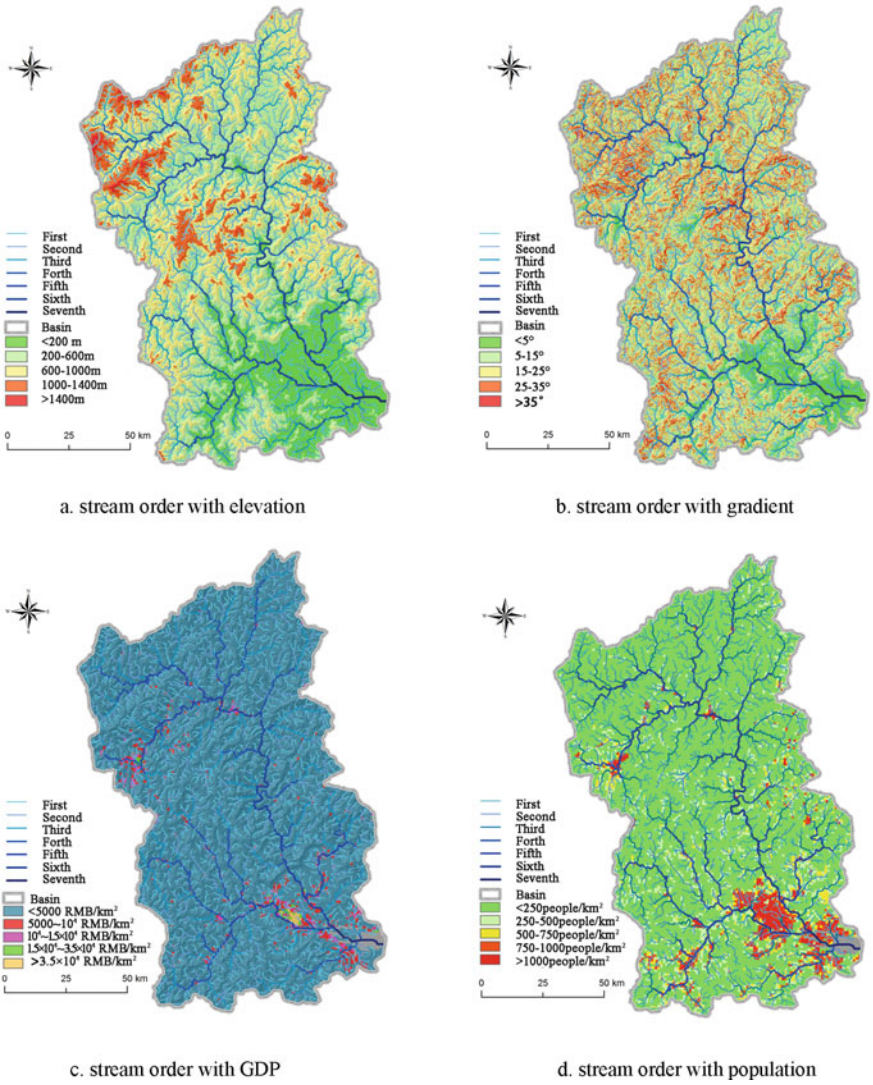

Fig. 1 The relationship of stream orders with natural and social factors

3.4 Spatial Pattern of Rivers Under the Distribution of Social Environmental Factors

Population Density. The population density hierarchical areas were shown in Table 5 which indicated that rivers in areas with a population less than 250 people/km^2 and a population greater than 1000 people/km^2 were longer than that in the other 3 zones

(Fig. 1c). Without regard to areas with a population greater than 1000 people/km^2, there was a downturn in both quantities and length of rivers in different grades. Combining site investigation, it is clear that the grade-7-streams was the tidal watercourse of the basin science it was divided by estuary islands, its three tributaries ran into the sea. The river, in the buffering zones studied, belonged to the ocean area and the beach area and its population was not counted.

GDP. The GDP hierarchical zones and distribution in the basin are shown in Table 6 from which we can found that the quantities and length of rivers in different GDP hierarchical zones varies similarly as its changes between population densities, which is a trend of decreasing (Fig. 1d). Areas with the lowest GDP grade have the largest number of rivers and the longest rivers, which outdistance that of the other four grade. Areas with a GDP greater than 10^7 RMB/km^2 show an abnormal trend in both quantities and length. Similar to the census, the crumple zone of the seventh-order is mainly consisted of ocean and beach and its GDP is not counted.

4 Discussions

Jiulongjiang basin locates in the southern part of Fujian province, and is a representative of mountainous river with subtropical moist climate. The basin, suffered from the intense influence caused by the river cascade hydropower development (Zhang et al. 2002), it shows a trend of variation tendency related to the natural environment factor (Tables 2 and 3) and the social environmental factors (Tables 4 and 5) like the population and the GDP. Vannote et al. (1980) pointed out that river is a continuous integration, and they emphasis that there is a unification between the structure and function of the ecosystem and the basin where it is located. The unification between the upriver and the downriver not only means the geological connection but also the connection of the structure, function and ecological process between the two ecosystems. Because of the impact led by the physical, chemical and biological factors, rivers show a continuous graded distribution which is more obvious in the lower grade rivers. These rivers are merely influenced by human behaviors, thus, easier for keeping their natural succession.

Zhang (1995) pointed out that the differences between the size of rivers and the size of basins can reflect the differences of its dynamic property (especially its fluviation). Therefore, various basin geomorphic elements such as: gradient, width, incise depth and the maximum altitude intercept also have obvious distinctions. Asa et al. (2007) discovered those rivers of different grades and their natural conditions like: topographies, geologies, soil, precipitation and human impacts have extinctions and show a regular distributional pattern. According to this research, the Jiulongjiang basin is mainly consisted of lower grade rivers which have the largest number of rivers and the longest rivers in all the grades (Table 1). Its origin where the geological lithology was formed form cretaceous intrusive rock that has little water permeability and strong erosion resistance, while the geological lithology in its downriver was mainly formed from sedimentary rock and sandstone, which led to the distributional

Table 5 Spatial pattern of river structure of different population density grade in Jiulongjiang river

Population density (people/km^2)	First		Second		Third		Fourth		Fifth		Sixth		Seventh		Total number	Total length
	Number	Length	Number	Length	Number	Length	Number	Length	Number	Number	Length	Number	Length	Number		
≤250	1840	2747.1	446	1188.6	122	57.4	29	40.8	6	93.2	2	13.5	2	11.4	**2447**	**4152**
250 ~ ≤500	768	530.6	278	314.7	87	45.2	27	42.6	7	37.9	2	16.2	1	1.9	1170	989.1
500 ~ ≤750	373	251.1	146	156.1	43	81.5	18	49.9	4	31.5	2	13.1	1	1.2	587	584.4
750 ~ ≤1000	144	107.8	72	71.4	22	159.6	10	97.7	3	5.3	2	35.3	3	2.5	256	479.6
>1000	164	162.9	48	102.7	24	701.8	11	321.8	4	15.7	2	116.8	3	4.4	256	1426.1

Note The river length unit: km

Table 6 Spatial pattern of river structure under different GDP grade in Jiulongjiang river

GDP (YUAN/km^2)	First		Second		Third		Fourth		Fifth		Sixth		Seventh		Total number	Total length
	Number	Length	Number	Length	Number	Length	Number	Length	Number	Length	Number	Length	Number	Length		
$\leq 2.5 \times 10^6$	1994	3147.6	491	1424.6	127	783.7	29	379.4	6	91.3	2	105.0	3	21.5	**2652**	**5953.1**
$2.5 \times 10^6 \sim \leq 5.0 \times 10^6$	191	115.6	89	70.3	41	46.3	16	30.4	4	9.0	2	8.2			343	279.8
$5.0 \times 10^6 \sim \leq 7.5 \times 10^6$	184	101.0	73	49.0	35	39.3	12	22.9	6	16.6	2	6.7			312	235.5
$7.5 \times 10^6 \sim \leq 1.0 \times 10^7$	117	65.4	70	49.7	31	26.7	14	19.5	4	9.0	2	7.4			238	177.7
$>10^7$	414	369.1	190	240.0	67	150.0	21	101.2	2	57.9	2	67.0	2	4.3	698	989.5

Note The river length unit: km

distinctions between different regions (Li 2005). Khomo and Rogers (2009) also discovered the unification between the hierarchy and the landform of rivers. With the change of the hierarchy, the landform on both sides of the rivers changes, presenting an according regularity. This research also indicates that the hierarchical distribution of rivers is closely related to the latitude and gradient (Tables 3 and 4). Strahler found that the divergence rate of rivers with little architectonical impact is generally 3.0–3.5 (Li 2005). It is generally acknowledged that once the development of the main river is weaker than that of its tributaries, there must be an indication that the river suffered from the impact of strong crustal movement and tectonic process (Armitage and Pardo 1995). This study shows that there were little tectonic impact on the grade 3 and grade 5 rivers while there was obvious tectonic movement in the grade 2 and grade 6 rivers. According to the materials of geological surveys, these areas mainly consist of coal bearing psepholite and sandstone. On the other hand, the river divergence rates here are generally lower than the average rate, representing a gentle slope zone. It is shown by Khomo and Rogers' study that the drainage net density is lower in areas with little water permeability, strong erosion resistance and high vegetation coverage rate with moist climate than that of other areas (Khomo and Rogers 2009). The spatial distribution of Jiulongjiang basin is influenced by the latitude, gradient, geological lithology, land cover, et al., like the ordinary river basins (Chen et al. 1999).

We can see from the distribution of rivers of different grades in various ecological function zones that the grade 1 rivers cover all the functional zones in the basin, grade 6 rivers cover 5 kinds of ecological zones and only one is covered by the grade 7 rivers. The number of functional zone covered by rivers decreases with the increase of the hierarchy of rivers, which is partly because that the number of rivers in high grade zones is lower than that in the low grade zones, on the other hand, the landform where high grade river locates in is always plain and are on a low latitude coupling with the limitation of the high population density, thus simplified its ecological functional zones. The ecological functional zone covered by grade 1 to grade 7 rivers varies a lot, some of the functional zones, for instance, mountainous natural ecosystem recovering and water reserving function zones, mountainous natural ecosystem recovering and water protecting and soil erosion controlling function zones, highland agricultural, culture heritage protecting and eco-touring function zones and drinking water catchment area protecting function zones in which no high grade rivers locate and are mainly taken by the low grade rivers. We can get the same conclusion by comparing the length of rivers of different hierarchies. The conclusion is that almost every high grade river locates where people gathered or with prosperity of economy and both low latitude and gentle slopes which is easier for the formation of high grade rivers, or in areas in the valleys with gentle slopes.

It is found in this research that the total number and length of rivers decreases with the increase of population density, however, areas with a population greater than 1000 people/km^2 have an adverse trend which is due to the increase in its hierarchy, the decrease in latitude and gradient and the river's turning to a gentler, wider and more suitable state for human. Since humankind first came into the world, rivers are closely linked to humanity and the development of human society (Chen and

Jia 2017). In areas with a population density between 750 and 1000 people/km^2, and areas with a population density greater than 1000 people/km^2, grade 3, 4, 5 and 6 rivers the length of rivers are longer than that of the low grade ones. With the increase of the rivers' hierarchy, the population influenced by them increases, so does the human impact. In areas with a low population density, locates a large numbers of low grade rivers whose number and length are longer than that of rivers in other hierarchies, which is due to its high latitude, steep slope and a severe living condition. However, in areas with a population density greater than 1000 people/km^2, locates cities and towns (Shao and Zhu 2007). When it comes to the development of cities, it has been taken granted that cities depends on rivers and humankind has a trend of living near the rivers. The site survey indicates that in the high latitude zones, rivers are having a stronger impact of its surroundings where the types of the substrate and the vegetation have great similarities with that on both side of its bank. Thanks to the high latitude and lower human disturbance, rivers keep their natural state. Rivers with lower latitude are wider and maintaining a great flux, and on its bank lays the typical vegetation. These areas have more human disturbance, so does the human impact. The distribution of high population density and GDP are mainly in areas with high grade rivers, which confirms the theory above (Tables 5 and 6). It was found by Zhang et al. that the hierarchy of river is directly related to the gradient, which is the lower the hierarchy is the larger the range of gradient is. Study shows that relationship between the hierarchy of the Jiulongjiang basin and its gradient is similar to the law above (Zhang et al. 2002). With the increase of the river's hierarchy the number of its downriver decreases obviously (Table 1). The currents gather in a minority of watercourses leading to a high flowing mobility which sharpened the erosion and the incision to the watercourse and its banks, making the river cut its way down and widen its surface width, thus, making its downriver tributaries gentle and the gradient to decrease.

Take a look at the three cities related to the Jiulongjiang basin, the population of Fujian province in 2005 is 35,350,000 people in total, the population density is 291.00 people/km^2 while the population of Longyan, Zhangzhou and Xiamen are 51.89, 124.74 and 310.31% of the total population of Fujian province respectively, which indicates that there is a great impact at the high grade areas downriver, bringing a great pressure to the ecological environment, and may become an obstacle that limits the development in the future. Therefore, solving the problem earnestly is need, which is also a great issue with universality when studying the basin ecological environment.

As for the relation between sustainable development and population, people live on extorting their demands from the water resources, that is to say the basin can provide the material basis that is necessary for humankind and can receive the waste produced by human behavior. If the population of a basin is immense and it has great rate of increase, the pollutants released by human behaviors will be increasing continuously. With the development of modern industry and population density increases, large amounts of untreated sewage and industrial wastewater directly into water bodies, leading to water pollution, increased. In the urbanization process of the Jiulongjiang basin, not only does the concentrated treatment of municipal sewage

and the sewage recycling but also the agricultural usage and ecological treatment of the sewage in rural areas should be paid great attention to. Once the problem of reusing the sewage in rural areas solved, it would be a great way for remitting the contradiction of water shortage and reduce the cost of sewage treating process at the same time and is also a good method to reduce the use of fertilizer and to partly solve the pollution caused by fertilizer, achieving many things at one stroke. Also, it is found in this research that in the Jiulongjiang basin, the GDP and population have a trend of converging at high grade rivers. Where there is a high population density and GDP where there locates high grade rivers, which is due to the landform and its fitness for mankind to live on and to develop their industry, also, the human nature of living by waters. On the other hand, both industrial and agricultural development cannot be parted from water. So, the higher the GDP on both sides of the river the higher the GDP will be.

According to Strahler's grading method, low grade River is the origin of higher grade rivers while high grade river is the convergence of lower grade rivers (Yu et al. 2009). The hydrographic and ecological status of high grade river can be influenced by lower grade rivers. The drought and flood downriver are directly related to the damage of the upriver ecosystem of the low grade rivers.

We often spend much money and resources on controlling the downstream, but pay less attention on the upstream of river's management and protection measures, leading to soil and water loss in upper reaches and flooding in lower reaches. The managing method of the Jiulongjiang basin should be Hierarchical Management Strategy in which enhancing the protection of grade 1 and 2 rivers and repairing some of the damaged habitats, taking adequate consideration on the ecological water demand and keeping the connectivity between habitats in the grade 3 and 4 rivers, keeping the ecological health of the rivers downriver and paying more attention to the influence on the rivers' health status caused by non-point source pollution in the grade 5 to grade 7 rivers.

5 Conclusions

This research based on the Jiulongjiang basin analyzed the relationship between the hierarchies of rivers and the latitude, gradient, population and regional GDP. The research indicates that the basin can be divided into 7 grades in which the number of rivers and their lengths in the grade 1 rivers were greater than 50% of that in other rivers of different grades, making up the main drainage net of the basin.

It was also an important part of the ecosystem integrity. Most of the rivers and the longest ones located in both the tea and fruit planting areas, the soil reserving ecological zones and the mountainous water reserving areas. Culture heritage protecting zones contained the least number of rivers while the mountainous ecosystem recovering and protecting areas and the soil erosion controlling areas contain the shortest rivers. As for the distribution with altitude, the higher grade streams located mostly in areas with lower altitude. For the distribution with gradient, the higher grade rivers

located mostly in areas with a lower gradient. With the population density, the distribution of rivers showed a decreasing trend with the increase of population; however, it was adverse in the areas with a population greater than 1000 people/km^2. Similar to the population density, the number of rivers and their length decreased with the increase of GDP; however, in the areas with the largest GDP, the two indexes tend to be repeating.

This study discussed the spatial distribution of river hierarchical, providing an important reference for exploiting the river environment and the river resources. Given the important function the river had to its ecosystem, the next step should be focus on the spatial distribution of river, especially on the relationship between its distribution and factors like: population, GDP and built up areas etc. thus, playing a guiding role in regional economic development and providing feedback mechanism.

Acknowledgements The study is supported by National Natural Science Foundation of China (No. 51509094, 31500394), the Subsidized Project for Cultivating Postgraduates' Innovative Ability in Scientific Research of Huaqiao University.

References

Armitage PD, Pardo I (1995) Impact assessment of regulation at the reach level using macro invertebrate information from mesohabitats. Rivers Res Manag 10(2–4):147–158

Asa B, Nilsson C, Svante H (2007) The potential role of tributaries as seed sources to an impoundment in northern Sweden: a field experiment with seed mimics. River Res Appl 23(10):1049–1057

Atlas of Fujian, China, 2009. Fujian Map Press, Fuzhou

Chen LF, Jia WY (2017) Research of the relationship between the river and core blocks of county-level cities in Shandong province. Geogr Sci Res 6(1):9–19

Chen JQ, Londo HA, Megown RA, Zhang QF, Boelema WJ, Hoefferle AM, LaCroix JJ, Londo AJ, Markovic KA, Olson ML, Owens KE (1999) Stream structure across five mountainous watersheds in the continental United States. Acta Ecol Sin 19(1):30–41

Deng WQ, Sun R, Li XM, Lu D, Yang Q, Lu KY (2013) Flora study of riparian plants on the mountain river banks of the Jiulongjiang river headstream. Plant Sci J 31(5):467–476

Dong ZR (2009) Framework of research on fluvial ecosystem. J Hydraul Eng 40(2):129–137

Grave A, Davy P (1997) Scaling relationships of channel networks at large scales: examples from two large-magnitude watersheds in Brittany, France. Tectonophysics 269(1–2):91–111

Han LX, Zhu Y, Yang JD (2004) Analysis of influence of local variation of water system on water regime and water quality of river networks. Water Resour Prot 20(4):31–41

Hong HS, Cao JL, Cao WZ (2008) Agricultural non-point source contamination mechanism and control technology in Jiulongjiang river watershed. Science Press, Beijing

Khomo L, Rogers KH (2009) Stream order controls geomorphic heterogeneity and plant distribution in a savanna landscape. Austral Ecol 34(2):170–178

Li CJ (2005) Characteristics of water system by the GIS analysis in Hunchun river basin. J Yanbian University (Nat Sci) 31(4):308–311

Merot P, Walter C, Montreuil O, Mourier B (2009) Using the stream order to model the internal structure and function of the wetlands within a catchment from the head water to the sea. Geophys Res Abstr 11(4):2009–3022

Puente CE, Castillo PA (1996) On the fractal structure of networks and dividers within a watershed. J Hydrol 187(1–2):173–181

Rui XF (2004) Principles of hydrology. China Water Press, Beijing

Shao HY, Zhu Y (2007) 'In situ urbanization' in the desakota region of the surrounding area of large cities: case study from Fuzhou municipality. Market Demographic Anal 13(1):12–19
Sun R, Deng WQ, Yuan XZh, Liu H, Zhang YW (2014) Riparian vegetation after dam construction on mountain rivers in China. Ecohydrology 7(4):1187–1195
Sun R, Liang ShM, Qiu ShK, Deng W (2017) Patterns of plant species richness along the drawdown zone of the Three Gorges Reservoir 5 years after submergence. Water Sci Technol 75(10):2299–2308
Vannote RL, Minshall GW, Cummins KW, Sedell JR, Cushing CE (1980) The river continuum concept. Can J Fish Aquat Sci 37(1):130–137
Wang Q, Zou XQ, Zhu DK (2002) On the dimensions of Qinhuai river networks based on the GIS technology. Adv Water Sci 13(6):513–526
Yu J, Sun MM, Cao Y, Lin BY, Yan QB (2009) The river hierarchical classification based on ecological function: a case of Zhejiang province. Geogr Res 28(4):1115–1127
Yuan W, Yang K, Wu JP (2007) River structure characteristics and classification system in river network plain during and course of urbanization. Sci Geogr Sinica 27(3):401–407
Zhang GK (1995) A study of varied nature of mountains river. J Sichuan Union University (Eng Sci Ed) 3(1):11–19
Zhang J, Jiu GS, Ge JP (2002) Model and analysis of structure for watershed and river in mountain area of northeast of China. J Beijing Normal University (Nat Sci) 38(3):231–234

Index

R. Sun and L. Fei (eds.), *Sustainable Development of Water and Environment*, Environmental Science and Engineering,
https://doi.org/10.1007/978-3-030-16729-5